Mixed Structure-Preserving Numerical Methods for Coupled Finite-Strain Continuum Mechanics within Variational, Port-Hamiltonian and GENERIC Frameworks

Zur Erlangung des akademischen Grades eines

DOKTORS DER INGENIEURWISSENSCHAFTEN (Dr.-Ing.)

von der KIT-Fakultät für
Bauingenieur-, Geo- und Umweltwissenschaften
des Karlsruher Instituts für Technologie (KIT)

genehmigte

DISSERTATION

von

Moritz Hille, M.Sc.
aus Augsburg

Tag der mündlichen Prüfung: 19.10.2026

Hauptreferent: Prof. Dr.-Ing. habil. Peter Betsch
Korreferent: Prof. Dr.-Ing. Michael Groß

Karlsruhe 2026

Abstract

Numerical methods for nonlinear continuum mechanics often need to account for large deformations, pronounced temperature changes, nonlinear material responses, and, in many applications, interactions between coupled physical fields. An important requirement for such numerical methods is that the spatial and temporal discretizations respect structural properties of the underlying model, such as conservation laws, power balances, or thermodynamic consistency. With this objective in mind, this thesis develops mixed structure-preserving formulations for finite-strain continuum mechanics.

Hu-Washizu-type mixed formulations enlarge the set of unknowns by introducing additional fields that are linked to the deformation through weakly imposed constraints or compatibility equations. In this work, the additional variables are motivated by polyconvexity-inspired finite-strain elasticity and consist of strain-type quantities such as the right Cauchy–Green tensor, its cofactor, and the determinant or a related volumetric measure. This Hu–Washizu-type setting provides a flexible multi-field description in which the additional variables can be combined with energy-based and thermodynamic modeling frameworks.

The thesis shows systematic ways to construct mixed formulations from purely mechanical elastodynamics to highly coupled multi-physics. In a first step, coupled electro-thermo-elastodynamical models are obtained by augmenting the mixed mechanical equations with thermodynamic and electrostatic field equations. Furthermore, mixed compatibility relations are reformulated at rate level in order to embed the additional variables into port-Hamiltonian formulations of finite elasticity. Eventually, the same idea is transferred to the General Equation for Non-Equilibrium Reversible-Irreversible Coupling (GENERIC). This yields mixed formulations in which reversible mechanical dynamics and irreversible heat conduction are represented within a thermodynamically consistent operator structure.

The corresponding spatial and temporal discretizations are constructed to preserve the relevant structure of the respective formulation. Discrete derivatives are used to obtain energy–momentum consistent schemes for the mechanical and multiphysics settings, while the GENERIC-based formulation leads to energy–momentum–entropy consistent schemes for thermodynamically coupled systems. Compatible mixed finite element discretizations retain the variational, port-Hamiltonian, or GENERIC structure at the discrete level. In the latter case, the resulting schemes preserve the total energy of closed systems while producing entropy consistently.

Overall, this thesis establishes systematic methodologies for integrating polyconvexity-inspired mixed formulations into structure-preserving frameworks for nonlinear continuum mechanics. The resulting formulations show how additional kinematic fields can be incorporated into variational, port-Hamiltonian, and GENERIC descriptions while retaining the relevant energy balances, power balances, and entropy-production properties of the respective frameworks.

Keywords: nonlinear continuum mechanics • large deformations • polyconvexity-inspired formulations • Hu–Washizu formulations • port-Hamiltonian systems • GENERIC • mixed finite elements • structure-preserving time integration

Kurzfassung

Numerische Verfahren für die nichtlineare Kontinuumsmechanik müssen häufig große Deformationen, ausgeprägte Temperaturänderungen, nichtlineares Materialverhalten und Wechselwirkungen zwischen gekoppelten physikalischen Feldern berücksichtigen. Eine wichtige Anforderung an solche Verfahren ist, dass die räumlichen und zeitlichen Diskretisierungen strukturelle Eigenschaften des zugrunde liegenden Modells erhalten, etwa Erhaltungssätze, Leistungsbilanzen oder thermodynamische Konsistenz. Mit diesem Ziel werden in dieser Arbeit gemischte strukturerhaltende Formulierungen in der Kontinuumsmechanik bei großen Deformationen entwickelt.

Gemischte Hu–Washizu-artige Formulierungen erweitern die Menge der Unbekannten durch zusätzliche Felder, die über schwach eingeforderte Zwangs- oder Kompatibilitätsgleichungen mit der Deformation verknüpft sind. In dieser Arbeit werden diese Variablen durch polykonvexitätsinspirierte Formulierungen der nichtlinearen Elastizität motiviert. Sie umfassen Verzerrungsgrößen wie den rechten Cauchy–Green-Tensor, dessen Kofaktor und die Determinante beziehungsweise ein verwandtes Volumenmaß. Diese Mehrfeldbeschreibung ermöglicht die Kombination der zusätzlichen Variablen mit energiebasierten und thermodynamischen Modellierungsansätzen.

Die Arbeit zeigt Wege, gemischte Formulierungen mit strukturerhaltenden Modellierungsrahmen für mechanische, multiphysikalische und thermodynamisch gekoppelte Probleme zu verbinden. Zunächst werden elektro-thermo-elastodynamische Modelle durch Augmentierung der gemischten mechanischen Gleichungen um thermodynamische und elektrostatische Feldgleichungen konstruiert. Anschließend werden gemischte Kompatibilitätsbedingungen auf Ratenebene formuliert, um die zusätzlichen Variablen in port-Hamiltonsche Formulierungen der finiten Elastizität einzubetten. Derselbe Ansatz wird schließlich auf den Formalismus der General Equation for Non-Equilibrium Reversible-Irreversible Coupling (GENERIC) übertragen, wodurch reversible mechanische Dynamik und irreversible Wärmeleitung in einer thermodynamisch konsistenten Operatorstruktur beschrieben werden.

Die zugehörigen räumlichen und zeitlichen Diskretisierungen werden so konstruiert, dass sie die relevante Struktur der jeweiligen Formulierung erhalten. Diskrete Gradienten führen zu energie- und impulskonsistenten Verfahren für die mechanischen und multiphysikalischen Formulierungen, während die GENERIC-basierte Formulierung energie-, impuls- und entropiekonsistente Verfahren für thermodynamisch gekoppelte Systeme ermöglicht. Kompatible gemischte Finite-Elemente-Diskretisierungen erhalten die variationelle, port-Hamiltonsche oder GENERIC-Struktur auf diskreter Ebene; im GENERIC-Fall werden Gesamtenergie geschlossener Systeme und Entropieproduktion konsistent abgebildet.

Insgesamt etabliert diese Arbeit systematische Methodiken zur Integration polykonvexitätsinspirierter gemischter Formulierungen in strukturerhaltende Ansätze der nichtlinearen Kontinuumsmechanik. Die resultierenden Formulierungen zeigen, wie zusätzliche kinematische Felder in variationelle, port-Hamiltonsche und GENERIC-Beschreibungen eingebettet werden können, wobei die jeweils relevanten Energiebilanzen, Leistungsbilanzen und Eigenschaften der Entropieproduktion erhalten bleiben.

Schlüsselwörter: nichtlineare Kontinuumsmechanik • große Deformationen • polykonvexitätsinspirierte Formulierungen • Hu–Washizu-Formulierungen • port-Hamiltonsche Systeme • GENERIC • gemischte Finite-Elemente • strukturerhaltende Zeitintegration

Acknowledgments

I would like to express my sincere gratitude to everyone who has accompanied me throughout the past years and contributed, in one way or another, to the completion of this dissertation.

First and foremost, I would like to thank Peter Betsch for giving me the opportunity to pursue my doctoral research at the Institute of Mechanics and for his continuous guidance throughout these years. I am particularly grateful for the trust he placed in me and his willingness to offer advice whenever needed. Beyond scientific matters, I have always appreciated his open door and his genuine interest in the individual circumstances of his colleagues. On several occasions, he took the time to understand my personal challenges and helped me find solutions tailored to my situation. His considerate approach has contributed greatly to the working environment in which this thesis was developed.

My sincere thanks also go to Michael Groß for serving as co-examiner of this dissertation. I particularly appreciate the time and effort he invested in studying my work and the thoughtful discussions that arose from our correspondence even before the doctoral examination. His detailed questions and constructive suggestions provided valuable perspectives on my research.

I am especially grateful to Marlon Franke, who has accompanied my academic journey from its very beginning. What started with an invitation to write my bachelor's thesis after an examination in continuum mechanics eventually led to my position as a student assistant and, ultimately, to this dissertation. Throughout these years, I have greatly valued his guidance, his openness to new ideas, and the many discussions we had on both scientific and personal matters. His willingness to listen, to discuss questions on equal terms, and to involve everyone in the work of our group has made him an exceptional supervisor, colleague, and friend.

Furthermore, I would like to thank everyone at the Institute of Mechanics for creating such an enjoyable and welcoming working environment. The friendships that developed during this time have made my doctoral studies a particularly rewarding experience.

My friendship with Robin Pfefferkorn goes back to our student days, long before either of us began our doctoral research. I fondly remember the countless study sessions on the fifth floor of the new Civil Engineering building, as well as the celebrations and the construction competition we took part in together. Later, Robin supervised my master's thesis during his own doctoral studies and thereby played an important role in my decision to pursue a doctorate at the Institute of Mechanics. I am grateful that our paths have crossed at so many different stages of our academic lives.

I owe special thanks to Marc Schiebl, whose previous research on the GENERIC formalism at the institute laid important groundwork for my own dissertation. Even after leaving the institute, he continued to contribute to my research through valuable advice, new ideas, and countless helpful discussions. I am especially grateful for his willingness to remain involved in my work and share his knowledge.

I am equally grateful to Simeon Schneider, with whom I shared many years of doctoral research and countless discussions about challenging mathematical and mechanical concepts. His determination to understand even the most difficult questions in depth, and his seemingly endless curiosity about the

fundamental principles governing our world, have made these conversations particularly memorable. Beyond our scientific exchanges, I have always appreciated his kindness and his efforts to bring people together and ensure that everyone felt included.

My special thanks also go to Bianca Seith for our Tuesday walks after lunch. These walks offered a welcome break from everyday work and an opportunity for stimulating conversations about all kinds of topics.

I would also like to thank Paul Wasmer, Vanessa Valdes Y Beck, Philipp Kinon, Felix Zähringer, Marvin May, Luis Hartmann, and Tim Pleßke for their friendship, collegiality, and the many good moments we shared at the institute.

Beyond the academic environment, I am deeply grateful to my friends and family, whose encouragement and understanding have accompanied me throughout my studies and doctoral research.

I would particularly like to thank Daniel Liermann, my longest-standing friend from my hometown of Augsburg. We share numerous interests and passions, from competitive dancing to our fascination with science and the world around us. I deeply value our ability to talk about virtually anything and everything. Even when life keeps us apart for longer periods, spending time with him always feels like coming home.

My heartfelt thanks also go to Denis Mayer, my closest friend in Karlsruhe. We have shared much of our student years, even while pursuing our studies in different parts of the city. Over the past years, our shared passion for cinema has become a cherished weekly tradition through our visits to the Sneak Preview at the Schauburg. These evenings and the conversations surrounding them are memories I will always treasure. As Denis prepares to move to Taiwan to be with his long-term partner, I am genuinely happy for him and this new chapter of his life, even though I know I will miss having him nearby.

I am profoundly grateful to my parents and siblings for their unconditional support and the close bond we share. Knowing that I can always rely on them, regardless of the circumstances, means more to me than I can express.

Finally, my deepest gratitude goes to Elena. Over the past three years, she has brought an extraordinary amount of happiness into my life and has been a constant source of encouragement and support. Thank you for your understanding, your patience, and for always finding a way to gently point me in the right direction when needed. Sharing both the challenges and the achievements of these past years with you has meant more to me than words can express. I am grateful for everything we have experienced together and look forward to all that lies ahead.

Karlsruhe, November 2026 Moritz Hille

Contents

Abstract . . . . . **i**

Kurzfassung . . . . . **iii**

Acknowledgments . . . . . **v**

1. Introduction **1**
1.1. Motivation and methods 1
1.1.1. Mixed formulations 1
1.1.2. Structure-preserving modeling 3
1.1.3. Mixed structure-preserving formulations 5
1.2. Research gaps and aims 5
1.3. Main contributions 6
1.4. Outline of the thesis 7

2. Mixed variational multiphysics formulation **9**
2.1. Introduction 9
2.2. Framework 10
2.2.1. Elastodynamics 10
2.2.2. Thermodynamics and electrostatics 12
2.2.3. Constitutive equations 12
2.2.4. Mixed thermo-electro-mechanical strong form 13
2.3. Discretization 13
2.3.1. Structure-preserving time integration 14
2.3.2. Finite element method 14
2.4. Numerical examples 15
2.4.1. Flying L-Shape 15
2.4.2. Microfluid pumping device 16
2.5. Conclusions 18

3. Mixed port-Hamiltonian formulation **21**
3.1. Introduction 21
3.2. Port-Hamiltonian formulation of nonlinear elastodynamics 23
3.2.1. Quantities of continuum mechanics and tensor cross product 23
3.2.2. Polyconvex energy density function and equations of motion 24
3.2.3. Port-Hamiltonian form of the local field equations 26
3.2.4. Weak form 28
3.2.5. Conservation properties 29
3.2.6. Alternative size-reduced port-Hamiltonian formulations 30
3.3. Discretization in time 32
3.3.1. Time-discrete conservation of energy 34
3.3.2. Time-discrete conservation of angular momentum 34

3.4. Discretization in space . . . 35
3.4.1. Approximation of the test and trial functions . . . 35
3.4.2. Space-discrete formulation as discrete port-Hamiltonian system . . . 39
3.5. Spatial and temporal discretization . . . 40
3.5.1. Fully mixed element based on the strain-type fields $\{\mathbf{C}, \mathbf{G}, J\}$ . . . 41
3.5.2. Mixed element based on the strain-type fields $\{\mathbf{G}, J\}$ . . . 43
3.5.3. Displacement-based element . . . 44
3.6. Numerical examples . . . 46
3.6.1. Dynamical investigations of an L-shaped body . . . 48
3.6.2. Dynamics of a bending and twisting beam . . . 50
3.7. Conclusion . . . 52
3.A. Appendix . . . 54
3.A.1. Nodal operator matrix . . . 54
3.A.2. Matrix related to the tensor cross product . . . 55
3.A.3. Update formula for the reduced mixed formulation . . . 55

4. Mixed GENERIC formulation . . . 57
4.1. Introduction . . . 57
4.2. The GENERIC formalism . . . 59
4.3. Continuum mechanical and thermodynamical preliminaries . . . 60
4.3.1. Quantities of continuum mechanics . . . 60
4.3.2. Tensor cross product and polyconvex energy density function . . . 60
4.3.3. Thermodynamical quantities . . . 61
4.4. The mixed GENERIC framework . . . 63
4.4.1. Hu-Washizu-type functional for $\{\mathbf{C}, \mathbf{G}, J\}$ . . . 63
4.4.2. Special form of GENERIC . . . 64
4.5. Discretization in time . . . 72
4.5.1. Time-discrete conservation of energy . . . 74
4.5.2. Time-discrete entropy production . . . 75
4.6. Discretization in space . . . 76
4.6.1. Finite element approximation . . . 76
4.6.2. GENERIC-consistent semi-discrete formulation . . . 82
4.6.3. Verification of the discrete energy balance . . . 85
4.6.4. Verification of discrete entropy production . . . 85
4.7. Numerical examples . . . 86
4.7.1. Material models and discretization . . . 86
4.7.2. Flying L-shape benchmark . . . 90
4.8. Conclusion . . . 94
4.9. Appendix . . . 94
4.9.1. Nodal operator matrix . . . 94
4.9.2. Matrix related to the tensor cross product . . . 95

5. Conclusion . . . 97
5.1. Summary . . . 97
5.2. Outlook . . . 98

Declaration of authorship . . . 101

Publications and talks . . . 103

List of figures **105**

List of tables **107**

Bibliography **109**

1. Introduction

The reliable numerical simulation of nonlinear continuum mechanical systems is a central task in computational mechanics. In many applications, the governing equations involve large deformations, nonlinear material behavior, and interactions between different physical fields. Such problems do not only require accurate spatial and temporal approximations, but also numerical methods that respect the underlying mechanical and thermodynamic structure of the model.

This thesis is concerned with mixed formulations for nonlinear continuum mechanics and their integration into structure-preserving modeling and discretization frameworks. The common theme of the following chapters is the use of additional independent fields to obtain flexible mixed descriptions and the construction of numerical methods that preserve essential structural properties of the continuous system.

1.1. Motivation and methods

We first introduce the two methodological pillars on which the thesis is based (see Figure 1.1). The first pillar is formed by **mixed formulations**, represented here by Hu–Washizu-type formulations and mixed finite elements, with particular emphasis on polyconvexity-inspired approaches for finite-strain solid mechanics. The second pillar is formed by **structure-preserving modeling**, comprising structure-preserving time discretization in the form of energy–momentum methods and their energy–momentum–entropy extensions for thermodynamically coupled systems, as well as port-Hamiltonian systems and the General Equation for Non-Equilibrium Reversible-Irreversible Coupling (GENERIC) framework. The section concludes by explaining how these two viewpoints are combined in the present thesis. Figure 1.1 provides a schematic overview of the methodological viewpoint pursued in this thesis and illustrates how mixed formulations and structure-preserving modeling are combined in the three article-based chapters.

1.1.1. Mixed formulations

Mixed formulations constitute a classical and widely used concept in computational mechanics and numerical analysis. Their central idea is to provide flexibility by enlarging the set of primary unknowns by additional fields and by enforcing selected kinematic, constitutive, or constraint equations only in a weak or variational sense. This additional freedom is often exploited to improve approximation properties, to avoid locking phenomena, or to construct finite element formulations with enhanced robustness. Classical examples include Hu–Washizu-type variational formulations, assumed strain approaches, and mixed and hybrid finite element methods for solid mechanics [11, 15, 77, 79, 88, 89].

In nonlinear solid mechanics, the role of mixed formulations becomes particularly important in the finite-strain regime. Large deformations, nearly incompressible material behavior, and strong constitutive nonlinearities often challenge purely displacement-based finite element methods. Introducing additional independent fields, such as pressure, strain-type variables, stress-type quantities, or suitable

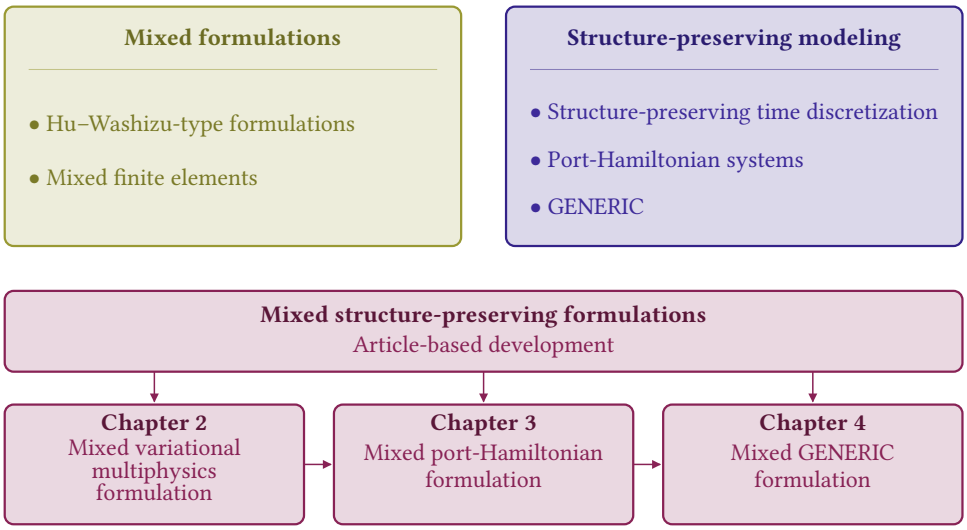


Figure 1.1.: Conceptual structure of the thesis. The two methodological pillars of mixed formulations and structure-preserving frameworks are combined into mixed structure-preserving formulations and developed further in the three article-based chapters.

kinematic measures, provides a systematic way to improve the numerical behavior of the resulting discretization. In this context, mixed formulations based on independent approximations of additional deformation-related quantities provide a flexible framework for finite-strain solid mechanics and have been successfully applied in representative finite element discretizations [7, 48, 74].

A closely related motivation arises from the mathematical structure of nonlinear elasticity. The concept of polyconvexity provides a well-established framework for the formulation of stored energy functions at finite strains. In its classical form, a stored energy function is called polyconvex if it can be represented as a convex function of the components of the deformation gradient, its cofactor, and its determinant. This is a constitutive property of a specific material model. In contrast, the term polyconvexity-inspired is used in this thesis in a broader methodological sense: the kinematic quantities appearing in polyconvex representations are introduced as independent fields and are employed to construct mixed formulations, even if the complete coupled material model is not necessarily proven to be polyconvex in all arguments. Since these quantities have a direct geometric interpretation in terms of line, area, and volume changes, they provide a natural motivation for multi-variable formulations in finite elasticity. In addition, using strain-type quantities such as the right Cauchy–Green tensor and its derived measures yields an objective formulation, since these variables are invariant under superposed rigid body motions [3, 13, 14, 22, 50].

This methodological viewpoint underlies several developments in large-strain computational mechanics. Bonet, Gil, Ortigosa and co-workers employed polyconvexity-based and polyconvexity-inspired formulations for nonlinear solid mechanics and coupled field problems, using the geometric structure of the deformation gradient, its cofactor, and its determinant as a basis for robust multi-field descriptions [13, 14, 30, 60, 61]. In a subsequent development, Betsch, Janz and Hesch [7] transferred this idea to an objective Hu–Washizu-type setting based on the right Cauchy–Green tensor, its cofactor, and the squared Jacobian. Their formulation treats these quantities as independent fields and relates them to the deformation map through variationally enforced kinematic constraints. It thereby provides a mixed variational basis for finite-strain elastodynamics and, at the same time, a convenient starting point for the construction of energy–momentum consistent time integration schemes. The present thesis builds

on this line of work and studies how such mixed formulations can be extended to coupled multiphysics systems and embedded into broader structure-preserving modeling frameworks.

Throughout this thesis, the mixed continuum formulations are ultimately combined with finite element discretizations. The role of the finite element method is not to introduce a separate modeling principle, but to provide compatible approximation spaces for the primary unknowns, the additional mixed fields, and the corresponding test functions [89, 92]. In the article-based chapters, standard Bubnov-Galerkin-type finite element discretizations are employed together with suitable choices of continuous and discontinuous approximation spaces. This is particularly important for the local treatment of the additional mixed variables, the possible use of static condensation, and the preservation of the structural properties inherited from the underlying variational, port-Hamiltonian, or GENERIC formulation.

1.1.2. Structure-preserving modeling

The second methodological pillar of this thesis is structure-preserving modeling. It comprises modeling frameworks and discretization techniques that aim to retain essential structural properties of the underlying physical system at the continuous, semi-discrete, or fully discrete level. Depending on the problem under consideration, these properties may include the conservation of total energy and momenta in closed mechanical systems, the preservation of energy or power balances in open systems, or the consistent production of entropy in thermodynamically coupled systems.

Structure-preserving time discretization

Structure-preserving time discretization aims at transferring such structural properties to the time-discrete level. In particular, energy–momentum methods for conservative mechanical systems, energy–momentum–entropy methods for thermodynamically coupled systems, and related discrete-derivative approaches provide prominent examples of structure-preserving time integration schemes [5, 6, 31, 32, 35, 78].

Energy–momentum schemes are closely connected to the variational and geometric structure of mechanical systems. Their construction is guided by the aim of reproducing the fundamental conservation laws of the continuous problem at the discrete level. This is particularly relevant in nonlinear elastodynamics, where standard time integration schemes may exhibit artificial energy drift, energy blowup, or loss of robustness, especially in long-term simulations. Discrete derivatives provide a systematic tool for replacing continuous derivatives of energy functions by algorithmic counterparts in such a way that exact discrete energy balances can be obtained. This makes them especially suitable for nonlinear material models and for formulations in which the stored energy is expressed in terms of several independent variables.

Port-Hamiltonian systems

Port-Hamiltonian systems provide an energy-based framework for the modeling, analysis, simulation, and control of dynamical systems. Originating from finite-dimensional port-controlled Hamiltonian systems [51], the framework was later extended to distributed-parameter systems by means of Stokes–Dirac structures and boundary energy flow [86]. In this setting, the Hamiltonian represents the stored energy of the system, while the interconnection and dissipation structures encode the exchange, conservation, and dissipation of power. This makes port-Hamiltonian formulations particularly attractive for open systems and multiphysics problems, where subsystems interact through power-conjugate variables [23, 70, 85].

A major line of research concerns the development of structure-preserving spatial discretizations for port-Hamiltonian systems. Such methods aim at transferring the underlying power balance, interconnection structure, and port variables to the discrete level. Weak-form and finite-element-based discretizations have therefore become increasingly important, since they provide a natural way to approximate distributed-parameter systems while retaining the port-Hamiltonian structure [47, 54]. In computational mechanics, recent developments include port-Hamiltonian formulations and discretizations for thermoelasticity, plates, beams, poroelastic systems, geometrically exact strings, and hyperelastic continua [1, 16–18, 44, 46, 68, 69].

Despite these developments, the integration of mixed Hu–Washizu-type formulations for finite-strain elasticity into the port-Hamiltonian framework remains nontrivial. The additional independent fields of a mixed formulation are not merely auxiliary discretization variables, but have to be interpreted consistently as part of the energy-based state description. This requires a suitable rate formulation of the kinematic compatibility relations and a corresponding weak form that preserves the power balance. This issue is one of the central topics of this thesis.

GENERIC

For thermodynamically coupled systems, the GENERIC framework provides a general structure for nonequilibrium thermodynamics. Originally developed by Grmela and Öttinger [34, 63], and later summarized and extended in monographic treatments [62, 66], GENERIC decomposes the evolution of a system into reversible and irreversible contributions generated by the total energy and the total entropy, respectively. The reversible part is governed by a skew-adjoint operator, whereas the irreversible part is governed by a symmetric positive semi-definite operator. Together with the non-interaction conditions, this structure encodes compatibility with the first and second laws of thermodynamics.

Recent developments show that GENERIC continues to evolve beyond classical thermo-mechanical solid mechanics. On the theoretical side, recent works have further clarified the geometric foundations of non-equilibrium thermodynamics and related GENERIC to rate formulations, cotangent lifts and Onsager-type variational principles [24, 25]. Further mathematical developments have investigated how GENERIC systems may arise from Hamiltonian systems by coarse graining [58]. At the same time, GENERIC has been applied to fluid dynamics, reactive flows, and rarefied gas dynamics, where it provides a thermodynamically consistent way of combining reversible transport with dissipative mechanisms such as viscosity, heat conduction, diffusion, and chemical reactions [4, 64, 80, 90]. More recently, GENERIC has also been used as an inductive bias in scientific machine learning, for instance in neural-network architectures that enforce energy conservation, entropy production, and the associated degeneracy conditions by construction [38, 65, 84, 87, 91]. These developments illustrate the broad current relevance of GENERIC as a structure-preserving framework for both model formulation and data-driven discovery.

In continuum mechanics, GENERIC has been used to formulate thermodynamically consistent models for dissipative material behavior and coupled thermo-mechanical systems [40, 56, 72]. In particular, the GENERIC structure provides a natural foundation for the construction of energy–momentum–entropy consistent time integration schemes. For finite-strain thermoelasticity, GENERIC-based formulations and discretizations have been developed that allow different choices of thermodynamic state variables and preserve the essential thermodynamic structure at the semi-discrete and fully discrete levels [8, 9]. Related developments have also addressed thermo-viscoelasticity and more general dissipative materials [57, 59, 73].

However, most existing GENERIC-based formulations in nonlinear continuum mechanics are formulated in terms of classical mechanical and thermal variables. The systematic inclusion of additional mixed

kinematic fields, as they arise in Hu–Washizu-type formulations inspired by polyconvexity, requires a reformulation of the reversible and irreversible dynamics. In particular, the compatibility conditions for the mixed variables have to be expressed at the rate level, and the resulting formulation has to preserve the GENERIC degeneracy conditions and the associated energy and entropy balances. This provides the second major structural extension investigated in this thesis.

1.1.3. Mixed structure-preserving formulations

The preceding sections outline two complementary developments in computational mechanics. Mixed formulations provide additional fields and constraints that can improve the modeling and discretization of nonlinear continuum problems. Structure-preserving frameworks, in contrast, provide mathematical structures that encode fundamental mechanical and thermodynamic principles such as energy conservation in closed systems, energy or power balances in open systems, and entropy production in thermodynamically coupled systems. The central viewpoint of this thesis is that these two developments can be combined in a systematic way.

From this perspective, the additional variables introduced in mixed Hu–Washizu-type formulations should not be regarded merely as auxiliary finite element quantities. Instead, they become part of the structured description of the continuum system. This raises several nontrivial questions. The compatibility relations defining the mixed variables have to be formulated in a way that is consistent with the underlying energy, power, or entropy structure. Moreover, the resulting weak forms and discrete equations have to preserve the structural properties of the corresponding continuous framework.

The present thesis investigates this idea in three consecutive steps. First, a polyconvexity-inspired mixed formulation is extended to coupled electro-thermo-elastodynamics by augmenting the variationally derived mechanical equations with non-potential field equations [B3, A1]. Second, the mixed formulation is recast in rate form and embedded into the port-Hamiltonian framework [A2]. Third, the same guiding principle is transferred to the GENERIC framework in order to obtain a mixed and thermodynamically consistent formulation for nonlinear thermoelasticity [A3]. In all three steps, the development of compatible structure-preserving discretization methods in space and time is an essential part of the formulation.

1.2. Research gaps and aims

The preceding section has outlined the methodological background of this thesis. Mixed Hu–Washizu-type formulations provide a flexible framework for finite-strain continuum mechanics, while structure-preserving approaches such as energy–momentum and energy–momentum–entropy methods, port-Hamiltonian systems, and GENERIC encode fundamental mechanical and thermodynamic principles at the continuous or discrete level. Despite substantial progress in each of these areas, their systematic combination remains only partially explored.

The key difficulty is that mixed formulations introduce additional independent fields that are not present in classical displacement-, momentum-, or temperature-based descriptions. These fields are often highly advantageous from the viewpoint of constitutive modeling and finite element discretization. However, in structure-preserving frameworks they cannot be regarded as mere auxiliary discretization variables. Instead, they have to be incorporated consistently into the underlying energy-, power-, or entropy-based description. This affects the formulation of the kinematic compatibility relations, the

interpretation of associated stress-type quantities, and the construction of weak forms and discrete schemes.

Against this background, the developments presented in this thesis are motivated by two principal research gaps.

Research gap 1: Mixed Hu–Washizu-type formulations and structure-preserving continuum modeling frameworks have mostly been developed from different perspectives. While mixed formulations emphasize additional independent fields, weakly enforced constraints, and improved discretization properties, port-Hamiltonian and GENERIC formulations emphasize energy, power, and thermodynamic structure. These observations define the first research gap addressed in this thesis: the systematic incorporation of mixed Hu–Washizu-type formulations into such structure-preserving frameworks. This concerns, in particular, the consistent treatment of additional kinematic fields and their compatibility relations within variational, port-Hamiltonian, and GENERIC descriptions.

Research gap 2: The integration of mixed formulations into structure-preserving frameworks requires spatial and temporal discretization techniques that are compatible with the resulting mixed structure. Existing structure-preserving time integration schemes, port-Hamiltonian discretizations, and GENERIC-based discretizations are typically tailored to specific state spaces and formulations. They cannot be transferred directly to mixed multiphysics systems or to thermodynamically consistent mixed formulations with additional kinematic variables. These observations define the second research gap addressed in this thesis: the development of structure-preserving discretization methods for such mixed systems.

To address these research gaps, the thesis pursues the following research aims.

Research aim 1: Development of a systematic methodology for incorporating mixed Hu–Washizu-type formulations into structure-preserving continuum modeling frameworks, including variational multiphysics formulations, port-Hamiltonian systems, and GENERIC.

Research aim 2: Development of compatible structure-preserving spatial and temporal discretization techniques for the resulting mixed formulations, with particular emphasis on energy consistency in closed systems, power balances in open systems, and thermodynamic consistency in dissipative systems.

1.3. Main contributions

The scientific contributions of this thesis are presented in the three article-based Chapters 2–4, which are based on two published articles and one manuscript submitted for publication. Together, they develop mixed structure-preserving formulations in three consecutive steps: from a variational multiphysics formulation, to a port-Hamiltonian formulation, and finally to a GENERIC formulation.

Contribution 1: The first contribution extends a polyconvexity-inspired mixed Hu–Washizu-type formulation to coupled nonlinear electro-thermo-elastodynamics [A1]. Starting from a variationally derived mixed mechanical formulation, non-potential field equations from thermodynamics and electrostatics are incorporated at the level of the strong and weak forms. This provides a systematic way to augment the mixed mechanical framework by additional physical fields while preserving the advantages of the underlying mixed formulation. Moreover, an energy–momentum consistent time integration scheme based on discrete derivatives is developed for the resulting coupled system.

Contribution 2: The second contribution embeds a mixed formulation for finite-strain elasticity into the port-Hamiltonian framework [A2]. To this end, the mixed kinematic compatibility conditions are reformulated at the rate level and incorporated into an energy-based state description. The resulting formulation combines the flexibility of mixed Hu–Washizu-type continuum descriptions with the power-based structure of port-Hamiltonian systems. In addition, the work shows how the corresponding weak form and finite element discretization can be constructed in a structure-preserving way.

Contribution 3: The third contribution transfers the rate-based mixed formulation principle to the GENERIC framework [A3]. A newly mixed GENERIC formulation for nonlinear thermoelasticity is developed in which reversible mechanical dynamics and irreversible heat conduction are represented within a thermodynamically consistent operator structure. The additional mixed kinematic fields are incorporated in a way that preserves the GENERIC degeneracy conditions. Furthermore, structure-preserving temporal and spatial discretization techniques are constructed such that the resulting schemes preserve the total energy of closed systems while ensuring consistent entropy production.

Taken together, these contributions establish a systematic pathway for integrating mixed Hu–Washizu-type continuum formulations into increasingly general structure-preserving modeling frameworks. At the same time, they provide corresponding discretization techniques that preserve the relevant mechanical, power-based, or thermodynamic structure of the respective formulation.

1.4. Outline of the thesis

This cumulative dissertation consists of the present introductory chapter, three article-based chapters, and a concluding chapter. The article-based chapters are arranged in chronological order. They follow the methodological development from a mixed variational formulation for coupled multiphysics problems, through a port-Hamiltonian formulation of finite elasticity, to a mixed GENERIC formulation for nonlinear thermoelasticity.

Chapter 2 is based on the first article on coupled nonlinear electro-thermo-elastodynamics. Chapter 3 is based on the second article on the port-Hamiltonian formulation of finite elasticity. Chapter 4 is based on the third article on the mixed GENERIC formulation of nonlinear thermoelasticity. Finally, Chapter 5 summarizes the main findings and discusses possible directions for future research.

2. Structure-preserving discretization of a polyconvexity-inspired formulation for coupled nonlinear electro-thermo-elastodynamics

This chapter is based on:*
Hille M, Franke M, Zähringer F, and Betsch P. "Structure-Preserving Discretization of a Polyconvexity-Inspired Formulation for Coupled Nonlinear Electro-Thermo-Elastodynamics". In: *IFAC-PapersOnLine*, 58(6): 113–118, 2024. DOI: 10.1016/j.ifacol.2024.08.266

Abstract: A consistent, structure-preserving space-time discretization for coupled nonlinear electro-thermo-elastodynamical problems is presented. The underlying polyconvexity-inspired mixed framework is facilitated by the properties of the tensor cross product. The elastodynamic problem is then extended by the energy balance as well as Gauss's and Faraday's law to integrate the thermodynamic and electrostatic contribution, respectively. A suitable polyconvexity-inspired internal energy function is chosen to complete the nonlinear, fully coupled electro-thermo-elastodynamical formulation. Additionally, we present a structure-preserving, second-order accurate time integration scheme, utilizing discrete derivatives in the sense of [31], ensuring a stable and robust simulation even for large time steps. Finally, we assess the numerical performance of our newly developed method through representative examples also showing the possibilities of the framework in the field of boundary control.

Keywords: nonlinear electro-thermo-elastodynamics • polyconvexity • tensor cross product • structure-preserving discretization

* Adapted from the cited work. © 2024 The Authors. Published by Elsevier B.V. This is an open access article under the CC BY-NC-ND 4.0 license. Peer review under responsibility of the International Federation of Automatic Control. The original publication is available via the DOI stated above.

2.1. Introduction

Dielectric elastomers (DEs) are classified as smart materials within the group of electroactive polymers, showcasing great potential in the field of control owing to their electrically induced actuation properties. In their basic configuration, DEs comprise an elastomer layer sandwiched between two electrodes. The application of a voltage results in a Coulomb force, leading to a compression of the elastomer layer. DEs can undergo large deformations, with area expansions of up to 1600% ([43]), albeit exhibiting sensitivity to temperature variations (see e.g. [52]). Thus, this paper provides a fully coupled nonlinear thermo-electro-mechanical framework to simulate DEs.

For long-term time-dependent finite element simulations of DEs, employing a stable and robust spatial and temporal discretization is crucial. Energy-momentum (EM) time integration schemes offer superior stability and robustness compared to other classical time integration methods ([78]). This superiority

arises from their inherent ability to preserve the conservation of the total energy, total linear momentum, and total angular momentum of the system.

[7] leveraged the tensor cross product, originally introduced by [10] and reintroduced to the field of nonlinear continuum mechanics by [14]. They subsequently adapted an EM scheme based on discrete gradients in the sense of [31], to suit a mixed polyconvexity-inspired elastodynamic framework. To achieve the desired multiphysics framework, we incorporate the mixed polyconvexity-inspired elastodynamics formulation by [7]. This formulation is then extended by introducing additional fields from thermodynamics and electrostatics.

The paper is therefore organized as follows: In Section 2.2, fundamental concepts are presented, including the basics of the tensor cross products, a mixed Hu-Washizu-like variational potential for elastodynamics, balance equations derived from thermodynamics and electrostatics, and a suitable coupling energy density function. These elements collectively give rise to the mixed polyconvexity-inspired thermo-electro-mechanical framework. The temporal and spatial discretization is then discussed in Section 2.3. Using two examples, the structure-preserving properties of the formulation are investigated in Section 2.4, before brief conclusions are drawn in Section 2.5.

2.2. Framework

In this section we give an overview of the balance equations of elastodynamics, thermodynamics and electrostatics along with a suitable material model yielding the fully coupled, mixed, polyconvexity-inspired framework we use.

2.2.1. Elastodynamics

We start with the elastodynamic part of the framework. The deformation gradient $\mathbf{F}$ defined as

$$\mathrm{d}\mathbf{x} = \mathbf{F}\,\mathrm{d}\mathbf{X} \tag{2.1}$$

maps infinitesimal line elements $\mathrm{d}\mathbf{X} \in \Omega_0$ to their spatial counterparts $\mathrm{d}\mathbf{x} \in \Omega_t$, where Ω_0 and Ω_t represent a body Ω in its reference and current configuration, respectively.

To describe the elastodynamic behaviour of the material under consideration we assume an energy density function of the form

$$\widehat{\mathcal{W}}(\mathbf{C}) = \widetilde{\mathcal{W}}(\mathbf{C}, \mathrm{cof}(\mathbf{C}), \det(\mathbf{C})) \tag{2.2}$$

with the right Cauchy Green tensor

$$\mathbf{C} = \mathbf{F}^{\mathrm{T}}\mathbf{F}. \tag{2.3}$$

We then utilize the tensor cross product[1] between two second-order tensors $\mathbf{A}, \mathbf{B} \in \mathbb{R}^3$ defined in index notation as

$$(\mathbf{A} \overset{\times}{\times} \mathbf{B})_{ij} = \epsilon_{i\alpha\beta}\epsilon_{jab}\mathbf{A}_{\alpha a}\mathbf{B}_{\beta b}, \tag{2.4}$$

[1] The tensor cross product was described in [10] and later introduced to the field of nonlinear continuum mechanics by [14].

where ϵ_{ijk} denotes the third-order permutation tensor. This operation allows us to rewrite the cofactor and the determinant of $\mathbf{C}$ as

$$\operatorname{cof}(\mathbf{C}) = \frac{1}{2}\,\mathbf{C}\,\overline{\times}\,\mathbf{C}, \tag{2.5}$$

$$\det(\mathbf{C}) = \frac{1}{6}\big(\mathbf{C}\,\overline{\times}\,\mathbf{C}\big) : \mathbf{C}, \tag{2.6}$$

respectively.[2]

Note that the energy density function (2.2) can be viewed as objective version of the underlying polyconvex energy density function $\overline{\mathcal{W}}(\mathbf{F}, \operatorname{cof}(\mathbf{F}), \det(\mathbf{F}))$.

We introduce the set of independent variables $\boldsymbol{\Sigma} = (\mathbf{C}, \mathbf{G}, C)$ for the right Cauchy Green tensor, its cofactor and its determinant along with the cascade like kinematic set

$$\begin{aligned} \mathbf{C} &= (\nabla\boldsymbol{\varphi})^{\top}\nabla\boldsymbol{\varphi}, \\ \mathbf{G} &= \frac{1}{2}\,\mathbf{C}\,\overline{\times}\,\mathbf{C}, \\ C &= \frac{1}{3}\,\mathbf{G} : \mathbf{C}. \end{aligned} \tag{2.7}$$

With a re-expressed energy density function

$$\widehat{\mathcal{W}}(\mathbf{C}) = \bar{\mathcal{W}}(\mathbf{C}, \mathbf{G}, C) \tag{2.8}$$

we can extend the classic variational potential for the pure displacement formulation by enforcing the kinematic set (2.7) via Lagrange multipliers $\boldsymbol{\Lambda} = (\boldsymbol{\Lambda}^{\mathbf{C}}, \boldsymbol{\Lambda}^{\mathbf{G}}, \Lambda^{C})$ yielding the 7-field Hu-Washizu type formulation

$$\begin{aligned} \Pi^{\mathrm{m}}(\boldsymbol{\varphi}, \boldsymbol{\Sigma}, \boldsymbol{\Lambda}) = \int_{\Omega_0} \bar{\mathcal{W}}(\mathbf{C}, \mathbf{G}, C) + \boldsymbol{\Lambda}^{\mathbf{C}} : \big((\nabla\boldsymbol{\varphi})^{\top}\nabla\boldsymbol{\varphi} - \mathbf{C}\big) \\ + \boldsymbol{\Lambda}^{\mathbf{G}} : \big(\frac{1}{2}\,\mathbf{C}\,\overline{\times}\,\mathbf{C} - \mathbf{G}\big) + \Lambda^{C} : \big(\frac{1}{3}\,\mathbf{G} : \mathbf{C} - C\big)\,\mathrm{d}V + \Pi^{\mathrm{m,ext}}(\boldsymbol{\varphi}), \end{aligned} \tag{2.9}$$

where $\boldsymbol{\varphi}$ is the displacement field. A variation of (2.9) yields the seven stationary conditions

$$\begin{aligned} \delta_{\boldsymbol{\varphi}}\tilde{\Pi}^{\mathrm{m}} &= \int_{\Omega_0} \boldsymbol{\Lambda}^{\mathbf{C}} : \big((\nabla\delta\boldsymbol{\varphi})^{\top}\nabla\boldsymbol{\varphi} + (\nabla\boldsymbol{\varphi})^{\top}\nabla\delta\boldsymbol{\varphi}\big)\,\mathrm{d}V + \Pi^{\mathrm{m,ext}}(\delta\boldsymbol{\varphi}) = 0, \\ \delta_{\mathbf{C}}\tilde{\Pi}^{\mathrm{m}} &= \int_{\Omega_0} \delta\mathbf{C} : \big(\partial_{\mathbf{C}}\bar{\mathcal{W}} - \boldsymbol{\Lambda}^{\mathbf{C}} + \boldsymbol{\Lambda}^{\mathbf{G}}\,\overline{\times}\,\mathbf{C} + \tfrac{1}{3}\,\Lambda^{C}\mathbf{G}\big)\,\mathrm{d}V = 0, \\ \delta_{\mathbf{G}}\tilde{\Pi}^{\mathrm{m}} &= \int_{\Omega_0} \delta\mathbf{G} : \big(\partial_{\mathbf{G}}\bar{\mathcal{W}} - \boldsymbol{\Lambda}^{\mathbf{G}} + \frac{1}{3}\,\Lambda^{C}\mathbf{C}\big)\,\mathrm{d}V = 0, \\ \delta_{C}\tilde{\Pi}^{\mathrm{m}} &= \int_{\Omega_0} \delta C\big(\partial_{C}\bar{\mathcal{W}} - \Lambda^{C}\big)\,\mathrm{d}V = 0, \\ \delta_{\boldsymbol{\Lambda}_{\mathbf{C}}}\tilde{\Pi}^{\mathrm{m}} &= \int_{\Omega_0} \delta\boldsymbol{\Lambda}^{\mathbf{C}} : \big((\nabla\boldsymbol{\varphi})^{\top}\nabla\boldsymbol{\varphi} - \mathbf{C}\big)\,\mathrm{d}V = 0, \\ \delta_{\boldsymbol{\Lambda}_{\mathbf{G}}}\tilde{\Pi}^{\mathrm{m}} &= \int_{\Omega_0} \delta\boldsymbol{\Lambda}^{\mathbf{G}} : \big(\frac{1}{2}\mathbf{C}\,\overline{\times}\,\mathbf{C} - \mathbf{G}\big)\,\mathrm{d}V = 0, \\ \delta_{\Lambda^{C}}\tilde{\Pi}^{\mathrm{m}} &= \int_{\Omega_0} \delta\Lambda^{C}\big(\frac{1}{3}\,\mathbf{G} : \mathbf{C} - C\big)\,\mathrm{d}V = 0. \end{aligned} \tag{2.10}$$

[2] For an overview on helpful properties and calculation rules for the tensor cross product cf. [7].

Due to the arbitrariness of the variations we afterwards transform these equations into a set of differential equations to be able to augment our framework with the balance equations of the non-potential thermodynamic and the electrostatic field. We want to emphasize that the method shown here allows one to augment the elastodynamic field with arbitrary not necessarily potential-based fields.

2.2.2. Thermodynamics and electrostatics

For the thermodynamic extension we use the local energy balance

$$\vartheta\dot{\eta} = \bar{R} - \operatorname{Div}\mathbf{Q} \tag{2.11}$$

with the absolute temperature ϑ, the entropy density η, a prescribed heat source $\bar{R}$ and the Piola heat flux vector $\mathbf{Q}$. The formulation is completed by suitable thermal boundary and initial values.

For the electrostatic extension we take Maxwell's equations and neglect all transient and magnetic effects yielding Gauss's and Faraday's law

$$\begin{aligned} \operatorname{Div}\mathbf{D}_0 &= \bar{\rho}_0^{\mathrm{e}}, \\ \mathbf{E}_0 &= -\nabla\Phi \end{aligned} \tag{2.12}$$

with the electric potential Φ, the electric field $\mathbf{E}_0$, the electric displacement field $\mathbf{D}_0$ and a prescribed electric volume charge $\bar{\rho}_0^{\mathrm{e}}$. The formulation is completed by suitable boundary values for the electric potential and the electric surface charge. The present electrostatic formulation will later on result in a mixed finite element method in terms of Φ and $\mathbf{D}_0$, first presented by [28].

2.2.3. Constitutive equations

We extend the energy density function (2.8) to obtain a fully coupled thermo-electro-mechanical material model. For the numerical examples below we used the energy density function

$$\mathcal{W}(\mathbf{C}, \mathbf{G}, C, \mathbf{D}_0, \vartheta) = f_\vartheta(\vartheta)\mathcal{W}_{\mathrm{em}}(\mathbf{C}, \mathbf{G}, C, \mathbf{D}_0) + \mathcal{W}_{\mathrm{tm}}(C, \vartheta) + \mathcal{W}_{\mathrm{t}}(\vartheta), \tag{2.13}$$

where $\mathcal{W}_{\mathrm{em}}(\mathbf{C}, \mathbf{G}, C, \mathbf{D}_0)$ is a compressible Mooney-Rivlin model with an ideal dielectric elastomer model. The full coupling of the model comes from the temperature dependent prefactor $f_\vartheta(\vartheta) = \vartheta/\vartheta_{\mathrm{R}}$. The thermomechanical and purely thermal contributions are given by

$$\mathcal{W}_{\mathrm{tm}}(C, \vartheta) = -3\beta e(C-1)(\vartheta - \vartheta_{\mathrm{R}}), \tag{2.14}$$

$$\mathcal{W}_{\mathrm{t}}(\vartheta) = \kappa\big(\vartheta - \vartheta_{\mathrm{R}} - \vartheta\log\big(\frac{\vartheta}{\vartheta_{\mathrm{R}}}\big)\big) \tag{2.15}$$

with the thermodynamical parameters β and e along with the reference temperature ϑ_{R} and the specific heat capacity κ. The given material model is convex with respect to $\{\mathbf{C}, \mathbf{G}, C, \mathbf{D}_0\}$ and concave with respect to ϑ. Note that while the energy density function's convexity is not mandatory, its presence not only enhances the stability of the formulation but also results in simpler equations when combined with the tensor cross product.

The description of the material model is completed by the constitutive equations of the three fields. The second Piola Kirchhoff stress tensor[3] denotes

$$\mathbf{S} = 2\big(\partial_{\mathbf{C}}\mathcal{W} + \partial_{\mathbf{G}}\mathcal{W} \overset{\otimes}{\times} \mathbf{C} + \partial_{C}\mathcal{W}\mathbf{G}\big) \tag{2.16}$$

and the constitutive equations for the electrostatic and the thermodynamic fields are

$$\mathbf{E}_0 = \partial_{\mathbf{D}_0}\mathcal{W} \quad , \quad \eta = -\partial_{\vartheta}\mathcal{W}. \tag{2.17}$$

Finally, we use Fourier's law for thermal isotropy

$$\mathbf{Q} = -\mathbf{K}\nabla\vartheta \quad , \quad \mathbf{K} = k_0 C^{-1}\mathbf{G} \tag{2.18}$$

with the thermal conductivity coefficient k_0 to conclude the material model.

2.2.4. Mixed thermo-electro-mechanical strong form

We combine the mixed mechanical equations in strong form from Section 2.2.1 with the differential equations of thermodynamics (2.11) and electrostatics (2.12) which leads to the mixed strong formulation for thermo-electro-mechanics[4]

$$\begin{aligned}
\rho_0(\dot{\boldsymbol{\varphi}} - \mathbf{v}) &= \mathbf{0} \\
\operatorname{Div}(2\mathbf{F}\boldsymbol{\Lambda}^{\mathbf{C}}) + \bar{\mathbf{B}} &= \rho_0\dot{\mathbf{v}} \\
\vartheta\dot{\eta} + \operatorname{Div}\mathbf{Q} - \bar{R} &= 0 \\
\operatorname{Div}\mathbf{D}_0 - \bar{\rho}_0^{\mathrm{e}} &= 0 \\
\partial_{\mathbf{D}_0}\mathcal{W} + \nabla\Phi &= \mathbf{0} \\
\partial_{\mathbf{C}}\mathcal{W} - \boldsymbol{\Lambda}^{\mathbf{C}} + \boldsymbol{\Lambda}^{\mathbf{G}} \overset{\otimes}{\times} \mathbf{C} + \frac{1}{3}\Lambda^{C}\mathbf{G} &= \mathbf{0} \\
\partial_{\mathbf{G}}\mathcal{W} - \boldsymbol{\Lambda}^{\mathbf{G}} + \frac{1}{3}\Lambda^{C}\mathbf{C} &= \mathbf{0} \\
\partial_{C}\mathcal{W} - \Lambda^{C} &= 0 \\
(\nabla\boldsymbol{\varphi})^{\top}\nabla\boldsymbol{\varphi} - \mathbf{C} &= \mathbf{0} \\
\frac{1}{2}\mathbf{C} \overset{\otimes}{\times} \mathbf{C} - \mathbf{G} &= \mathbf{0} \\
\frac{1}{3}\mathbf{G} : \mathbf{C} - C &= 0.
\end{aligned} \tag{2.19}$$

In order to arrive at the corresponding weak formulation, we multiply the equations from (2.19) with admissible test functions $\mathbf{w}_{(\bullet)}$, integrate over the entire body and apply integration by parts as usual.

2.3. Discretization

In this section, we conduct the temporal and spatial discretization of the weak form outlined in Section 2.2.4 starting with the temporal one.

[3] It is important to remark, that on a continuum level, (2.16) does not deviate from the well-known classical stress formula. However, the algorithmic form of the second Piola-Kirchhoff stress tensor will play a crucial role in preserving the energy conservation of the discrete system. The partial derivatives included are considerably simpler to calculate, due to the incorporation of both the polyconvex framework and the tensor cross product.

[4] The Lagrange multiplier $\boldsymbol{\Lambda}^{\mathbf{C}}$ can be understood as half of the second Piola-Kirchhoff stress tensor, i.e. $\mathbf{S} = 2\boldsymbol{\Lambda}^{\mathbf{C}}$.

2.3.1. Structure-preserving time integration

For the temporal discretization we adopt the notion of discrete gradient introduced in [31]. Within this scheme the midpoint evaluations of the partial derivatives of $\mathcal{W}$ are substituted with discrete derivatives $\mathrm{D}_{\mathcal{V}}\mathcal{W}$, which can be understood as algorithmic or time-discrete counterparts of $\partial_{\mathcal{V}}\mathcal{W}$ with $\mathcal{V} \in \{\mathbf{C}, \mathbf{G}, C, \mathbf{D}_0, \vartheta\}$. These discrete derivatives fulfill the so-called directionality condition

$$\mathcal{W}(\mathcal{V}_{n+1}) - \mathcal{W}(\mathcal{V}_n) = \mathrm{D}_{\mathbf{C}}\mathcal{W} : \Delta\mathbf{C} + \mathrm{D}_{\mathbf{G}}\mathcal{W} : \Delta\mathbf{G} + \mathrm{D}_{C}\mathcal{W}\Delta C + \mathrm{D}_{\mathbf{D}_0}\mathcal{W} \cdot \Delta\mathbf{D}_0 + \mathrm{D}_{\vartheta}\mathcal{W}\Delta\vartheta \tag{2.20}$$

with $\Delta(\bullet) = (\bullet)_{n+1} - (\bullet)_n$ thereby achieving the desired property of energy conservation - an aspect lacking in the classical midpoint evaluation.[5]

If we apply the time discretization including the discrete derivatives to the weak form, we obtain the semi-discrete set of equations

$$\begin{aligned}
&\int_{\Omega_0} \mathbf{w}_{\mathbf{v}} \cdot \big(\frac{1}{\Delta t}(\boldsymbol{\varphi}_{n+1} - \boldsymbol{\varphi}_n) - \mathbf{v}_{n+1/2}\big)\rho_0 \,\mathrm{d}V = 0,\\
&\int_{\Omega_0} \mathbf{w}_{\boldsymbol{\varphi}} \cdot \frac{\rho_0}{\Delta t}(\mathbf{v}_{n+1} - \mathbf{v}_n) + \boldsymbol{\Lambda}^{\mathbf{C}}_{n+1} : \big(\big(\nabla\mathbf{w}_{\boldsymbol{\varphi}}\big)^{\top}\nabla\boldsymbol{\varphi}_{n+1/2} + \big(\nabla\boldsymbol{\varphi}_{n+1/2}\big)^{\top}\nabla\mathbf{w}_{\boldsymbol{\varphi}}\big)\,\mathrm{d}V + \Pi^{\mathrm{m,ext}}_{n+1/2}(\mathbf{w}_{\boldsymbol{\varphi}}) = 0,\\
&\int_{\Omega_0} w_{\vartheta}\big(\frac{1}{\Delta t}\big(\vartheta_{n+1}\eta_{n+1} - \vartheta_n\eta_n\big) + \frac{1}{\Delta t}(\vartheta_{n+1} - \vartheta_n)\mathrm{D}_{\vartheta}\mathcal{W}\big)\,\mathrm{d}V - \int_{\Omega_0} \nabla w_{\vartheta} \cdot \mathbf{Q}_{n+1/2}\,\mathrm{d}V + \Pi^{\mathrm{t,ext}}_{n+1/2}(w_{\vartheta}) = 0,\\
&\int_{\Omega_0} \nabla w_{\Phi} \cdot \mathbf{D}_{0\,n+1/2}\,\mathrm{d}V + \Pi^{\mathrm{e,ext}}_{n+1/2}(w_{\Phi}) = 0,\\
&\int_{\Omega_0} \mathbf{w}_{\mathbf{D}_0} \cdot \big(\mathrm{D}_{\mathbf{D}_0}\mathcal{W} + \nabla\Phi_{n+1/2}\big)\,\mathrm{d}V = 0,\\
&\int_{\Omega_0} \mathbf{w}_{\mathbf{C}} : \big(\mathrm{D}_{\mathbf{C}}\mathcal{W} - \boldsymbol{\Lambda}^{\mathbf{C}}_{n+1} + \boldsymbol{\Lambda}^{\mathbf{G}}_{n+1} \overset{\otimes}{\otimes} \mathbf{C}_{n+1/2} + \frac{1}{3}\Lambda^{C}_{n+1}\mathbf{G}_{n+1/2}\big)\,\mathrm{d}V = 0,\\
&\int_{\Omega_0} \mathbf{w}_{\mathbf{G}} : \big(\mathrm{D}_{\mathbf{G}}\mathcal{W} - \boldsymbol{\Lambda}^{\mathbf{G}}_{n+1} + \frac{1}{3}\Lambda^{C}_{n+1}\mathbf{C}_{n+1/2}\big)\,\mathrm{d}V = 0,\\
&\int_{\Omega_0} w_{C}\big(\mathrm{D}_{C}\mathcal{W} - \Lambda^{C}_{n+1}\big)\,\mathrm{d}V = 0\\
&\int_{\Omega_0} \mathbf{w}_{\Lambda_{\mathbf{C}}} : \big(\big(\nabla\boldsymbol{\varphi}_{n+1}\big)^{\top}\nabla\boldsymbol{\varphi}_{n+1} - \mathbf{C}_{n+1}\big)\,\mathrm{d}V = 0,\\
&\int_{\Omega_0} \mathbf{w}_{\Lambda_{\mathbf{G}}} : \big(\frac{1}{2}\mathbf{C}_{n+1} \overset{\otimes}{\otimes} \mathbf{C}_{n+1} - \mathbf{G}_{n+1}\big)\,\mathrm{d}V = 0,\\
&\int_{\Omega_0} w_{\Lambda^{C}}\big(\frac{1}{3}\mathbf{G}_{n+1} : \mathbf{C}_{n+1} - C_{n+1}\big)\,\mathrm{d}V = 0.
\end{aligned} \tag{2.21}$$

where $f_{(\bullet)}$ denotes the evaluation of a variable f at time $t_{(\bullet)}$ along with $f_{n+1/2} = \frac{1}{2}(f_n + f_{n+1})$.

2.3.2. Finite element method

For the spatial discretization we employ the classic Bubnov-Galerkin finite element method along with the isoparametric concept. The continuous variables - namely, the displacement $\boldsymbol{\varphi}$, the temperature ϑ and the electric potential Φ - are approximated using 20-node serendipity shape functions. Regarding

[5] For the detailed construction rules of the discrete derivatives we refer to [B3].

the mixed variables, which include the electric displacement vector $\mathbf{D}_0$ and the three mixed mechanical variables $\mathbf{C}$, $\mathbf{G}$ and C along with their corresponding Lagrange multipliers $\boldsymbol{\Lambda}_{\mathbf{C}}$, $\boldsymbol{\Lambda}_{\mathbf{G}}$ and Λ^C, we employ discontinuous trilinear Lagrange shape functions on eight-node cube elements. This enables the implementation of a static condensation, thereby reducing the numerical costs to approximately the level of a three-field thermo-electro-mechanical formulation.

2.4. Numerical examples

In this section we present two numerical examples showing the structure preserving properties of the formulation along with the possibilities in the field of boundary control.

2.4.1. Flying L-Shape

The first example is a technical one, where an L-shaped specimen can freely fly through space. Figure

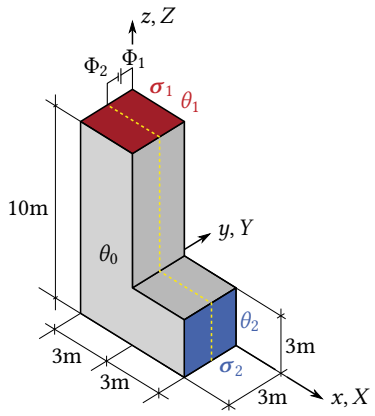


Figure 2.1.: Flying L-Shape: reference configuration with boundary and initial conditions.

2.1 shows the specimens reference configuration along with its initial and boundary conditions. For the spatial discretization a total of 288 elements is used. The colored surfaces indicate initial temperatures of $\vartheta_1 = 250\text{K}$ and $\vartheta_2 = 300\text{K}$, whereas the remainder of the body starts with an initial temperature of $\vartheta_0 = 293.15\text{K}$. For the first 5 seconds of the simulation, we apply mechanical Neumann boundary conditions in the form of two stresses

$$\boldsymbol{\sigma}_1(t) = -\boldsymbol{\sigma}_2(t) = f(t) \begin{pmatrix} 1 \\ 2 \\ 3 \end{pmatrix} \frac{\text{N}}{\text{m}^2} \tag{2.22}$$

with

$$f(t) = \begin{cases} \frac{256}{9} t & \text{for} \quad t \leq 2.5\text{s} \\ \frac{256}{9}(5 - t) & \text{for} \quad 2.5 \leq t \leq 5\text{s} \\ 0 & \text{for} \quad t > 5\text{s} \end{cases} \tag{2.23}$$

onto the two colored surfaces. Simultaneously, electrical Dirichlet boundary conditions corresponding to two electric potentials $\Phi_1(X, Y = 0, Z) = 0\text{V}$ and $\Phi_2(X, Y = -1.5, Z) = 6 \cdot 10^6 \sin(\frac{\pi}{5} t)\text{V}$ are applied on the back surface of the specimen and the surface indicated by the yellow dotted line (see Figure 2.1).

The system is simulated over a total time $T = 40\text{s}$ with a time step size $\Delta t = 0.8\text{s}$. After the initial 5 seconds, as no additional energy is introduced into the system, the discrete gradient is able to preserve both the total energy E and the total angular momentum $\|\mathbf{L}\|$ as illustrated in Figures 2.2 and 2.3. Unlike the discrete gradient, the classic midpoint rule fails to preserve the total energy, resulting in an energy blow-up after a few seconds. Since the midpoint rule and the EM-scheme produce exactly the same results for the total angular momentum, only the EM-scheme is depicted in the right plots of Figures 2.2 and 2.3.

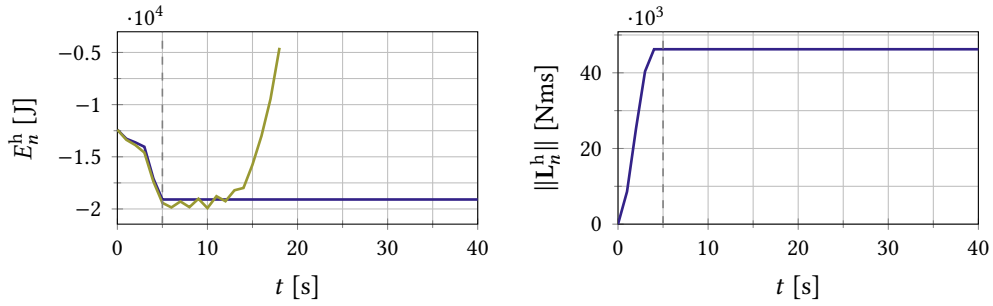


Figure 2.2.: Flying L-Shape: total energy E_n^h for the EM scheme —— and the MP scheme —— (left); total angular momentum $\|\mathbf{L}_n^h\|$ for the EM scheme —— (right).

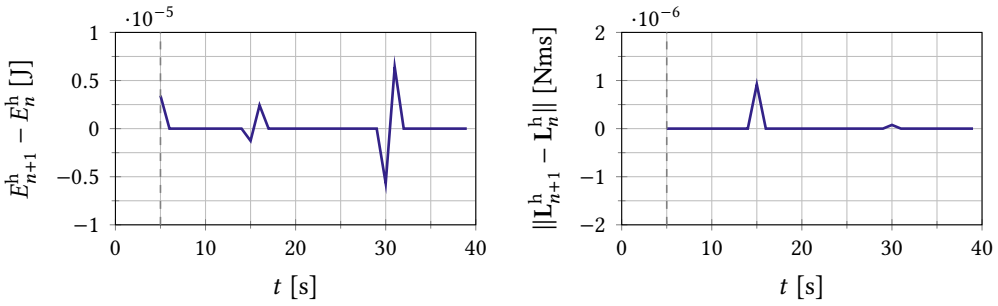


Figure 2.3.: Flying L-Shape: difference of total energy $E_{n+1}^h - E_n^h$ for the EM scheme —— (left); difference of total angular momentum $\|\mathbf{L}_{n+1}^h - \mathbf{L}_n^h\|$ for the EM scheme —— (right).

2.4.2. Microfluid pumping device

As a second example, we illustrate a more practical application: a microfluid pump employed, for instance, to deliver drugs through the bloodstream. This example is intended to demonstrate both the long-term stability of the formulation and the possible applications in the area of boundary control. The microfluidic pumping device under consideration closely resembles the one discussed in e.g. [53] and was also presented in [B3]. Similarly, it does not account for fluid-structure interaction. Both the complete shape of the cylindrical pumping device and its dimensioning are depicted in Figures 2.4 and 2.5, where all lengths are provided in micrometers (μm). Due to the three symmetry axes, it is sufficient to simulate only one-eighth of the pumping corpus comprised of 320 finite elements, along with suitable symmetric mechanical Dirichlet boundary conditions. The simulation is conducted with a total simulation time of $T = 100\text{s}$ and a time step size of $\Delta t = 0.1\text{s}$. The heating of the pumped liquid is

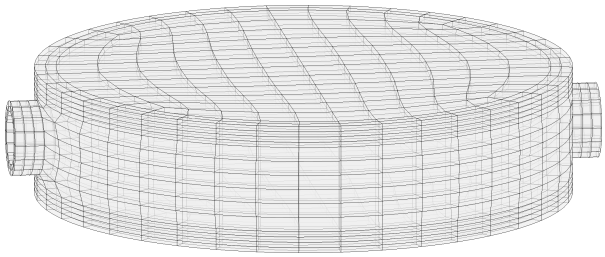


Figure 2.4.: Microfluid pump: initial configuration.

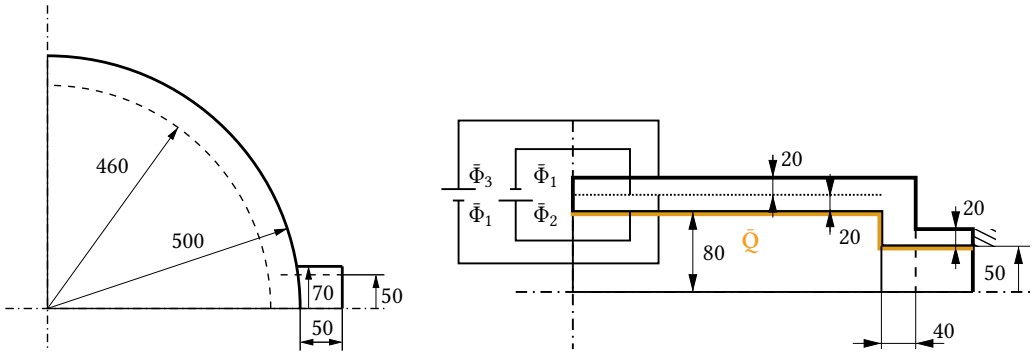


Figure 2.5.: Microfluid pump: top view (left) and side view (right) of one eighth of the pumping corpus.

simulated by a thermal Neumann boundary condition

$$\bar{Q} = 0.8 \begin{cases} t & \text{for } t \leq 2\,\text{s} \\ 4 - t & \text{for } 2\,\text{s} < t \leq 4\,\text{s} \\ 0 & \text{for } t > 4\,\text{s} \end{cases} \quad \left[\frac{\text{W}}{\text{m}^2}\right], \tag{2.24}$$

applied to the interior of the pump for the initial 4 seconds of the simulation (illustrated in orange in Figure 2.5). For the pumping purpose two elastomer layers are sandwiched between two compliant electrodes on the top and bottom walls of the corpus, respectively. Specifically, mimicking the pumping movement involves applying Dirichlet boundary conditions in the form of electrical potentials $\bar{\Phi}_1$ to $\bar{\Phi}_3$, where $\bar{\Phi}_1 = 0\text{V}$ at all times, while $\bar{\Phi}_2$ and $\bar{\Phi}_3$ follow a periodic pattern, as depicted in Figure 2.6. After

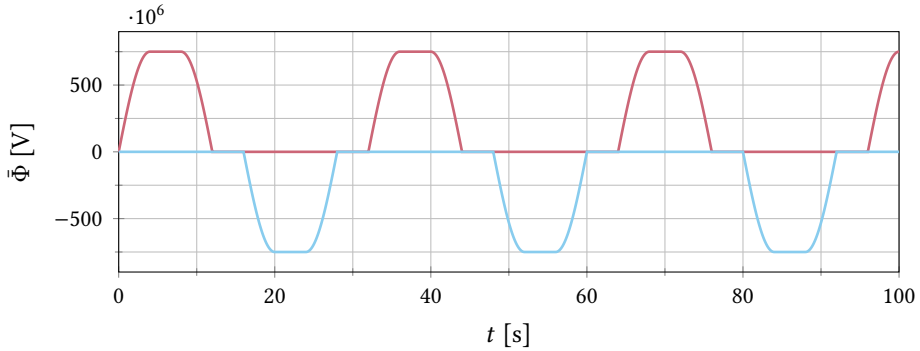


Figure 2.6.: Microfluid pump: periodically applied electric Dirichlet boundary conditions $\bar{\Phi}_2$ and $\bar{\Phi}_3$.

the heating phase and during constant phases of the applied electric potential fields the proposed EM integration scheme is able to correctly reproduce the conservation of the total energy of the system.

Figure 2.7 shows the total energy and the energy difference[6] of the simulation with the proposed EM scheme. Finally, in Figure 2.8 snapshots of the simulation are shown, where in column one to three

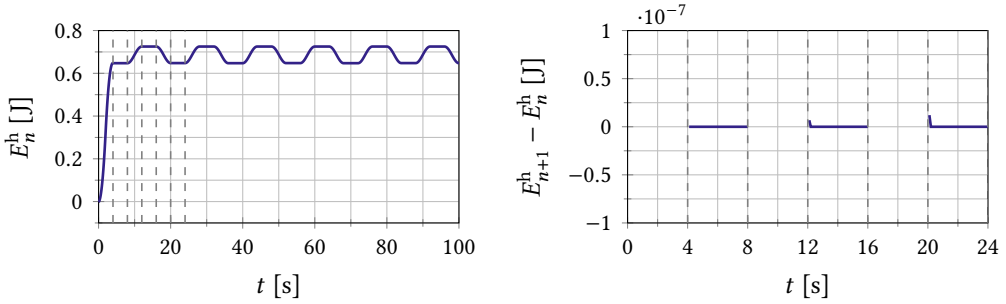


Figure 2.7.: Microfluid pump: total energy E_n^h for the EM scheme —— (left); energy difference $E_{n+1}^h - E_n^h$ for the EM scheme —— (right), plotted during constant electric potential phases.

the electric potential, the temperature and the von Mises stress are depicted. The top snapshot of each column takes place at time $t = 0$s, the middle one at time $t = 6$s and the bottom one shows each quantity at time $t = 22$s. The snapshots show that the formulation can accurately reproduce both the

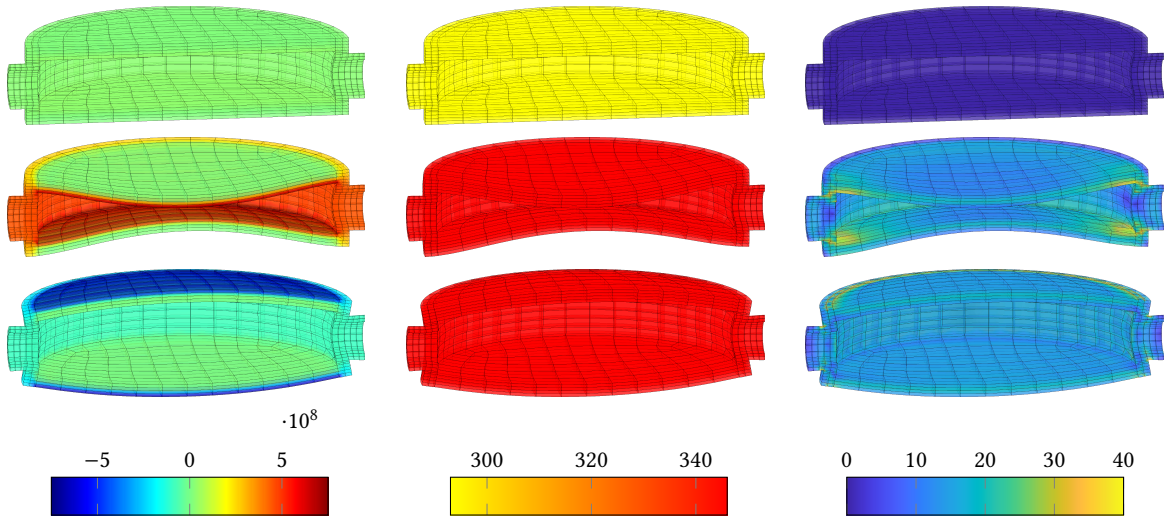


Figure 2.8.: Microfluid pump: snapshots of the electric potential field Φ [V] (left), the absolute temperature field ϑ [K] (center) and the von Mises stress σ_{vM} [Pa] (right) at times $t = 0$s (top), $t = 6$s (middle) and $t = 22$s (bottom).

heating of the pump induced by the thermal Neumann boundary condition and the movement of the pump induced by the electrical Dirichlet boundary conditions.

2.5. Conclusions

This paper introduces a structure-preserving space-time discretization method for coupled nonlinear thermo-electro-elastodynamics. This approach is built upon the polyconvex mixed framework developed by [7], which has been further extended to accommodate multiphysics. To achieve this, the

[6] Note that the discrete energy difference is only plotted during time intervals when constant electric potential fields are applied.

mixed Hu-Washizu-like seven-field variational potential was transformed into its corresponding strong form. Subsequently, it was augmented with the requisite multiphysic fields, specifically incorporating thermodynamics and electrostatics in our case. In this augmentation, the selection of coupled fields is not confined solely to potential fields. The elastodynamic formulation's polyconvex structure derives advantages from the utilization of both the tensor cross product in conjunction with the cascade-like formulation of kinematic constraints and a polyconvex material model. The latter reflects the behavior of dielectric elastomers and is pivotal for the coupling within the formulation.

The result is a fully coupled mixed thermo-electro-elastodynamic framework, which was discretized in a next step using the finite element method and a structure-preserving time integration via discrete gradient in the sense of [31] in space and time, respectively. Finally, two numerical examples were presented to demonstrate that the formulation exhibits numerical stability even in long-term simulations. Furthermore, the proposed method is capable to accurately preserve both the total energy and the total angular momentum of the system.

We see potential in transcribing the present formulation into the GENERIC formalism (see [62] and [73]). GENERIC (General Equation for the Non-Equilibrium Reversible Irreversible Coupling) offers a thermodynamically consistent framework that splits the underlying evolution equations additively into reversible and irreversible parts. This aligns seamlessly with a possible extension of the formulation to incorporate viscoelastic material behavior, providing an even more accurate description of the behavior of dielectric elastomers.

3. Port-Hamiltonian formulation and structure-preserving discretization of finite elasticity based on a mixed Hu-Washizu-type formulation

This chapter is based on:*
Hille M, Betsch P, and Franke M. "Port-Hamiltonian Formulation and Structure-Preserving Discretization of Finite Elasticity Based on a Mixed Hu–Washizu-Type Formulation". In: *Computer Methods in Applied Mechanics and Engineering*, 458: 118790, 2026. DOI: 10.1016/j.cma.2026.118790

Abstract: We propose a port-Hamiltonian formulation and structure-preserving discretization of finite elasticity. The energy functional (or Hamiltonian) is based on a polyconvex representation of the stored energy and gives rise to three strain-type fields, which play the role of energy variables in the port-Hamiltonian formulation. We show that a Hu-Washizu-type extension of the variational principle of Livens can be used (i) to derive the continuous port-Hamiltonian formulation and (ii) to perform a structure-preserving spatial discretization. In particular, we show that the spatial finite element discretization of the underlying mixed formulation yields a discrete port-Hamiltonian system. Moreover, the temporal discretization of the underlying continuous formulation yields a new energy-momentum consistent framework, which accommodates alternative finite element formulations. The new framework, in particular, covers mixed finite elements that have been shown to be well suited for handling quasi-incompressible material behavior. Numerical examples are provided to evaluate the numerical performance and stability of the newly devised energy-momentum schemes.

Keywords: nonlinear elastodynamics • Livens principle • Hu-Washizu principle • port-Hamiltonian formulation • mixed finite elements • energy-momentum methods

* Adapted from the cited work. This open access article is licensed under CC BY 4.0. © 2026 The Authors. Published by Elsevier B.V.

3.1. Introduction

The port-Hamiltonian (pH) formulation of evolution equations related to multiphysics systems provides an appealing framework for modeling, simulation, and control [23, 85]. The energy-based pH description takes into account dissipation and interaction with the environment by means of ports, and can thus be considered as an extension of classical Hamiltonian systems to open systems.

Finite-dimensional pH systems have been originally introduced in [51] and are based on a Dirac structure, which encodes system properties such as passivity and energy consistency into system equations. The extension of the pH modeling paradigm to infinite-dimensional systems is based on a Stokes-Dirac structure and can be traced back to [86]. Since then, distributed pH systems have been subject to extensive research in the areas of multiphysics system modeling, analysis and design of control

techniques, and structure-preserving discretization methods, as categorized in the comprehensive literature review [70].

The design of structure-preserving discretization techniques is a natural objective in preserving the intrinsic structure and properties of pH systems, such as passivity and energy consistency. Galerkin-based numerical methods for the structure-preserving discretization of pH systems have become more popular only recently [47]. In particular, finite element methods have been applied to discretize pH formulations of viscoelastic strings [46], beams [18, 21, 44, 68], plates [16], the wave equation [20], poroelasticity [1], and thermoelasticity [17]. It is important to note that the typical use of energy variables in the pH approach inherently gives rise to mixed finite element formulations.

Interestingly, the field of nonlinear elastodynamics has been addressed only very recently within the pH framework. The pH structure of the so-called velocity-stress formulation proposed in [83] led to the design of a linear implicit energy-consistent time-stepping scheme. Similarly, the linearly implicit energy-momentum (EM) scheme developed in [19] is based on a mixed finite element description relying on the approximation of the displacement, velocity and stress fields. Both works [19, 83] are closely related to the Hellinger-Reissner variational formulation and restricted to the St. Venant-Kirchhoff material. The pH formulation proposed in [69] is based on the approximation of displacement, linear momentum density, and Green-Lagrangian strain fields and takes into account general hyperelastic constitutive laws. While the semi-discrete equations of motion in [69] retain the pH structure, the Störmer-Verlet scheme or the midpoint rule are used in the temporal discretization, thus generally compromising the balance law for energy in the discrete model.

The above summarized developments in the framework of the pH formulation complement earlier works on the design of EM schemes for nonlinear elastodynamics. In fact, the quest for numerically stable time-stepping schemes led to the first EM scheme for non-linear elastodynamics proposed in the pioneering work [78]. This method has been developed in the framework of purely displacement-based finite elements and relies on a modification of the implicit midpoint rule on the constitutive level. This modification was then generalized for arbitrary hyperelastic materials applying the notion of discrete derivative in [32]. In essence, the application of discrete derivatives at the constitutive level yields specific stress formulas that are a prominent feature of EM methods [71]. It should be noted that EM schemes can also be designed by applying Galerkin methods in time [5]. In particular, higher-order EM schemes have been devised in [35]. EM schemes have also been developed in the framework of mixed finite elements resulting from a polyconvex representation of hyperelastic materials [7].

In the present work, we propose a new pH-based avenue for the design of EM schemes for finite-deformation elastodynamics. Similarly to [7], we start from a polyconvex representation of hyperelastic materials. The proposed pH-based approach makes it possible to accommodate alternative mixed finite element formulations, leading to related EM methods. In this way, previously developed mixed finite elements which have been shown to perform well in finite-deformation problems, including quasi-imcompressible material behavior, can be extended to the dynamic regime. This will be shown by incorporating the family of mixed finite elements developed in [48, 74] into the present approach.

The outline of the rest of the paper is as follows. Section 3.2 provides a mixed variational principle for finite strain elastodynamics, from which the continuous pH formulation will be derived. The corresponding weak form of the fully mixed formulation provides the starting point for the energy-momentum consistent temporal discretization, as discussed in Section 3.3. Section 3.4 shows that the spatial discretization of the fully mixed weak form yields semidiscrete equations of motion which fit into the framework of discrete pH systems. Starting from the time-discrete weak form of the underlying fully mixed description, alternative spatial discretizations are incorporated in Section 3.5, leading to

corresponding EM schemes. Numerical investigations are presented in Section 3.6 and conclusions are drawn in Section 3.7.

3.2. Port-Hamiltonian formulation of nonlinear elastodynamics

This section introduces the theoretical framework underlying the proposed pH formulation of nonlinear elastodynamics. We begin by reviewing the fundamentals of continuum mechanics and the tensor cross product. A polyconvex energy density function is introduced afterwards, and a variational principle is used to derive the strong form of the governing equations. The local field equations are reformulated in port-Hamiltonian form, and alternative reduced-order pH formulations are briefly discussed. We proceed with the derivation of the weak form and conclude by verifying the balance laws for energy and angular momentum.

3.2.1. Quantities of continuum mechanics and tensor cross product

We consider a deformable body in the reference configuration $\Omega_0 \subset \mathbb{R}^3$, depicted in Fig. 3.1, which can be described by material points $\mathbf{X} \in \mathbb{R}^3$. The mapping $\mathbf{x}(t) = \boldsymbol{\varphi}(\mathbf{X}, t)$ maps points $\mathbf{X}$ to their corresponding points $\mathbf{x} = \mathbf{x}(t) \in \mathbb{R}^3$ of the body in the spatial configuration Ω at time t, i.e. $\Omega(t) = \boldsymbol{\varphi}(\Omega_0, t) \subset \mathbb{R}^3$ for a time $t \in \mathcal{I} = [t_0, t_N]$, where $\mathcal{I}$ is the time interval of interest. The boundary of the domain $\partial\Omega_0$ is disjointly decomposed into the Dirichlet boundary $\partial_\varphi\Omega_0$ with prescribed placements $\bar{\boldsymbol{\varphi}}(t)$, and the Neumann boundary $\partial_\sigma\Omega_0$ with prescribed tractions $\bar{\mathbf{t}} = \bar{\mathbf{t}}(t)$. In addition, there are prescribed body forces $\bar{\mathbf{g}} = \bar{\mathbf{g}}(t) \in \mathbb{R}^3$ and distributed body control forces $\bar{\mathbf{b}} = \bar{\mathbf{b}}(t) \in \mathbb{R}^3$ acting on the body.

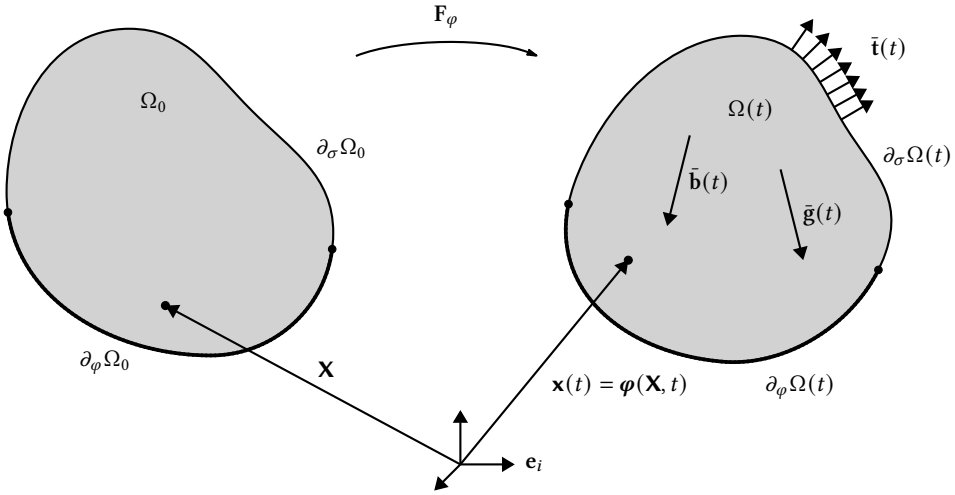


Figure 3.1.: Configuration and kinematics of a deformable body Ω.

To map material line elements $\mathrm{d}\mathbf{X}$ to their spatial counterparts $\mathrm{d}\mathbf{x}$, we introduce the deformation gradient $\mathbf{F}_\varphi$, a second-order tensor given by

$$\mathrm{d}\mathbf{x} = \mathbf{F}_\varphi \mathrm{d}\mathbf{X}, \quad \mathbf{F}_\varphi = \nabla\boldsymbol{\varphi}(\mathbf{X}, t), \tag{3.1}$$

where ∇ denotes the gradient with respect to the material coordinates. Note that the notation $\mathbf{F}_\varphi$ explicitly indicates that the deformation gradient depends on the deformation map. This notation is used in the sequel to distinguish deformation-dependent quantities from associated quantities of the mixed formulation.

In this paper, we use the so-called tensor cross product[1] between two second-order tensors $\mathbf{A}, \mathbf{B} \in \mathbb{R}^{3\times3}$ given by

$$(\mathbf{A} \boxtimes \mathbf{B})_{ij} = \epsilon_{i\alpha\beta}\epsilon_{jab}A_{\alpha a}B_{\beta b}, \tag{3.2}$$

where repeated indices $a, b, \alpha, \beta, i, j \in \{1, 2, 3\}$ imply summation according to Einstein's convention and ϵ_{ijk} denotes the third-order permutation tensor. The tensor cross product can be used to rewrite the cofactor and the determinant of a second-order tensor $\mathbf{A}$ as

$$\begin{aligned} \operatorname{cof}(\mathbf{A}) &= \frac{1}{2}\,\mathbf{A} \boxtimes \mathbf{A}, \\ \det(\mathbf{A}) &= \frac{1}{6}\left(\mathbf{A} \boxtimes \mathbf{A}\right) : \mathbf{A}. \end{aligned} \tag{3.3}$$

This reformulation allows for some straightforward calculations due to suitable properties of the tensor cross product, given by

$$\begin{aligned} \mathbf{A} \boxtimes \mathbf{B} &= \mathbf{B} \boxtimes \mathbf{A} \\ \mathbf{A} \boxtimes (\mathbf{B} + \mathbf{C}) &= \mathbf{A} \boxtimes \mathbf{B} + \mathbf{A} \boxtimes \mathbf{C} \\ (\mathbf{A} \boxtimes \mathbf{B}) : \mathbf{C} &= (\mathbf{A} \boxtimes \mathbf{C}) : \mathbf{B} = (\mathbf{B} \boxtimes \mathbf{C}) : \mathbf{A}. \end{aligned} \tag{3.4}$$

In addition to the deformation gradient $\mathbf{F}_\varphi$, further kinematic measures can be introduced. These include the right Cauchy–Green deformation tensor, defined as

$$\mathbf{C}_\varphi = \mathbf{F}_\varphi^\top \mathbf{F}_\varphi, \tag{3.5}$$

as well as its cofactor,

$$\mathbf{G}_\varphi = \operatorname{cof}(\mathbf{C}_\varphi) = \frac{1}{2}\,\mathbf{C}_\varphi \boxtimes \mathbf{C}_\varphi, \tag{3.6}$$

and the determinant of the deformation gradient,

$$J_\varphi = \det(\mathbf{F}_\varphi) = \frac{1}{6}\left(\mathbf{F}_\varphi \boxtimes \mathbf{F}_\varphi\right) : \mathbf{F}_\varphi = \sqrt{\det(\mathbf{C}_\varphi)}. \tag{3.7}$$

The latter two expressions have been reformulated in terms of the tensor cross product to facilitate its efficient numerical implementation.

3.2.2. Polyconvex energy density function and equations of motion

Polyconvexity is a widely accepted notion for hyperelastic materials in the large-deformation regime. Consequently, we assume that the material behavior under consideration can be described by a polyconvex energy density function

$$W = \widehat{W}(\mathbf{F}_\varphi) = \widetilde{\mathcal{W}}\left(\mathbf{F}_\varphi, \operatorname{cof}(\mathbf{F}_\varphi), \det(\mathbf{F}_\varphi)\right), \tag{3.8}$$

where $\widetilde{\mathcal{W}}$ is constructed to be convex with respect to its arguments. To obtain an objective representation, W is re-expressed as

$$W = \widehat{\mathcal{W}}(\mathbf{C}_\varphi) = \widetilde{\mathcal{W}}\left(\mathbf{C}_\varphi, \mathbf{G}_\varphi, J_\varphi\right) \tag{3.9}$$

with the kinematic measures $\mathbf{C}_\varphi$, $\mathbf{G}_\varphi$ and J_φ defined in (3.6) and (3.7).

[1] The tensor cross product can be found in [10] and its advantageous use has been more recently advocated in [14].

To derive the governing equations for the motion of an elastic body, we employ a Hu-Washizu-type extension of Livens' principle based on the variational functional, defined as

$$\begin{aligned}\mathcal{S} = \int_{t_0}^{t_N} \int_{\Omega_0} \Big[&\frac{1}{2}\rho_0 \mathbf{v}\cdot\mathbf{v} - \widetilde{\mathcal{W}}\left(\mathbf{C},\mathbf{G},J\right) + \boldsymbol{\pi}\cdot\left(\dot{\boldsymbol{\varphi}}-\mathbf{v}\right) \\ &- \boldsymbol{\Lambda}_{\mathbf{C}} : \left(\mathbf{C}_{\varphi}-\mathbf{C}\right) - \boldsymbol{\Lambda}_{\mathbf{G}} : \left(\mathbf{G}_{\varphi}-\mathbf{G}\right) - \lambda\left(J_{\varphi}-J\right)\Big] \,\mathrm{d}V\,\mathrm{d}t \\ + \int_{t_0}^{t_N} \Big[&\int_{\Omega_0} (\bar{\mathbf{g}}+\bar{\mathbf{b}})\cdot\boldsymbol{\varphi}\,\mathrm{d}V + \int_{\partial_\sigma\Omega_0} \bar{\mathbf{t}}\cdot\boldsymbol{\varphi}\,\mathrm{d}A\Big]\,\mathrm{d}t,\end{aligned} \tag{3.10}$$

where $\rho_0 = \rho_0(\mathbf{X})$ is the mass density in reference configuration. Here, the displacement field $\boldsymbol{\varphi} \in \mathcal{V}_\varphi$ is sought in the function space

$$\mathcal{V}_\varphi = \left\{\boldsymbol{\varphi} : \Omega_0 \to \mathbb{R}^3 \,|\, \varphi_i \in H^1(\Omega_0) \wedge \boldsymbol{\varphi} = \bar{\boldsymbol{\varphi}} \text{ on } \partial_\varphi\Omega_0\right\}, \tag{3.11}$$

where $H^1(\Omega_0)$ is the Sobolev space. Similarly, the velocity field $\mathbf{v} \in \mathcal{V}_v$, where the function space $\mathcal{V}_v$ is defined as

$$\mathcal{V}_v = \left\{\mathbf{v} : \Omega_0 \to \mathbb{R}^3 \,|\, v_i \in L^2(\Omega_0)\right\}, \tag{3.12}$$

where $L^2(\Omega_0)$ is the space of square-integrable functions on Ω_0. The kinematic variables $\mathbf{C} \in \mathcal{V}_C$, $\mathbf{G} \in \mathcal{V}_G$ and $J \in \mathcal{V}_J$ are introduced as independent fields representing the right Cauchy–Green tensor, its cofactor, and the determinant of the deformation gradient, respectively. Their equivalence with deformation-dependent measures $\mathbf{C}_\varphi$, $\mathbf{G}_\varphi$, and J_φ is enforced via the tensor-valued Lagrange multipliers $\boldsymbol{\Lambda}_{\mathbf{C}} \in \mathcal{V}_C$, $\boldsymbol{\Lambda}_{\mathbf{G}} \in \mathcal{V}_G$ and the scalar-valued Lagrange multiplier $\lambda \in \mathcal{V}_J$. The function spaces of the mixed variables and their Lagrange multipliers are defined as

$$\begin{aligned}\mathcal{V}_C = \mathcal{V}_G &= \left\{\mathbf{A} : \Omega_0 \to \mathbb{S} \,|\, A_{ij} \in L^2(\Omega_0)\right\}, \\ \mathcal{V}_J &= \left\{J : \Omega_0 \to \mathbb{R}_+ \setminus \{0\} \,|\, J \in L^2(\Omega_0)\right\},\end{aligned} \tag{3.13}$$

where $\mathbb{S}$ is the space of symmetric 3×3 matrices. Note that in the functional $\mathcal{S}$, the velocity field $\mathbf{v} \in \mathcal{V}_v$ is introduced as an independent field that is linked to the time derivative of the deformation field $\dot{\boldsymbol{\varphi}}$ through the vector-valued Lagrange multiplier $\boldsymbol{\pi} \in \mathcal{V}_v$.

Imposing the stationarity of the functional $\mathcal{S}$ yields the associated Euler-Lagrange equations. Accordingly, we obtain $\boldsymbol{\pi} = \rho_0\mathbf{v}$, such that the multiplier $\boldsymbol{\pi}$ corresponds to the linear momentum density. In addition to that, the remaining stationary conditions read

$$\left.\begin{aligned}\dot{\boldsymbol{\varphi}} &= \mathbf{v} \\ \rho_0\,\dot{\mathbf{v}} &= \mathrm{Div}(\mathbf{F}_\varphi\mathbf{S}) + \bar{\mathbf{g}} + \bar{\mathbf{b}} \\ \boldsymbol{\Lambda}_{\mathbf{C}} &= \partial_{\mathbf{C}}\widetilde{\mathcal{W}}(\mathbf{C},\mathbf{G},J) \\ \boldsymbol{\Lambda}_{\mathbf{G}} &= \partial_{\mathbf{G}}\widetilde{\mathcal{W}}(\mathbf{C},\mathbf{G},J) \\ \lambda &= \partial_J\widetilde{\mathcal{W}}(\mathbf{C},\mathbf{G},J) \\ \mathbf{C} &= \mathbf{C}_\varphi \\ \mathbf{G} &= \mathbf{G}_\varphi \\ J &= J_\varphi\end{aligned}\right\} \text{ in } \Omega_0\times\mathcal{I}, \tag{3.14}$$

where the second Piola-Kirchhoff stress tensor is given by

$$\mathbf{S} = 2\boldsymbol{\Lambda}_{\mathbf{C}} + 2\boldsymbol{\Lambda}_{\mathbf{G}} \barwedge \mathbf{C}_\varphi + \frac{\lambda}{J_\varphi}\mathbf{G}_\varphi. \tag{3.15}$$

Note that in (3.14), the velocity field has been preferred over the linear momentum density field, since in the discretization process we prefer to use the velocity field.

In addition to the local field equations (3.14), the stationarity of functional $\mathcal{S}$ implies the boundary condition

$$\mathbf{F}_{\varphi}\mathbf{S}\mathbf{N} = \bar{\mathbf{t}} \text{ on } \partial_{\sigma}\Omega_0, \tag{3.16}$$

where $\mathbf{N}$ denotes the unit outward normal vector on the boundary $\partial_{\sigma}\Omega_0$. Note that during the imposition of the stationarity of functional $\mathcal{S}$, the usual end point conditions on the deformation field at times t_0 and t_N have been taken into account for all $\mathbf{X} \in \Omega_0$.

Remark 3.1. *Functional $\mathcal{S}$ in* (3.10) *can be viewed as a combination of Livens' variational principle (see [45]) and the Hu-Washizu principle (see the 'generalized principle' in [88]) adapted to polyconvex elasticity. In addition to the Lagrange multipliers $\boldsymbol{\pi}$ and $\{\boldsymbol{\Lambda}_{\mathrm{C}}, \boldsymbol{\Lambda}_{\mathrm{G}}, \lambda\}$, another vector-valued Lagrange multiplier could be used to enforce Dirichlet boundary conditions $\boldsymbol{\varphi} = \bar{\boldsymbol{\varphi}}$ on $\partial_{\varphi}\Omega_0$ (cf. [88]). This contrasts to our present approach, in which the Dirichlet boundary conditions are taken into account by choosing $\boldsymbol{\varphi} \in \mathcal{V}_{\varphi}$.*

3.2.3. Port-Hamiltonian form of the local field equations

Next, we bring the local field equations into port-Hamiltonian form. To identify the energy variables relevant for the port-Hamiltonian formulation, we introduce the total energy of the elastic body, also called the *Hamiltonian* functional. Accordingly, we define

$$\mathcal{H}(\mathbf{x}) = \int_{\Omega_0} \left(\frac{1}{2}\rho_0 \mathbf{v}\cdot\mathbf{v} + \widetilde{\mathcal{W}}(\mathbf{C}, \mathbf{G}, J) - \bar{\mathbf{g}}\cdot\boldsymbol{\varphi}\right) \mathrm{d}V. \tag{3.17}$$

Note that the potential of body forces $\bar{\mathbf{g}}$ has been included in the Hamiltonian, while external tractions $\bar{\mathbf{t}}$ acting on the boundary of the elastic body, as well as distributed control body forces $\bar{\mathbf{b}}$ are treated as inputs in the port-Hamiltonian formulation. The specific form of (3.17) gives rise to the energy variables

$$\mathbf{x} = \begin{bmatrix} \boldsymbol{\varphi} \\ \mathbf{v} \\ \mathbf{C} \\ \mathbf{G} \\ J \end{bmatrix}. \tag{3.18}$$

Now, the functional derivative of the Hamiltonian can be written as

$$\delta_{\mathbf{x}}\mathcal{H}(\mathbf{x}) = \begin{bmatrix} -\bar{\mathbf{g}} \\ \rho_0\mathbf{v} \\ \partial_{\mathrm{C}}\widetilde{\mathcal{W}} \\ \partial_{\mathrm{G}}\widetilde{\mathcal{W}} \\ \partial_{J}\widetilde{\mathcal{W}} \end{bmatrix}. \tag{3.19}$$

The goal is now to bring the local field equations of the present problem into pH form, which is given by

$$\begin{aligned} \mathcal{E}\dot{\mathbf{x}} &= \mathcal{J}(\mathbf{x})\mathbf{z}(\mathbf{x}) + \mathcal{B}\mathbf{u}, \\ \mathbf{y} &= \mathcal{B}^{*}\mathbf{z}(\mathbf{x}), \end{aligned} \tag{3.20}$$

where

$$\mathcal{E}^{\top}\mathbf{z}(\mathbf{x}) = \delta_{\mathbf{x}}\mathcal{H}(\mathbf{x}) \tag{3.21}$$

(see [54, 55]). In particular, we need to identify the differential operator $\mathcal{J}(\mathbf{x})$ along with matrix $\mathcal{E}$ from the local field equations. Note that $\mathcal{B}$ is a differential operator that can account for distributed controls $\mathbf{u}$ acting on the system. The collocated and power-conjugated outputs $\mathbf{y}$ are defined in the second equation of (3.20), where $\mathcal{B}^*$ denotes the adjoint of $\mathcal{B}$. The vector-valued function $\mathbf{z}(\mathbf{x})$ is defined in equation (3.21) in terms of the variational derivative of the Hamiltonian. We first rewrite the local field equations (3.14) as

$$\left.\begin{aligned} \dot{\boldsymbol{\varphi}} &= \mathbf{v} \\ \rho_0\,\dot{\mathbf{v}} &= \mathrm{Div}(\mathbf{F}_\varphi \mathbf{S}) + \bar{\mathbf{g}} + \bar{\mathbf{b}} \\ \boldsymbol{\Lambda}_{\mathrm{C}} &= \partial_{\mathrm{C}}\widetilde{\mathcal{W}}(\mathbf{C},\mathbf{G},J) \\ \boldsymbol{\Lambda}_{\mathrm{G}} &= \partial_{\mathrm{G}}\widetilde{\mathcal{W}}(\mathbf{C},\mathbf{G},J) \\ \lambda &= \partial_J\widetilde{\mathcal{W}}(\mathbf{C},\mathbf{G},J) \\ \dot{\mathbf{C}} &= \tfrac{\mathrm{d}}{\mathrm{d}t}\mathbf{C}_\varphi = 2\,\mathrm{sym}(\mathbf{F}_\varphi^\top \nabla\mathbf{v}) \\ \dot{\mathbf{G}} &= \tfrac{\mathrm{d}}{\mathrm{d}t}\mathbf{G}_\varphi = 2\mathbf{C}_\varphi \barwedge \mathrm{sym}(\mathbf{F}_\varphi^\top \nabla\mathbf{v}) \\ \dot{J} &= \tfrac{\mathrm{d}}{\mathrm{d}t}J_\varphi = J_\varphi^{-1}\mathbf{G}_\varphi : \mathrm{sym}(\mathbf{F}_\varphi^\top \nabla\mathbf{v}) \end{aligned}\right\} \text{ in } \Omega_0 \times \mathcal{I}, \tag{3.22}$$

Note that the second Piola-Kirchhoff stress tensor $\mathbf{S}$ has been defined in (3.15) and thus follows from the constitutive relations for the Lagrange multipliers $\{\boldsymbol{\Lambda}_{\mathrm{C}}, \boldsymbol{\Lambda}_{\mathrm{G}}, \lambda\}$ in (3.22). The last three equations in (3.22) comprise the kinematic relationships in rate form, as required by the pH form (3.20). It is now straightforward to put (3.22) in pH form (3.20) by substituting the expressions for the Lagrange multipliers from (3.22) into (3.15). Consequently, we arrive at the differential operator $\mathcal{J}(\mathbf{x})$ given by the expression

$$\mathcal{J}(\mathbf{x}) = \begin{bmatrix} 0 & I & 0 & 0 & 0 \\ -I & 0 & \mathrm{Div}(2\mathbf{F}_\varphi \square) & \mathrm{Div}(2\mathbf{F}_\varphi \mathbf{C}_\varphi \barwedge \square) & \mathrm{Div}(J_\varphi^{-1}\mathbf{F}_\varphi \mathbf{G}_\varphi \square) \\ 0 & 2\,\mathrm{sym}(\mathbf{F}_\varphi^\top \nabla(\square)) & 0 & 0 & 0 \\ 0 & 2\mathbf{C}_\varphi \barwedge \mathrm{sym}(\mathbf{F}_\varphi^\top \nabla(\square)) & 0 & 0 & 0 \\ 0 & J_\varphi^{-1}\mathbf{G}_\varphi : \mathrm{sym}(\mathbf{F}_\varphi^\top \nabla(\square)) & 0 & 0 & 0 \end{bmatrix}, \tag{3.23}$$

together with matrices $\mathcal{E}$ and $\mathcal{B}$, which assume the form

$$\mathcal{E} = \mathcal{E}^\top = \begin{bmatrix} I & 0 & 0 & 0 & 0 \\ 0 & \rho_0 I & 0 & 0 & 0 \\ 0 & 0 & I & 0 & 0 \\ 0 & 0 & 0 & I & 0 \\ 0 & 0 & 0 & 0 & I \end{bmatrix} \quad \text{and} \quad \mathcal{B} = \begin{bmatrix} 0 & 0 & 0 & 0 & 0 \\ 0 & I & 0 & 0 & 0 \\ 0 & 0 & 0 & 0 & 0 \\ 0 & 0 & 0 & 0 & 0 \\ 0 & 0 & 0 & 0 & 0 \end{bmatrix}. \tag{3.24}$$

In (3.23) and (3.24), I denotes the identity operator. The vector of distributed controls $\mathbf{u}$ in (3.20) contains the distributed control body forces $\bar{\mathbf{b}}$.

Note that the differential operator $\mathcal{J}(\mathbf{x})$ is formally skew-adjoint, i.e., $\mathcal{J}(\mathbf{x}) = -\mathcal{J}(\mathbf{x})^*$. This property is reflected in the power balance as can be seen below. Taking the time derivative of the Hamiltonian yields

$$\dot{\mathcal{H}}(\mathbf{x}) = \langle \delta_{\mathbf{x}}\mathcal{H}(\mathbf{x}), \dot{\mathbf{x}} \rangle\,, \tag{3.25}$$

where the brackets represent the duality pairing. Using (3.20), we obtain

$$\begin{aligned} \dot{\mathcal{H}}(\mathbf{x}) &= \left\langle \mathcal{E}^\top \mathbf{z}(\mathbf{x}), \dot{\mathbf{x}} \right\rangle \\ &= \langle \mathbf{z}(\mathbf{x}), \mathcal{E}\dot{\mathbf{x}} \rangle \\ &= \langle \mathbf{z}(\mathbf{x}), \mathcal{J}(\mathbf{x})\mathbf{z}(\mathbf{x}) \rangle + \langle \mathbf{z}(\mathbf{x}), \mathcal{B}\mathbf{u} \rangle\,. \end{aligned} \tag{3.26}$$

Now, after a straightforward calculation, the first term on the right-hand side of the last equation yields

$$\begin{aligned}\langle \mathbf{z}(\mathbf{x}), \mathcal{J}(\mathbf{x})\mathbf{z}(\mathbf{x})\rangle &= \left\langle \mathbf{v}, \mathrm{Div}(\mathbf{F}_\varphi \mathbf{S})\right\rangle + \left\langle \nabla \mathbf{v}, \mathbf{F}_\varphi \mathbf{S}\right\rangle \\ &= \int_{\partial_\sigma \Omega_0} \bar{\mathbf{t}} \cdot \mathbf{v} \, \mathrm{d}A,\end{aligned} \tag{3.27}$$

where Green's theorem along with the Neumann boundary condition have been used. Furthermore, the second term on the right-hand side of (3.26) leads to

$$\langle \mathbf{z}(\mathbf{x}), \mathcal{B}\mathbf{u}\rangle = \langle \mathcal{B}^* \mathbf{z}(\mathbf{x}), \mathbf{u}\rangle = \langle \mathbf{y}, \mathbf{u}\rangle \,. \tag{3.28}$$

Thus, the resulting power balance takes the form

$$\dot{\mathcal{H}}(\mathbf{x}) = \int_{\partial_\sigma \Omega_0} \bar{\mathbf{t}} \cdot \mathbf{v} \, \mathrm{d}A + \langle \mathbf{y}, \mathbf{u}\rangle \,. \tag{3.29}$$

Note that the contribution to the power balance of the potential body forces $\bar{\mathbf{g}}$ emanates from the Hamiltonian on the left-hand side of the last equation.

3.2.4. Weak form

In the following, we introduce the weak form associated with the pH formulation of the local field equations dealt with in Section 3.2.3. We therefore start with the set of equations given in (3.22). Multiplying these equations by admissible test functions $\{\mathbf{w}_\pi, \mathbf{w}_\varphi\}$, $\{\mathbf{w}_{\Lambda_\mathrm{C}}, \mathbf{w}_{\Lambda_\mathrm{G}}, w_\lambda\}$ and $\{\mathbf{w}_\mathrm{C}, \mathbf{w}_\mathrm{G}, w_J\}$, subsequently integrating over body Ω_0 and performing an integration by parts yields the weak form

$$\begin{aligned}
&\int_{\Omega_0} \mathbf{w}_\pi \cdot (\dot{\boldsymbol{\varphi}} - \mathbf{v}) \, \mathrm{d}V = 0 \\
&\int_{\Omega_0} \mathbf{w}_\varphi \cdot \rho_0 \dot{\mathbf{v}} + 2\,\mathrm{sym}(\mathbf{F}_\varphi^\top \nabla \mathbf{w}_\varphi) : \big(\boldsymbol{\Lambda}_\mathrm{C} + \boldsymbol{\Lambda}_\mathrm{G} \barwedge \mathbf{C}_\varphi + \frac{\lambda}{2J_\varphi}\mathbf{G}_\varphi\big) \, \mathrm{d}V \\
&\qquad = \int_{\Omega_0} \mathbf{w}_\varphi \cdot (\bar{\mathbf{g}} + \bar{\mathbf{b}}) \, \mathrm{d}V + \int_{\partial\Omega_0} \mathbf{w}_\varphi \cdot \bar{\mathbf{t}} \, \mathrm{d}A \\
&\int_{\Omega_0} \mathbf{w}_\mathrm{C} : \Big[\boldsymbol{\Lambda}_\mathrm{C} - \partial_\mathrm{C}\widetilde{\mathcal{W}}(\mathbf{C}, \mathbf{G}, J)\Big] \, \mathrm{d}V = 0 \\
&\int_{\Omega_0} \mathbf{w}_\mathrm{G} : \Big[\boldsymbol{\Lambda}_\mathrm{G} - \partial_\mathrm{G}\widetilde{\mathcal{W}}(\mathbf{C}, \mathbf{G}, J)\Big] \, \mathrm{d}V = 0 \\
&\int_{\Omega_0} w_J \Big[\lambda - \partial_J \widetilde{\mathcal{W}}(\mathbf{C}, \mathbf{G}, J)\Big] \, \mathrm{d}V = 0 \\
&\int_{\Omega_0} \mathbf{w}_{\Lambda_\mathrm{C}} : \big[\dot{\mathbf{C}} - 2\ \mathrm{sym}(\mathbf{F}_\varphi^\top \nabla \mathbf{v})\big] \, \mathrm{d}V = 0 \\
&\int_{\Omega_0} \mathbf{w}_{\Lambda_\mathrm{G}} : \big[\dot{\mathbf{G}} - 2\mathbf{C}_\varphi \barwedge \mathrm{sym}(\mathbf{F}_\varphi^\top \nabla \mathbf{v})\big] \, \mathrm{d}V = 0 \\
&\int_{\Omega_0} w_\lambda \big[\dot{J} - J_\varphi^{-1}\mathbf{G}_\varphi : \mathrm{sym}(\mathbf{F}_\varphi^\top \nabla \mathbf{v})\big] \, \mathrm{d}V = 0.
\end{aligned} \tag{W}$$

These equations hold for arbitrary $\mathbf{w}_\varphi \in \mathcal{V}_\varphi^0$ with

$$\mathcal{V}_\varphi^0 = \big\{\mathbf{w}_\varphi : \Omega_0 \to \mathbb{R}^3 \,|\, w_{\varphi_i} \in H^1(\Omega_0) \wedge \mathbf{w}_\varphi = \mathbf{0} \text{ on } \partial_\varphi \Omega_0\big\} \tag{3.30}$$

as well as arbitrary $\mathbf{w}_\pi \in \mathcal{V}_v$, $\mathbf{w}_\mathbf{C}, \mathbf{w}_\mathbf{G}, \mathbf{w}_{\mathbf{\Lambda}_\mathbf{C}}, \mathbf{w}_{\mathbf{\Lambda}_\mathbf{G}} \in \mathcal{V}_C$, and $w_J, w_\lambda \in \mathcal{V}_J$.

Note that we retain the constitutive equations for the Lagrange multipliers resulting from the underlying variational principle in weak form (W). As will be shown in the sequel, this facilitates an energy-momentum consistent spatial discretization in general (see also Remark 3.4).

3.2.5. Conservation properties

In the next step, conservation properties of the newly developed formulation are discussed. In particular, this is conservation of total energy and total angular momentum.

3.2.5.1. Conservation of total energy

Energy conservation in the time-continuous case is ensured if the time derivative of the Hamiltonian $\mathcal{H}$, defined in (3.17), vanishes, i.e.,

$$\dot{\mathcal{H}} = \frac{\mathrm{d}}{\mathrm{d}t}\left[\int_{\Omega_0} \left(\frac{1}{2}\rho_0 \mathbf{v}\cdot\mathbf{v} + \widetilde{\mathcal{W}}(\mathbf{C},\mathbf{G},J) - \bar{\mathbf{g}}\cdot\boldsymbol{\varphi}\right)\mathrm{d}V\right] = 0. \tag{3.31}$$

To verify this, we choose the test functions $\mathbf{w}_\pi = -\rho_0\dot{\mathbf{v}}$, $\mathbf{w}_\varphi = \dot{\boldsymbol{\varphi}}$, $\mathbf{w}_\mathbf{C} = -\dot{\mathbf{C}}$, $\mathbf{w}_\mathbf{G} = -\dot{\mathbf{G}}$, $w_J = -\dot{J}$, $\mathbf{w}_{\mathbf{\Lambda}_\mathbf{C}} = \mathbf{\Lambda}_\mathbf{C}$, $\mathbf{w}_{\mathbf{\Lambda}_\mathbf{G}} = \mathbf{\Lambda}_\mathbf{G}$, and $w_\lambda = \lambda$, and insert them into (W). Summing the resulting equations yields

$$\begin{aligned}\int_{\Omega_0} \rho_0\dot{\mathbf{v}}\cdot\mathbf{v} + \partial_\mathbf{C}\widetilde{\mathcal{W}} : \dot{\mathbf{C}} + \partial_\mathbf{G}\widetilde{\mathcal{W}} : \dot{\mathbf{G}} + \partial_J\widetilde{\mathcal{W}}\dot{J} - \dot{\boldsymbol{\varphi}}\cdot\bar{\mathbf{g}}\,\mathrm{d}V \\ = \int_{\partial_\sigma\Omega_0} \dot{\boldsymbol{\varphi}}\cdot\bar{\mathbf{t}}\,\mathrm{d}A + \int_{\Omega_0}\dot{\boldsymbol{\varphi}}\cdot\bar{\mathbf{b}}\,\mathrm{d}V,\end{aligned} \tag{3.32}$$

which coincides with (3.31) precisely in the absence of boundary tractions and distributed control body forces, that is, $\bar{\mathbf{t}} = \mathbf{0}$ and $\bar{\mathbf{b}} = \mathbf{0}$. It should be noted that the kinematic relation $\dot{\boldsymbol{\varphi}} = \mathbf{v}$ is used to obtain (3.32).

3.2.5.2. Conservation of angular momentum

The angular momentum of the body Ω_0 is defined as

$$\mathbf{L} = \int_{\Omega_0} \boldsymbol{\varphi}\times\mathbf{v}\rho_0\,\mathrm{d}V. \tag{3.33}$$

It is conserved if the time derivative of $\mathbf{L}$ vanishes, i.e.,

$$\dot{\mathbf{L}} = \int_{\Omega_0} \frac{\mathrm{d}}{\mathrm{d}t}\left(\boldsymbol{\varphi}\times\mathbf{v}\rho_0\right)\,\mathrm{d}V = \mathbf{0}. \tag{3.34}$$

In analogy to the energy conservation proof, we select the test functions $\mathbf{w}_\varphi = \boldsymbol{\zeta}\times\boldsymbol{\varphi}$ and $\mathbf{w}_\pi = -\rho_0\boldsymbol{\zeta}\times\dot{\boldsymbol{\varphi}}$ to derive the angular momentum balance. Here, $\boldsymbol{\zeta} \in \mathbb{R}^3$ is an arbitrary but constant vector. Using vector calculus, the cross product $\boldsymbol{\zeta}\times\mathbf{a}$ can be expressed as a matrix-vector product $\hat{\boldsymbol{\zeta}}\mathbf{a}$ for any $\mathbf{a} \in \mathbb{R}^3$,

where $\hat{\boldsymbol{\zeta}} \in \mathbb{R}^{3\times 3}$ denotes the skew-symmetric matrix associated with $\boldsymbol{\zeta}$. Inserting these test functions into (W) and summing the first two equations of (W) yields

$$\begin{aligned}&\int_{\Omega_0} (-\rho_0 \boldsymbol{\zeta}\times\dot{\boldsymbol{\varphi}}) \cdot (\dot{\boldsymbol{\varphi}} - \mathbf{v}) \,\mathrm{d}V \\ &\quad + \int_{\Omega_0} (\boldsymbol{\zeta}\times\boldsymbol{\varphi}) \cdot \rho_0 \dot{\mathbf{v}} + (\hat{\boldsymbol{\zeta}}\nabla\boldsymbol{\varphi}) : (\mathbf{F}_\varphi \mathbf{S}) - (\boldsymbol{\zeta}\times\boldsymbol{\varphi}) \cdot (\bar{\mathbf{g}} + \bar{\mathbf{b}}) \,\mathrm{d}V \\ &\quad - \int_{\partial_\sigma \Omega_0} (\boldsymbol{\zeta}\times\boldsymbol{\varphi}) \cdot \bar{\mathbf{t}} \,\mathrm{d}A = 0.\end{aligned} \tag{3.35}$$

Due to the symmetry of the second Piola-Kirchhoff stress tensor $\mathbf{S}$ and the skew-symmetry of $\hat{\boldsymbol{\zeta}}$, the term $\hat{\boldsymbol{\zeta}} : (\mathbf{F}_\varphi \mathbf{S} \nabla \boldsymbol{\varphi}^\top)$ vanishes. Thus, expression (3.35) simplifies to

$$\boldsymbol{\zeta} \cdot \left[\int_{\Omega_0} \frac{\mathrm{d}}{\mathrm{d}t} (\boldsymbol{\varphi}\times\mathbf{v}\rho_0) - (\bar{\mathbf{g}} + \bar{\mathbf{b}})\times\boldsymbol{\varphi} \,\mathrm{d}V - \int_{\partial_\sigma \Omega_0} \bar{\mathbf{t}}\times\boldsymbol{\varphi} \,\mathrm{d}A \right] = \boldsymbol{\zeta} \cdot (\dot{\mathbf{L}} - \mathbf{m}^{\mathrm{ext}}) = 0. \tag{3.36}$$

Here, $\mathbf{m}^{\mathrm{ext}}$ denotes the external torque acting on the body and its boundary. Hence, the angular momentum is conserved iff $\mathbf{m}^{\mathrm{ext}} = \mathbf{0}$.

3.2.6. Alternative size-reduced port-Hamiltonian formulations

The present pH formulation is based on the introduction of independent strain-type fields $\{\mathbf{C}, \mathbf{G}, J\}$. Alternatively, a reduced number of independent strain-type fields may be used. For completeness, we outline the construction of size-reduced pH formulations. Since the procedure to setup the respective pH formulation closely follows the lines above, we merely sketch the main steps.

3.2.6.1. Size-reduced mixed port-Hamiltonian formulation based on mixed fields $\{\mathrm{G}, J\}$

In [48, 74] the independent fields $\{\mathbf{G}, J\}$ are introduced, while the right Cauchy-Green tensor is directly formulated in terms of the deformation map. In particular, instead of introducing the independent field $\mathbf{C}$, $\mathbf{C}_\varphi$, which is defined in (3.5), is used directly. The pH formulation associated with [48, 74] is based on the Hamiltonian

$$\mathcal{H}_1(\mathbf{x}_1) = \int_{\Omega_0} \left(\frac{1}{2} \rho_0 \mathbf{v} \cdot \mathbf{v} + \widetilde{\mathcal{W}}(\mathbf{C}_\varphi, \mathbf{G}, J) - \bar{\mathbf{g}} \cdot \boldsymbol{\varphi} \right) \mathrm{d}V, \tag{3.37}$$

implying the reduced set of energy variables

$$\mathbf{x}_1 = \begin{bmatrix} \boldsymbol{\varphi} \\ \mathbf{v} \\ \mathbf{G} \\ J \end{bmatrix}. \tag{3.38}$$

The functional derivative of Hamiltonian (3.37) is given by

$$\delta_{\mathbf{x}_1} \mathcal{H}_1(\mathbf{x}_1) = \begin{bmatrix} -\bar{\mathbf{g}} - \mathrm{Div}(2\mathbf{F}_\varphi \partial_{\mathbf{C}} \widetilde{\mathcal{W}}) \\ \rho_0 \mathbf{v} \\ \partial_{\mathbf{G}} \widetilde{\mathcal{W}} \\ \partial_J \widetilde{\mathcal{W}} \end{bmatrix}, \tag{3.39}$$

where $\widetilde{\mathcal{W}} = \widetilde{\mathcal{W}}(\mathbf{C}_\varphi, \mathbf{G}, J)$. The pH formulation of the local field equations again assumes the form (3.20), where the size-reduced differential operator is given by

$$\mathcal{J}_1 = \begin{bmatrix} 0 & I & 0 & 0 \\ -I & 0 & \mathrm{Div}(2\mathbf{F}_\varphi \mathbf{C}_\varphi \overset{\times}{\otimes} \square) & \mathrm{Div}(J_\varphi^{-1}\mathbf{F}_\varphi \mathbf{G}_\varphi \square) \\ 0 & 2\mathbf{C}_\varphi \overset{\times}{\otimes} \mathrm{sym}(\mathbf{F}_\varphi^\top \nabla(\square)) & 0 & 0 \\ 0 & J_\varphi^{-1}\mathbf{G}_\varphi : \mathrm{sym}(\mathbf{F}_\varphi^\top \nabla(\square)) & 0 & 0 \end{bmatrix}. \tag{3.40}$$

The operator $\mathcal{E}$ takes a similar form as in (3.24), differing only in size due to the reduced set of energy variables.

3.2.6.2. Size-reduced mixed port-Hamiltonian formulation based on mixed field E

The recently published works [19, 69, 83] rely on the introduction of the Green-Lagrangian strain tensor as an independent field. Since the Green-Lagrangian strain tensor is given by

$$\mathbf{E} = \frac{1}{2}\left(\mathbf{C} - \mathbf{I}\right), \tag{3.41}$$

we have $2\dot{\mathbf{E}} = \dot{\mathbf{C}}$ and we thus may use the right Cauchy-Green tensor again. Correspondingly, the Hamiltonian now assumes the form

$$\mathcal{H}_2(\mathbf{x}_2) = \int_{\Omega_0} \left(\frac{1}{2}\rho_0 \mathbf{v}\cdot\mathbf{v} + \widehat{\mathcal{W}}(\mathbf{C}) - \bar{\mathbf{g}}\cdot\boldsymbol{\varphi}\right) \mathrm{d}V, \tag{3.42}$$

where the stored energy $\widehat{\mathcal{W}}$ has been introduced in (3.9). Accordingly, the reduced set of energy variables is given by

$$\mathbf{x}_2 = \begin{bmatrix} \boldsymbol{\varphi} \\ \mathbf{v} \\ \mathbf{C} \end{bmatrix} \tag{3.43}$$

and the functional derivative of Hamiltonian (3.42) reads

$$\delta_{\mathbf{x}_2}\mathcal{H}_2(\mathbf{x}_2) = \begin{bmatrix} -\bar{\mathbf{g}} \\ \rho_0 \mathbf{v} \\ \partial_{\mathbf{C}}\widehat{\mathcal{W}} \end{bmatrix}. \tag{3.44}$$

The pH formulation of the local field equations again assumes the form (3.20), where the size-reduced differential operator is given by

$$\mathcal{J}_2 = \begin{bmatrix} 0 & I & 0 \\ -I & 0 & \mathrm{Div}(2\mathbf{F}_\varphi \square) \\ 0 & 2\,\mathrm{sym}(\mathbf{F}_\varphi^\top \nabla(\square)) & 0 \end{bmatrix}. \tag{3.45}$$

In analogy to Subsection 3.2.6.1, the operator $\mathcal{E}$ follows the same definition as in (3.24), differing only in its dimension.

It is worth noting that the constitutive law in [19, 83] is restricted to Saint Venant-Kirchhoff material from the outset. For Saint Venant-Kirchhoff material,

$$\mathbf{S} = 2\partial_{\mathbf{C}}\widehat{\mathcal{W}} = \mathbb{C} : \mathbf{E}, \tag{3.46}$$

where $\mathbb{C}$ is the fourth-order elasticity tensor. Consequently, in the pH formulation the independent right Cauchy-Green tensor can be replaced with the independent second Piola-Kirchhoff stress field by using the relations $\partial_{\mathbf{C}}\widehat{\mathcal{W}} = \frac{1}{2}\mathbf{S}$ and $\dot{\mathbf{C}} = 2\dot{\mathbf{E}} = 2\mathbb{C}^{-1} : \dot{\mathbf{S}}$. We refer to[19, 83] for further details of the resulting 'velocity-stress formulation'.

3.2.6.3. Fully size-reduced displacement-based pH formulation

In a further step one can consider a fully size-reduced displacement-based pH formulation in which the Hamiltonian is given by

$$\mathcal{H}_3(\mathbf{x}_3) = \int_{\Omega_0} \left(\frac{1}{2}\rho_0 \mathbf{v}\cdot\mathbf{v} + \widetilde{\mathcal{W}}(\mathbf{C}_\varphi, \mathbf{G}_\varphi, J_\varphi) - \bar{\mathbf{g}}\cdot\boldsymbol{\varphi}\right) \mathrm{d}V, \tag{3.47}$$

where the stored energy function $\widetilde{\mathcal{W}}$ has been introduced in (3.9). Hamiltonian (3.47) gives rise to the classic set of variables

$$\mathbf{x}_3 = \begin{bmatrix} \boldsymbol{\varphi} \\ \mathbf{v} \end{bmatrix} \tag{3.48}$$

associated with a pure displacement-based formulation. The functional derivative of the Hamiltonian (3.47) is then given by

$$\delta_{\mathbf{x}_3}\mathcal{H}_3(\mathbf{x}_3) = \begin{bmatrix} -\bar{\mathbf{g}} - \mathrm{Div}(2\mathbf{F}_\varphi(\partial_{\mathbf{C}}\widetilde{\mathcal{W}} + \mathbf{C}_\varphi \overset{\otimes}{\times} \partial_{\mathbf{G}}\widetilde{\mathcal{W}} + \tfrac{1}{2}J_\varphi^{-1}\partial_J\widetilde{\mathcal{W}}\mathbf{G}_\varphi)) \\ \rho_0\mathbf{v} \end{bmatrix}, \tag{3.49}$$

where $\widetilde{\mathcal{W}} = \widetilde{\mathcal{W}}(\mathbf{C}_\varphi, \mathbf{G}_\varphi, J_\varphi)$. Again, we obtain a pH formulation in the form of (3.20), where, however, the operator $\mathcal{J}_3$ reduces to its canonical form

$$\mathcal{J}_3 = \begin{bmatrix} 0 & I \\ -I & 0 \end{bmatrix}. \tag{3.50}$$

As in the previous subsections, the operator $\mathcal{E}$ follows the same definition as in (3.24), differing only in its dimension.

The displacement-based formulation lies at the heart of the first energy-momentum scheme for nonlinear elastodynamics devised in [78].

3.3. Discretization in time

In order to preserve the structural properties of the port-Hamiltonian formulation in numerical simulations, an appropriate time discretization scheme is essential. To this end, we introduce a variant of the implicit midpoint scheme, which relies on the notion of a discrete derivative. After presenting the time-discrete weak form, we show that the conservation laws are preserved under the proposed time discretization.

We begin by dividing the time interval $\mathcal{I}$ into discrete subintervals $\mathcal{I}_n = [t_n, t_{n+1}]$ for $n \in \{0, ..., N\}$ with time-step size $\Delta t_n = t_{n+1} - t_n$. The average value of a quantity $(\bullet)(t)$ over one time interval is defined as

$$(\bullet)_{n+1/2} = \frac{1}{2}\left[(\bullet)_n + (\bullet)_{n+1}\right], \tag{3.51}$$

where $(\bullet)_n = (\bullet)(t_n)$ and $(\bullet)_{n+1} = (\bullet)(t_{n+1})$. Furthermore, the time derivative $(\dot{\bullet})$ is approximated using finite differences given by

$$(\dot{\bullet}) \approx \frac{\Delta(\bullet)_n}{\Delta t_n} = \frac{(\bullet)_{n+1} - (\bullet)_n}{\Delta t_n}. \tag{3.52}$$

This leads to the time-discrete counterpart of the weak form (W), given by

$$
\begin{aligned}
&\int_{\Omega_0} \mathbf{w}_\pi \cdot \Big(\frac{\boldsymbol{\varphi}_{n+1} - \boldsymbol{\varphi}_n}{\Delta t_n} - \mathbf{v}_{n+1/2}\Big)\,\mathrm{d}V = 0\\
&\int_{\Omega_0} \mathbf{w}_\varphi \cdot \rho_0 \frac{\mathbf{v}_{n+1} - \mathbf{v}_n}{\Delta t_n} + \operatorname{sym}(\mathbf{F}^\top_{\boldsymbol{\varphi}_{n+1/2}} \nabla \mathbf{w}_\varphi) : \bar{\mathbf{S}}\,\mathrm{d}V\\
&\qquad = \int_{\Omega_0} \mathbf{w}_\varphi \cdot \Big(\bar{\mathbf{g}}_{n+1/2} + \bar{\mathbf{b}}_{n+1/2}\Big)\,\mathrm{d}V + \int_{\partial\Omega_0} \mathbf{w}_\varphi \cdot \bar{\mathbf{t}}_{n+1/2}\,\mathrm{d}A\\
&\int_{\Omega_0} \mathbf{w}_\mathbf{C} : \Big[\boldsymbol{\Lambda}_{\mathbf{C}_{n+1}} - \mathrm{D}_\mathbf{C}\widetilde{\mathcal{W}}\Big]\,\mathrm{d}V = 0\\
&\int_{\Omega_0} \mathbf{w}_\mathbf{G} : \Big[\boldsymbol{\Lambda}_{\mathbf{G}_{n+1}} - \mathrm{D}_\mathbf{G}\widetilde{\mathcal{W}}\Big]\,\mathrm{d}V = 0\\
&\int_{\Omega_0} w_J \Big[\lambda_{n+1} - \mathrm{D}_J\widetilde{\mathcal{W}}\Big]\,\mathrm{d}V = 0\\
&\int_{\Omega_0} \mathbf{w}_{\boldsymbol{\Lambda}_\mathbf{C}} : \Big[\frac{\mathbf{C}_{n+1} - \mathbf{C}_n}{\Delta t_n} - 2\operatorname{sym}(\mathbf{F}^\top_{\boldsymbol{\varphi}_{n+1/2}} \nabla \mathbf{v}_{n+1/2})\Big]\,\mathrm{d}V = 0\\
&\int_{\Omega_0} \mathbf{w}_{\boldsymbol{\Lambda}_\mathbf{G}} : \Big[\frac{\mathbf{G}_{n+1} - \mathbf{G}_n}{\Delta t_n} - 2\mathbf{C}_{\boldsymbol{\varphi}_{n+1/2}} \mathbin{\overset{\boxtimes}{}} \operatorname{sym}(\mathbf{F}^\top_{\boldsymbol{\varphi}_{n+1/2}} \nabla \mathbf{v}_{n+1/2})\Big]\,\mathrm{d}V = 0\\
&\int_{\Omega_0} w_\lambda \Big[\frac{J_{n+1} - J_n}{\Delta t_n} - (J_{\boldsymbol{\varphi}_{n+1/2}})^{-1}\mathbf{G}_{\boldsymbol{\varphi}_{n+1/2}} : \operatorname{sym}(\mathbf{F}^\top_{\boldsymbol{\varphi}_{n+1/2}} \nabla \mathbf{v}_{n+1/2})\Big]\,\mathrm{d}V = 0,
\end{aligned}
\tag{3.53}
$$

where the time-discrete second Piola-Kirchhoff stress tensor $\bar{\mathbf{S}}$ is defined by

$$
\bar{\mathbf{S}} = 2\boldsymbol{\Lambda}_{\mathbf{C}_{n+1}} + 2\boldsymbol{\Lambda}_{\mathbf{G}_{n+1}} \mathbin{\overset{\boxtimes}{}} \mathbf{C}_{\boldsymbol{\varphi}_{n+1/2}} + \frac{\lambda_{n+1}}{J_{\boldsymbol{\varphi}_{n+1/2}}}\mathbf{G}_{\boldsymbol{\varphi}_{n+1/2}}. \tag{3.54}
$$

In this time-discrete weak form, the partial derivatives of the energy density function, $\partial_{\mathcal{V}^i}\widetilde{\mathcal{W}}$ with $\mathcal{V}^i \in \{\mathbf{C}, \mathbf{G}, J\}$, are replaced by partitioned discrete derivatives $\mathrm{D}_{\mathcal{V}^i}\widetilde{\mathcal{W}}$ in the sense of [31] (cf. Example 1). An important property of discrete derivatives is the fulfillment of the so-called directionality property, which in the present case reads

$$
\Delta\widetilde{\mathcal{W}}_n = \widetilde{\mathcal{W}}_{n+1} - \widetilde{\mathcal{W}}_n = \mathrm{D}_\mathbf{C}\widetilde{\mathcal{W}} : \Delta\mathbf{C}_n + \mathrm{D}_\mathbf{G}\widetilde{\mathcal{W}} : \Delta\mathbf{G}_n + \mathrm{D}_J\widetilde{\mathcal{W}}\Delta J_n. \tag{3.55}
$$

In particular, the directionality property (3.55) facilitates the conservation of energy in the discrete setting.

To indicate the functional dependence of the present discrete derivatives, we occasionally write

$$
\mathrm{D}_{\mathcal{V}^i}\widetilde{\mathcal{W}} = \mathrm{D}_{\mathcal{V}^i}\widetilde{\mathcal{W}}(\mathcal{V}_n, \mathcal{V}_{n+1}), \tag{3.56}
$$

where $\mathcal{V} = (\mathbf{C}, \mathbf{G}, J)$.

Moreover, in the limit $\Delta\mathcal{V}^i_n \to 0$, the discrete derivatives coincide with the derivatives of the classical midpoint rule, that is,

$$
\lim_{\Delta\mathcal{V}^i_n \to 0} \Big(\mathrm{D}_{\mathcal{V}^i}\widetilde{\mathcal{W}}\Big) = \partial_{\mathcal{V}^i}\widetilde{\mathcal{W}}|_{\mathcal{V}_{n+1/2}}. \tag{3.57}
$$

Example 1. *Consider a separable stored energy function of the form*

$$
\widetilde{\mathcal{W}}(\mathbf{C}, \mathbf{G}, J) = \widetilde{\mathcal{W}}_1(\mathbf{C}) + \widetilde{\mathcal{W}}_2(\mathbf{G}) + \widetilde{\mathcal{W}}_3(J) \tag{3.58}
$$

and assume that the functions $\widetilde{\mathcal{W}}_1(\mathbf{C})$ *and* $\widetilde{\mathcal{W}}_2(\mathbf{G})$ *are at most quadratic, while* $\widetilde{\mathcal{W}}_3(J)$ *is a general nonlinear function. Then the partitioned discrete derivatives* $\mathrm{D}_{\mathcal{V}^i}\widetilde{\mathcal{W}}$ *are given by*

$$\begin{aligned}\mathrm{D}_{\mathrm{C}}\widetilde{\mathcal{W}} &= \partial_{\mathrm{C}}\widetilde{\mathcal{W}}(\mathbf{C}_{n+1/2})\\ \mathrm{D}_{\mathrm{G}}\widetilde{\mathcal{W}} &= \partial_{\mathrm{G}}\widetilde{\mathcal{W}}(\mathbf{G}_{n+1/2})\\ \mathrm{D}_{J}\widetilde{\mathcal{W}} &= \frac{\widetilde{\mathcal{W}}_3(J_{n+1}) - \widetilde{\mathcal{W}}_3(J_n)}{J_{n+1} - J_n},\end{aligned} \tag{3.59}$$

where $\mathrm{D}_J\widetilde{\mathcal{W}}$ *is known as the Greenspan formula [33].*

3.3.1. Time-discrete conservation of energy

A system conserves energy in the time-discrete setting if the difference in the Hamiltonian $\mathcal{H}$ between two time steps vanishes, that is,

$$\mathcal{H}_{n+1} - \mathcal{H}_n = \Delta\mathcal{H}_n = 0 \tag{3.60}$$

for each time step Δt_n, where

$$\Delta\mathcal{H}_n = \int_{\Omega_0} \Delta T_n + \Delta\widetilde{\mathcal{W}}_n + \Delta V_n \,\mathrm{d}V. \tag{3.61}$$

In the last equation, $T = \frac{1}{2}\rho_0\mathbf{v}\cdot\mathbf{v}$ and $V = -\bar{\mathbf{g}}\cdot\boldsymbol{\varphi}$. To prove energy conservation, we start from the time-discrete weak form, given in (3.53). Similarly to Section 3.2.5.1, we select admissible time-discrete test functions $\mathbf{w}_\varphi = {}^{\Delta\varphi_n}/_{\Delta t_n}$, $\mathbf{w}_\pi = -\rho_0{}^{\Delta\mathrm{v}_n}/_{\Delta t_n}$, $\mathbf{w}_C = -{}^{\Delta\mathrm{C}_n}/_{\Delta t_n}$, $\mathbf{w}_G = -{}^{\Delta\mathrm{G}_n}/_{\Delta t_n}$, $w_J = -{}^{\Delta J_n}/_{\Delta t_n}$, $\mathbf{w}_{\Lambda_\mathrm{C}} = \boldsymbol{\Lambda}_{\mathrm{C}_{n+1}}$, $\mathbf{w}_{\Lambda_\mathrm{G}} = \boldsymbol{\Lambda}_{\mathrm{G}_{n+1}}$ and $w_\lambda = \lambda_{n+1}$. Inserting these into the weak form (3.53) and summing the equations yields

$$\begin{aligned}&\int_{\Omega_0} \mathbf{v}_{n+1/2}\cdot\frac{\rho_0}{\Delta t_n}(\mathbf{v}_{n+1}-\mathbf{v}_n) + \frac{\Delta\mathbf{C}_n}{\Delta t_n} : \mathrm{D}_{\mathrm{C}}\widetilde{\mathcal{W}} + \frac{\Delta\mathbf{G}_n}{\Delta t_n} : \mathrm{D}_{\mathrm{G}}\widetilde{\mathcal{W}} + \frac{\Delta J_n}{\Delta t_n}\mathrm{D}_J\widetilde{\mathcal{W}}\,\mathrm{d}V\\ &\quad - \int_{\Omega_0}\frac{\Delta\boldsymbol{\varphi}_n}{\Delta t_n}\cdot\left(\bar{\mathbf{g}}_{n+1/2} + \bar{\mathbf{b}}_{n+1/2}\right)\mathrm{d}V - \int_{\partial\Omega_0}\frac{\Delta\boldsymbol{\varphi}_n}{\Delta t_n}\cdot\bar{\mathbf{t}}_{n+1/2}\,\mathrm{d}A = 0,\end{aligned} \tag{3.62}$$

which coincides with (3.60) iff $\bar{\mathbf{t}}_{n+1/2} = \mathbf{0}$ and $\bar{\mathbf{b}}_{n+1/2} = \mathbf{0}$. Note that the relation $\Delta\boldsymbol{\varphi}_n = \Delta t_n\mathbf{v}_{n+1/2}$ was used to obtain (3.62).

3.3.2. Time-discrete conservation of angular momentum

Following the approach in Section 3.2.5.2, we choose the time-discrete test functions $\mathbf{w}_\varphi = \boldsymbol{\zeta}\times\boldsymbol{\varphi}_{n+1/2}$ and $\mathbf{w}_\pi = -\rho_0\boldsymbol{\zeta}\times\frac{\Delta\varphi_n}{\Delta t_n}$ where again $\boldsymbol{\zeta}\in\mathbb{R}^3$ is an arbitrary but constant vector. Inserting these into (3.53) and summing the first two equations then yields

$$\begin{aligned}&\int_{\Omega_0}(-\rho_0\boldsymbol{\zeta}\times\Delta\boldsymbol{\varphi}_n)\cdot\left(\frac{\Delta\boldsymbol{\varphi}_n}{\Delta t_n} - \mathbf{v}_{n+1/2}\right)\mathrm{d}V\\ &\quad + \int_{\Omega_0}(\boldsymbol{\zeta}\times\boldsymbol{\varphi}_{n+1/2})\cdot\rho_0\frac{\Delta\mathbf{v}_n}{\Delta t_n} + (\hat{\boldsymbol{\zeta}}\nabla\boldsymbol{\varphi}_{n+1/2}) : (\mathbf{F}_{\boldsymbol{\varphi}_{n+1/2}}\bar{\mathbf{S}})\,\mathrm{d}V\\ &\quad - \int_{\Omega_0}(\boldsymbol{\zeta}\times\boldsymbol{\varphi}_{n+1/2})\cdot\left(\bar{\mathbf{g}}_{n+1/2} + \bar{\mathbf{b}}_{n+1/2}\right)\mathrm{d}V - \int_{\partial_\sigma\Omega_0}(\boldsymbol{\zeta}\times\boldsymbol{\varphi}_{n+1/2})\cdot\bar{\mathbf{t}}_{n+1/2}\,\mathrm{d}A = 0.\end{aligned} \tag{3.63}$$

Due to the symmetry of the time-discrete second Piola-Kirchhoff stress tensor $\bar{\mathbf{S}}$, the scalar product of $(\nabla \boldsymbol{\varphi}^{\top}_{n+1/2} \hat{\boldsymbol{\zeta}} \mathbf{F}_{n+1/2}) : \bar{\mathbf{S}}$ vanishes again. With some additional vector calculus, the last equation simplifies to

$$\begin{aligned} \boldsymbol{\zeta} \cdot \Bigg[\int_{\Omega_0} \frac{1}{\Delta t_n} \rho_0 \left(\boldsymbol{\varphi}_{n+1} \times \mathbf{v}_{n+1} - \boldsymbol{\varphi}_n \times \mathbf{v}_n \right) - \left(\bar{\mathbf{g}}_{n+1/2} + \bar{\mathbf{b}}_{n+1/2} \right) \times \boldsymbol{\varphi}_{n+1/2} \, \mathrm{d}V \\ - \int_{\partial_\sigma \Omega_0} \bar{\mathbf{t}}_{n+1/2} \times \boldsymbol{\varphi}_{n+1/2} \, \mathrm{d}A \Bigg] = \boldsymbol{\zeta} \cdot \left(\frac{\Delta \mathbf{L}_n}{\Delta t_n} - \mathbf{m}^{\mathrm{ext}}_{n+1/2} \right) = 0. \end{aligned} \tag{3.64}$$

Hence, the angular momentum is conserved in the sense that $\mathbf{L}_{n+1} = \mathbf{L}_n$ iff the time-discrete external torque $\mathbf{m}^{\mathrm{ext}}_{n+1/2}$ vanishes.

3.4. Discretization in space

This section addresses the spatial discretization of the fully mixed formulation. Furthermore, it is shown that the resulting space-discrete weak form can be recast as a discrete port-Hamiltonian system.

3.4.1. Approximation of the test and trial functions

Similarly to Section 3.3, we consider the weak form of the fully mixed formulation given in (W). In a first step, finite element approximations of the test and trial functions are introduced in order to discretize the governing equations in space in the framework of the Bubnov-Galerkin method.

For this purpose, we employ a standard isoparametric finite element concept as described, for example, in [89]. First, the finite element approximation of the deformation field $\boldsymbol{\varphi}$ is specified by

$$\boldsymbol{\varphi}^{\mathrm{h}} = \sum_{K=1}^{n_{\mathrm{node}}} N^K_\varphi \hat{\boldsymbol{\varphi}}^K = \mathbf{N}_\varphi \hat{\boldsymbol{\varphi}} \tag{3.65}$$

with

$$\begin{aligned} \hat{\boldsymbol{\varphi}} &= \begin{bmatrix} \hat{\varphi}^1_x & \hat{\varphi}^1_y & \hat{\varphi}^1_z & \cdots & \hat{\varphi}^{n_{\mathrm{node}}}_x & \hat{\varphi}^{n_{\mathrm{node}}}_y & \hat{\varphi}^{n_{\mathrm{node}}}_z \end{bmatrix}^{\top} \in \mathbb{R}^{3 n_{\mathrm{node}}}, \\ \mathbf{N}_\varphi &= \begin{bmatrix} N^1_\varphi \mathbf{I} & \cdots & N^{n_{\mathrm{node}}}_\varphi \mathbf{I} \end{bmatrix} \in \mathbb{R}^{3 \times 3 n_{\mathrm{node}}}, \end{aligned} \tag{3.66}$$

where N^K_φ are Lagrangian shape functions and $K = 1, \ldots, n_{\mathrm{node}}$ are n_{node} nodal points per element. The nodal position vectors $\hat{\boldsymbol{\varphi}}^K$ are summarized in the vector $\hat{\boldsymbol{\varphi}}$. Similarly, the shape functions are collected in the matrix $\mathbf{N}_\varphi$. Using standard finite element assembly procedures, we obtain a globally continuous discrete deformation field.

Similarly, the approximation of the velocity field $\mathbf{v}$ and the test functions $\{\mathbf{w}_\varphi, \mathbf{w}_\pi\}$ is given by

$$\begin{aligned} \mathbf{w}^{\mathrm{h}}_\varphi &= \sum_{K=1}^{n_{\mathrm{node}}} N^K_\varphi \hat{\mathbf{w}}^K_\varphi = \mathbf{N}_\varphi \hat{\mathbf{w}}_\varphi, \\ \mathbf{v}^{\mathrm{h}} &= \sum_{K=1}^{n_{\mathrm{node}}} N^K_\varphi \hat{\mathbf{v}}^K = \mathbf{N}_\varphi \hat{\mathbf{v}}, \\ \mathbf{w}^{\mathrm{h}}_\pi &= \sum_{K=1}^{n_{\mathrm{node}}} N^K_\varphi \hat{\mathbf{w}}^K_\pi = \mathbf{N}_\varphi \hat{\mathbf{w}}_\pi. \end{aligned} \tag{3.67}$$

For the tensor-valued mixed quantities $\{\mathbf{C}, \mathbf{G}\}$, their Lagrange multipliers $\{\boldsymbol{\Lambda}_{\mathbf{C}}, \boldsymbol{\Lambda}_{\mathbf{G}}\}$ and the corresponding test functions $\{\mathbf{w}_{\mathbf{C}}, \mathbf{w}_{\mathbf{G}}, \mathbf{w}_{\boldsymbol{\Lambda}_{\mathbf{C}}}, \mathbf{w}_{\boldsymbol{\Lambda}_{\mathbf{G}}}\}$, we make use of the Voigt notation to obtain an easier

implementation. We differentiate between stress-related and strain-related quantities. For a symmetric stress-like second-order tensor $\mathbf{A} = \mathbf{A}^\top$ and a symmetric strain-like second-order tensor $\mathbf{B} = \mathbf{B}^\top$, the Voigt notation is defined as

$$\begin{aligned} \{\mathbf{A}\}_\mathrm{V} &= \begin{bmatrix} A_{11} & A_{22} & A_{33} & A_{12} & A_{23} & A_{13} \end{bmatrix}^\top, \\ \{\mathbf{B}\}_\mathrm{V} &= \begin{bmatrix} B_{11} & B_{22} & B_{33} & 2B_{12} & 2B_{23} & 2B_{13} \end{bmatrix}^\top, \end{aligned} \tag{3.68}$$

respectively. With this in mind, we next provide the finite element approximations of the mixed fields, which do not require inter-element continuity. In fact, we focus on approximations of the mixed fields which are discontinuous across element boundaries. This way, static condensation can be applied to eliminate the corresponding local degrees of freedom on element level, see Section 3.5 for further details. The approximation of the right Cauchy-Green deformation tensor $\mathbf{C}$ is given by

$$\begin{aligned} \mathbf{C}^\mathrm{h} &= \sum_{L=1}^{m_\mathrm{node}} N_C^L \hat{\mathbf{C}}^L, \\ \{\mathbf{C}^\mathrm{h}\}_\mathrm{V} &= \mathbf{N}_C \{\hat{\mathbf{C}}\}_\mathrm{V}, \end{aligned} \tag{3.69}$$

where

$$\begin{aligned} \{\hat{\mathbf{C}}\}_\mathrm{V} &= \begin{bmatrix} \{\hat{\mathbf{C}}^1\}_\mathrm{V}^\top & \cdots & \{\hat{\mathbf{C}}^{m_\mathrm{node}}\}_\mathrm{V}^\top \end{bmatrix}^\top \in \mathbb{R}^{6m_\mathrm{node}}, \\ \mathbf{N}_C &= \begin{bmatrix} N_C^1 \mathbf{I}_6 & \cdots & N_C^{m_\mathrm{node}} \mathbf{I}_6 \end{bmatrix} \in \mathbb{R}^{6\times 6m_\mathrm{node}}. \end{aligned} \tag{3.70}$$

Here, m_node shape functions N_C^L are used per element. Furthermore, $\mathbf{I}_6$ is the identity matrix in $\mathbb{R}^{6\times 6}$. Note that although $\mathbf{C}^\mathrm{h}$ is defined only on a single element e, a superscript e is omitted here for the sake of readability.

Similarly, for the remaining matrix-valued mixed fields, we define

$$\begin{aligned} & & \{\mathbf{w}_\mathbf{C}^\mathrm{h}\}_\mathrm{V} &= \mathbf{N}_C \{\hat{\mathbf{w}}_\mathbf{C}\}_\mathrm{V}, \\ \{\mathbf{G}^\mathrm{h}\}_\mathrm{V} &= \mathbf{N}_C \{\hat{\mathbf{G}}\}_\mathrm{V}, & \{\mathbf{w}_\mathbf{G}^\mathrm{h}\}_\mathrm{V} &= \mathbf{N}_C \{\hat{\mathbf{w}}_\mathbf{G}\}_\mathrm{V}, \\ \{\mathbf{\Lambda}_\mathbf{C}^\mathrm{h}\}_\mathrm{V} &= \mathbf{N}_C \{\hat{\mathbf{\Lambda}}_\mathbf{C}\}_\mathrm{V}, & \{\mathbf{w}_{\mathbf{\Lambda}_\mathbf{C}}^\mathrm{h}\}_\mathrm{V} &= \mathbf{N}_C \{\hat{\mathbf{w}}_{\mathbf{\Lambda}_\mathbf{C}}\}_\mathrm{V}, \\ \{\mathbf{\Lambda}_\mathbf{G}^\mathrm{h}\}_\mathrm{V} &= \mathbf{N}_C \{\hat{\mathbf{\Lambda}}_\mathbf{G}\}_\mathrm{V}, & \{\mathbf{w}_{\mathbf{\Lambda}_\mathbf{G}}^\mathrm{h}\}_\mathrm{V} &= \mathbf{N}_C \{\hat{\mathbf{w}}_{\mathbf{\Lambda}_\mathbf{G}}\}_\mathrm{V}. \end{aligned} \tag{3.71}$$

Lastly, the remaining mixed fields $\{J, \lambda\}$ and the corresponding test functions $\{w_J, w_\lambda\}$ are discretized with shape functions N_J^L, where no Voigt notation is necessary. Consequently, we introduce

$$J^\mathrm{h} = \sum_{I=1}^{p_\mathrm{node}} N_J^I \hat{J}^I = \mathbf{N}_J \hat{\mathbf{J}}, \tag{3.72}$$

where

$$\begin{aligned} \hat{\mathbf{J}} &= \begin{bmatrix} \hat{J}^1 & \cdots & \hat{J}^{p_\mathrm{node}} \end{bmatrix}^\top \in \mathbb{R}^{p_\mathrm{node}}, \\ \mathbf{N}_J &= \begin{bmatrix} N_J^1 & \cdots & N_J^{p_\mathrm{node}} \end{bmatrix} \in \mathbb{R}^{p_\mathrm{node}} \end{aligned} \tag{3.73}$$

as well as

$$w_J^\mathrm{h} = \mathbf{N}_J \hat{\mathbf{w}}_J, \quad \lambda^\mathrm{h} = \mathbf{N}_J \hat{\boldsymbol{\lambda}}, \quad w_\lambda^\mathrm{h} = \mathbf{N}_J \hat{\mathbf{w}}_\lambda. \tag{3.74}$$

Based on the stored energy $\widetilde{\mathcal{W}}$, we define the stored energy functional

$$\mathcal{U} = \int_{\Omega_0} \widetilde{\mathcal{W}}(\mathbf{C}, \mathbf{G}, J) \, \mathrm{d}V. \tag{3.75}$$

Inserting the space-discrete versions of $\mathbf{C}$, $\mathbf{G}$ and J, we obtain the discretized stored energy functional

$$\begin{aligned}\mathcal{U}^{\mathrm{h}} := \int_{\Omega_0} \widetilde{\mathcal{W}}^{\mathrm{h}}\,\mathrm{d}V &= \int_{\Omega_0} \widetilde{\mathcal{W}}(\mathbf{C}^{\mathrm{h}}, \mathbf{G}^{\mathrm{h}}, J^{\mathrm{h}})\,\mathrm{d}V \\ &= \int_{\Omega_0} \widetilde{\mathcal{W}}(N_C^L \hat{\mathbf{C}}^L, N_C^L \hat{\mathbf{G}}^L, N_J^I \hat{J}^I)\,\mathrm{d}V =: U\left(\{\hat{\mathbf{C}}\}_{\mathrm{V}}, \{\hat{\mathbf{G}}\}_{\mathrm{V}}, \hat{\mathbf{J}}\right),\end{aligned} \tag{3.76}$$

where Einstein's summation convention is applied to the arguments of the function $\widetilde{\mathcal{W}}$. Taking the time derivative and applying the chain rule yields

$$\begin{aligned}\frac{\mathrm{d}}{\mathrm{d}t}U &= \int_{\Omega_0} \partial_{\mathrm{C}}\widetilde{\mathcal{W}}^{\mathrm{h}} : \frac{\mathrm{d}}{\mathrm{d}t}\left(N_C^L \hat{\mathbf{C}}^L\right) + \partial_{\mathrm{G}}\widetilde{\mathcal{W}}^{\mathrm{h}} : \frac{\mathrm{d}}{\mathrm{d}t}\left(N_C^L \hat{\mathbf{G}}^L\right) + \partial_J \widetilde{\mathcal{W}}^{\mathrm{h}} \frac{\mathrm{d}}{\mathrm{d}t}\left(N_J^I \hat{J}^I\right)\,\mathrm{d}V \\ &= \left\{\dot{\hat{\mathbf{C}}}\right\}_{\mathrm{V}}^{\top} \int_{\Omega_0} \mathbf{N}_C^{\top}\left\{\partial_{\mathrm{C}}\widetilde{\mathcal{W}}^{\mathrm{h}}\right\}_{\mathrm{V}}\mathrm{d}V + \left\{\dot{\hat{\mathbf{G}}}\right\}_{\mathrm{V}}^{\top} \int_{\Omega_0} \mathbf{N}_C^{\top}\left\{\partial_{\mathrm{G}}\widetilde{\mathcal{W}}^{\mathrm{h}}\right\}_{\mathrm{V}}\mathrm{d}V + \dot{\hat{\mathbf{J}}}^{\top} \int_{\Omega_0} \mathbf{N}_J^{\top}\partial_J\widetilde{\mathcal{W}}^{\mathrm{h}}\,\mathrm{d}V.\end{aligned} \tag{3.77}$$

Consequently, the partial derivatives of the discrete stored energy function U defined in (3.76) are given by

$$\begin{aligned}\partial_{\hat{\mathbf{C}}} U &= \int_{\Omega_0} \mathbf{N}_C^{\top}\left\{\partial_{\mathrm{C}}\widetilde{\mathcal{W}}^{\mathrm{h}}\right\}_{\mathrm{V}}\,\mathrm{d}V, \\ \partial_{\hat{\mathbf{G}}} U &= \int_{\Omega_0} \mathbf{N}_C^{\top}\left\{\partial_{\mathrm{G}}\widetilde{\mathcal{W}}^{\mathrm{h}}\right\}_{\mathrm{V}}\,\mathrm{d}V, \\ \partial_{\hat{J}} U &= \int_{\Omega_0} \mathbf{N}_J^{\top}\partial_J\widetilde{\mathcal{W}}^{\mathrm{h}}\,\mathrm{d}V.\end{aligned} \tag{3.78}$$

To avoid clumsy notation, $\partial_{\hat{\mathbf{C}}} U$ and $\partial_{\hat{\mathbf{G}}} U$ represent $\partial U / \partial\{\hat{\mathbf{C}}\}_{\mathrm{V}}$ and $\partial U / \partial\{\hat{\mathbf{G}}\}_{\mathrm{V}}$. Taking into account the above approximations of the test and trial functions, weak form (W) can be written as

$$\begin{aligned}&\int_{\Omega_0} \mathbf{w}_{\pi}^{\mathrm{h}} \cdot (\dot{\boldsymbol{\varphi}}^{\mathrm{h}} - \mathbf{v}^{\mathrm{h}})\,\mathrm{d}V = 0 \\ &\int_{\Omega_0} \mathbf{w}_{\varphi}^{\mathrm{h}} \cdot \rho_0 \dot{\mathbf{v}}^{\mathrm{h}} + 2\,\mathrm{sym}(\mathbf{F}_{\boldsymbol{\varphi}^{\mathrm{h}}}^{\top}\nabla\mathbf{w}_{\varphi}^{\mathrm{h}}) : \left(\boldsymbol{\Lambda}_{\mathrm{C}}^{\mathrm{h}} + \boldsymbol{\Lambda}_{\mathrm{G}}^{\mathrm{h}} \barwedge \mathbf{C}_{\boldsymbol{\varphi}^{\mathrm{h}}} + \frac{\lambda^{\mathrm{h}}}{2J_{\boldsymbol{\varphi}^{\mathrm{h}}}}\mathbf{G}_{\boldsymbol{\varphi}^{\mathrm{h}}}\right)\mathrm{d}V \\ &\qquad = \int_{\Omega_0} \mathbf{w}_{\varphi}^{\mathrm{h}} \cdot \left(\bar{\mathbf{g}} + \bar{\mathbf{b}}\right)\,\mathrm{d}V + \int_{\partial\Omega_0} \mathbf{w}_{\varphi}^{\mathrm{h}} \cdot \bar{\mathbf{t}}\,\mathrm{d}A \\ &\int_{\Omega_0} \mathbf{w}_{\mathrm{C}}^{\mathrm{h}} : \left[\boldsymbol{\Lambda}_{\mathrm{C}}^{\mathrm{h}} - \partial_{\mathrm{C}}\widetilde{\mathcal{W}}^{\mathrm{h}}\right]\,\mathrm{d}V = 0 \\ &\int_{\Omega_0} \mathbf{w}_{\mathrm{G}}^{\mathrm{h}} : \left[\boldsymbol{\Lambda}_{\mathrm{G}}^{\mathrm{h}} - \partial_{\mathrm{G}}\widetilde{\mathcal{W}}^{\mathrm{h}}\right]\,\mathrm{d}V = 0 \\ &\int_{\Omega_0} w_J^{\mathrm{h}}\left[\lambda^{\mathrm{h}} - \partial_J\widetilde{\mathcal{W}}^{\mathrm{h}}\right]\,\mathrm{d}V = 0 \\ &\int_{\Omega_0} \mathbf{w}_{\boldsymbol{\Lambda}_{\mathrm{C}}}^{\mathrm{h}} : \left[\dot{\mathbf{C}}^{\mathrm{h}} - 2\ \mathrm{sym}(\mathbf{F}_{\boldsymbol{\varphi}^{\mathrm{h}}}^{\top}\nabla\mathbf{v}^{\mathrm{h}})\right]\,\mathrm{d}V = 0 \\ &\int_{\Omega_0} \mathbf{w}_{\boldsymbol{\Lambda}_{\mathrm{G}}}^{\mathrm{h}} : \left[\dot{\mathbf{G}}^{\mathrm{h}} - 2\mathbf{C}_{\boldsymbol{\varphi}^{\mathrm{h}}} \barwedge \mathrm{sym}(\mathbf{F}_{\boldsymbol{\varphi}^{\mathrm{h}}}^{\top}\nabla\mathbf{v}^{\mathrm{h}})\right]\,\mathrm{d}V = 0 \\ &\int_{\Omega_0} w_{\lambda}^{\mathrm{h}}\left[\dot{J}^{\mathrm{h}} - J_{\boldsymbol{\varphi}^{\mathrm{h}}}^{-1}\mathbf{G}_{\boldsymbol{\varphi}^{\mathrm{h}}} : \mathrm{sym}(\mathbf{F}_{\boldsymbol{\varphi}^{\mathrm{h}}}^{\top}\nabla\mathbf{v}^{\mathrm{h}})\right]\,\mathrm{d}V = 0.\end{aligned} \tag{3.79}$$

Inserting the specific finite element approximations into (3.79), we obtain the following system of equations

$$\begin{aligned}
\dot{\hat{\boldsymbol{\varphi}}} - \hat{\mathbf{v}} &= \mathbf{0} \\
\hat{\mathbf{w}}_{\varphi}^{\top} \left[\mathbf{M}_{\varphi}^{\rho} \dot{\hat{\mathbf{v}}} + \boldsymbol{\Phi}(\hat{\boldsymbol{\varphi}}) \left\{ \hat{\boldsymbol{\Lambda}}_{\mathrm{C}} \right\}_{\mathrm{V}} + \boldsymbol{\Psi}(\hat{\boldsymbol{\varphi}}) \left\{ \hat{\boldsymbol{\Lambda}}_{\mathrm{G}} \right\}_{\mathrm{V}} + \boldsymbol{\Xi}(\hat{\boldsymbol{\varphi}}) \hat{\boldsymbol{\lambda}} - \mathbf{g} - \mathbf{b} - \mathbf{t} \right] &= 0 \\
\left\{ \hat{\mathbf{w}}_{\mathrm{C}} \right\}_{\mathrm{V}}^{\top} \left[\mathbf{M}_{\mathrm{C}} \left\{ \hat{\boldsymbol{\Lambda}}_{\mathrm{C}} \right\}_{\mathrm{V}} - \partial_{\hat{\mathrm{C}}} U \right] &= 0 \\
\left\{ \hat{\mathbf{w}}_{\mathrm{G}} \right\}_{\mathrm{V}}^{\top} \left[\mathbf{M}_{\mathrm{C}} \left\{ \hat{\boldsymbol{\Lambda}}_{\mathrm{G}} \right\}_{\mathrm{V}} - \partial_{\hat{\mathrm{G}}} U \right] &= 0 \\
\hat{\mathbf{w}}_{J}^{\top} \left[\mathbf{M}_{J} \hat{\boldsymbol{\lambda}} - \partial_{\hat{J}} U \right] &= 0 \\
\left\{ \hat{\mathbf{w}}_{\Lambda_{\mathrm{C}}} \right\}_{\mathrm{V}}^{\top} \left[\mathbf{M}_{\mathrm{C}} \left\{ \dot{\hat{\mathrm{C}}} \right\}_{\mathrm{V}} - \boldsymbol{\Phi}^{\top}(\hat{\boldsymbol{\varphi}}) \hat{\mathbf{v}} \right] &= 0 \\
\left\{ \hat{\mathbf{w}}_{\Lambda_{\mathrm{G}}} \right\}_{\mathrm{V}}^{\top} \left[\mathbf{M}_{\mathrm{C}} \left\{ \dot{\hat{\mathrm{G}}} \right\}_{\mathrm{V}} - \boldsymbol{\Psi}^{\top}(\hat{\boldsymbol{\varphi}}) \hat{\mathbf{v}} \right] &= 0 \\
\hat{\mathbf{w}}_{\lambda}^{\top} \left[\mathbf{M}_{J} \dot{\hat{\mathbf{J}}} - \boldsymbol{\Xi}^{\top}(\hat{\boldsymbol{\varphi}}) \hat{\mathbf{v}} \right] &= 0.
\end{aligned} \tag{3.80}$$

Here, the matrices $\left\{ \mathbf{M}_{\varphi}^{\rho}, \mathbf{M}_{\mathrm{C}}, \mathbf{M}_{J} \right\}$ and $\{ \boldsymbol{\Phi}(\hat{\boldsymbol{\varphi}}), \boldsymbol{\Psi}(\hat{\boldsymbol{\varphi}}), \boldsymbol{\Xi}(\hat{\boldsymbol{\varphi}}), \mathbf{g}, \mathbf{b}, \mathbf{t} \}$ are defined as

$$\begin{aligned}
\mathbf{M}_{\varphi}^{\rho} &= \int_{\Omega_0} \rho_0 \mathbf{N}_{\varphi}^{\top} \mathbf{N}_{\varphi} \, \mathrm{d}V \\
\mathbf{M}_{\mathrm{C}} &= \int_{\Omega_0} \mathbf{N}_{C}^{\top} \mathbf{N}_{C} \, \mathrm{d}V \\
\mathbf{M}_{J} &= \int_{\Omega_0} \mathbf{N}_{J}^{\top} \mathbf{N}_{J} \, \mathrm{d}V \\
\boldsymbol{\Phi}(\hat{\boldsymbol{\varphi}}) &= \int_{\Omega_0} 2 \mathbb{B}_{\hat{\boldsymbol{\varphi}}}^{\top} \mathbf{N}_{C} \, \mathrm{d}V \\
\boldsymbol{\Psi}(\hat{\boldsymbol{\varphi}}) &= \int_{\Omega_0} 2 \mathbb{B}_{\hat{\boldsymbol{\varphi}}}^{\top} \mathcal{D}(\mathbf{C}_{\boldsymbol{\varphi}^{\mathrm{h}}}) \mathbf{N}_{C} \, \mathrm{d}V \\
\boldsymbol{\Xi}(\hat{\boldsymbol{\varphi}}) &= \int_{\Omega_0} \mathbb{B}_{\hat{\boldsymbol{\varphi}}}^{\top} J_{\boldsymbol{\varphi}^{\mathrm{h}}}^{-1} \left\{ \mathbf{G}_{\boldsymbol{\varphi}^{\mathrm{h}}} \right\}_{\mathrm{V}} \mathbf{N}_{J} \, \mathrm{d}V \\
\mathbf{g} &= \int_{\Omega_0} \mathbf{N}_{\varphi}^{\top} \bar{\mathbf{g}} \, \mathrm{d}V \\
\mathbf{b} &= \int_{\Omega_0} \mathbf{N}_{\varphi}^{\top} \bar{\mathbf{b}} \, \mathrm{d}V \\
\mathbf{t} &= \int_{\partial\Omega_0} \mathbf{N}_{\varphi}^{\top} \bar{\mathbf{t}} \, \mathrm{d}A.
\end{aligned} \tag{3.81}$$

Within these definitions, $\mathbb{B}_{\hat{\boldsymbol{\varphi}}} \in \mathbb{R}^{6 \times 3 n_{\mathrm{node}}}$ is the classic nodal operator matrix defined through

$$\operatorname{sym}(\mathbf{F}_{\boldsymbol{\varphi}^{\mathrm{h}}}^{\top} \nabla \mathbf{w}_{\varphi}^{\mathrm{h}}) : \mathbf{A} = \left\{ \mathbf{A} \right\}_{\mathrm{V}}^{\top} \mathbb{B}_{\hat{\boldsymbol{\varphi}}} \hat{\mathbf{w}}_{\varphi}. \tag{3.82}$$

For completeness, the nodal operator matrix is contained in Appendix 3.A.1.

The matrix $\mathcal{D}(\square) \in \mathbb{R}^{6 \times 6}$ corresponds to the Voigt notation of the tensor cross product that fulfills the following relationship

$$\left(\mathbf{O} \overset{\times}{\otimes} \mathbf{P} \right) : \mathbf{Q} = \left\{ \mathbf{O} \right\}_{\mathrm{V}}^{\top} \mathcal{D}(\mathbf{Q}) \left\{ \mathbf{P} \right\}_{\mathrm{V}}, \tag{3.83}$$

where $\mathbf{O}$ is a symmetric strain-like second-order tensor and $\mathbf{P}$ is a symmetric stress-like second-order tensor. An explicit representation of $\mathcal{D}(\square)$ can be found in Appendix 3.A.2.

3.4.2. Space-discrete formulation as discrete port-Hamiltonian system

We next show that the space-discrete formulation emanating from (3.80) can be brought into the form of a discrete pH system. To this end, we take into account the arbitrariness of the nodal values pertaining to the discrete test functions and perform a static condensation of the Lagrange multipliers $\left\{\hat{\boldsymbol{\Lambda}}_{\mathrm{C}}\right\}_{\mathrm{V}}$, $\left\{\hat{\boldsymbol{\Lambda}}_{\mathrm{G}}\right\}_{\mathrm{V}}$ and $\hat{\boldsymbol{\lambda}}$ on element level. Correspondingly,

$$\begin{aligned}\left\{\hat{\boldsymbol{\Lambda}}_{\mathrm{C}}\right\}_{\mathrm{V}} &= \mathbf{M}_{\mathrm{C}}^{-1}\partial_{\hat{\mathrm{C}}}U,\\ \left\{\hat{\boldsymbol{\Lambda}}_{\mathrm{G}}\right\}_{\mathrm{V}} &= \mathbf{M}_{\mathrm{C}}^{-1}\partial_{\hat{\mathrm{G}}}U,\\ \hat{\boldsymbol{\lambda}} &= \mathbf{M}_{J}^{-1}\partial_{\hat{J}}U,\end{aligned} \tag{3.84}$$

and (3.80) can be recast in the form

$$\begin{aligned}\dot{\hat{\boldsymbol{\varphi}}} &= \hat{\mathbf{v}}\\ \mathbf{M}_{\varphi}^{\rho}\dot{\hat{\mathbf{v}}} &= -\boldsymbol{\Phi}(\hat{\boldsymbol{\varphi}})\mathbf{M}_{\mathrm{C}}^{-1}\partial_{\hat{\mathrm{C}}}U - \boldsymbol{\Psi}(\hat{\boldsymbol{\varphi}})\mathbf{M}_{\mathrm{C}}^{-1}\partial_{\hat{\mathrm{G}}}U - \boldsymbol{\Xi}(\hat{\boldsymbol{\varphi}})\mathbf{M}_{J}^{-1}\partial_{\hat{J}}U + \mathbf{g} + \mathbf{b} + \mathbf{t}\\ \mathbf{M}_{\mathrm{C}}\left\{\dot{\hat{\mathrm{C}}}\right\}_{\mathrm{V}} &= \boldsymbol{\Phi}^{\top}(\hat{\boldsymbol{\varphi}})\hat{\mathbf{v}}\\ \mathbf{M}_{\mathrm{C}}\left\{\dot{\hat{\mathrm{G}}}\right\}_{\mathrm{V}} &= \boldsymbol{\Psi}^{\top}(\hat{\boldsymbol{\varphi}})\hat{\mathbf{v}}\\ \mathbf{M}_{J}\dot{\hat{\mathbf{J}}} &= \boldsymbol{\Xi}^{\top}(\hat{\boldsymbol{\varphi}})\hat{\mathbf{v}}.\end{aligned} \tag{3.85}$$

Note that on element level, $\left\{\dot{\hat{\mathrm{C}}}\right\}_{\mathrm{V}}$, $\left\{\dot{\hat{\mathrm{G}}}\right\}_{\mathrm{V}}$ and $\dot{\hat{\mathbf{J}}}$ can be expressed in terms of the nodal quantities $\hat{\boldsymbol{\varphi}}$ and $\hat{\mathbf{v}}$ by using the last three equations of (3.85). This implies that after the temporal discretization, the degrees of freedom corresponding to the strain-type fields C^{h}, G^{h} and J^{h} can be eliminated by static condensation on element level (see Section 3.5.1.2). However, before proceeding with the time discretization, we first show that (3.85) gives rise to a discrete pH system. For that purpose, we rewrite (3.85) in the form

$$\begin{aligned}&\begin{bmatrix}\mathbf{I} & 0 & 0 & 0 & 0\\ 0 & \mathbf{M}_{\varphi}^{\rho} & 0 & 0 & 0\\ 0 & 0 & \mathbf{M}_{\mathrm{C}} & 0 & 0\\ 0 & 0 & 0 & \mathbf{M}_{\mathrm{C}} & 0\\ 0 & 0 & 0 & 0 & \mathbf{M}_{\mathrm{J}}\end{bmatrix}\begin{bmatrix}\dot{\hat{\boldsymbol{\varphi}}}\\ \dot{\hat{\mathbf{v}}}\\ \left\{\dot{\hat{\mathrm{C}}}\right\}_{\mathrm{V}}\\ \left\{\dot{\hat{\mathrm{G}}}\right\}_{\mathrm{V}}\\ \dot{\hat{\mathbf{J}}}\end{bmatrix} =\\ &\begin{bmatrix}0 & \mathbf{I} & 0 & 0 & 0\\ -\mathbf{I} & 0 & -\boldsymbol{\Phi}(\hat{\boldsymbol{\varphi}}) & -\boldsymbol{\Psi}(\hat{\boldsymbol{\varphi}}) & -\boldsymbol{\Xi}(\hat{\boldsymbol{\varphi}})\\ 0 & \boldsymbol{\Phi}^{\top}(\hat{\boldsymbol{\varphi}}) & 0 & 0 & 0\\ 0 & \boldsymbol{\Psi}^{\top}(\hat{\boldsymbol{\varphi}}) & 0 & 0 & 0\\ 0 & \boldsymbol{\Xi}^{\top}(\hat{\boldsymbol{\varphi}}) & 0 & 0 & 0\end{bmatrix}\begin{bmatrix}-\mathbf{g}\\ \hat{\mathbf{v}}\\ \mathbf{M}_{\mathrm{C}}^{-1}\partial_{\hat{\mathrm{C}}}U\\ \mathbf{M}_{\mathrm{C}}^{-1}\partial_{\hat{\mathrm{G}}}U\\ \mathbf{M}_{J}^{-1}\partial_{\hat{J}}U\end{bmatrix} + \begin{bmatrix}0 & 0\\ \mathbf{I} & \mathbf{I}\\ 0 & 0\\ 0 & 0\\ 0 & 0\end{bmatrix}\begin{bmatrix}\mathbf{b}\\ \mathbf{t}\end{bmatrix}.\end{aligned} \tag{3.86}$$

The above system of ordinary differential equations can be rewritten as

$$\mathbf{E}\dot{\hat{\mathbf{x}}} = \mathbf{J}(\hat{\boldsymbol{\varphi}})\mathbf{z}(\hat{\mathbf{x}}) + \mathbf{B}\hat{\mathbf{u}}, \tag{3.87}$$

where

$$\mathbf{E}^{\top}\mathbf{z}(\hat{\mathbf{x}}) = \nabla H(\hat{\mathbf{x}}). \tag{3.88}$$

Similarly to the continuous version of the pH system in (3.20) and (3.21), the two equations (3.87) and (3.88) constitute a discrete pH system [54, 55]. It can be easily observed that the structure matrix $\mathbf{J}$ is

skew-symmetric. Moreover, the discrete Hamiltonian $H(\hat{\mathbf{x}})$ follows from the Hamiltonian (3.17) by inserting the space-discrete approximations dealt with previously. Consequently,

$$\begin{aligned} H(\hat{\mathbf{x}}) := \mathcal{H}^{\mathrm{h}} &= \int_{\Omega_0} \left(\frac{1}{2}\rho_0 \mathbf{v}^{\mathrm{h}} \cdot \mathbf{v}^{\mathrm{h}} + \widetilde{\mathcal{W}}(\mathbf{C}^{\mathrm{h}}, \mathbf{G}^{\mathrm{h}}, J^{\mathrm{h}}) - \bar{\mathbf{g}} \cdot \boldsymbol{\varphi}^{\mathrm{h}}\right) \mathrm{d}V \\ &= \frac{1}{2}\hat{\mathbf{v}}^T \mathbf{M}_{\varphi}^{\rho} \hat{\mathbf{v}} + U\left(\left\{\hat{\mathbf{C}}\right\}_{\mathrm{V}}, \left\{\hat{\mathbf{G}}\right\}_{\mathrm{V}}, \hat{\mathbf{J}}\right) - \hat{\boldsymbol{\varphi}}^T \mathbf{g}, \end{aligned} \tag{3.89}$$

where the discrete stored energy U has been introduced in (3.76). Now, the derivative of the discrete Hamiltonian can be calculated to be

$$\nabla H(\hat{\mathbf{x}}) = \begin{bmatrix} -\mathbf{g} \\ \mathbf{M}_{\varphi}^{\rho}\hat{\mathbf{v}} \\ \partial_{\hat{\mathbf{C}}} U \\ \partial_{\hat{\mathbf{G}}} U \\ \partial_{\hat{J}} U \end{bmatrix}. \tag{3.90}$$

Note that the derivatives $\partial_{\hat{\mathbf{C}}} U$, $\partial_{\hat{\mathbf{G}}} U$ and $\partial_{\hat{J}} U$ have been defined in (3.78). The validity of (3.88) can now be easily verified.

Remark 3.2. *The discrete pH system on the element level gives rise to a corresponding discrete pH system on the system level, since (i) the power-preserving interconnection of discrete pH systems yields again a discrete pH system, and (ii) the finite element assembly procedure can be viewed as power-preserving interconnection of the element contributions.*

Remark 3.3. *The pH form of the semi-discrete equations of motion guarantees the energy consistency of the space-discrete formulation. To see this, consider*

$$\begin{aligned} \frac{\mathrm{d}}{\mathrm{d}t} H(\hat{\mathbf{x}}) &= \nabla H(\hat{\mathbf{x}}) \cdot \dot{\hat{\mathbf{x}}} \\ &= \left(\mathbf{E}^{\top} \mathbf{z}(\hat{\mathbf{x}})\right) \cdot \dot{\hat{\mathbf{x}}} \\ &= \mathbf{z}(\hat{\mathbf{x}}) \cdot \mathbf{E}\dot{\hat{\mathbf{x}}} \\ &= \mathbf{z}(\hat{\mathbf{x}}) \cdot \left(\mathbf{J}(\hat{\boldsymbol{\varphi}})\mathbf{z}(\hat{\mathbf{x}}) + \mathbf{B}\hat{\mathbf{u}}\right) \\ &= \mathbf{z}(\hat{\mathbf{x}}) \cdot \mathbf{B}\hat{\mathbf{u}} \\ &= \hat{\mathbf{y}} \cdot \hat{\mathbf{u}} \end{aligned} \tag{3.91}$$

where $\hat{\mathbf{y}} = \mathbf{B}^{\top}\mathbf{z}(\hat{\mathbf{x}})$ *is the discrete output. Consequently, the total energy is conserved iff no external control forces* $\hat{\mathbf{u}}$ *act on the system.*

Remark 3.4. *In order for* (3.87) *and* (3.88) *to form a discrete pH system, the fulfillment of* (3.88) *is crucial. It should be noted that the presence of constitutive equations for the Lagrange multipliers in the weak form is required during the spatial discretization process to satisfy* (3.88) *in general. However, there is the following exception: The pointwise enforcement of the constitutive equations for the Lagrange multipliers is sufficient in the case of constant approximations for the strain-type mixed fields* $\mathbf{C}$, $\mathbf{G}$ *and* J*. In this case,* $\mathbf{N}_C = \mathbf{I}_6$ *and* $\mathbf{N}_J = 1$*, leading to* $\mathbf{M}_{\mathrm{C}} = V_e \mathbf{I}_6$ *and* $\mathbf{M}_J = V_e$*, where* V_e *is the volume of the element in the reference configuration.*

3.5. Spatial and temporal discretization

In this section, the time-discrete weak form (3.53), introduced in Section 3.3, is further discretized in space. Although we shall deal with alternative spatial discretizations, we always start from the time-discrete weak form (3.53) corresponding to the fully mixed formulation.

3.5.1. Fully mixed element based on the strain-type fields $\{\mathrm{C}, \mathrm{G}, J\}$

In a first step, we apply the fully mixed finite element formulation devised in Section 3.4. Consequently, the time-discrete weak form (3.53) gives rise to

$$
\begin{aligned}
&\int_{\Omega_0} \mathbf{w}_\pi^{\mathrm{h}} \cdot \big(\frac{\boldsymbol{\varphi}_{n+1}^{\mathrm{h}} - \boldsymbol{\varphi}_n^{\mathrm{h}}}{\Delta t_n} - \mathbf{v}_{n+1/2}^{\mathrm{h}}\big)\,\mathrm{d}V = 0 \\
&\int_{\Omega_0} \mathbf{w}_\varphi^{\mathrm{h}} \cdot \rho_0 \frac{\mathbf{v}_{n+1}^{\mathrm{h}} - \mathbf{v}_n^{\mathrm{h}}}{\Delta t_n} \\
&\qquad + 2\,\mathrm{sym}(\mathbf{F}_{\varphi_{n+1/2}^{\mathrm{h}}}^{\top} \nabla \mathbf{w}_\varphi^{\mathrm{h}}) : \big(\boldsymbol{\Lambda}_{\mathrm{C}_{n+1}}^{\mathrm{h}} + \boldsymbol{\Lambda}_{\mathrm{G}_{n+1}}^{\mathrm{h}} \barwedge \mathbf{C}_{\varphi_{n+1/2}^{\mathrm{h}}} + \frac{\lambda^{\mathrm{h}}}{2J_{\varphi_{n+1/2}^{\mathrm{h}}}} \mathbf{G}_{\varphi_{n+1/2}^{\mathrm{h}}}\big)\,\mathrm{d}V \\
&\quad = \int_{\Omega_0} \mathbf{w}_\varphi^{\mathrm{h}} \cdot \Big(\bar{\mathbf{g}}_{n+1/2} + \bar{\mathbf{b}}_{n+1/2}\Big)\,\mathrm{d}V + \int_{\partial\Omega_0} \mathbf{w}_\varphi^{\mathrm{h}} \cdot \bar{\mathbf{t}}_{n+1/2}\,\mathrm{d}A \\
&\int_{\Omega_0} \mathbf{w}_{\mathrm{C}}^{\mathrm{h}} : \Big[\boldsymbol{\Lambda}_{\mathrm{C}_{n+1}}^{\mathrm{h}} - \mathrm{D}_{\mathrm{C}}\widetilde{\mathcal{W}}^{\mathrm{h}}\Big]\,\mathrm{d}V = 0 \\
&\int_{\Omega_0} \mathbf{w}_{\mathrm{G}}^{\mathrm{h}} : \Big[\boldsymbol{\Lambda}_{\mathrm{G}_{n+1}}^{\mathrm{h}} - \mathrm{D}_{\mathrm{G}}\widetilde{\mathcal{W}}^{\mathrm{h}}\Big]\,\mathrm{d}V = 0 \\
&\int_{\Omega_0} w_J^{\mathrm{h}} \Big[\lambda_{n+1}^{\mathrm{h}} - \mathrm{D}_J\widetilde{\mathcal{W}}^{\mathrm{h}}\Big]\,\mathrm{d}V = 0 \\
&\int_{\Omega_0} \mathbf{w}_{\Lambda_{\mathrm{C}}}^{\mathrm{h}} : \big[\frac{\mathbf{C}_{n+1}^{\mathrm{h}} - \mathbf{C}_n^{\mathrm{h}}}{\Delta t_n} - 2\,\mathrm{sym}(\mathbf{F}_{\varphi_{n+1/2}^{\mathrm{h}}}^{\top} \nabla \mathbf{v}_{n+1/2}^{\mathrm{h}})\big]\,\mathrm{d}V = 0 \\
&\int_{\Omega_0} \mathbf{w}_{\Lambda_{\mathrm{G}}}^{\mathrm{h}} : \big[\frac{\mathbf{G}_{n+1}^{\mathrm{h}} - \mathbf{G}_n^{\mathrm{h}}}{\Delta t_n} - 2\mathbf{C}_{\varphi_{n+1/2}^{\mathrm{h}}} \barwedge \mathrm{sym}(\mathbf{F}_{\varphi_{n+1/2}^{\mathrm{h}}}^{\top} \nabla \mathbf{v}_{n+1/2}^{\mathrm{h}})\big]\,\mathrm{d}V = 0 \\
&\int_{\Omega_0} w_\lambda^{\mathrm{h}} \big[\frac{J_{n+1}^{\mathrm{h}} - J_n^{\mathrm{h}}}{\Delta t_n} - (J_{\varphi_{n+1/2}^{\mathrm{h}}})^{-1} \mathbf{G}_{\varphi_{n+1/2}^{\mathrm{h}}} : \mathrm{sym}(\mathbf{F}_{\varphi_{n+1/2}^{\mathrm{h}}}^{\top} \nabla \mathbf{v}_{n+1/2}^{\mathrm{h}})\big]\,\mathrm{d}V = 0.
\end{aligned}
\tag{3.92}
$$

Note that the discrete derivatives $\mathrm{D}_{\mathcal{V}^i}\widetilde{\mathcal{W}}(\mathcal{V}_n, \mathcal{V}_{n+1})$, $\mathcal{V}^i \in \{\mathbf{C}^{\mathrm{h}}, \mathbf{G}^{\mathrm{h}}, J^{\mathrm{h}}\}$, have been introduced in Section 3.3.

3.5.1.1. Fully mixed discrete port-Hamiltonian formulation

Since time and space discretization of the fully mixed formulation commutes, the scheme emanating from (3.92) can also be written in the form

$$
\mathbf{E}\,(\hat{\mathbf{x}}_{n+1} - \hat{\mathbf{x}}_n) = \Delta t_n \left(\mathbf{J}(\hat{\boldsymbol{\varphi}}_{n+1/2})\bar{\mathbf{z}}(\hat{\mathbf{x}}_n, \hat{\mathbf{x}}_{n+1}) + \mathbf{B}\hat{\mathbf{u}}_{n+1/2}\right), \tag{3.93}
$$

where

$$
\mathbf{E}^{\top}\bar{\mathbf{z}}(\hat{\mathbf{x}}_n, \hat{\mathbf{x}}_{n+1}) = \bar{\nabla} H(\hat{\mathbf{x}}_n, \hat{\mathbf{x}}_{n+1}). \tag{3.94}
$$

Here, the matrices $\mathbf{E}$, $\mathbf{J}(\hat{\boldsymbol{\varphi}})$, and $\mathbf{B}$ can be again inferred from the discrete pH system (3.86). Moreover, the discrete derivative of the discrete Hamiltonian (3.89) is given by

$$
\bar{\nabla} H(\hat{\mathbf{x}}_n, \hat{\mathbf{x}}_{n+1}) = \begin{bmatrix} -\mathbf{g}_{n+1/2} \\ \mathbf{M}_\varphi^\rho \hat{\mathbf{v}}_{n+1/2} \\ \mathrm{D}_{\hat{\mathrm{C}}} U \\ \mathrm{D}_{\hat{\mathrm{G}}} U \\ \mathrm{D}_{\hat{J}} U \end{bmatrix}, \tag{3.95}
$$

where, similar to (3.78), the partitioned discrete derivatives of the discrete stored energy function assume the form

$$\begin{aligned} \mathrm{D}_{\hat{\mathrm{C}}} U &= \int_{\Omega_0} \mathbf{N}_C^{\top} \left\{ \mathrm{D}_{\mathrm{C}} \widetilde{\mathcal{W}}^{\mathrm{h}} \right\}_{\mathrm{V}} \mathrm{d}V, \\ \mathrm{D}_{\hat{\mathrm{G}}} U &= \int_{\Omega_0} \mathbf{N}_C^{\top} \left\{ \mathrm{D}_{\mathrm{G}} \widetilde{\mathcal{W}}^{\mathrm{h}} \right\}_{\mathrm{V}} \mathrm{d}V, \\ \mathrm{D}_{\hat{J}} U &= \int_{\Omega_0} \mathbf{N}_J \mathrm{D}_J \widetilde{\mathcal{W}}^{\mathrm{h}} \, \mathrm{d}V. \end{aligned} \tag{3.96}$$

It should be noted that algorithmic conservation of the total energy and total angular momentum can be shown starting from (3.92) along the lines of Sections 3.3.1 and 3.3.2, respectively. Alternatively, the algorithmic conservation of energy can be verified using (3.93) and (3.94). Consequently, due to the directionality property of the discrete derivative, we obtain

$$\begin{aligned} H(\hat{\mathbf{x}}_{n+1}) - H(\hat{\mathbf{x}}_n) &= \bar{\nabla} H(\hat{\mathbf{x}}_n, \hat{\mathbf{x}}_{n+1}) \cdot (\hat{\mathbf{x}}_{n+1} - \hat{\mathbf{x}}_n) \\ &= (\hat{\mathbf{x}}_{n+1} - \hat{\mathbf{x}}_n) \cdot \mathbf{E}^{\top} \bar{\mathbf{z}}(\hat{\mathbf{x}}_n, \hat{\mathbf{x}}_{n+1}) \\ &= \bar{\mathbf{z}}(\hat{\mathbf{x}}_n, \hat{\mathbf{x}}_{n+1}) \cdot \mathbf{E} \, (\hat{\mathbf{x}}_{n+1} - \hat{\mathbf{x}}_n) \\ &= \Delta t_n \bar{\mathbf{z}}(\hat{\mathbf{x}}_n, \hat{\mathbf{x}}_{n+1}) \cdot \left(\mathbf{J}(\hat{\boldsymbol{\varphi}}_{n+1/2}) \bar{\mathbf{z}}(\hat{\mathbf{x}}_n, \hat{\mathbf{x}}_{n+1}) + \mathbf{B} \hat{\mathbf{u}}_{n+1/2} \right) \\ &= \Delta t_n \left(\mathbf{B}^{\top} \bar{\mathbf{z}}(\hat{\mathbf{x}}_n, \hat{\mathbf{x}}_{n+1}) \right) \cdot \hat{\mathbf{u}}_{n+1/2} \\ &= \Delta t_n \hat{\mathbf{y}}_{n+1/2} \cdot \hat{\mathbf{u}}_{n+1/2}, \end{aligned} \tag{3.97}$$

where $\hat{\mathbf{y}}_{n+1/2} = \mathbf{B}^{\top} \bar{\mathbf{z}}(\hat{\mathbf{x}}_n, \hat{\mathbf{x}}_{n+1})$ is the discrete output at time $t_{n+1/2}$.

3.5.1.2. Notes on the implementation

An efficient implementation of the fully mixed formulation can be reached by applying static condensation of the mixed strain-type variables and expressing the nodal velocities $\hat{\mathbf{v}}_{n+1}$ in terms of the nodal position vectors $\hat{\boldsymbol{\varphi}}_{n+1}$. At the element level, the fully discrete equations (3.93) and (3.94) can be written in the form

$$\begin{aligned} \hat{\boldsymbol{\varphi}}_{n+1} - \hat{\boldsymbol{\varphi}}_n &= \Delta t_n \hat{\mathbf{v}}_{n+1/2} \\ \frac{1}{\Delta t_n} \mathbf{M}_{\varphi}^{\rho} \left(\hat{\mathbf{v}}_{n+1} - \hat{\mathbf{v}}_n \right) &= -\boldsymbol{\Phi}(\hat{\boldsymbol{\varphi}}_{n+1/2}) \mathbf{M}_{\mathrm{C}}^{-1} \mathrm{D}_{\hat{\mathrm{C}}} U - \boldsymbol{\Psi}(\hat{\boldsymbol{\varphi}}_{n+1/2}) \mathbf{M}_{\mathrm{C}}^{-1} \mathrm{D}_{\hat{\mathrm{G}}} U \\ &\quad - \boldsymbol{\Xi}(\hat{\boldsymbol{\varphi}}_{n+1/2}) \mathbf{M}_J^{-1} \mathrm{D}_{\hat{J}} U + \mathbf{g}_{n+1/2} + \mathbf{b}_{n+1/2} + \mathbf{t}_{n+1/2} \\ \frac{1}{\Delta t_n} \mathbf{M}_{\mathrm{C}} \left(\left\{ \hat{\mathbf{C}}_{n+1} \right\}_{\mathrm{V}} - \left\{ \hat{\mathbf{C}}_n \right\}_{\mathrm{V}} \right) &= \boldsymbol{\Phi}^{\top}(\hat{\boldsymbol{\varphi}}_{n+1/2}) \hat{\mathbf{v}}_{n+1/2} \\ \frac{1}{\Delta t_n} \mathbf{M}_{\mathrm{C}} \left(\left\{ \hat{\mathbf{G}}_{n+1} \right\}_{\mathrm{V}} - \left\{ \hat{\mathbf{G}}_n \right\}_{\mathrm{V}} \right) &= \boldsymbol{\Psi}^{\top}(\hat{\boldsymbol{\varphi}}_{n+1/2}) \hat{\mathbf{v}}_{n+1/2} \\ \frac{1}{\Delta t_n} \mathbf{M}_J \left(\hat{\mathbf{J}}_{n+1} - \hat{\mathbf{J}}_n \right) &= \boldsymbol{\Xi}^{\top}(\hat{\boldsymbol{\varphi}}_{n+1/2}) \hat{\mathbf{v}}_{n+1/2} \end{aligned} \tag{3.98}$$

(cf. (3.85)). We now introduce the element residual vector

$$\begin{aligned} \mathbf{R}(\hat{\boldsymbol{\varphi}}_{n+1}) := \frac{2}{\Delta t_n} \mathbf{M}_{\varphi}^{\rho} \left(\hat{\boldsymbol{\varphi}}_{n+1} - \hat{\boldsymbol{\varphi}}_n \right) - 2 \mathbf{M}_{\varphi}^{\rho} \hat{\mathbf{v}}_n + \Delta t_n \boldsymbol{\Phi}(\hat{\boldsymbol{\varphi}}_{n+1/2}) \mathbf{M}_{\mathrm{C}}^{-1} \mathrm{D}_{\hat{\mathrm{C}}} U \\ + \Delta t_n \left(\boldsymbol{\Psi}(\hat{\boldsymbol{\varphi}}_{n+1/2}) \mathbf{M}_{\mathrm{C}}^{-1} \mathrm{D}_{\hat{\mathrm{G}}} U + \boldsymbol{\Xi}(\hat{\boldsymbol{\varphi}}_{n+1/2}) \mathbf{M}_J^{-1} \mathrm{D}_{\hat{J}} U - \mathbf{g}_{n+1/2} - \mathbf{b}_{n+1/2} - \mathbf{t}_{n+1/2} \right), \end{aligned} \tag{3.99}$$

where the discrete derivatives of the discrete stored energy, $\mathrm{D}_{\hat{\mathrm{C}}}U$, $\mathrm{D}_{\hat{\mathrm{G}}}U$ and $\mathrm{D}_{\hat{J}}U$, are defined in (3.96). Thus, to calculate the residual vector (3.99), one first has to calculate

$$\begin{aligned}\left\{\hat{\mathbf{C}}_{n+1}\right\}_{\mathrm{V}} &= \left\{\hat{\mathbf{C}}_{n}\right\}_{\mathrm{V}} + \Delta t_n \mathbf{M}_{\mathrm{C}}^{-1}\boldsymbol{\Phi}^{\mathrm{T}}(\hat{\boldsymbol{\varphi}}_{n+1/2})\hat{\mathbf{v}}_{n+1/2}\\ \left\{\hat{\mathbf{G}}_{n+1}\right\}_{\mathrm{V}} &= \left\{\hat{\mathbf{G}}_{n}\right\}_{\mathrm{V}} + \Delta t_n \mathbf{M}_{\mathrm{C}}^{-1}\boldsymbol{\Psi}^{\mathrm{T}}(\hat{\boldsymbol{\varphi}}_{n+1/2})\hat{\mathbf{v}}_{n+1/2}\\ \hat{\mathbf{J}}_{n+1} &= \hat{\mathbf{J}}_{n} + \Delta t_n \mathbf{M}_{J}^{-1}\Xi^{\mathrm{T}}(\hat{\boldsymbol{\varphi}}_{n+1/2})\hat{\mathbf{v}}_{n+1/2}.\end{aligned} \tag{3.100}$$

These equations result from the last three equations in (3.98). In this context, $\hat{\mathbf{v}}_{n+1/2} = {}^{(\hat{\boldsymbol{\varphi}}_{n+1}-\hat{\boldsymbol{\varphi}}_n)}/_{\Delta t_n}$ results from the first equation in (3.98). Now,

$$\begin{aligned}\left\{\mathbf{C}^{\mathrm{h}}_{n+1}\right\}_{\mathrm{V}} &= \mathbf{M}\left\{\hat{\mathbf{C}}_{n+1}\right\}_{\mathrm{V}},\\ \left\{\mathbf{G}^{\mathrm{h}}_{n+1}\right\}_{\mathrm{V}} &= \mathbf{M}\left\{\hat{\mathbf{G}}_{n+1}\right\}_{\mathrm{V}},\\ J^{\mathrm{h}}_{n+1} &= \bar{\mathbf{M}}\hat{\mathbf{J}}_{n+1}\end{aligned} \tag{3.101}$$

can be used to evaluate the discrete derivatives (3.56) required to determine $\mathrm{D}_{\hat{\mathrm{C}}}U$, $\mathrm{D}_{\hat{\mathrm{G}}}U$ and $\mathrm{D}_{\hat{J}}U$ through (3.96).

The residual vector of the whole system can be obtained from the assembly of the element contributions (3.99) by applying standard finite element procedures. It should be noted that static condensation of mixed strain-type unknowns at element level leads to history-type quantities $\left\{\hat{\mathbf{C}}_n\right\}_{\mathrm{V}}$, $\left\{\hat{\mathbf{G}}_n\right\}_{\mathrm{V}}$ and $\hat{\mathbf{J}}_n$ in (3.100), which must be recovered from storage in each time step. We eventually emphasize that after finite element assembly, merely the nodal position vectors at time t_{n+1} remain as unknowns of the resulting nonlinear algebraic system, which can be solved iteratively by applying Newton's method. Consequently, the numerical effort to solve the global algebraic system is comparable to that of the purely displacement-based formulation treated in Section 3.5.3.

3.5.2. Mixed element based on the strain-type fields $\{\mathrm{G}, J\}$

We next show that the time-discrete weak form (3.53) can also accommodate the mixed finite element formulation developed in [48, 74], which is based on independent finite element approximations of mixed fields $\mathbf{G}$ and J. The corresponding size reduction of the time-discrete weak form (3.53) is based on the following two steps:

1. Choose the test function $\mathbf{w}_{\mathrm{C}}$ in (3.53) to be of the form

$$\mathbf{w}_{\mathrm{C}} = -2\,\mathrm{sym}(\mathbf{F}^{\mathrm{T}}_{\boldsymbol{\varphi}_{n+1/2}}\nabla\mathbf{w}_{\varphi}) \tag{3.102}$$

   for arbitrary $\mathbf{w}_{\varphi} \in \mathcal{V}^0_{\varphi}$.

2. Due to the arbitrariness of $\mathbf{w}_{\Lambda_{\mathrm{C}}} \in \mathcal{V}_C$, the update formula for $\mathbf{C}_{n+1}$ in (3.53) can be evaluated at Gauss point level, leading to

$$\mathbf{C}_{n+1} = \mathbf{C}_n + \Delta t_n 2\,\mathrm{sym}(\mathbf{F}^{\mathrm{T}}_{\boldsymbol{\varphi}_{n+1/2}}\nabla\mathbf{v}_{n+1/2}). \tag{3.103}$$

   Provided that $\mathbf{C}_n = \mathbf{C}_{\varphi^{\mathrm{h}}_n}$, a straightforward calculation based on (3.103) shows that $\mathbf{C}_{n+1} = \mathbf{C}_{\varphi^{\mathrm{h}}_{n+1}}$. For completeness, this is shown in Appendix 3.A.3.

The remaining equations of the time-discrete weak form (3.53) can now be used to accommodate the mixed finite element formulation due to [48, 74]. The resulting scheme emanates from

$$
\begin{aligned}
&\int_{\Omega_0} \mathbf{w}_\pi^{\mathrm{h}} \cdot \big(\frac{\boldsymbol{\varphi}_{n+1}^{\mathrm{h}} - \boldsymbol{\varphi}_n^{\mathrm{h}}}{\Delta t_n} - \mathbf{v}_{n+1/2}^{\mathrm{h}}\big)\,\mathrm{d}V = 0 \\
&\int_{\Omega_0} \mathbf{w}_\varphi^{\mathrm{h}} \cdot \rho_0 \frac{\mathbf{v}_{n+1}^{\mathrm{h}} - \mathbf{v}_n^{\mathrm{h}}}{\Delta t_n} \\
&\qquad + 2\,\mathrm{sym}(\mathbf{F}^{\mathrm{h}\top}_{\varphi^{\mathrm{h}}_{n+1/2}} \nabla \mathbf{w}_\varphi^{\mathrm{h}}) : \big(\mathrm{D}_{\mathbf{C}}\widetilde{\mathcal{W}}^{\mathrm{h}} + \boldsymbol{\Lambda}^{\mathrm{h}}_{\mathbf{G}_{n+1}} \barwedge \mathbf{C}_{\varphi^{\mathrm{h}}_{n+1/2}} + \frac{\lambda^{\mathrm{h}}_{n+1}}{2J_{\varphi^{\mathrm{h}}_{n+1/2}}} \mathbf{G}_{\varphi^{\mathrm{h}}_{n+1/2}}\big)\,\mathrm{d}V \\
&\quad = \int_{\Omega_0} \mathbf{w}_\varphi^{\mathrm{h}} \cdot \Big(\bar{\mathbf{g}}_{n+1/2} + \bar{\mathbf{b}}_{n+1/2}\Big)\,\mathrm{d}V + \int_{\partial\Omega_0} \mathbf{w}_\varphi^{\mathrm{h}} \cdot \bar{\mathbf{t}}_{n+1/2}\,\mathrm{d}A \\
&\int_{\Omega_0} \mathbf{w}_{\mathbf{G}}^{\mathrm{h}} : \Big[\boldsymbol{\Lambda}^{\mathrm{h}}_{\mathbf{G}_{n+1}} - \mathrm{D}_{\mathbf{G}}\widetilde{\mathcal{W}}^{\mathrm{h}}\Big]\,\mathrm{d}V = 0 \\
&\int_{\Omega_0} w_J^{\mathrm{h}} \Big[\lambda^{\mathrm{h}}_{n+1} - \mathrm{D}_J\widetilde{\mathcal{W}}^{\mathrm{h}}\Big]\,\mathrm{d}V = 0 \\
&\int_{\Omega_0} \mathbf{w}_{\boldsymbol{\Lambda}_{\mathbf{G}}}^{\mathrm{h}} : \big[\frac{\mathbf{G}^{\mathrm{h}}_{n+1} - \mathbf{G}^{\mathrm{h}}_n}{\Delta t_n} - 2\mathbf{C}_{\varphi^{\mathrm{h}}_{n+1/2}} \barwedge \mathrm{sym}(\mathbf{F}^{\mathrm{h}\top}_{\varphi^{\mathrm{h}}_{n+1/2}} \nabla \mathbf{v}^{\mathrm{h}}_{n+1/2})\big]\,\mathrm{d}V = 0 \\
&\int_{\Omega_0} w_\lambda^{\mathrm{h}} \big[\frac{J^{\mathrm{h}}_{n+1} - J^{\mathrm{h}}_n}{\Delta t_n} - (J_{\varphi^{\mathrm{h}}_{n+1/2}})^{-1}\mathbf{G}_{\varphi^{\mathrm{h}}_{n+1/2}} : \mathrm{sym}(\mathbf{F}^{\mathrm{h}\top}_{\varphi^{\mathrm{h}}_{n+1/2}} \nabla \mathbf{v}^{\mathrm{h}}_{n+1/2})\big]\,\mathrm{d}V = 0
\end{aligned}
\tag{3.104}
$$

with

$$
\mathbf{C}_{n+1} = \mathbf{C}_{\varphi^{\mathrm{h}}_{n+1}} \qquad \text{and} \qquad \mathbf{C}_n = \mathbf{C}_{\varphi^{\mathrm{h}}_n}. \tag{3.105}
$$

The finite element approximation of the remaining fields in (3.104) can be done in complete analogy to the fully mixed formulation as described in Section 3.4.1.

Algorithmic conservation of the total energy and total angular momentum can be shown by following similar lines as in Sections 3.3.1 and 3.3.2, respectively.

The implementation of the resulting EM scheme again relies on static condensation of the remaining mixed fields and can be performed in complete analogy to the fully mixed formulation (see Section 3.5.1.2).

3.5.3. Displacement-based element

We next show that the time-discrete weak form (3.53) can also accommodate purely displacement-based elements. The corresponding size reduction of the time-discrete weak form (3.53) is based on the following two steps:

1. Choose the test functions $\mathbf{w}_{\mathbf{C}}$, $\mathbf{w}_{\mathbf{G}}$ and w_J in (3.53) to be of the form

$$
\begin{aligned}
\mathbf{w}_{\mathbf{C}} &= -2\,\mathrm{sym}(\mathbf{F}^{\top}_{\boldsymbol{\varphi}_{n+1/2}} \nabla \mathbf{w}_\varphi) \\
\mathbf{w}_{\mathbf{G}} &= -2\,\mathrm{sym}(\mathbf{F}^{\top}_{\boldsymbol{\varphi}_{n+1/2}} \nabla \mathbf{w}_\varphi) \barwedge \mathbf{C}_{\boldsymbol{\varphi}_{n+1/2}} \\
w_J &= -J^{-1}_{\boldsymbol{\varphi}_{n+1/2}}\,\mathrm{sym}(\mathbf{F}^{\top}_{\boldsymbol{\varphi}_{n+1/2}} \nabla \mathbf{w}_\varphi) : \mathbf{G}_{\boldsymbol{\varphi}_{n+1/2}}
\end{aligned}
\tag{3.106}
$$

   for arbitrary $\mathbf{w}_\varphi \in \mathcal{V}^0_\varphi$.

2. Due to the arbitrariness of $\mathbf{w}_{\Lambda_C}, \mathbf{w}_{\Lambda_G} \in \mathcal{V}_C$ and $w_\lambda \in \mathcal{V}_J$, the update formulas for $\mathbf{C}_{n+1}$, $\mathbf{G}_{n+1}$ and J_{n+1} in (3.53) can be evaluated at Gauss point level leading to

$$\begin{aligned} \mathbf{C}_{n+1} &= \mathbf{C}_{\varphi^{\mathrm{h}}_{n+1}} \\ \mathbf{G}_{n+1} &= \mathbf{G}_n + 2\Delta t_n \mathbf{C}_{\varphi^{\mathrm{h}}_{n+1/2}} \overset{\ast}{\otimes} \mathrm{sym}(\mathbf{F}^{\top}_{\varphi^{\mathrm{h}}_{n+1/2}} \nabla \mathbf{v}^{\mathrm{h}}_{n+1/2}) \\ J_{n+1} &= J_n + \frac{\Delta t_n}{J_{\varphi^{\mathrm{h}}_{n+1/2}}} \mathbf{G}_{\varphi^{\mathrm{h}}_{n+1/2}} : \mathrm{sym}(\mathbf{F}^{\top}_{\varphi^{\mathrm{h}}_{n+1/2}} \nabla \mathbf{v}^{\mathrm{h}}_{n+1/2}). \end{aligned} \tag{3.107}$$

Here, $(3.107)_1$ again results from (3.103) as shown in Appendix 3.A.3

Inserting the test functions from (3.106) into (3.53) gives rise to the following displacement-based formulation

$$\begin{aligned} &\int_{\Omega_0} \mathbf{w}^{\mathrm{h}}_{\pi} \cdot \Big(\frac{\boldsymbol{\varphi}^{\mathrm{h}}_{n+1} - \boldsymbol{\varphi}^{\mathrm{h}}_{n}}{\Delta t_n} - \mathbf{v}^{\mathrm{h}}_{n+1/2} \Big) \, \mathrm{d}V = 0 \\ &\int_{\Omega_0} \mathbf{w}^{\mathrm{h}}_{\varphi} \cdot \rho_0 \frac{\mathbf{v}^{\mathrm{h}}_{n+1} - \mathbf{v}^{\mathrm{h}}_{n}}{\Delta t_n} + \mathrm{sym}(\mathbf{F}^{\top}_{\varphi^{\mathrm{h}}_{n+1/2}} \nabla \mathbf{w}^{\mathrm{h}}_{\varphi}) : \mathbf{S}_{\mathrm{A}} \, \mathrm{d}V \\ &\qquad = \int_{\Omega_0} \mathbf{w}^{\mathrm{h}}_{\varphi} \cdot \Big(\bar{\mathbf{g}}_{n+1/2} + \bar{\mathbf{b}}_{n+1/2} \Big) \, \mathrm{d}V + \int_{\partial\Omega_0} \mathbf{w}^{\mathrm{h}}_{\varphi} \cdot \bar{\mathbf{t}}_{n+1/2} \, \mathrm{d}A \end{aligned} \tag{3.108}$$

with algorithmic stress formula

$$\mathbf{S}_{\mathrm{A}} = 2\mathrm{D}_{\mathbf{C}} \widetilde{\mathcal{W}} + 2\mathrm{D}_{\mathbf{G}} \widetilde{\mathcal{W}} \overset{\ast}{\otimes} \mathbf{C}_{\varphi^{\mathrm{h}}_{n+1/2}} + \frac{\mathrm{D}_J \widetilde{\mathcal{W}}}{J_{\varphi^{\mathrm{h}}_{n+1/2}}} \mathbf{G}_{\varphi^{\mathrm{h}}_{n+1/2}}, \tag{3.109}$$

in which strain-type quantities (3.107) are required to calculate the discrete derivatives $\mathrm{D}_{\mathcal{V}^i} \widetilde{\mathcal{W}}(\mathcal{V}_n, \mathcal{V}_{n+1})$, $\mathcal{V}^i \in \{\mathbf{C}, \mathbf{G}, J\}$, at the Gauss point level. Note that $\mathbf{G}_n$ and J_n play the role of history variables that must be retrieved from storage at each time step to calculate $\mathbf{G}_{n+1}$ and J_{n+1} from $(3.107)_{2,3}$. In contrast to that, $\mathbf{C}_{n+1}$ can be obtained directly from $\boldsymbol{\varphi}^{\mathrm{h}}_{n+1}$ by applying $(3.107)_1$.

Algorithmic conservation of the total energy can be shown following lines similar to those in Section 3.3.1. Consequently, choosing $\mathbf{w}^{\mathrm{h}}_{\varphi} = \mathbf{v}^{\mathrm{h}}_{n+1/2}$ and taking into account (3.107), a straightforward calculation shows the conservation of the total energy in the absence of external forces. Similarly to Section 3.3.2, conservation of angular momentum can be shown by choosing $\mathbf{w}^{\mathrm{h}}_{\varphi} = \boldsymbol{\zeta} \times \mathbf{v}^{\mathrm{h}}_{n+1/2}$.

Remark 3.5. *The distinguishing features of the present approach to the formulation of EM schemes are (i) the partitioned form of the algorithmic stress formula* (3.109) *relying on partial discrete derivatives of the strain energy* $\widetilde{\mathcal{W}}(\mathbf{C}, \mathbf{G}, J)$ *(cf. Example 1) and (ii) the update formulas* (3.107) *for the strain-type variables relying on history variables* $\mathbf{G}_n$ *and* J_n*.*
This is in contrast to previous developments [32, 71] relying on discrete derivatives of the strain energy $\widehat{\mathcal{W}}(\mathbf{C}_\varphi)$ *defined in* (3.9)*. In particular, applying the discrete derivative proposed in [32] yields an algorithmic stress formula of the form* $\mathbf{S}_{\mathrm{A}} = 2\mathrm{D}_{\mathbf{C}} \widehat{\mathcal{W}}$*, where*

$$\mathrm{D}_{\mathbf{C}} \widehat{\mathcal{W}} = \nabla_{\mathbf{C}} \widehat{\mathcal{W}}(\mathbf{C}_{n+1/2}) + \frac{\widehat{\mathcal{W}}(\mathbf{C}_{n+1}) - \widehat{\mathcal{W}}(\mathbf{C}_n) - \nabla_{\mathbf{C}} \widehat{\mathcal{W}}(\mathbf{C}_{n+1/2}) : \Delta\mathbf{C}}{\Delta\mathbf{C} : \Delta\mathbf{C}} \Delta\mathbf{C}. \tag{3.110}$$

Here, $\mathbf{C}_n = \mathbf{C}_{\varphi^h_n}$, $\mathbf{C}_{n+1} = \mathbf{C}_{\varphi^h_{n+1}}$ *and* $\Delta\mathbf{C} = \mathbf{C}_{n+1} - \mathbf{C}_n$*.*

3.6. Numerical examples

This section presents numerical examples dealing with finite elastodynamics by applying various finite element formulations. In particular, we apply the newly developed EM schemes resulting from the fully mixed (FM) formulation (Section 3.5.1), the size-reduced mixed (RM) formulation (Section 3.5.2) and the size-reduced displacement (RD) formulation (Section 3.5.3). For comparison, we also apply the standard displacement-based (SD) formulation in combination with the implicit midpoint rule and the 'projection-based' EM scheme (cf. [32] and Remark 3.5). The mixed formulations rely on globally continuous tri-linear or tri-quadratic interpolations for the displacements and velocities, while the mixed quantities are interpolated one order lower, discontinuously across the element boundaries allowing for a static condensation as described in Sections 3.4 and 3.5. The various formulations under investigation are summarized in Table 3.1.

Table 3.1.: Considered discretizations and associated abbreviations.

Method	Description
FM-Q_2Q_1-EM	fully mixed formulation (see Section 3.5.1): spatially continuous triquadratic Q_2-elements for $\mathbf{v}$, $\boldsymbol{\varphi}$, and discontinuous trilinear Q_1-elements for $\mathbf{C}$, $\mathbf{G}$, J, $\boldsymbol{\Lambda}_\mathbf{C}$, $\boldsymbol{\Lambda}_\mathbf{G}$, λ; EM scheme
FM-Q_1Q_0-EM	fully mixed formulation (see Section 3.5.1): spatially continuous trilinear Q_1-elements for $\mathbf{v}$, $\boldsymbol{\varphi}$, and discontinuous constant Q_0-elements for $\mathbf{C}$, $\mathbf{G}$, J, $\boldsymbol{\Lambda}_\mathbf{C}$, $\boldsymbol{\Lambda}_\mathbf{G}$, λ; EM scheme
RM-Q_2Q_1-EM	size-reduced mixed formulation (see Section 3.5.2): spatially continuous triquadratic Q_2-elements for $\mathbf{v}$, $\boldsymbol{\varphi}$, and discontinuous trilinear Q_1-elements for $\mathbf{G}$, J, $\boldsymbol{\Lambda}_\mathbf{G}$, λ; EM scheme
RM-Q_1Q_0-EM	size-reduced mixed formulation (see Section 3.5.2): spatially continuous trilinear Q_1-elements for $\mathbf{v}$, $\boldsymbol{\varphi}$, and discontinuous constant Q_0-elements for $\mathbf{G}$, J, $\boldsymbol{\Lambda}_\mathbf{G}$, λ; EM scheme
RD-Q_1-EM	size-reduced displacement formulation (see Section 3.5.3): spatially continuous trilinear Q_1-elements for $\mathbf{v}$, $\boldsymbol{\varphi}$; EM scheme
SD-Q_1-MP	standard displacement-based formulation: spatially continuous trilinear Q_1-elements for $\mathbf{v}$, $\boldsymbol{\varphi}$; implicit midpoint rule
SD-Q_1-EM	standard displacement-based formulation: spatially continuous trilinear Q_1-elements for $\mathbf{v}$, $\boldsymbol{\varphi}$; EM scheme (see Remark 3.5)

Two hyperelastic material models are considered. A Mooney-Rivlin model (cf. [7]) with a stored energy function, defined as

$$\widetilde{\mathcal{W}}^{\mathrm{MR}} = a\,(\mathrm{tr}(\mathbf{C}) - 3) + b\,(\mathrm{tr}(\mathbf{G}) - 3) + \frac{c}{2}\,(J-1)^2 - d\ln(J), \tag{3.111}$$

with independent parameters $a, b, c \in \mathbb{R}^+$ and dependent parameter $d = 2\,(a + 2\,b)$ that ensures stress normalization (stress-free reference configuration). For more details, refer to [27]. Furthermore, a modified Mooney-Rivlin model (cf. [74]), whose stored energy is given by

$$\widetilde{\mathcal{W}}^{\mathrm{mMR}} = \frac{\alpha}{2}\left((\mathrm{tr}(\mathbf{C}))^2 - 9\right) + \frac{\beta}{2}\left((\mathrm{tr}(\mathbf{G}))^2 - 9\right) - \gamma\ln(J) + \epsilon_1\left(J^{2\epsilon_2} + J^{-2\epsilon_2} - 2\right), \tag{3.112}$$

is considered, where the independent parameters $\alpha, \beta, \epsilon_1, \epsilon_2 \in \mathbb{R}^+$ are introduced and dependent parameter $\gamma = 6\,(\alpha + 2\,\beta)$ ensures stress normalization[2].

The specific model parameters for the numerical study of the first example (Section 3.6.1) are listed in Table 3.2 and result in a compressible material behavior. In contrast, the second example (Section 3.6.2) deals with quasi-incompressible material behavior. The parameters are listed in Tables 3.3 and 3.4. In both cases, a linearization of the employed material model about the reference configuration leads to a quasi-incompressible material behavior with an effective Poisson's ratios of $\nu = 0.495$ and $\nu = 0.499$, respectively.

Table 3.2.: Mooney–Rivlin model parameters from [27].

Parameter	Value	Unit	Description
a	831.25	Pa	material parameter
b	166.25	Pa	material parameter
c	10000	Pa	volumetric parameter
$d = 2(a + 2b)$	2327.5	Pa	material parameter
ρ_0	100	$\mathrm{kg\,m^{-3}}$	mass density

Table 3.3.: Modified Mooney–Rivlin model parameters from [74] with effective Poisson's ratio of $\nu = 0.495$.

Parameter	Value	Unit	Description
α	42000	Pa	material parameter
β	84000	Pa	material parameter
$\gamma = 6(\alpha + 2\beta)$	1260000	Pa	material parameter
ϵ_1	100000	Pa	volumetric parameter
ϵ_2	10	-	volumetric exponent
ρ_0	225	$\mathrm{kg\,m^{-3}}$	mass density

Table 3.4.: Modified Mooney–Rivlin model parameters inspired from [74] with effective Poisson's ratio of $\nu = 0.499$.

Parameter	Value	Unit	Description
α	42000	Pa	material parameter
β	84000	Pa	material parameter
$\gamma = 6(\alpha + 2\beta)$	1260000	Pa	material parameter
ϵ_1	150000	Pa	volumetric parameter
ϵ_2	17.7	-	volumetric exponent
ρ_0	225	$\mathrm{kg\,m^{-3}}$	mass density

The discrete derivatives of the stored energy functions required in the fully mixed formulation (Section 3.5.1), the size-reduced mixed formulation (Section 3.5.2), and the size-reduced displacement formulation (Section 3.5.3) can now be easily calculated. For the stored energy of the Mooney-Rivlin model (3.111) we obtain

$$\begin{aligned} \mathrm{D}_{\mathrm{C}}\widetilde{\mathcal{W}} &= a\mathbf{I}, \\ \mathrm{D}_{\mathrm{G}}\widetilde{\mathcal{W}} &= b\mathbf{I}, \\ \mathrm{D}_J\widetilde{\mathcal{W}} &= \frac{\frac{c}{2}(J_{n+1}-1)^2 - d\ln(J_{n+1}) - \left(\frac{c}{2}(J_n-1)^2 - d\ln(J_n)\right)}{J_{n+1}-J_n}. \end{aligned} \tag{3.113}$$

[2] It should be emphasized that the above formulation differs from the one presented in [74] solely by an energy normalization (energy-free reference configuration), consistent with the standard Mooney–Rivlin model (3.111) (see also [27] for more details).

Similarly, the discrete derivatives of the modified Mooney-Rivlin model (3.112) are given by

$$\begin{aligned} \mathrm{D}_{\mathrm{C}}\widetilde{\mathcal{W}} &= \alpha\,\mathrm{tr}(\mathbf{C}_{n+1/2})\mathbf{I}, \\ \mathrm{D}_{\mathrm{G}}\widetilde{\mathcal{W}} &= \beta\,\mathrm{tr}(\mathbf{G}_{n+1/2})\mathbf{I}, \\ \mathrm{D}_{J}\widetilde{\mathcal{W}} &= \frac{-\gamma\left(\ln(J_{n+1}) - \ln(J_n)\right) + \epsilon_1\left(J_{n+1}^{2\epsilon_2} - J_n^{2\epsilon_2} + J_{n+1}^{-2\epsilon_2} - J_n^{-2\epsilon_2}\right)}{J_{n+1} - J_n}. \end{aligned} \tag{3.114}$$

Note that both stored energy functions under consideration are separable as outlined in Example 1.

3.6.1. Dynamical investigations of an L-shaped body

The objective of this first investigation is to assess the robustness, long-term stability, and discrete conservation properties of the newly developed formulations and integrators, compared to the standard midpoint integrator.

We consider the initial boundary value problem of an L-shaped body, following the work of [7, 26, 78].

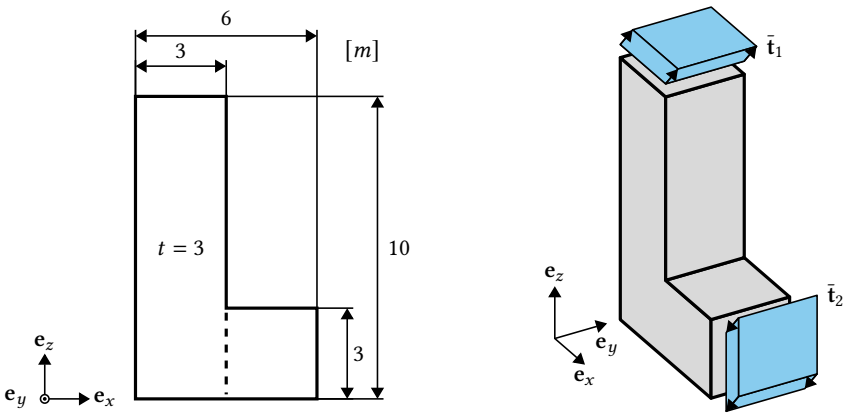


Figure 3.2.: Flying L-Shape: 2D projection of the geometry (left) and 3D illustration of the boundary conditions (right).

The geometry and initial setting with boundary conditions are shown in Figure 3.2. In particular, the applied external tractions are

$$\bar{\mathbf{t}}_1(t) = -\bar{\mathbf{t}}_2(t) = f(t)\,\frac{1}{9}\begin{bmatrix}256\\512\\768\end{bmatrix}\frac{\mathrm{N}}{\mathrm{m}^2}, \quad f(t) = \begin{cases} t & \text{for } t \le 2.5\mathrm{s} \\ 5 - t & \text{for } 2.5\mathrm{s} < t \le 5\mathrm{s} \\ 0 & \text{for } t > 5\mathrm{s}. \end{cases}$$

The L-shaped domain is discretized with 117 finite elements, and the simulation time is set to $T = 100\,\mathrm{s}$. In Figure 3.3, snapshots of the motion are shown with the corresponding von Mises stress distribution, clearly showing the occurrence of large rotations, deformations, and stresses. The energies obtained with the integrators under investigation are shown in Figure 3.4. Note that after $t = 5\mathrm{s}$, no external forces are acting on the system, so that the total energy should be a constant of motion. The total angular momentum obtained with the integrators under investigation is shown in Figure 3.5.

As evident in the energy diagram (see Figure 3.4), the implicit midpoint rule applied to the standard displacement formulation *SD*-Q_1-MP leads to a simulation failure due to an energy blow-up. In contrast,

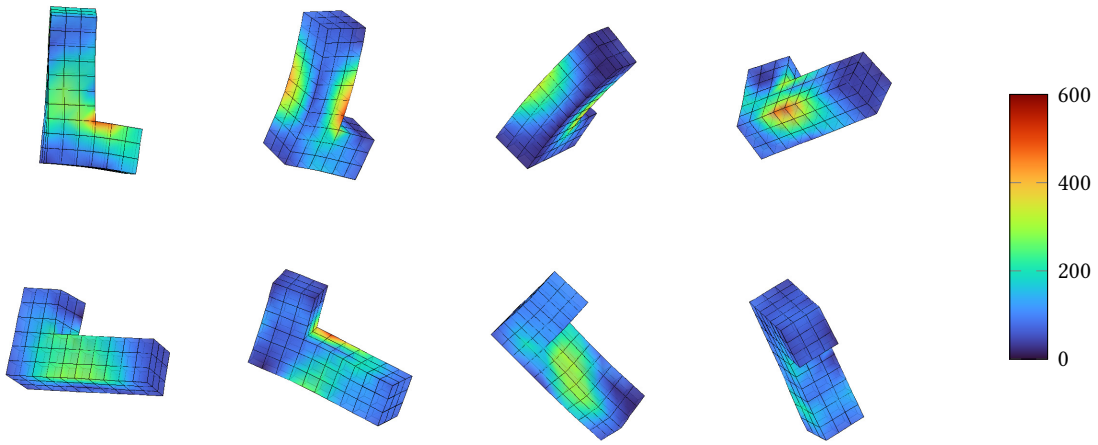


Figure 3.3.: Fyling L-Shape: snapshots with von Mises stress distribution σ_{vM} [Pa] of the *FM*-Q_1Q_0-EM formulation at times $t \in \{3.0, 6.0, 9.0, 12.0, 15.0, 18.0, 21.0, 24.0\}$s.

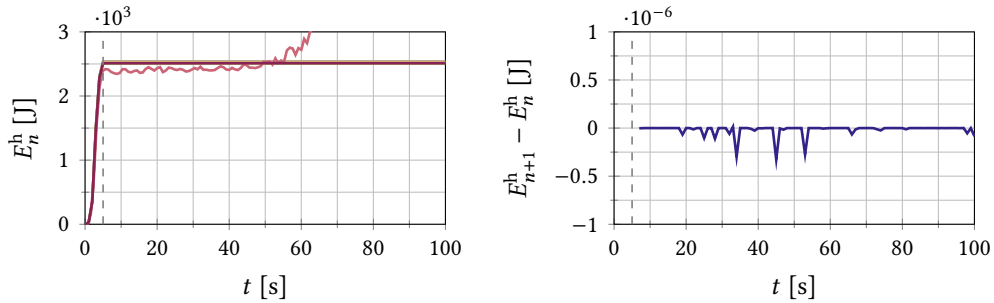


Figure 3.4.: Flying L-Shape: total energy E_n^{h} (left) for *FM*-Q_1Q_0-EM ——, *RM*-Q_1Q_0-EM ——, *RD*-Q_1-EM ——, *SD*-Q_1-MP ——, *SD*-Q_1-EM ——; energy difference $E_{n+1}^{\mathrm{h}} - E_n^{\mathrm{h}}$ for the *FM*-Q_1Q_0-EM —— formulation (right), with Newton tolerance $\epsilon = 10^{-6}$.

the size-reduced displacement formulation *RD*-Q_1Q_0-EM yields both numerical stability and exact energy conservation (after the loading phase $t > 5$ s), as illustrated in Figure 3.4.

It should be noted that the other formulations considered, *FM*-Q_1Q_0-EM, *RM*-Q_1Q_0-EM and *SD*-Q_1-EM, also conserve the energy exactly (after the loading phase $t > 5$s). In addition to that, all considered integrators conserve the angular momentum (after the loading phase $t > 5$s).

Furthermore, we examine the order of accuracy of the proposed integrators. Analogously to the implicit midpoint rule, second-order convergence is expected. To assess this, we define the relative L_2-norm of the error for a quantity $(\bullet)$ as

$$||e(\bullet)||_{L_2} = \frac{||(\bullet) - (\bullet)_{\mathrm{r}}||_{L^2}}{||(\bullet)_{\mathrm{r}}||_{L^2}}, \tag{3.115}$$

with

$$||(\bullet)||_{L_2} = \sqrt{\int_{\mathcal{B}_0} ((\bullet) \cdot (\bullet))\, \mathrm{d}V}. \tag{3.116}$$

Here, $(\bullet)_{\mathrm{r}}$ denotes the reference solution of $(\bullet)$, obtained using the smallest time-step size. For validation, we consider the free-flight motion of the L-shaped block in the time interval $5\mathrm{s} \leq t \leq 6\mathrm{s}$. As illustrated in Figure 3.6 in a double logarithmic scale, the proposed *RD*-Q_1Q_0-EM and *FM*-Q_1Q_0-EM formulations exhibit second-order accuracy.

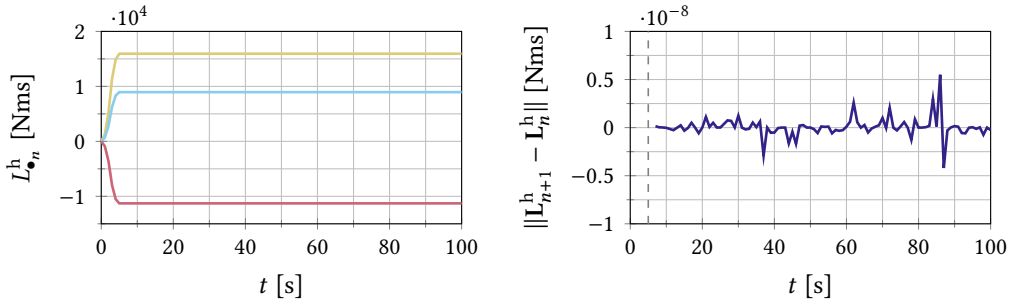


Figure 3.5.: Flying L-Shape: angular momentum components $L^{\mathrm{h}}_{i,n}$, $i \in \{1$ ——, 2 ——, 3 ——$\}$ (left) and norm of the angular momentum difference $\|\Delta\mathbf{L}^{\mathrm{h}}_{n}\|$ —— (right), obtained with *FM*-Q_1Q_0-EM, $\Delta t_n = 1$ s.

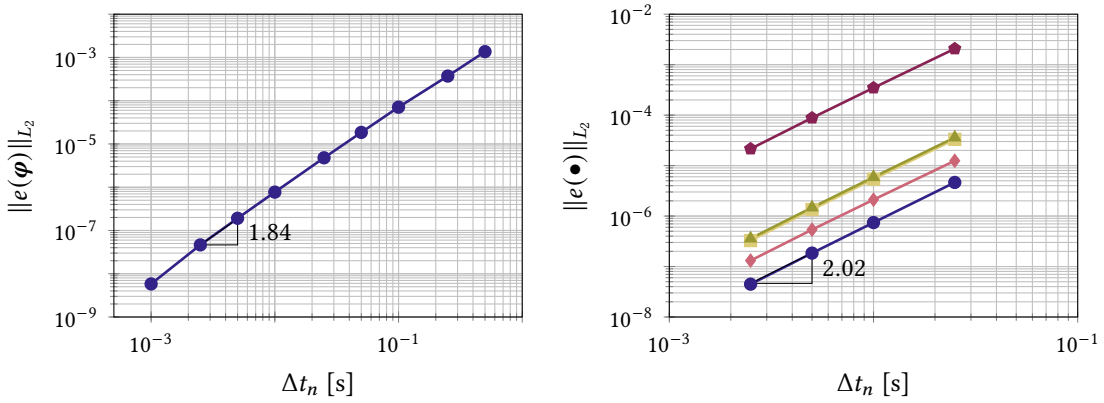


Figure 3.6.: Flying L-Shape: numerical accuracy in the relative L_2-error for *RD*-Q_1-EM (left): $\|e(\boldsymbol{\varphi})\|_{L_2}$ ——●——; *FM*-Q_1Q_0-EM (right): $\|e(\boldsymbol{\varphi})\|_{L_2}$ ——●——, $\|e(\mathrm{C})\|_{L_2}$ ——■——, $\|e(\mathrm{G})\|_{L_2}$ ——▲——, $\|e(J)\|_{L_2}$ ——◆——, $\|e(\mathrm{S})\|_{L_2}$ ——⬟——.

3.6.2. Dynamics of a bending and twisting beam

The objective of this second example is to investigate numerical robustness and discrete conservation properties in the case of quasi-incompressible material behavior. We primarily apply the size-reduced mixed formulation (Section 3.5.2), i.e. *RM*-Q_1Q_0-EM and *RM*-Q_2Q_1-EM, since the underlying mixed finite element formulation has been shown to be well suited for quasi-incompressible finite elasticity (see [48, 74]).

The underlying examples originate from [29, 75]. For the pure bending beam, see also [19]. The geometry and initial setting with boundary conditions are shown in Figure 3.7. In particular, the initial velocities for bending and twisting, respectively, illustrated in Figure 3.7, are given by

$$\mathbf{v}^{\text{bending}}(\mathbf{x}, t=0) = \begin{bmatrix} 5y/3 \\ 0 \\ 0 \end{bmatrix} \left[\tfrac{\mathrm{m}}{\mathrm{s}}\right], \quad \mathbf{v}^{\text{twisting}}(\mathbf{x}, t=0) = 100 \sin\left(\frac{\pi y}{12}\right) \begin{bmatrix} z \\ 0 \\ -x \end{bmatrix} \left[\tfrac{\mathrm{m}}{\mathrm{s}}\right].$$

Accordingly, due to the asymmetric clamping with respect to the coordinate system and the initial velocity, the bending beam problem is non-symmetric. In contrast to the examples in [75], which employ a Saint-Venant-Kirchhoff constitutive model, and [19, 29], which both use a neo-Hookean model, we consider the modified Mooney-Rivlin model (3.112) with parameters given in Table 3.3, both taken from [74]. The parameters lead to nearly incompressible material behavior.

To obtain comparable deformations as in [19, 75], we choose a density (see Table 3.3) that is one-quarter of the value used in [19, 75]. A $2\times12\times2$ finite element mesh is used. The simulations are carried out with

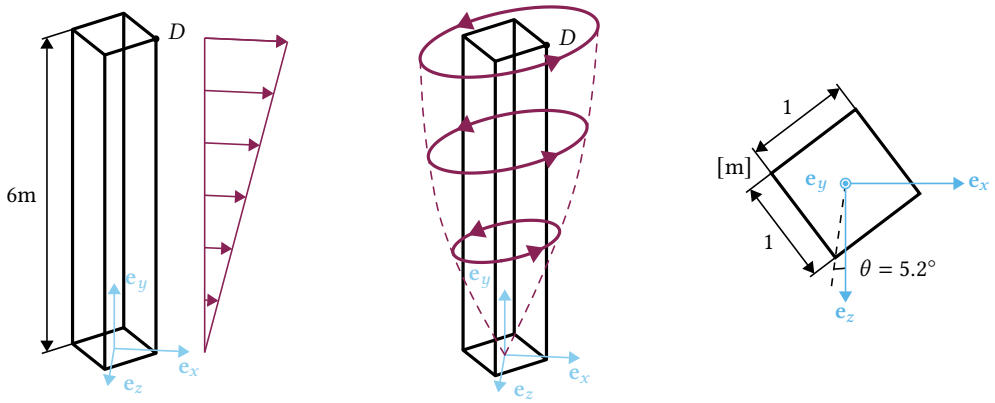


Figure 3.7.: Bending and Twisting beam: geometric setup of the beam in its initial configuration and initial velocities: bending beam (left), twisting beam (center), and top view (right).

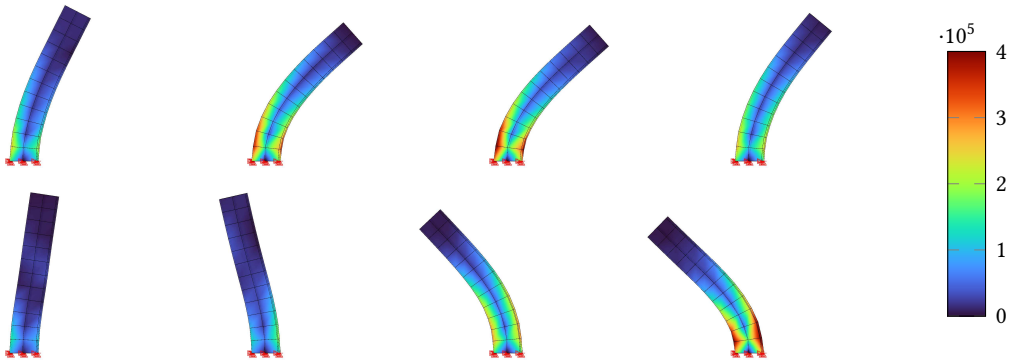


Figure 3.8.: Bending beam: snapshots for the *RM*-Q_1Q_0-EM formulation with von Mises stress distribution σ_{vM} [Pa] at times $t \in \{0.2, 0.4, 0.6, 0.8, 1.0, 1.2, 1.4, 1.6\}$s.

the *RM*-Q_1Q_0-EM formulation for the bending beam and the *RM*-Q_2Q_1-EM formulation for the twisting beam. In the case of the bending beam, a total time of $T = 20$s is considered, using a time step size of $\Delta t_n = 0.05$s and a Newton tolerance of $\epsilon = 5e\text{-}5$. For the twisting beam, the parameters are set to $T = 4$ s and $\epsilon = 5e\text{-}6$. The time-step size is chosen as $\Delta t_n = 0.01$ s for the material parameters given in Table 3.3 and $\Delta t_n = 0.002$ s for the material parameters given in Table 3.4. Note that a smaller time-step size is required for the more demanding combination of twisting deformation and near-incompressibility ($\nu = 0.499$).

Snapshots of the deformation and von Mises stress distribution are shown in Figure 3.8 for the *RM*-Q_1Q_0-EM formulation and Figure 3.9 for the *RM*-Q_2Q_1-EM formulation, respectively, while the total energy is depicted in Figure 3.10.

Additionally, we compute the *RM*-Q_1Q_0-EM and *RM*-Q_2Q_1-EM formulations for the modified Mooney-Rivlin model with parameters given in Table 3.4, corresponding to a Poisson's ratio of $\nu = 0.499$. The resulting total energies are shown in Figure 3.11. Furthermore, we investigate how accurately quasi-incompressibility is enforced (see Figure 3.12) by evaluating the mean error

$$\bar{\mathcal{E}}_J = \frac{1}{V}\int_{\Omega_0} |J-1| \, \mathrm{d}V, \quad \bar{\mathcal{E}}_{J_\varphi} = \frac{1}{V}\int_{\Omega_0} |J_\varphi - 1| \, \mathrm{d}V,$$

where the total reference volume is given by

$$V = \int_{\Omega_0} \mathrm{d}V.$$

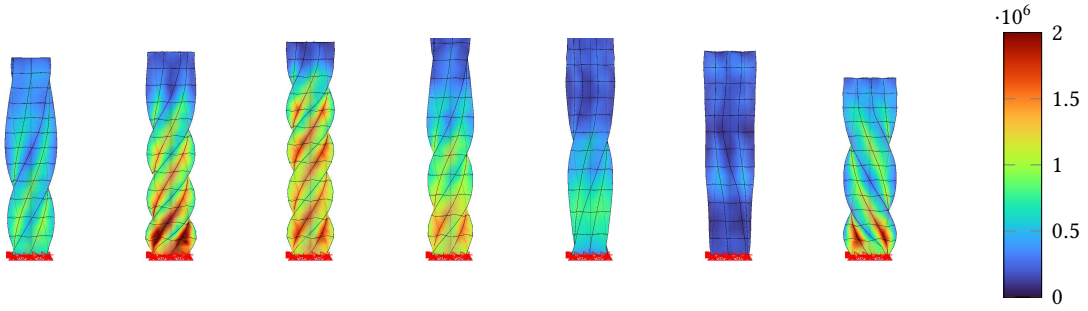


Figure 3.9.: Twisting beam: snapshots for the *RM*-Q_2Q_1-EM formulation with von Mises stress distribution σ_{vM} [Pa] at times $t \in \{0.04, 0.08, 0.12, 0.16, 0.20, 0.24, 0.28\}$s.

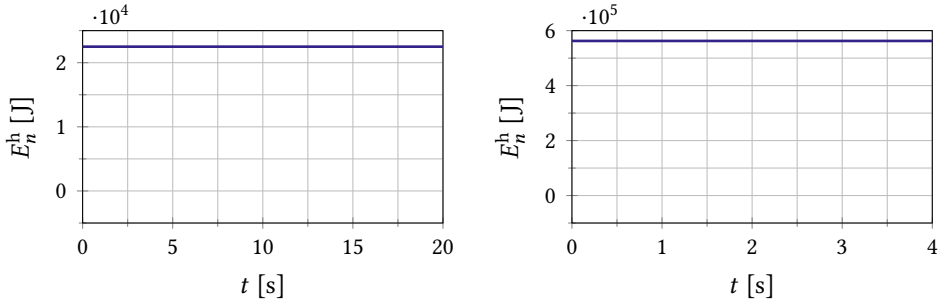


Figure 3.10.: Bending and twisting beam: total energy E_n^h of the bending (left, *RM*-Q_1Q_0-EM ——) and twisting (right, *RM*-Q_2Q_1-EM ——) beam for quasi-incompressible material ($\nu = 0.495$, Table 3.3).

Due to the new rate-type pH formulation, a drift between J and J_φ can be observed. The mixed quantity J therefore tends to fulfill the incompressibility constraint more accurately. This tendency becomes more pronounced in the nearly incompressible case (cf. $\nu = 0.495$ in Figure 3.12, left, versus $\nu = 0.499$ in Figure 3.12, right). Although the drift between J and J_φ is of interest, only J enters the strain energy in the formulation, and the incompressibility constraint associated with J is satisfied to a very good degree, as can be observed in Figure 3.12.

Despite the relatively coarse time step sizes, the *RM*-Q_1Q_0-EM formulation for the bending beam and the *RM*-Q_2Q_1-EM formulation for the twisting beam remain stable with energy conserved throughout these fully conservative setups.

It should be noted that the fully mixed formulations, i.e. *FM*-Q_1Q_0-EM and *FM*-Q_2Q_1-EM, produce nearly identical results, conserving energy and maintaining stability throughout the entire simulation.

3.7. Conclusion

We have proposed a new port-Hamiltonian formulation of finite elasticity along with its structure-preserving discretization in space and time. We have shown that the combination of Livens' variational principle with a Hu-Washizu-type extension adapted to polyconvex finite elasticity can be used to (i) derive the continuous pH formulation and (ii) construct a fully mixed weak formulation which provides the foundation for the structure-preserving discretization in space and time.

We have seen that the straightforward spatial discretization of the fully mixed weak formulation leads to semi-discrete equations of motion, which can be put in the form of a discrete pH system. Moreover, the direct temporal discretization of the fully mixed weak formulation provides a framework

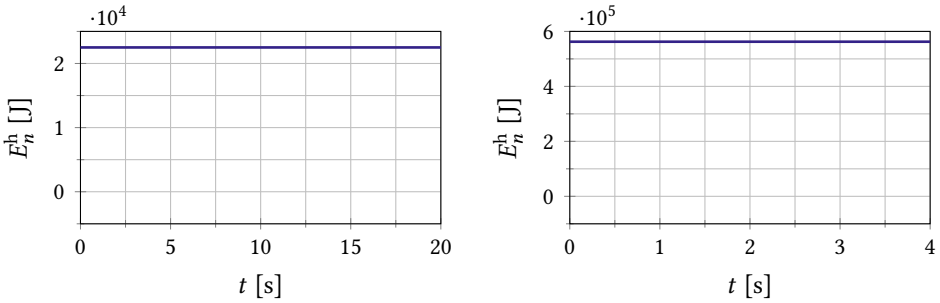


Figure 3.11.: Bending and twisting beam: total energy E_n^h of the bending (left, RM-Q_1Q_0-EM ——) and twisting (right, RM-Q_2Q_1-EM ——) beam for quasi-incompressible material ($\nu = 0.499$, Table 3.4).

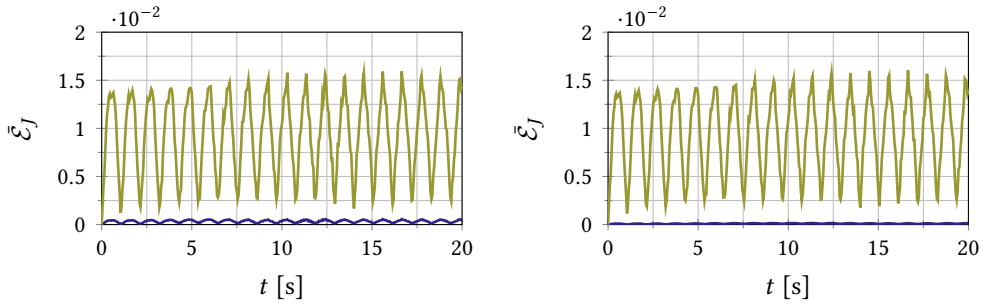


Figure 3.12.: Bending beam: verification of quasi-incompressibility (RM-Q_1Q_0-EM, $\Delta t_n = 0.05$ s): mean error $\bar{\mathcal{E}}_J$ for J —— and J_φ ——; left: $\nu = 0.495$ (Table 3.3) and right: $\nu = 0.499$ (Table 3.4).

that accommodates alternative finite element formulations and leads to structure-preserving energy-momentum schemes. In this way, alternative finite elements suitable for handling quasi-incompressible finite elasticity can be chosen and extended to the dynamic regime. This was shown, in particular, for the mixed finite element formulation developed in [48, 74].

A unique feature of the underlying pH description is that the strain-displacement relations are written in rate form. In this respect, the present approach bears some similarities with previous developments in [12] and [75]. The main advantage of the present pH-based approach is that it facilitates the design of energy-momentum-consistent methods in a natural way. This has been shown in the context of second-order accurate time-stepping schemes by employing the midpoint rule together with the notion of discrete derivatives applied to the stored energy function.

In essence, the underlying rate form of the strain-displacement relations makes possible the design of energy-momentum-consistent methods for a whole family of mixed finite element formulations that fit into the structure provided by the fully mixed weak form. The corresponding size reduction procedure has been shown for mixed finite elements due to [48, 74] (Section 3.5.2) and pure displacement elements (Section 3.5.3). This is in contrast to previous related work [7], which requires a specific cascade form of strain-type variables and thus precludes the use of other previously developed mixed finite elements for finite elastostatics, which in general do not comply with the cascade form of strain-type variables.

On the other hand, the versatility of the present pH-based approach comes at the expense of strain-type history variables that need to be retrieved from storage at the element level in each time step. In particular, strain-type history variables emerge in the static condensation procedure of mixed finite elements and for fully reduced displacement elements. In fact, this specific feature distinguishes the pH-based approach from previously designed EM methods. Similar observations have been made in the context of the nonlinear beam model investigated in [44].

Future research can address the extension of the present approach to multiphysics as well as inelastic material models, further exhausting the possibilities of the port-Hamiltonian framework. The present approach also opens promising avenues for the area of control, where energy-based formulations are of central importance.

Appendix to Chapter 3

3.A. Appendix

3.A.1. Nodal operator matrix

The nodal operator matrix $\mathbb{B}_{\hat{\boldsymbol{\varphi}}}$ is defined such that

$$\operatorname{sym}(\mathbf{F}_{\boldsymbol{\varphi}^{\mathrm{h}}}^{\top} \nabla \mathbf{w}_{\varphi}^{\mathrm{h}}) : \mathbf{A} = \left\{\mathbf{A}\right\}_{\mathrm{V}}^{\top} \mathbb{B}_{\hat{\boldsymbol{\varphi}}} \hat{\mathbf{w}}_{\varphi} \tag{3.117}$$

holds for any symmetric second-order tensor $\mathbf{A}$. Since

$$\begin{aligned} \operatorname{sym}(\mathbf{F}_{\boldsymbol{\varphi}^{\mathrm{h}}}^{\top} \nabla \mathbf{w}_{\varphi}^{\mathrm{h}}) : \mathbf{A} &= \mathbf{A} : \left(\mathbf{F}_{\boldsymbol{\varphi}^{\mathrm{h}}}^{\top} \nabla \mathbf{w}_{\varphi}^{\mathrm{h}}\right) \\ &= \operatorname{tr}\left(\mathbf{A}^{\top} \mathbf{F}_{\boldsymbol{\varphi}^{\mathrm{h}}}^{\top} \nabla \mathbf{w}_{\varphi}^{\mathrm{h}}\right) \\ &= \sum_{K=1}^{n_{\mathrm{node}}} \operatorname{tr}\left(\mathbf{A}^{\top} \mathbf{F}_{\boldsymbol{\varphi}^{\mathrm{h}}}^{\top} \hat{\mathbf{w}}_{\varphi}^{K} \otimes \nabla N_{\varphi}^{K}\right) \\ &= \sum_{K=1}^{n_{\mathrm{node}}} \nabla N_{\varphi}^{K} \cdot \left(\mathbf{A}^{\top} \mathbf{F}_{\boldsymbol{\varphi}^{\mathrm{h}}}^{\top} \hat{\mathbf{w}}_{\varphi}^{K}\right) \\ &= \left\{\mathbf{A}\right\}_{\mathrm{V}}^{\top} \Big(\sum_{K=1}^{n_{\mathrm{node}}} \mathbb{B}_{\hat{\boldsymbol{\varphi}}}^{K} \hat{\mathbf{w}}_{\varphi}^{K} \Big). \end{aligned} \tag{3.118}$$

Note that $\mathbb{B}_{\hat{\boldsymbol{\varphi}}}^{K}$ is linear in the nodal position vectors, because

$$\mathbf{F}_{\boldsymbol{\varphi}^{\mathrm{h}}} = \nabla \boldsymbol{\varphi}^{\mathrm{h}} = \sum_{K=1}^{n_{\mathrm{node}}} \hat{\boldsymbol{\varphi}}^{K} \otimes \nabla N_{\varphi}^{K}. \tag{3.119}$$

Now, it can be inferred from (3.118) that the nodal operator matrix $\mathbb{B}_{\hat{\boldsymbol{\varphi}}}$ is given by

$$\mathbb{B}_{\hat{\boldsymbol{\varphi}}} = \begin{bmatrix} \mathbb{B}_{\hat{\boldsymbol{\varphi}}}^{1} & \cdots & \mathbb{B}_{\hat{\boldsymbol{\varphi}}}^{n_{\mathrm{node}}} \end{bmatrix}, \tag{3.120}$$

where

$$\mathbb{B}_{\hat{\boldsymbol{\varphi}}}^{K} = \begin{bmatrix} F_{11} N_{,x}^{K} & F_{21} N_{,x}^{K} & F_{31} N_{,x}^{K} \\ F_{12} N_{,y}^{K} & F_{22} N_{,y}^{K} & F_{32} N_{,y}^{K} \\ F_{13} N_{,z}^{K} & F_{23} N_{,z}^{K} & F_{33} N_{,z}^{K} \\ F_{11} N_{,y}^{K} + F_{12} N_{,x}^{K} & F_{21} N_{,y}^{K} + F_{22} N_{,x}^{K} & F_{31} N_{,y}^{K} + F_{32} N_{,x}^{K} \\ F_{12} N_{,z}^{K} + F_{13} N_{,y}^{K} & F_{22} N_{,z}^{K} + F_{23} N_{,y}^{K} & F_{32} N_{,z}^{K} + F_{33} N_{,y}^{K} \\ F_{11} N_{,z}^{K} + F_{13} N_{,x}^{K} & F_{21} N_{,z}^{K} + F_{23} N_{,x}^{K} & F_{31} N_{,z}^{K} + F_{33} N_{,x}^{K} \end{bmatrix}. \tag{3.121}$$

3.A.2. Matrix related to the tensor cross product

The matrix representation of the tensor cross product of second-order tensors is defined such that the relationship

$$\left(\mathbf{O}\overset{\otimes}{\times}\mathbf{P}\right) : \mathbf{Q} = \left\{\mathbf{O}\right\}_{\mathrm{V}}^{\top}\mathcal{D}(\mathbf{Q})\left\{\mathbf{P}\right\}_{\mathrm{V}} \tag{3.122}$$

holds for a symmetric second-order tensor $\mathbf{Q}$, a symmetric strain-like second-order tensor $\mathbf{O}$ and a symmetric stress-like second-order tensor $\mathbf{P}$. Using definition (3.2) of the tensor cross product, the last equation can be written in index notation as

$$\begin{aligned}\left(\mathbf{O}\overset{\otimes}{\times}\mathbf{P}\right) : \mathbf{Q} &= \epsilon_{i\alpha\beta}\epsilon_{jab}O_{\alpha a}P_{\beta b}Q_{ij}\\ &= O_{\alpha a}Q_{ij}\epsilon_{i\alpha\beta}\epsilon_{jab}P_{\beta b}\end{aligned} \tag{3.123}$$

Now, comparing the last equation with the right-hand side of (3.122) and taking into account the summation convention, the properties of the permutation symbol along with the Voigt notations in (3.68), one obtains

$$\mathcal{D}(\mathbf{Q}) = \begin{bmatrix} 0 & Q_{33} & Q_{22} & 0 & -2Q_{23} & 0\\ Q_{33} & 0 & Q_{11} & 0 & 0 & -2Q_{13}\\ Q_{22} & Q_{11} & 0 & -2Q_{12} & 0 & 0\\ 0 & 0 & -Q_{12} & -Q_{33} & Q_{13} & Q_{23}\\ -Q_{23} & 0 & 0 & Q_{13} & -Q_{11} & Q_{12}\\ 0 & -Q_{13} & 0 & Q_{23} & Q_{12} & -Q_{22} \end{bmatrix}. \tag{3.124}$$

Note that matrix $\mathcal{D}(\mathbf{Q})$ is not symmetric, since the Voigt notation for $\mathbf{O}$ and $\mathbf{P}$ differs in off-diagonal terms. Additionally, it should be noted that the matrix $\mathcal{D}(\mathbf{Q})$ would be symmetric if Mandel notation was employed in place of classical Voigt notation.

3.A.3. Update formula for the reduced mixed formulation

We show that for the reduced mixed formulations dealt with in Sections 3.5.2 and 3.5.3, the update formula for $\mathbf{C}_{n+1}$ in (3.53) yields the result $\mathbf{C}_{n+1} = \mathbf{C}_{\varphi^{\mathrm{h}}_{n+1}}$. Thus, from (3.53), we have

$$\int_{\Omega_0} \mathbf{w}_{\Lambda_{\mathrm{C}}} : \left[\mathbf{C}_{n+1} - \mathbf{C}_n - 2\Delta t_n \,\mathrm{sym}(\mathbf{F}^{\top}_{\varphi^{\mathrm{h}}_{n+1/2}}\nabla\mathbf{v}^{\mathrm{h}}_{n+1/2})\right] \mathrm{d}V = 0. \tag{3.125}$$

Due to the arbitrariness of $\mathbf{w}_{\Lambda_{\mathrm{C}}} \in \mathcal{V}_C$, the last equation yields

$$\mathbf{C}_{n+1} - \mathbf{C}_n = \Delta t_n 2\,\mathrm{sym}(\mathbf{F}^{\top}_{\boldsymbol{\varphi}^{\mathrm{h}}_{n+1/2}}\nabla\mathbf{v}^{\mathrm{h}}_{n+1/2}). \tag{3.126}$$

Now,

$$2\,\mathrm{sym}(\mathbf{F}^{\top}_{\boldsymbol{\varphi}^{\mathrm{h}}_{n+1/2}}\nabla\mathbf{v}^{\mathrm{h}}_{n+1/2}) = \mathbf{F}^{\top}_{\boldsymbol{\varphi}^{\mathrm{h}}_{n+1/2}}\nabla\mathbf{v}^{\mathrm{h}}_{n+1/2} + (\nabla\mathbf{v}^{\mathrm{h}}_{n+1/2})^{\top}\mathbf{F}_{\boldsymbol{\varphi}^{\mathrm{h}}_{n+1/2}}. \tag{3.127}$$

Taking into account

$$\begin{aligned}\mathbf{F}_{\boldsymbol{\varphi}^{\mathrm{h}}_{n+1/2}} &= \nabla\boldsymbol{\varphi}^{\mathrm{h}}_{n+1/2} = \frac{1}{2}\left(\nabla\boldsymbol{\varphi}^{\mathrm{h}}_{n} + \nabla\boldsymbol{\varphi}^{\mathrm{h}}_{n+1}\right)\\ \nabla\mathbf{v}^{\mathrm{h}}_{n+1/2} &= \frac{1}{\Delta t_n}\nabla\left(\boldsymbol{\varphi}^{\mathrm{h}}_{n+1} - \boldsymbol{\varphi}^{\mathrm{h}}_{n}\right) = \frac{1}{\Delta t_n}\left(\nabla\boldsymbol{\varphi}^{\mathrm{h}}_{n+1} - \nabla\boldsymbol{\varphi}^{\mathrm{h}}_{n}\right),\end{aligned} \tag{3.128}$$

we obtain

$$\begin{aligned}\Delta t_n 2\,\mathrm{sym}(\mathbf{F}^{\top}_{\boldsymbol{\varphi}^{\mathrm{h}}_{n+1/2}} \nabla \mathbf{v}^{\mathrm{h}}_{n+1/2}) &= (\nabla \boldsymbol{\varphi}^{\mathrm{h}}_{n+1})^{\top} \nabla \boldsymbol{\varphi}^{\mathrm{h}}_{n+1} - (\nabla \boldsymbol{\varphi}^{\mathrm{h}}_{n})^{\top} \nabla \boldsymbol{\varphi}^{\mathrm{h}}_{n} \\ &= \mathbf{C}_{\varphi^{\mathrm{h}}_{n+1}} - \mathbf{C}_{\varphi^{\mathrm{h}}_{n}}.\end{aligned} \tag{3.129}$$

Consequently, (3.126) yields

$$\mathbf{C}_{n+1} - \mathbf{C}_n = \mathbf{C}_{\varphi^{\mathrm{h}}_{n+1}} - \mathbf{C}_{\varphi^{\mathrm{h}}_{n}} \tag{3.130}$$

and thus $\mathbf{C}_{n+1} = \mathbf{C}_{\varphi^{\mathrm{h}}_{n+1}}$ provided that $\mathbf{C}_n = \mathbf{C}_{\varphi^{\mathrm{h}}_{n}}$.

4. Structure-preserving mixed GENERIC formulation for nonlinear thermoelasticity

This chapter is based on:*
Hille M, Betsch P, and Franke M. *Structure-Preserving Mixed GENERIC Formulation for Nonlinear Thermoelasticity*. Manuscript submitted to Journal of Computational Physics. Preprint available at SSRN. 2026. DOI: 10.2139/ssrn.7029051

Abstract: We propose a mixed and structure-preserving discretization framework for finite-strain thermoelasticity based on General Equation for Non-Equilibrium Reversible-Irreversible Coupling (GENERIC). GENERIC provides a systematic decomposition of the dynamics into reversible and irreversible contributions while guaranteeing consistency with the first and second laws of thermodynamics. Starting from a Hu–Washizu-type extension of the variational principle of Livens and a polyconvex representation of the internal energy, a mixed thermo-mechanical GENERIC framework is constructed. The resulting formulation introduces additional mixed fields associated with thermodynamic driving forces arising from the internal energy and entropy representation. A central aspect of the proposed approach is that the kinematic compatibility conditions are enforced at the rate level, which naturally opens the framework to broader classes of mixed finite element formulations. The temporal discretization is based on so-called discrete derivatives and yields a time-discrete formulation preserving the total energy for closed systems while guaranteeing consistent entropy production. Furthermore, the spatial discretization of the underlying weak form leads to a mixed finite element formulation preserving the thermodynamic structure of the semi-discrete problem. Numerical examples are presented to investigate the numerical performance, thermodynamic consistency, and stability properties of the proposed framework.

Keywords: GENERIC • nonlinear thermoelasticity • Hu-Washizu • mixed finite elements • structure-preserving discretization • thermodynamic consistency

* Adapted from the cited manuscript.

4.1. Introduction

The modeling and numerical simulation of coupled thermo-mechanical systems at finite strains require mathematical frameworks that consistently account for both reversible and irreversible processes. In particular, the preservation of fundamental thermodynamic principles at the discrete level has become an important objective in the design of modern computational methods. Structure-preserving discretization techniques aim at retaining intrinsic properties of the underlying continuum model, such as conservation of total energy and consistent entropy production, thereby improving long-term stability and physical consistency of numerical simulations.

A systematic framework for the modeling of thermodynamically consistent evolution equations is provided by the General Equation for Non-Equilibrium Reversible-Irreversible Coupling (GENERIC).

GENERIC was originally introduced in [34]. Detailed expositions of its mathematical structure, thermodynamic foundations, and subsequent developments are provided in the monographs [62, 66]. The GENERIC formalism decomposes the evolution of a thermodynamic system into reversible and irreversible contributions generated by the total energy and entropy, respectively. The structure of the associated operators directly guarantees compatibility with the first and second laws of thermodynamics. In this way, GENERIC provides a unified operator-based framework in which reversible and irreversible mechanisms can be treated consistently at both the continuous and discrete levels.

Owing to its generality, GENERIC has been applied to a broad range of problems in nonequilibrium thermodynamics and continuum mechanics. In particular, [56] introduced a special form of GENERIC that allows transformations between different sets of state variables and forms the theoretical foundation of the present work. Further developments in the context of continuum mechanics include, for example, [9, 40, 72] and, more recently, [57, 59]. Moreover, the structure-preserving discretization of GENERIC systems has attracted increasing interest in recent years, particularly in connection with geometric integration techniques and thermodynamically consistent time integration methods such as [8, 26]. The cited works are intended only as representative examples within a broad and continuously growing body of literature.

In the context of nonlinear continuum mechanics, mixed variational formulations have proven to be particularly attractive for the treatment of finite-deformation problems. In particular, formulations based on polyconvex energy representations provide a mathematically robust framework for hyperelasticity while naturally introducing additional kinematic variables, such as the right Cauchy–Green tensor, its cofactor, and the Jacobian of the deformation gradient. Corresponding mixed formulations have been successfully employed in the design of finite element methods exhibiting favorable numerical properties, especially in nearly incompressible regimes and finite-strain applications (e.g. [7, 48, 74]). In addition, polyconvexity-inspired mixed formulations provide a natural setting for the construction of energy-momentum consistent time integration schemes based on discrete derivatives [B3, A2].

Despite these developments, the systematic incorporation of mixed finite element formulations into thermodynamically consistent GENERIC-based discretization frameworks remains largely unexplored. The present work aims to bridge this gap by developing a mixed GENERIC framework for finite-strain thermoelasticity together with corresponding structure-preserving discretization techniques in time and space. Starting from a Hu–Washizu-type mixed variational principle based on a polyconvex representation of the internal energy, a coupled thermo-mechanical GENERIC formulation is constructed. The resulting weak form introduces additional mixed fields associated with the energetic and entropic driving forces.

For the temporal discretization, a discrete derivative approach in the sense of Gonzalez [31, 32] is employed, yielding a thermodynamically consistent extension of midpoint-type schemes. The resulting time-discrete formulation is shown to preserve the total energy for closed systems while guaranteeing consistent entropy production.

Subsequently, a mixed finite element discretization is developed for the spatial approximation of the coupled system. The proposed spatial discretization preserves the underlying thermodynamic structure at the semi-discrete level and naturally leads to a semi-discrete GENERIC formulation.

A central aspect of the present approach is that the kinematic compatibility conditions associated with the underlying mixed formulation are enforced at the rate level rather than through exact pointwise consistency of the strain measures at the discrete configuration level. As a consequence, the proposed GENERIC-based construction is not restricted to the specific polyconvex mixed setting considered in this work, but can be extended to a broader class of mixed finite element formulations, including

classical Hu–Washizu- and Hellinger–Reissner-type approaches as well as mixed methods for quasi-incompressible finite elasticity.

The remainder of the paper is organized as follows. Section 4.2 briefly reviews the GENERIC formalism and its fundamental structural properties. Section 4.3 introduces the continuum-mechanical and thermodynamic preliminaries together with the polyconvex representation employed throughout the work. The mixed GENERIC framework and the associated weak formulation are developed in Section 4.4. Section 4.5 presents the structure-preserving time discretization and establishes discrete conservation and entropy properties. The spatial discretization by means of mixed finite elements is discussed in Section 4.6, where the corresponding semi-discrete thermodynamic consistency is shown. Numerical examples are presented in Section 4.7, followed by concluding remarks in Section 4.8.

4.2. The GENERIC formalism

Let $X(t)$ denote the state of a thermodynamic system. Then the GENERIC evolution equation is given by

$$\dot{X} = \mathcal{L}(X)\,\frac{\delta E(X)}{\delta X} + \mathcal{K}(X)\,\frac{\delta S(X)}{\delta X}, \tag{4.1}$$

where $E(X)$ denotes the total energy and $S(X)$ the total entropy of the system. Furthermore, $\delta E/\delta X$ and $\delta S/\delta X$ denote the corresponding functional derivatives with respect to the state variable X, interpreted as elements of the dual space associated with the state space. The first term represents the reversible part of the dynamics, while the second term accounts for irreversible processes. Thermodynamic consistency is ensured by structural properties of the operators $\mathcal{L}$ and $\mathcal{K}$. The operator $\mathcal{L}$ governing the reversible dynamics is assumed to be formally skew-adjoint with respect to the underlying duality pairing, i.e.

$$\langle \eta, \mathcal{L}\xi\rangle = -\langle \mathcal{L}\eta, \xi\rangle \qquad \forall\, \eta, \xi \text{ in the domain of } \mathcal{L}, \tag{4.2}$$

which implies conservation of total energy along the reversible flow. The operator $\mathcal{K}$ associated with irreversible processes is assumed to be formally self-adjoint and positive semi-definite, i.e.

$$\langle \eta, \mathcal{K}\xi\rangle = \langle \mathcal{K}\eta, \xi\rangle, \qquad \langle \xi, \mathcal{K}\xi\rangle \geq 0, \tag{4.3}$$

ensuring non-negative entropy production.[1] In addition, the operators are subject to the so-called non-interaction condition, i.e.

$$\mathcal{L}(X)\,\frac{\delta S(X)}{\delta X} = 0, \qquad \mathcal{K}(X)\,\frac{\delta E(X)}{\delta X} = 0, \tag{4.4}$$

which guarantees that the reversible dynamics does not contribute to entropy production and that irreversible processes do not alter the total energy. As a consequence, the GENERIC formulation satisfies the first and second laws of thermodynamics by construction, independent of the specific constitutive assumptions made for $\mathcal{L}$ and $\mathcal{K}$.

For a detailed treatment of the GENERIC framework and its applications, the reader is referred to [62, 66].

[1] At this stage, the notions of formal skew-adjointness of $\mathcal{L}$ and formal self-adjointness and positive semidefiniteness of $\mathcal{K}$ are understood purely in terms of the duality pairing between the state space and its dual. In particular, no inner product structure and no explicit adjoint operators are assumed at this point. Such additional structure will be introduced later when specializing the GENERIC framework and constructing concrete realizations and discretizations.

4.3. Continuum mechanical and thermodynamical preliminaries

In this Section, we introduce the continuum-mechanical and thermodynamic concepts required for the application to nonlinear thermo-mechanical problems.

4.3.1. Quantities of continuum mechanics

A continuous body Ω_0 is described in its reference configuration by material points $\mathbf{X} \in \Omega_0 \subset \mathbb{R}^3$ (see Fig. 4.1). Let $\mathcal{I} = [t_0, t_N] \subset \mathbb{R}$ denote a given time interval, with $t \in \mathcal{I}$. The motion of the body is characterized by a bijective mapping $\boldsymbol{\varphi} : \Omega_0 \times \mathcal{I} \to \mathbb{R}^3$, $\mathbf{x} = \boldsymbol{\varphi}(\mathbf{X}, t)$, which maps each material point $\mathbf{X}$ to its current position $\mathbf{x}$ in the spatial configuration. The corresponding current configuration is therefore given by $\Omega(t) = \boldsymbol{\varphi}(\Omega_0, t)$. The boundary of the body $\partial\Omega$ is disjointly decomposed into a Dirichlet and a Neumann part, i.e. $\partial\Omega = \partial_\varphi\Omega \cup \partial_t\Omega$ and $\partial_\varphi\Omega \cap \partial_t\Omega = \emptyset$, on which displacements $\bar{\boldsymbol{\varphi}}(t) \in \mathbb{R}^3$ and surface tractions $\bar{\mathbf{t}}(t) \in \mathbb{R}^3$ are prescribed, respectively. Additionally, there is a body force $\bar{\mathbf{b}}(t) \in \mathbb{R}^3$ acting on the body.

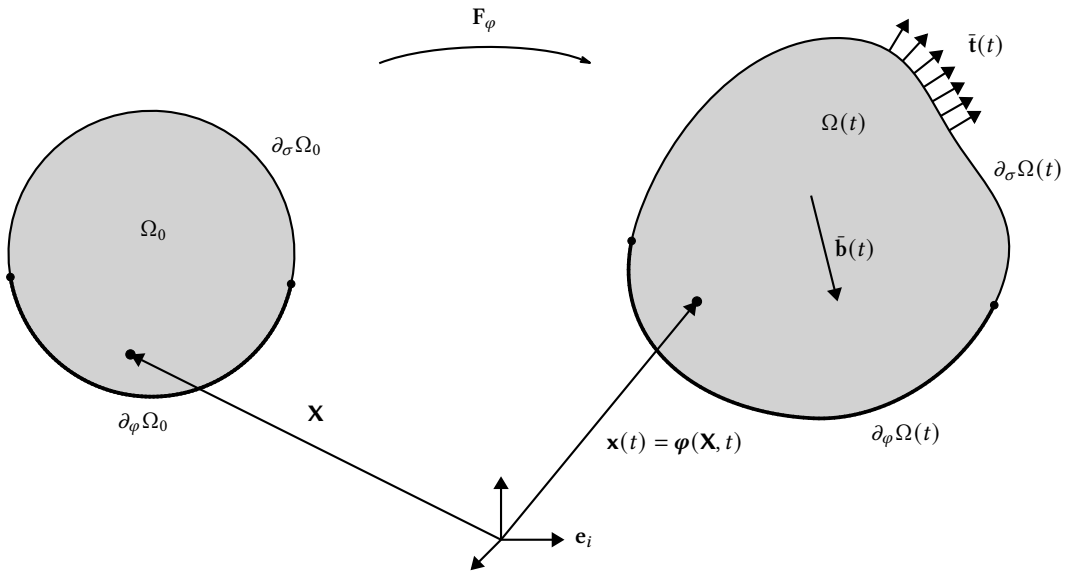


Figure 4.1.: Configuration and kinematics of a deformable body Ω with mechanical boundaries.

The deformation gradient $\mathbf{F}_\varphi$ given by

$$\mathrm{d}\mathbf{x} = \mathbf{F}_\varphi \mathrm{d}\mathbf{X}, \quad \mathbf{F}_\varphi = \nabla\boldsymbol{\varphi}(\mathbf{X}, t) \tag{4.5}$$

maps material line elements $\mathrm{d}\mathbf{X}$ to their spatial counterparts $\mathrm{d}\mathbf{x}$. Additionally, ∇ denotes the gradient with respect to the material coordinates.[2]

4.3.2. Tensor cross product and polyconvex energy density function

In the large-deformation regime, polyconvex stored energy density functions provide a well-established framework ensuring material stable (see e.g. [22, 30]). In the present work, we therefore assume that

[2] Note that the index $(\bullet)_\varphi$ indicates the dependency on the deformation map $\boldsymbol{\varphi}$ to explicitly distinguish deformation-dependent quantities from associated quantities of the mixed formulation dealt with in Section 4.4.

the elastic response is described by an objective representation of a polyconvex stored energy density function of the form

$$\chi = \chi(\mathbf{C}_\varphi, \mathbf{G}_\varphi, J_\varphi), \tag{4.6}$$

where $\mathbf{C}_\varphi$ denotes the right Cauchy-Green deformation tensor

$$\mathbf{C}_\varphi = \mathbf{F}_\varphi^\top \mathbf{F}_\varphi, \tag{4.7}$$

$\mathbf{G}_\varphi$ its cofactor, and J_φ the determinant of the deformation gradient. The usage of $\mathbf{C}_\varphi$ ensures objectivity of the energy functional, while the additional kinematic quantities $\mathbf{G}_\varphi$ and J_φ account for area and volume changes, respectively.

For a compact and numerically convenient representation of these quantities, we make use of the tensor cross product (cf. [10, 14]) between two second-order tensors $\mathbf{A}, \mathbf{B} \in \mathbb{R}^{3\times3}$, defined componentwise as

$$(\mathbf{A} \boxtimes \mathbf{B})_{ij} = \epsilon_{i\alpha\beta}\, \epsilon_{jab}\, A_{\alpha a} B_{\beta b}, \tag{4.8}$$

where ϵ_{ijk} denotes the third-order permutation tensor and Einstein summation is implied.

Using this definition, the cofactor of $\mathbf{C}_\varphi$ and the Jacobian of the deformation can be expressed as

$$\begin{aligned} \mathbf{G}_\varphi &= \operatorname{cof}(\mathbf{C}_\varphi) = \frac{1}{2}\mathbf{C}_\varphi \boxtimes \mathbf{C}_\varphi, \\ J_\varphi &= \det(\mathbf{F}_\varphi) = \frac{1}{6}(\mathbf{F}_\varphi \boxtimes \mathbf{F}_\varphi) : \mathbf{F}_\varphi = \sqrt{\det(\mathbf{C}_\varphi)}. \end{aligned} \tag{4.9}$$

Based on the introduced kinematic quantities and the polyconvex representation of the stored energy density , the total mechanical energy density of the system is defined as

$$e_{\text{mechancial}} = e_{\text{mechancial}}(\boldsymbol{\varphi}, \mathbf{v}, \mathbf{C}_\varphi, \mathbf{G}_\varphi, J_\varphi) = T(\mathbf{v}) + \chi(\mathbf{C}_\varphi, \mathbf{G}_\varphi, J_\varphi) + V(\boldsymbol{\varphi}), \tag{4.10}$$

where the kinetic energy density is given by $T(\mathbf{v}) = \frac{1}{2}\rho_0 \mathbf{v}\cdot\mathbf{v}$ with the reference mass density $\rho_0 = \rho_0(\mathbf{X})$ and the specific potential of external body forces by $V(\boldsymbol{\varphi}) = -\bar{\mathbf{b}} \cdot \boldsymbol{\varphi}$. The corresponding global energies read

$$\mathcal{E}_{\text{mech}} = \int_{\Omega_0} e_{\text{mech}}\, \mathrm{d}V, \quad \mathcal{T} = \int_{\Omega_0} T(\mathbf{v})\, \mathrm{d}V, \quad \mathcal{V} = \int_{\Omega_0} V(\boldsymbol{\varphi})\, \mathrm{d}V. \tag{4.11}$$

4.3.3. Thermodynamical quantities

In addition to the mechanical fields introduced above, the thermomechanical description of the body requires the specification of appropriate thermal state variables and boundary conditions. Figure 4.2 illustrates the thermal amendment of the mechanical setting shown in Fig. 4.1.

We consider a thermomechanical body that occupies the reference configuration Ω_0 and evolves over the time interval $\mathcal{I} = [t_0, t_N]$. The thermal state of the body is described by suitable thermodynamic fields defined per unit reference volume. Depending on the chosen thermodynamic representation, these may include the absolute temperature $\vartheta(\mathbf{X}, t)$, the internal energy density $u(\mathbf{X}, t)$, or the entropy density $\eta(\mathbf{X}, t)$.

Heat exchange with the environment occurs through the boundary $\partial\Omega_0$, which is disjointly decomposed into a thermal Dirichlet part $\partial_\theta\Omega_0$ and a thermal Neumann part $\partial_q\Omega_0$, such that $\partial\Omega_0 = \partial_\theta\Omega_0 \cup \partial_q\Omega_0$, $\partial_\theta\Omega_0 \cap \partial_q\Omega_0 = \emptyset$. On $\partial_\theta\Omega_0$, the temperature is prescribed as $\vartheta = \bar{\vartheta}(t)$, whereas on $\partial_q\Omega_0$ a heat flux $\bar{q}(t)$ is prescribed.

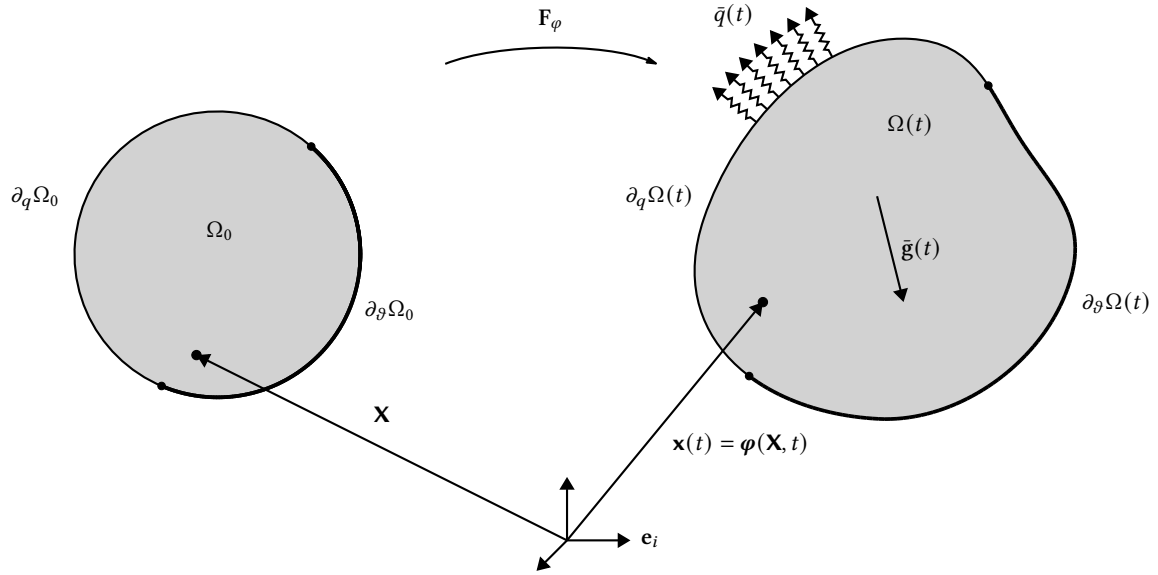


Figure 4.2.: Configuration and kinematics of a deformable body Ω with thermal boundaries.

In addition to the mechanical contributions introduced previously, the thermodynamic behavior of the system is characterized by a thermal energy contribution, which is assumed to depend on one of the suitable thermodynamic fields, e.g. the temperature field ϑ, yielding

$$\psi_{\text{thermal}} = \psi_{\text{thermal}}(\vartheta). \tag{4.12}$$

To account for interactions between mechanical and thermal fields, we introduce an additional coupling contribution

$$\psi_{\text{coupling}} = \psi_{\text{coupling}}(\mathbf{C}_\varphi, \mathbf{G}_\varphi, J_\varphi, \vartheta), \tag{4.13}$$

which represents energetic effects that depend simultaneously on mechanical and thermal state variables.

The Helmholtz free energy density ψ is introduced by augmenting the purely mechanical stored energy density χ with additional thermal and thermo-mechanical coupling contributions, i.e.

$$\psi = \psi(\mathbf{C}_\varphi, \mathbf{G}_\varphi, J_\varphi, \vartheta) = \chi(\mathbf{C}_\varphi, \mathbf{G}_\varphi, J_\varphi) + \psi_{\text{thermal}}(\vartheta) + \psi_{\text{coupling}}(\mathbf{C}_\varphi, \mathbf{G}_\varphi, J_\varphi, \vartheta), \tag{4.14}$$

which provides a natural additive decomposition into purely mechanical, purely thermal, and coupling contributions.

The internal energy density is obtained from the Helmholtz free energy density by the Legendre transformation

$$u = \psi + \vartheta\eta, \tag{4.15}$$

where $\eta = \eta(\mathbf{C}_\varphi, \mathbf{G}_\varphi, J_\varphi, \vartheta)$ is the systems entropy density. With the above, we are able to define the global internal energy and the global entropy as

$$\mathcal{U} = \int_{\Omega_0} u \, \mathrm{d}V, \quad \mathcal{S} = \int_{\Omega_0} \eta \, \mathrm{d}V. \tag{4.16}$$

The total energy density of the coupled thermomechanical system can then be written as

$$e = e(\boldsymbol{\varphi}, \mathbf{v}, \mathbf{C}_\varphi, \mathbf{G}_\varphi, J_\varphi, \vartheta) = T(\mathbf{v}) + u(\mathbf{C}_\varphi, \mathbf{G}_\varphi, J_\varphi, \vartheta) + V(\boldsymbol{\varphi}), \tag{4.17}$$

leading to the global counterpart

$$\mathcal{E} = \int_{\Omega_0} e \, \mathrm{d}V = \mathcal{T} + \mathcal{U} + \mathcal{V}. \tag{4.18}$$

4.4. The mixed GENERIC framework

This section introduces the fundamental framework underlying the development of the mixed GENERIC formulation. As a first step, a purely mechanical system is considered, which is based on a mixed Hu–Washizu functional with a polyconvex representation of the stored energy. The functional is reformulated in such a way that it can be consistently embedded into the mechanical part of the GENERIC formalism. Building on this mechanical core, the framework is subsequently extended to incorporate thermodynamic effects. The irreversible contribution of the GENERIC formulation is derived from the classical heat conduction equation. The resulting system of evolution equations finally leads to the weak form of the underlying mixed coupled thermo-mechanical initial-boundary value problem.

4.4.1. Hu-Washizu-type functional for $\{\mathrm{C}, \mathrm{G}, J\}$

We begin by formulating the governing equations for a purely mechanical elastic body within a Hu–Washizu-type variational setting. The construction is based on a mixed extension of Livens' principle [45] and employs a polyconvex stored energy density. The corresponding action functional is given by

$$\begin{aligned} \mathcal{F} = \int_{t_0}^{t_N} \int_{\Omega_0} \Big[& \frac{1}{2}\rho_0 \mathbf{v} \cdot \mathbf{v} - \chi\left(\mathbf{C}, \mathbf{G}, J\right) + \boldsymbol{\pi} \cdot \left(\dot{\boldsymbol{\varphi}} - \mathbf{v}\right) \\ & - \boldsymbol{\chi}_{\mathrm{C}} : \left(\mathbf{C}_{\varphi} - \mathbf{C}\right) - \boldsymbol{\chi}_{\mathrm{G}} : \left(\mathbf{G}_{\varphi} - \mathbf{G}\right) - \chi_J \left(J_{\varphi} - J\right) \Big] \, \mathrm{d}V \, \mathrm{d}t \\ & + \int_{t_0}^{t_N} \left[\int_{\Omega_0} \bar{\mathbf{b}} \cdot \boldsymbol{\varphi} \, \mathrm{d}V + \int_{\partial_\sigma \Omega_0} \bar{\mathbf{t}} \cdot \boldsymbol{\varphi} \, \mathrm{d}A \right] \mathrm{d}t. \end{aligned} \tag{4.19}$$

The primary unknowns consist of the deformation field $\boldsymbol{\varphi}$ and the velocity field $\mathbf{v}$, supplemented by the independent kinematic fields $\mathbf{C}$, $\mathbf{G}$, and J, which represent the right Cauchy–Green tensor, its cofactor, and the Jacobian of the deformation gradient, respectively.

The admissible displacement field is chosen from

$$V_{\varphi} = \left\{ \boldsymbol{\varphi} : \Omega_0 \to \mathbb{R}^3 | \varphi_i \in H^1(\Omega_0), \ \boldsymbol{\varphi} = \bar{\boldsymbol{\varphi}} \text{ on } \partial_{\varphi}\Omega_0 \right\}, \tag{4.20}$$

where $H^1(\Omega_0)$ denotes the Sobolev space of square-integrable functions with square-integrable first derivatives. The velocity field belongs to

$$V_v = \left\{ \mathbf{v} : \Omega_0 \to \mathbb{R}^3 | v_i \in H^1(\Omega_0), \ \mathbf{v} = \bar{\mathbf{v}} \text{ on } \partial_{\varphi}\Omega_0 \right\}. \tag{4.21}$$

The additional kinematic variables are defined on corresponding L^2-based function spaces

$$\begin{aligned} V_C = V_G &= \left\{ \mathbf{A} : \Omega_0 \to \mathbb{S} \,|\, A_{ij} \in L^2(\Omega_0) \right\} \\ V_J &= \left\{ J : \Omega_0 \to \mathbb{R}_+ \,|\, J \in L^2(\Omega_0) \right\}, \end{aligned} \tag{4.22}$$

where $\mathbb{S}$ is the space of symmetric 3×3 matrices and $L^2(\Omega_0)$ is the space of square-integrable functions on Ω_0. The consistency of the mixed kinematic fields with the deformation is enforced via Lagrange

multipliers, namely tensor-valued multipliers $\boldsymbol{\chi}_{\mathbf{C}} \in V_C$ and $\boldsymbol{\chi}_{\mathbf{G}} \in V_G$ for $\mathbf{C} \in V_C$ and $\mathbf{G} \in \mathcal{V}_G$ and a scalar multiplier $\chi_J \in V_J$ for $J \in V_J$.[3]

In the present Liven's based formulation, the velocity is introduced as an independent field and coupled to the time derivative of the deformation through the multiplier $\boldsymbol{\pi} \in \mathcal{V}_v$.

Stationarity of the functional $\mathcal{F}$ yields the Euler–Lagrange system. In particular, one obtains $\boldsymbol{\pi} = \rho_0 \mathbf{v}$, identifying $\boldsymbol{\pi}$ with the linear momentum density. The remaining stationarity conditions read

$$\left.\begin{aligned} \dot{\boldsymbol{\varphi}} &= \mathbf{v} \\ \rho_0\, \dot{\mathbf{v}} &= \mathrm{Div}(\mathbf{F}_\varphi \mathbf{S}_{\text{mechanical}}) + \bar{\mathbf{b}} \\ \boldsymbol{\chi}_{\mathbf{C}} &= \partial_{\mathbf{C}} \chi(\mathbf{C}, \mathbf{G}, J) \\ \boldsymbol{\chi}_{\mathbf{G}} &= \partial_{\mathbf{G}} \chi(\mathbf{C}, \mathbf{G}, J) \\ \chi_J &= \partial_J \chi(\mathbf{C}, \mathbf{G}, J) \\ \mathbf{C} &= \mathbf{C}_\varphi \\ \mathbf{G} &= \mathbf{G}_\varphi \\ J &= J_\varphi \end{aligned}\right\} \text{ in } \Omega_0 \times \mathcal{I}. \tag{4.23}$$

The associated second Piola–Kirchhoff stress tensor is given by

$$\mathbf{S}_{\text{mechanical}} = 2\boldsymbol{\chi}_{\mathbf{C}} + 2\boldsymbol{\chi}_{\mathbf{G}} \barwedge \mathbf{C}_\varphi + \frac{\chi_J}{J_\varphi} \mathbf{G}_\varphi. \tag{4.24}$$

The formulation implies the natural boundary condition

$$\mathbf{F}_\varphi \mathbf{S}_{\text{mechanical}} \mathbf{N} = \bar{\mathbf{t}}_{\text{mechanical}} \quad \text{on } \partial_\sigma \Omega_0 \tag{4.25}$$

with $\mathbf{N}$ denoting the outward unit normal vector on the Neumann boundary $\partial_\sigma \Omega_0$.

4.4.2. Special form of GENERIC

To incorporate the mixed mechanical framework into the GENERIC setting, we recall the special form introduced by [56], in which the operators $\mathcal{L}$ and $\mathcal{K}$ in (4.1) are represented as

$$\mathcal{L} = \mathcal{M}_{\mathcal{S}} \mathcal{L}_0 \mathcal{M}_{\mathcal{S}}^*, \quad \mathcal{K} = \mathcal{M}_{\mathcal{E}} \mathcal{K}_0 \mathcal{M}_{\mathcal{E}}^*, \tag{4.26}$$

such that the GENERIC evolution equation reads

$$\dot{X} = \mathcal{M}_{\mathcal{S}} \mathcal{L}_0 \mathcal{M}_{\mathcal{S}}^* \mathrm{D}\mathcal{E}(X) + \mathcal{M}_{\mathcal{E}} \mathcal{K}_0 \mathcal{M}_{\mathcal{E}}^* \mathrm{D}\mathcal{S}(X). \tag{4.27}$$

The state vector is decomposed as $X = [\xi, \tau]^\top$, where ξ collects the mechanical variables $\xi = [\boldsymbol{\varphi}, \mathbf{p}, \mathbf{C}, \mathbf{G}, J]^\top$ and τ denotes a general thermodynamic scalar variable. Depending on the modeling context, τ may represent the absolute temperature ϑ, the internal energy u, or the entropy η.

The representation (4.27) enables a systematic transformation between different thermodynamic descriptions. While the transformation operators $\mathcal{M}_\square$ follow from the chosen thermodynamic variable, the construction of the canonical operators $\mathcal{L}_0$ and $\mathcal{K}_0$ reflects the intrinsic physical structure of the system.

[3] While Lagrange multipliers are classically denoted by λ, the present notation is chosen to reflect their connection to specific partial derivatives. As follows from the Euler–Lagrange equations (4.23), the multipliers in the purely mechanical setting are given by the corresponding partial derivatives of the stored energy. In the thermomechanical extension, these quantities become derivatives of the internal energy. This anticipates the analogy to the mixed variables introduced later, which are associated with derivatives of the entropy.

4.4.2.1. Reversible part

We first consider the reversible contribution

$$\dot{X} = \mathcal{M}_{\mathcal{S}} \mathcal{L}_0 \mathcal{M}_{\mathcal{S}}^* \mathrm{D}\mathcal{E}(X), \tag{4.28}$$

where the variational derivatives of the total energy read

$$\mathrm{D}\mathcal{E}(X) = \begin{bmatrix} \delta_{\boldsymbol{\varphi}} \mathcal{V} \\ \delta_{\mathrm{p}} \mathcal{T} \\ \delta_{\mathrm{C}} \mathcal{U} \\ \delta_{\mathrm{G}} \mathcal{U} \\ \delta_J \mathcal{U} \\ \delta_\tau \mathcal{U} \end{bmatrix} = \begin{bmatrix} -\bar{\mathbf{b}} \\ \mathbf{v} \\ \partial_{\mathrm{C}} u \\ \partial_{\mathrm{G}} u \\ \partial_J u \\ \partial_\tau u \end{bmatrix}. \tag{4.29}$$

The operator $\mathcal{L}$ attains its canonical form $\mathcal{L}_0$ when the entropy η is chosen as thermodynamic variable, i.e.,

$$\dot{X}' = \mathcal{L}_0 \mathrm{D}\mathcal{E}'(X'), \qquad X' = [\xi, \eta]^\top. \tag{4.30}$$

In this case, the mixed mechanical system (4.23) can be rewritten in rate form and extended by the entropy variable. Note that since we now consider a thermomechanical system, instead of the stored energy density χ, the internal energy density u is used. Due to the non-interaction condition $\mathcal{L}_0 \mathrm{D}\mathcal{S}' = 0$, the reversible dynamics does not contribute to entropy evolution, yielding the trivial identity $\dot{\eta} = 0$. This manifests itself as a vanishing row in the operator representation. Consequently, (4.23) gives rise to

$$\begin{aligned} \dot{\boldsymbol{\varphi}} &= \mathbf{v} \\ \rho_0 \dot{\mathbf{v}} &= \mathrm{Div}(2\mathbf{F}_\varphi \partial_{\mathrm{C}} u) + \mathrm{Div}(2\mathbf{F}_\varphi (\partial_{\mathrm{G}} u \barwedge \mathbf{C}_\varphi)) \\ &\quad + \mathrm{Div}(\partial_J u J_\varphi^{-1} \mathbf{F}_\varphi \mathbf{G}_\varphi) + \bar{\mathbf{b}} \\ \dot{\mathbf{C}} &= 2\,\mathrm{sym}(\mathbf{F}_\varphi^\top \nabla \mathbf{v}) \\ \dot{\mathbf{G}} &= \mathbf{C}_\varphi \barwedge 2\,\mathrm{sym}(\mathbf{F}_\varphi^\top \nabla \mathbf{v}) \\ \dot{J} &= J_\varphi^{-1} \mathbf{G}_\varphi : \mathrm{sym}(\mathbf{F}_\varphi^\top \nabla \mathbf{v}) \\ \dot{\eta} &= 0. \end{aligned} \tag{4.31}$$

Now, the operator $\mathcal{L}_0$ can be inferred from (4.30) and (4.31) leading to

$$\mathcal{L}_0(\boldsymbol{\varphi}, \eta) = \begin{bmatrix} 0 & I & 0 & 0 & 0 & 0 \\ -I & 0 & \mathrm{Div}(2\mathbf{F}_\varphi \square) & \mathrm{Div}(2\mathbf{F}_\varphi (\square \barwedge \mathbf{C}_\varphi)) & \mathrm{Div}(J_\varphi^{-1} \mathbf{F}_\varphi \mathbf{G}_\varphi \square) & 0 \\ 0 & 2\,\mathrm{sym}(\mathbf{F}_\varphi^\top \nabla(\square)) & 0 & 0 & 0 & 0 \\ 0 & 2\mathbf{C}_\varphi \barwedge \mathrm{sym}(\mathbf{F}_\varphi^\top \nabla(\square)) & 0 & 0 & 0 & 0 \\ 0 & J_\varphi^{-1} \mathbf{G}_\varphi : \mathrm{sym}(\mathbf{F}_\varphi^\top \nabla(\square)) & 0 & 0 & 0 & 0 \\ 0 & 0 & 0 & 0 & 0 & 0 \end{bmatrix}, \tag{4.32}$$

where the symbol $\square$ denotes the argument slot of the corresponding operator entry, which is occupied by the associated component of the variational derivative $\mathrm{D}\mathcal{E}$.

To express the operator $\mathcal{L}$ with respect to a general thermodynamic variable τ, we introduce the constitutive relation

$$\eta = \eta(\mathbf{C}, \mathbf{G}, J, \tau), \tag{4.33}$$

which is assumed to be sufficiently smooth and invertible with respect to τ.

The transformation from the entropy-based variables X' to X induces, via the chain rule, the relation

$$\dot{\eta} = \partial_{\mathrm{C}}\eta : \dot{\mathbf{C}} + \partial_{\mathrm{G}}\eta : \dot{\mathbf{G}} + \partial_J\eta\, \dot{J} + \partial_\tau\eta\, \dot{\tau}, \tag{4.34}$$

which yields

$$\dot{\tau} = \frac{1}{\partial_\tau\eta}\left(\dot{\eta} - \partial_{\mathrm{C}}\eta : \dot{\mathbf{C}} - \partial_{\mathrm{G}}\eta : \dot{\mathbf{G}} - \partial_J\eta\, \dot{J}\right). \tag{4.35}$$

This defines the transformation of state rates in operator form as

$$\dot{X} = \mathcal{M}_{\mathcal{S}}\dot{X}', \tag{4.36}$$

with

$$\mathcal{M}_{\mathcal{S}} = \begin{bmatrix} I & 0 & 0 & 0 & 0 & 0 \\ 0 & I & 0 & 0 & 0 & 0 \\ 0 & 0 & I & 0 & 0 & 0 \\ 0 & 0 & 0 & I & 0 & 0 \\ 0 & 0 & 0 & 0 & I & 0 \\ 0 & 0 & -\frac{\partial_{\mathrm{C}}\eta}{\partial_\tau\eta} & -\frac{\partial_{\mathrm{G}}\eta}{\partial_\tau\eta} & -\frac{\partial_J\eta}{\partial_\tau\eta} & \frac{1}{\partial_\tau\eta} \end{bmatrix}. \tag{4.37}$$

The corresponding adjoint operator $\mathcal{M}_{\mathcal{S}}^*$ with respect to the duality pairing is defined by

$$\langle \mathrm{D}\mathcal{E}(X), \dot{X}\rangle = \langle \mathcal{M}_{\mathcal{S}}^*\mathrm{D}\mathcal{E}(X), \dot{X}'\rangle, \tag{4.38}$$

yielding

$$\mathcal{M}_{\mathcal{S}}^* = \begin{bmatrix} I & 0 & 0 & 0 & 0 & 0 \\ 0 & I & 0 & 0 & 0 & 0 \\ 0 & 0 & I & 0 & 0 & -\frac{\partial_{\mathrm{C}}\eta}{\partial_\tau\eta} \\ 0 & 0 & 0 & I & 0 & -\frac{\partial_{\mathrm{G}}\eta}{\partial_\tau\eta} \\ 0 & 0 & 0 & 0 & I & -\frac{\partial_J\eta}{\partial_\tau\eta} \\ 0 & 0 & 0 & 0 & 0 & \frac{1}{\partial_\tau\eta} \end{bmatrix}. \tag{4.39}$$

Finally, the transformed reversible operator is given by

$$\begin{aligned} \mathcal{L}(\boldsymbol{\varphi}, \tau) &= \mathcal{M}_{\mathcal{S}}\mathcal{L}_0(\boldsymbol{\varphi}, \eta)\mathcal{M}_{\mathcal{S}}^* \\ &= \begin{bmatrix} 0 & I & 0 & 0 & 0 & 0 \\ -I & 0 & \mathrm{Div}(2\mathbf{F}_\varphi\square) & \mathrm{Div}(2\mathbf{F}_\varphi(\square \barwedge \mathbf{C}_\varphi)) & \mathrm{Div}(J_\varphi^{-1}\mathbf{F}_\varphi\mathbf{G}_\varphi\square) & A(\square) \\ 0 & 2\,\mathrm{sym}(\mathbf{F}_\varphi^\top\nabla(\square)) & 0 & 0 & 0 & 0 \\ 0 & 2\mathbf{C}_\varphi \barwedge \mathrm{sym}(\mathbf{F}_\varphi^\top\nabla(\square)) & 0 & 0 & 0 & 0 \\ 0 & J_\varphi^{-1}\mathbf{G}_\varphi : \mathrm{sym}(\mathbf{F}_\varphi^\top\nabla(\square)) & 0 & 0 & 0 & 0 \\ 0 & B(\square) & 0 & 0 & 0 & 0 \end{bmatrix}, \end{aligned} \tag{4.40}$$

where $A(\square)$ and $B(\square)$ are given as

$$A(\square) = -\mathrm{Div}\left(\frac{\square}{\partial_\tau\eta}2\mathbf{F}_\varphi\partial_{\mathrm{C}}\eta + \frac{\square}{\partial_\tau\eta}2\mathbf{F}_\varphi(\partial_{\mathrm{G}}\eta \barwedge \mathbf{C}_\varphi) + \frac{\square}{\partial_\tau\eta}J_\varphi^{-1}\mathbf{F}_\varphi\mathbf{G}_\varphi\partial_J\eta\right), \tag{4.41}$$

and

$$\begin{aligned} B(\square) = &-\frac{\partial_{\mathrm{C}}\eta}{\partial_\tau\eta} : \left[2\,\mathrm{sym}(\mathbf{F}_\varphi^\top\nabla(\square))\right] - \frac{\partial_{\mathrm{G}}\eta}{\partial_\tau\eta} : \left[\mathbf{C}_\varphi \barwedge 2\,\mathrm{sym}(\mathbf{F}_\varphi^\top\nabla(\square))\right] \\ &- \frac{\partial_J\eta}{\partial_\tau\eta}J_\varphi^{-1}\mathbf{G}_\varphi : \mathrm{sym}(\mathbf{F}_\varphi^\top\nabla(\square)). \end{aligned} \tag{4.42}$$

This construction preserves the GENERIC structure. In particular, the skew-adjointness of $\mathcal{L}$ is retained, and the additional coupling terms can be directly attributed to the dependence of the entropy on the kinematic variables.

4.4.2.2. Irreversible part

In analogy to the reversible contribution, we now consider the irreversible part of the dynamics, given by

$$\dot{X} = \mathcal{M}_{\mathcal{E}} \mathcal{K}_0 \mathcal{M}_{\mathcal{E}}^{*} \, \mathrm{D}\mathcal{S}(X), \tag{4.43}$$

where the functional derivative of the systems total entropy is given by

$$\mathrm{D}\mathcal{S}(X) = \begin{bmatrix} \delta_{\boldsymbol{\varphi}}\mathcal{S} \\ \delta_{\mathrm{p}}\mathcal{S} \\ \delta_{\mathrm{C}}\mathcal{S} \\ \delta_{\mathrm{G}}\mathcal{S} \\ \delta_{J}\mathcal{S} \\ \delta_{\tau}\mathcal{S} \end{bmatrix} = \begin{bmatrix} 0 \\ 0 \\ \partial_{\mathrm{C}}\eta \\ \partial_{\mathrm{G}}\eta \\ \partial_{J}\eta \\ \partial_{\tau}\eta \end{bmatrix}. \tag{4.44}$$

The operator $\mathcal{K}$ attains its canonical representation $\mathcal{K}_0$ when the total energy density e is chosen as thermodynamic variable, i.e.

$$\dot{X}'' = \mathcal{K}_0 \mathrm{D}\mathcal{S}''(X''), \qquad X'' = [\xi, e]^{\top}. \tag{4.45}$$

The non-interaction condition $\mathcal{K}_0 \mathrm{D}\mathcal{E}'' = 0$ ensures that the irreversible dynamics does not contribute to the evolution of the total energy.

In the absence of mechanical dissipation mechanisms, the irreversible part reduces to a heat conduction model of Fourier type. The corresponding canonical operator is given by

$$\mathcal{K}_0(\boldsymbol{\varphi}, e) = \begin{bmatrix} 0 & 0 & 0 & 0 & 0 & 0 \\ 0 & 0 & 0 & 0 & 0 & 0 \\ 0 & 0 & 0 & 0 & 0 & 0 \\ 0 & 0 & 0 & 0 & 0 & 0 \\ 0 & 0 & 0 & 0 & 0 & 0 \\ 0 & 0 & 0 & 0 & 0 & K_{\mathrm{heat}}(\square) \end{bmatrix}, \tag{4.46}$$

where the heat conduction operator is defined by

$$K_{\mathrm{heat}}(\square) = -\mathrm{Div}\big(\tilde{\mathbf{K}} \nabla(\square)\big), \qquad \tilde{\mathbf{K}} = (\Theta)^2 \, \mathbf{K}_{\mathrm{H}}, \qquad \mathbf{K}_{\mathrm{H}} = k J_{\varphi} \mathbf{C}_{\varphi}^{-1} = k \, J_{\varphi}^{-1} \, \mathbf{G}_{\varphi}, \tag{4.47}$$

k is the coefficient of thermal conductivity, and

$$\Theta = \frac{1}{\partial_e \eta} = \frac{1}{\partial_u \eta}. \tag{4.48}$$

The constitutive relation

$$e = e(\boldsymbol{\varphi}, \mathbf{p}, \mathbf{C}, \mathbf{G}, J, \tau) \tag{4.49}$$

is assumed to be sufficiently smooth and locally invertible with respect to τ. Applying the chain rule yields

$$\dot{e} = \partial_{\varphi} e \cdot \dot{\boldsymbol{\varphi}} + \partial_{p} e \cdot \dot{\mathbf{p}} + \partial_{\mathrm{C}} e : \dot{\mathbf{C}} + \partial_{\mathrm{G}} e : \dot{\mathbf{G}} + \partial_{J} e \, \dot{J} + \partial_{\tau} e \, \dot{\tau}, \tag{4.50}$$

which can be rewritten as

$$\dot{\tau} = \frac{1}{\partial_{\tau} e} \big(\dot{e} - \partial_{\varphi} e \cdot \dot{\boldsymbol{\varphi}} - \partial_{p} e \cdot \dot{\mathbf{p}} - \partial_{\mathrm{C}} e : \dot{\mathbf{C}} - \partial_{\mathrm{G}} e : \dot{\mathbf{G}} - \partial_{J} e \, \dot{J} \big). \tag{4.51}$$

The corresponding transformation of variables is encoded via the operators $\mathcal{M}_{\mathcal{E}}$ and $\mathcal{M}_{\mathcal{E}}^*$, which are given by

$$\mathcal{M}_{\mathcal{E}} = \begin{bmatrix} I & 0 & 0 & 0 & 0 & 0 \\ 0 & I & 0 & 0 & 0 & 0 \\ 0 & 0 & I & 0 & 0 & 0 \\ 0 & 0 & 0 & I & 0 & 0 \\ 0 & 0 & 0 & 0 & I & 0 \\ -\frac{\partial_\varphi e}{\partial_\tau e} & -\frac{\partial_p e}{\partial_\tau e} & -\frac{\partial_{\mathrm{C}} e}{\partial_\tau e} & -\frac{\partial_{\mathrm{G}} e}{\partial_\tau e} & -\frac{\partial_J e}{\partial_\tau e} & \frac{1}{\partial_\tau e} \end{bmatrix}, \tag{4.52}$$

$$\mathcal{M}_{\mathcal{E}}^* = \begin{bmatrix} I & 0 & 0 & 0 & 0 & -\frac{\partial_\varphi e}{\partial_\tau e} \\ 0 & I & 0 & 0 & 0 & -\frac{\partial_p e}{\partial_\tau e} \\ 0 & 0 & I & 0 & 0 & -\frac{\partial_{\mathrm{C}} e}{\partial_\tau e} \\ 0 & 0 & 0 & I & 0 & -\frac{\partial_{\mathrm{G}} e}{\partial_\tau e} \\ 0 & 0 & 0 & 0 & I & -\frac{\partial_J e}{\partial_\tau e} \\ 0 & 0 & 0 & 0 & 0 & \frac{1}{\partial_\tau e} \end{bmatrix}. \tag{4.53}$$

The transformed irreversible operator is then obtained as

$$\mathcal{K}(\boldsymbol{\varphi}, \tau) = \mathcal{M}_{\mathcal{E}} \mathcal{K}_0(\boldsymbol{\varphi}, e) \mathcal{M}_{\mathcal{E}}^*, \tag{4.54}$$

which preserves the block-diagonal structure of the dissipation mechanism and results in a heat conduction operator of the form

$$\mathcal{K}(\boldsymbol{\varphi}, \tau) = \begin{bmatrix} 0 & 0 & 0 & 0 & 0 & 0 \\ 0 & 0 & 0 & 0 & 0 & 0 \\ 0 & 0 & 0 & 0 & 0 & 0 \\ 0 & 0 & 0 & 0 & 0 & 0 \\ 0 & 0 & 0 & 0 & 0 & 0 \\ 0 & 0 & 0 & 0 & 0 & \frac{1}{\partial_\tau e} K_{\mathrm{heat}}\left(\frac{\square}{\partial_\tau e}\right) \end{bmatrix}. \tag{4.55}$$

4.4.2.3. GENERIC form of the local field equations and associated weak form

With the results gained in Sections 4.4.2.1 and 4.4.2.2, a more explicit form of (4.27) can be written as

$$\begin{aligned} \dot{\boldsymbol{\varphi}} &= \mathbf{v} \\ \dot{\mathbf{p}} &= \mathrm{Div}(\mathbf{F}_\varphi \mathbf{S}) + \bar{\mathbf{b}} \\ \dot{\mathbf{C}} &= 2\,\mathrm{sym}(\mathbf{F}_\varphi^\top \nabla \mathbf{v}) \\ \dot{\mathbf{G}} &= \mathbf{C}_\varphi \overset{\otimes}{\cdot} 2\,\mathrm{sym}(\mathbf{F}_\varphi^\top \nabla \mathbf{v}) \\ \dot{J} &= J_\varphi^{-1} \mathbf{G}_\varphi : \mathrm{sym}(\mathbf{F}_\varphi^\top \nabla \mathbf{v}) \\ \dot{\tau} &= -\frac{1}{\partial_\tau \eta} \partial_{\mathrm{C}} \eta : \left[2\,\mathrm{sym}(\mathbf{F}_\varphi^\top \nabla(\mathbf{v}))\right] - \frac{1}{\partial_\tau \eta} \partial_{\mathrm{G}} \eta : \left[\mathbf{C}_\varphi \overset{\otimes}{\cdot} 2\,\mathrm{sym}(\mathbf{F}_\varphi^\top \nabla(\mathbf{v}))\right] \\ &\quad - \frac{1}{\partial_\tau \eta} \partial_J \eta J_\varphi^{-1} \mathbf{G}_\varphi : \mathrm{sym}(\mathbf{F}_\varphi \nabla \mathbf{v}) - \frac{1}{\partial_\tau e} \mathrm{Div}(\mathbf{Q}). \end{aligned} \tag{4.56}$$

In this set of equations, the second Piola Kirchhoff stress tensor $\mathbf{S}$ assumes the form

$$\mathbf{S} = 2\partial_{\mathrm{C}} u + 2\partial_{\mathrm{G}} u \overset{\otimes}{\cdot} \mathbf{C}_\varphi + J_\varphi^{-1} \mathbf{G}_\varphi \partial_J u - \Theta\left(2\partial_{\mathrm{C}} \eta + 2\partial_{\mathrm{G}} \eta \overset{\otimes}{\cdot} \mathbf{C}_\varphi + J_\varphi^{-1} \mathbf{G}_\varphi \partial_J \eta\right) \tag{4.57}$$

and the heat flux vector $\mathbf{Q}$ is given by

$$\mathbf{Q} = \Theta^2 k J_\varphi^{-1} \mathbf{G}_\varphi \nabla(\frac{1}{\Theta}). \tag{4.58}$$

The attentive reader may notice a certain analogy in (4.57) between the three terms involving partial derivatives of the internal energy density u and the three terms involving partial derivatives of the entropy density η. The second Piola–Kirchhoff stress tensor retains the same structural form as in the corresponding minimal (or non-mixed) formulation (cf. [56]), namely

$$\mathbf{S} = 2\,(\partial_{\mathbf{C}_\varphi} u - \Theta\,\partial_{\mathbf{C}_\varphi} \eta), \tag{4.59}$$

where in our mixed formulation $\partial_{\mathbf{C}_\varphi} \square = \partial_{\mathbf{C}} \square + \partial_{\mathbf{G}} \square \barwedge \mathbf{C}_\varphi + {}^1\!/_2 J_\varphi^{-1} \mathbf{G}_\varphi \partial_J \square$.

In the next step we introduce the weak form associated with the GENERIC type strong form presented in (4.56). Before proceeding with the standard derivation of the weak formulation, the system of equations in (4.56) is augmented by additional constitutive relations. To this end, we introduce the Lagrange-type quantities $\mathbf{u}_\mathbf{C}$, $\mathbf{u}_\mathbf{G}$, and u_J, associated with the partial derivatives of the internal energy with respect to the kinematic variables $\mathbf{C}$, $\mathbf{G}$, and J, respectively. These quantities take over the role previously played by the multipliers $\boldsymbol{\chi}_\mathbf{C}$, $\boldsymbol{\chi}_\mathbf{G}$, and χ_J in the purely mechanical setting. In addition, the scalar-valued multiplier u_τ is introduced to represent the partial derivative of the internal energy with respect to the thermodynamic variable τ. Analogously, we introduce additional Lagrange-type quantities $\boldsymbol{\eta}_\mathbf{C}$, $\boldsymbol{\eta}_\mathbf{G}$, η_J, and η_τ, corresponding to the partial derivatives of the entropy with respect to its arguments. Altogether, this extends the set of equations (4.56) to the following coupled system:

$$\begin{aligned}
\dot{\boldsymbol{\varphi}} &= \mathbf{v} \\
\dot{\mathbf{p}} &= \mathrm{Div}(\mathbf{F}_\varphi \mathbf{S}) + \bar{\mathbf{b}} \\
\dot{\mathbf{C}} &= 2\,\mathrm{sym}(\mathbf{F}_\varphi^\top \nabla \mathbf{v}) \\
\dot{\mathbf{G}} &= \mathbf{C}_\varphi \barwedge 2\,\mathrm{sym}(\mathbf{F}_\varphi^\top \nabla \mathbf{v}) \\
\dot{J} &= J_\varphi^{-1} \mathbf{G}_\varphi : \mathrm{sym}(\mathbf{F}_\varphi^\top \nabla \mathbf{v}) \\
\dot{\tau} &= -\frac{1}{\eta_\tau} \boldsymbol{\eta}_\mathbf{C} : \big[2\,\mathrm{sym}(\mathbf{F}_\varphi^\top \nabla \mathbf{v})\big] - \frac{1}{\eta_\tau} \boldsymbol{\eta}_\mathbf{G} : \big[\mathbf{C}_\varphi \barwedge 2\,\mathrm{sym}(\mathbf{F}_\varphi^\top \nabla \mathbf{v})\big] \\
&\quad - \frac{1}{\eta_\tau} \eta_J J_\varphi^{-1} \mathbf{G}_\varphi : \mathrm{sym}(\mathbf{F}_\varphi^\top \nabla \mathbf{v}) - \frac{1}{u_\tau} \mathrm{Div}(\mathbf{Q}) \\
\mathbf{u}_\mathbf{C} &= \partial_\mathbf{C} u(\mathbf{C}, \mathbf{G}, J, \tau) \\
\mathbf{u}_\mathbf{G} &= \partial_\mathbf{G} u(\mathbf{C}, \mathbf{G}, J, \tau) \\
u_J &= \partial_J u(\mathbf{C}, \mathbf{G}, J, \tau) \\
u_\tau &= \partial_\tau u(\mathbf{C}, \mathbf{G}, J, \tau) \\
\boldsymbol{\eta}_\mathbf{C} &= \partial_\mathbf{C} \eta(\mathbf{C}, \mathbf{G}, J, \tau) \\
\boldsymbol{\eta}_\mathbf{G} &= \partial_\mathbf{G} \eta(\mathbf{C}, \mathbf{G}, J, \tau) \\
\eta_J &= \partial_J \eta(\mathbf{C}, \mathbf{G}, J, \tau) \\
\eta_\tau &= \partial_\tau \eta(\mathbf{C}, \mathbf{G}, J, \tau),
\end{aligned} \tag{4.60}$$

where the second Piola Kirchhoff stress tensor $\mathbf{S}$ is reformulated as

$$\mathbf{S} = 2\mathbf{u}_\mathbf{C} + 2\mathbf{u}_\mathbf{G} \barwedge \mathbf{C}_\varphi + J_\varphi^{-1} \mathbf{G}_\varphi u_J - \Theta\big(2\boldsymbol{\eta}_\mathbf{C} + 2\boldsymbol{\eta}_\mathbf{G} \barwedge \mathbf{C}_\varphi + J_\varphi^{-1} \mathbf{G}_\varphi \eta_J\big). \tag{4.61}$$

In (4.58) and (4.61), Θ is computed by

$$\Theta = \frac{u_\tau}{\eta_\tau}. \tag{4.62}$$

Subsequently, the standard steps leading to the weak formulation corresponding to (4.60) are carried out. To this end, the equations in (4.60) are multiplied by admissible test functions and integrated over the reference configuration Ω_0. Moreover, integration by parts is applied to the balance of linear momentum $(4.60)_2$ and the thermal evolution equation $(4.60)_6$ in order to transfer spatial derivatives onto the corresponding test functions and to naturally incorporate the associated Neumann boundary conditions. Altogether, this yields $\dot{\boldsymbol{\varphi}} = \mathbf{v}$ as well as the following weak form:

$$
\begin{aligned}
&\int_{\Omega_0} \mathbf{w}_{\boldsymbol{\varphi}} \cdot \rho_0 \dot{\mathbf{v}} + \operatorname{sym}(\mathbf{F}_\varphi^\top \nabla \mathbf{w}_{\boldsymbol{\varphi}}) : \mathbf{S} - \mathbf{w}_{\boldsymbol{\varphi}} \cdot \bar{\mathbf{b}} \, \mathrm{d}V - \int_{\partial_\sigma \Omega_0} \mathbf{w}_{\boldsymbol{\varphi}} \cdot \bar{\mathbf{t}} \, \mathrm{d}A = 0 \\
&\int_{\Omega_0} w_\tau \dot{\tau} + \frac{w_\tau}{\eta_\tau} \boldsymbol{\eta}_\mathrm{C} : \left[2 \operatorname{sym}(\mathbf{F}_\varphi^\top \nabla \mathbf{v}) \right] + \frac{w_\tau}{\eta_\tau} \boldsymbol{\eta}_\mathrm{G} : \left[\mathbf{C}_\varphi \barwedge 2 \operatorname{sym}(\mathbf{F}_\varphi^\top \nabla \mathbf{v}) \right] \\
&\qquad + \frac{w_\tau}{\eta_\tau} \eta_J J_\varphi^{-1} \mathbf{G}_\varphi : \operatorname{sym}(\mathbf{F}_\varphi^\top \nabla \mathbf{v}) - \nabla \Big(\frac{w_\tau}{u_\tau} \Big) \cdot \mathbf{Q} \, \mathrm{d}V - \int_{\partial_\sigma \Omega_0} w_\tau \bar{q} \, \mathrm{d}A = 0 \\
&\int_{\Omega_0} \mathbf{w}_\mathrm{C} : \left[\dot{\mathbf{C}} - 2 \operatorname{sym}(\mathbf{F}_\varphi^\top \nabla \mathbf{v}) \right] \mathrm{d}V = 0 \\
&\int_{\Omega_0} \mathbf{w}_\mathrm{G} : \left[\dot{\mathbf{G}} - 2 \mathbf{C}_\varphi \barwedge \operatorname{sym}(\mathbf{F}_\varphi^\top \nabla \mathbf{v}) \right] \mathrm{d}V = 0 \\
&\int_{\Omega_0} w_J \left[\dot{J} - J_\varphi^{-1} \mathbf{G}_\varphi : \operatorname{sym}(\mathbf{F}_\varphi^\top \nabla \mathbf{v}) \right] \mathrm{d}V = 0 \\
&\int_{\Omega_0} \mathbf{w}_{\boldsymbol{u}_\mathrm{C}} : \left[\mathbf{u}_\mathrm{C} - \partial_\mathrm{C} u(\mathbf{C}, \mathbf{G}, J, \tau) \right] \mathrm{d}V = 0 \\
&\int_{\Omega_0} \mathbf{w}_{\boldsymbol{u}_\mathrm{G}} : \left[\mathbf{u}_\mathrm{G} - \partial_\mathrm{G} u(\mathbf{C}, \mathbf{G}, J, \tau) \right] \mathrm{d}V = 0 \\
&\int_{\Omega_0} w_{u_J} \left[u_J - \partial_J u(\mathbf{C}, \mathbf{G}, J, \tau) \right] \mathrm{d}V = 0 \\
&\int_{\Omega_0} w_{u_\tau} \left[u_\tau - \partial_\tau u(\mathbf{C}, \mathbf{G}, J, \tau) \right] \mathrm{d}V = 0 \\
&\int_{\Omega_0} \mathbf{w}_{\boldsymbol{\eta}_\mathrm{C}} : \left[\boldsymbol{\eta}_\mathrm{C} - \partial_\mathrm{C} \eta(\mathbf{C}, \mathbf{G}, J, \tau) \right] \mathrm{d}V = 0 \\
&\int_{\Omega_0} \mathbf{w}_{\boldsymbol{\eta}_\mathrm{G}} : \left[\boldsymbol{\eta}_\mathrm{G} - \partial_\mathrm{G} \eta(\mathbf{C}, \mathbf{G}, J, \tau) \right] \mathrm{d}V = 0 \\
&\int_{\Omega_0} w_{\eta_J} \left[\eta_J - \partial_J \eta(\mathbf{C}, \mathbf{G}, J, \tau) \right] \mathrm{d}V = 0 \\
&\int_{\Omega_0} w_{\eta_\tau} \left[\eta_\tau - \partial_\tau \eta(\mathbf{C}, \mathbf{G}, J, \tau) \right] \mathrm{d}V = 0.
\end{aligned}
\tag{W}
$$

Note that, for the sake of clarity and readability, the ordering of the equations in the weak formulation (W) has been rearranged compared to the corresponding strong form (4.60).

The Neumann-type boundary data are given by the mechanical traction vector $\bar{\mathbf{t}}$, prescribed on $\partial_\sigma \Omega_0$ and corresponding, in the purely mechanical setting, to the boundary quantity $\bar{\mathbf{t}}_\mathrm{mechanical}$ introduced in (4.25), and by the prescribed heat flux $\bar{q} = \mathbf{Q} \cdot \mathbf{N}$, introduced on $\partial_q \Omega_0$, representing the Neumann boundary contribution associated with the thermal balance equation.

The test functions are chosen consistently with the underlying function spaces of the primary variables, see (4.20)-(4.22). Since the deformation field $\boldsymbol{\varphi}$ is constrained by Dirichlet boundary conditions, its associated test functions are defined in a homogeneous subspace

$$
V_{w_\varphi} = \left\{ \mathbf{w}_\varphi \in H^1(\Omega_0; \mathbb{R}^3) \;\middle|\; \mathbf{w}_\varphi = \mathbf{0} \text{ on } \partial_\varphi \Omega_0 \right\}. \tag{4.63}
$$

The remaining test functions of the velocity and the mixed kinematic variables are taken from the same spaces as their corresponding field variables, since no essential boundary conditions are imposed on these quantities. Consequently, admissible variations for $\mathbf{v}$, $\mathbf{C}$, $\mathbf{G}$, J and τ belong to V_v, V_C, V_G, V_J and V_τ, introduced in (4.20)-(4.22), respectively.

The thermodynamic variable τ is treated as an independent scalar field and is sought in the space

$$V_\tau = \left\{ \tau : \Omega_0 \longrightarrow \mathbb{R}_+ \,\middle|\, \tau \in H^1(\Omega_0),\ \tau = \bar{\tau} \text{ on } \partial_\tau \Omega_0 \right\}. \tag{4.64}$$

The test functions for the energy-related mixed fields are defined as

$$\mathbf{w}_{\boldsymbol{u}_\mathrm{C}} \in V_C, \qquad \mathbf{w}_{\boldsymbol{u}_\mathrm{G}} \in V_G, \qquad w_{u_J} \in V_J, \qquad w_{u_\tau} \in V_J, \tag{4.65}$$

while the corresponding entropy-related test functions satisfy

$$\mathbf{w}_{\boldsymbol{\eta}_\mathrm{C}} \in V_C, \qquad \mathbf{w}_{\boldsymbol{\eta}_\mathrm{G}} \in V_G, \qquad w_{\eta_J} \in V_J, \qquad w_{\eta_\tau} \in V_J. \tag{4.66}$$

Remark 4.1. *In the present continuous (non-discretized) setting, the weak formulation* (W) *together with the arbitrariness of admissible test functions implies that mixed variables and their deformation-based counterparts can be identified in a pointwise sense. In particular, relations such as* $\mathbf{C} = \mathbf{C}_\varphi$, $\mathbf{G} = \mathbf{G}_\varphi$ *and* $J = J_\varphi$ *are equivalent to the corresponding constitutive constraints in the strong form, and similarly* $\partial_\mathrm{C} u = \mathbf{u}_\mathrm{C}$, $\partial_\mathrm{G} u = \mathbf{u}_\mathrm{G}$, $\partial_J u = u_J$, $\partial_\tau u = u_\tau$, $\partial_\mathrm{C} \eta = \boldsymbol{\eta}_\mathrm{C}$, $\partial_\mathrm{G} \eta = \boldsymbol{\eta}_\mathrm{G}$, $\partial_J \eta = \eta_J$ *and* $\partial_\tau \eta = \eta_\tau$ *hold in the continuous formulation.*

This equivalence extends to the thermodynamic variable τ *if chosen to be the temperature field* ϑ*. Then, in the continuous setting, the quantity* $\theta := \frac{\partial_\tau u}{\partial_\tau \eta}$ *and the temperature field* ϑ *remain interchangeable.*

After temporal and spatial discretization, these identities are no longer satisfied exactly. At that stage, the choice of whether to retain deformation-induced or mixed variables becomes a modeling decision, which must be justified a posteriori, for instance via conservation or dissipation properties such as total energy balance and entropy production.

As a final step, we choose $\tau = \vartheta$ throughout the remainder of this work. For this choice of τ, the system's total entropy only depends on J and ϑ which implies that the remaining partial derivatives vanish, i.e.

$$\partial_\mathrm{C} \eta = \partial_\mathrm{G} \eta = \mathbf{0}. \tag{4.67}$$

Thus, the mixed entropy-related quantities $\boldsymbol{\eta}_\mathrm{C}$ and $\boldsymbol{\eta}_\mathrm{G}$ are no longer required, since the corresponding thermodynamic derivatives vanish identically. Consequently, the associated constitutive relations in

the weak formulation (W) do not contribute and can be omitted. This yields the following reduced set of weak equations:

$$
\begin{aligned}
&\int_{\Omega_0} \mathbf{w}_{\boldsymbol{\varphi}} \cdot \rho_0 \dot{\mathbf{v}} + \operatorname{sym}(\mathbf{F}_\varphi^\top \nabla \mathbf{w}_{\boldsymbol{\varphi}}) : \mathbf{S} - \mathbf{w}_{\boldsymbol{\varphi}} \cdot \bar{\mathbf{b}} \, \mathrm{d}V - \int_{\partial_\sigma \Omega_0} \mathbf{w}_{\boldsymbol{\varphi}} \cdot \bar{\mathbf{t}} \, \mathrm{d}A = 0 \\
&\int_{\Omega_0} w_\vartheta \dot{\vartheta} + \frac{w_\vartheta}{\eta_\vartheta} \eta_{\mathrm{C}} : \left[2 \operatorname{sym}(\mathbf{F}_\varphi^\top \nabla \mathbf{v}) \right] + \frac{w_\vartheta}{\eta_\vartheta} \eta_{\mathrm{G}} : \left[\mathbf{C}_\varphi \overset{\otimes}{\mathrm{s}} 2 \operatorname{sym}(\mathbf{F}_\varphi^\top \nabla \mathbf{v}) \right] \\
&\qquad + \frac{w_\vartheta}{\eta_\vartheta} \eta_J J_\varphi^{-1} \mathbf{G}_\varphi : \operatorname{sym}(\mathbf{F}_\varphi^\top \nabla \mathbf{v}) - \nabla \left(\frac{w_\vartheta}{u_\vartheta} \right) \cdot \mathbf{Q} \, \mathrm{d}V - \int_{\partial_\sigma \Omega_0} w_\vartheta \bar{q} \, \mathrm{d}A = 0 \\
&\int_{\Omega_0} \mathbf{w}_{\mathrm{C}} : \left[\dot{\mathbf{C}} - 2 \operatorname{sym}(\mathbf{F}_\varphi^\top \nabla \mathbf{v}) \right] \mathrm{d}V = 0 \\
&\int_{\Omega_0} \mathbf{w}_{\mathrm{G}} : \left[\dot{\mathbf{G}} - 2 \mathbf{C}_\varphi \overset{\otimes}{\mathrm{s}} \operatorname{sym}(\mathbf{F}_\varphi^\top \nabla \mathbf{v}) \right] \mathrm{d}V = 0 \\
&\int_{\Omega_0} w_J \left[\dot{J} - J_\varphi^{-1} \mathbf{G}_\varphi : \operatorname{sym}(\mathbf{F}_\varphi^\top \nabla \mathbf{v}) \right] \mathrm{d}V = 0 \\
&\int_{\Omega_0} \mathbf{w}_{\boldsymbol{u}_{\mathrm{C}}} : \left[\mathbf{u}_{\mathrm{C}} - \partial_{\mathrm{C}} u(\mathbf{C}, \mathbf{G}, J, \vartheta) \right] \mathrm{d}V = 0 \\
&\int_{\Omega_0} \mathbf{w}_{\boldsymbol{u}_{\mathrm{G}}} : \left[\mathbf{u}_{\mathrm{G}} - \partial_{\mathrm{G}} u(\mathbf{C}, \mathbf{G}, J, \vartheta) \right] \mathrm{d}V = 0 \\
&\int_{\Omega_0} w_{u_J} \left[u_J - \partial_J u(\mathbf{C}, \mathbf{G}, J, \vartheta) \right] \mathrm{d}V = 0 \\
&\int_{\Omega_0} w_{u_\vartheta} \left[u_\vartheta - \partial_\vartheta u(\mathbf{C}, \mathbf{G}, J, \vartheta) \right] \mathrm{d}V = 0 \\
&\int_{\Omega_0} w_{\eta_J} \left[\eta_J - \partial_J \eta(J, \vartheta) \right] \mathrm{d}V = 0 \\
&\int_{\Omega_0} w_{\eta_\vartheta} \left[\eta_\vartheta - \partial_\vartheta \eta(J, \vartheta) \right] \mathrm{d}V = 0.
\end{aligned}
\tag{4.68}
$$

4.5. Discretization in time

In this chapter, a time discretization scheme is introduced with the purpose of preserving the structural properties of the GENERIC formulation developed above. We present a variant of the implicit midpoint scheme, which relies on the notion of a discrete derivative. In the second part of this Section, we show that the structural properties of energy conservation and positive entropy production are preserved by the proposed time discretization scheme.

We partition the time interval $\mathcal{I} = [t_0, t_N]$ into a sequence of subintervals $\mathcal{I}_n = [t_n, t_{n+1}]$, $n = 0, \dots, N-1$, with time step sizes $\Delta t_n = t_{n+1} - t_n$. For a generic time-dependent quantity $(\bullet)(t)$, we introduce the midpoint evaluation

$$
(\bullet)_{n+1/2} := \frac{1}{2} \left[(\bullet)_n + (\bullet)_{n+1} \right], \tag{4.69}
$$

where $(\bullet)_n = (\bullet)(t_n)$ and $(\bullet)_{n+1} = (\bullet)(t_{n+1})$ denote the nodal values at the end points of $\mathcal{I}_n$.

Time derivatives are approximated by a finite difference quotient of the form

$$
(\dot{\bullet}) \approx \frac{(\bullet)_{n+1} - (\bullet)_n}{\Delta t_n}. \tag{4.70}
$$

Employing these definitions yields a time-discrete version of the weak formulation (4.68) as $\frac{\Delta \boldsymbol{\varphi}_n}{\Delta t_n} = \mathbf{v}_{n+1/2}$ and

$$
\begin{aligned}
&\int_{\Omega_0} \mathbf{w}_{\boldsymbol{\varphi}} \rho_0 \frac{\Delta \mathbf{v}_n}{\Delta t_n} + \operatorname{sym}(\mathbf{F}_{\varphi_{n+1/2}}^{\top} \nabla \mathbf{w}_{\boldsymbol{\varphi}}) : \mathbf{S}_{1/2} - \mathbf{w}_{\boldsymbol{\varphi}} \cdot \bar{\mathbf{b}} \, \mathrm{d}V \\
&\quad - \int_{\partial_\sigma \Omega_0} \mathbf{w}_{\boldsymbol{\varphi}} \cdot \bar{\mathbf{t}}_{n+1/2} \, \mathrm{d}A = 0 \\
&\int_{\Omega_0} w_\vartheta \frac{\Delta \vartheta_n}{\Delta t_n} + \frac{w_\vartheta}{\eta_{\vartheta_{n+1}}} \eta_{J_{n+1}} J_{\varphi_{n+1/2}}^{-1} \mathbf{G}_{\varphi_{n+1/2}} : \operatorname{sym}(\mathbf{F}_{\varphi_{n+1/2}}^{\top} \nabla \mathbf{v}_{n+1/2}) \\
&\quad - \nabla \big(\frac{w_\vartheta}{u_{\vartheta_{n+1}}} \big) \cdot \mathbf{Q}_{1/2} \, \mathrm{d}V - \int_{\partial \Omega_0} w_\vartheta \bar{q}_{n+1/2} \, \mathrm{d}A = 0 \\
&\int_{\Omega_0} \mathbf{w}_{\mathbf{C}} : \big[\frac{\Delta \mathbf{C}_n}{\Delta t_n} - 2 \operatorname{sym}(\mathbf{F}_{\varphi_{n+1/2}}^{\top} \nabla \mathbf{v}_{n+1/2}) \big] \, \mathrm{d}V = 0 \\
&\int_{\Omega_0} \mathbf{w}_{\mathbf{G}} : \big[\frac{\Delta \mathbf{G}_n}{\Delta t_n} - 2 \mathbf{C}_{\varphi_{n+1/2}} \barwedge \operatorname{sym}(\mathbf{F}_{\varphi_{n+1/2}}^{\top} \nabla \mathbf{v}_{n+1/2}) \big] \, \mathrm{d}V = 0 \\
&\int_{\Omega_0} w_J \big[\frac{\Delta J_n}{\Delta t_n} - J_{\varphi_{n+1/2}}^{-1} \mathbf{G}_{\varphi_{n+1/2}} : \operatorname{sym}(\mathbf{F}_{\varphi_{n+1/2}}^{\top} \nabla \mathbf{v}_{n+1/2}) \big] \, \mathrm{d}V = 0 \\
&\int_{\Omega_0} \mathbf{w}_{\boldsymbol{u}_{\mathbf{C}}} : \big[\mathbf{u}_{\mathbf{C}_{n+1}} - \mathrm{D}_{\mathbf{C}} u \big] \, \mathrm{d}V = 0 \\
&\int_{\Omega_0} \mathbf{w}_{\boldsymbol{u}_{\mathbf{G}}} : \big[\mathbf{u}_{\mathbf{G}_{n+1}} - \mathrm{D}_{\mathbf{G}} u \big] \, \mathrm{d}V = 0 \\
&\int_{\Omega_0} w_{u_J} \big[u_{J_{n+1}} - \mathrm{D}_J u \big] \, \mathrm{d}V = 0 \\
&\int_{\Omega_0} w_{u_\vartheta} (u_{\vartheta_{n+1}} - \mathrm{D}_\vartheta u) \, \mathrm{d}V = 0 \\
&\int_{\Omega_0} w_{\eta_J} (\eta_{J_{n+1}} - \mathrm{D}_J \eta) \, \mathrm{d}V = 0 \\
&\int_{\Omega_0} w_{\eta_\vartheta} (\eta_{\vartheta_{n+1}} - \mathrm{D}_\vartheta \eta) \, \mathrm{d}V = 0,
\end{aligned}
\tag{4.71}
$$

where $\Delta(\bullet)_n = (\bullet)_{n+1} - (\bullet)_n$. Additionally, the time discrete counterpart of the second Piola Kirchhoff stress tensor is given as

$$
\mathbf{S}_{1/2} = 2\mathbf{u}_{\mathbf{C}_{n+1}} + 2\mathbf{u}_{\mathbf{G}_{n+1}} \barwedge \mathbf{C}_{\varphi_{n+1/2}} + J_{\varphi_{n+1/2}}^{-1} \mathbf{G}_{\varphi_{n+1/2}} u_{J_{n+1}} - \Theta_{n+1} J_{\varphi_{n+1/2}}^{-1} \mathbf{G}_{\varphi_{n+1/2}} \eta_{J_{n+1}} \tag{4.72}
$$

The time discrete heat flux and temperature field follow as

$$
\mathbf{Q}_{1/2} = \Theta_{n+1}^2 k J_{\varphi_{n+1/2}}^{-1} \mathbf{G}_{\varphi_{n+1/2}} \nabla \big(\frac{1}{\Theta_{n+1}} \big) \tag{4.73}
$$

and

$$
\Theta_{n+1} = \frac{u_{\vartheta_{n+1}}}{\eta_{\vartheta_{n+1}}}, \tag{4.74}
$$

respectively.

The mixed quantities $\mathbf{u}_{\mathbf{C}}$, $\mathbf{u}_{\mathbf{G}}$, u_J, u_ϑ, η_J, and η_ϑ are assumed to be constant on each time interval $\mathcal{I}_n$. Consequently, only a single value per time step is introduced, which is denoted by the index $(n+1)$. The chosen notation emphasizes that the corresponding constitutive constraints are enforced consistently at the end point of the interval. The same interpretation applies to Θ_{n+1}, which is defined as the ratio of two mixed thermodynamic variables.

In the time-discrete setting, the classical partial derivatives of the thermodynamic potentials are replaced by partitioned discrete derivatives in the sense of [31]. More precisely, for a generic thermodynamic potential $\mathcal{A} = \mathcal{A}(\mathbf{C}, \mathbf{G}, J, \vartheta)$ and variables $\Phi^i \in \{\mathbf{C}, \mathbf{G}, J, \vartheta\}$, the continuous partial derivatives $\partial_{\Phi^i}\mathcal{A}$ are substituted by discrete counterparts

$$\mathrm{D}_{\Phi^i}\mathcal{A} = \mathrm{D}_{\Phi^i}\mathcal{A}(\Phi_n, \Phi_{n+1}), \tag{4.75}$$

where $\Phi = (\mathbf{C}, \mathbf{G}, J, \vartheta)$. A fundamental property of these discrete derivatives is the so-called directionality property, which in the present setting takes the form

$$\begin{aligned}\Delta\mathcal{A}_n &= \mathcal{A}_{n+1} - \mathcal{A}_n \\ &= \mathrm{D}_{\mathrm{C}}\mathcal{A} : \Delta\mathbf{C}_n + \mathrm{D}_{\mathrm{G}}\mathcal{A} : \Delta\mathbf{G}_n + \mathrm{D}_J\mathcal{A}\,\Delta J_n + \mathrm{D}_\vartheta\mathcal{A}\,\Delta\vartheta_n.\end{aligned} \tag{4.76}$$

This identity may be interpreted as a discrete counterpart of the classical chain rule and constitutes the key ingredient for proving the preservation of the thermodynamic structure at the time-discrete level.

Moreover, the discrete derivatives are consistent with the classical midpoint approximation in the limit of vanishing increments. In particular,

$$\lim_{\Delta\Phi^i_n \to 0} (\mathrm{D}_{\Phi^i}\mathcal{A}) = \partial_{\Phi^i}\mathcal{A}\big|_{\Phi_{n+1/2}}. \tag{4.77}$$

4.5.1. Time-discrete conservation of energy

The following derivation shows that the proposed temporal discretization preserves the total energy at the discrete level. The difference of the system's total energy between two time steps is given by

$$\Delta\mathcal{E}_n = \Delta\mathcal{T}_n + \Delta\mathcal{U}_n + \Delta\mathcal{V}_n = \int_{\Omega_0} \Delta T_n + \Delta u_n + \Delta V_n \,\mathrm{d}V, \tag{4.78}$$

where the directionality property (4.76) of the discrete derivative ensures that

$$\Delta u_n = \mathrm{D}_{\mathrm{C}}u : \Delta\mathbf{C}_n + \mathrm{D}_{\mathrm{G}}u : \Delta\mathbf{G}_n + \mathrm{D}_J u\Delta J_n + \mathrm{D}_\vartheta u\Delta\vartheta_n. \tag{4.79}$$

To ensure conservation of the system's total energy, the energy difference $\Delta\mathcal{E}_n$ must vanish for a conservative system, i.e. $\Delta\mathcal{E}_n = 0$ for every timestep Δt_n.

We select the admissible test functions

$$\begin{aligned}\mathbf{w}_{\boldsymbol{\varphi}} &= \frac{\Delta\boldsymbol{\varphi}_n}{\Delta t_n},\ w_\vartheta = u_{\vartheta_{n+1}},\ \mathbf{w}_{\mathrm{C}} = \mathbf{u}_{\mathrm{C}_{n+1}},\ \mathbf{w}_{\mathrm{G}} = \mathbf{u}_{\mathrm{G}_{n+1}},\ w_J = u_{J_{n+1}} \\ \mathbf{w}_{\boldsymbol{u}_{\mathrm{C}}} &= -\frac{\Delta\mathbf{C}_n}{\Delta t_n},\ \mathbf{w}_{\boldsymbol{u}_{\mathrm{G}}} = -\frac{\Delta\mathbf{G}_n}{\Delta t_n},\ w_{u_J} = -\frac{\Delta J_n}{\Delta t_n},\ w_{u_\vartheta} = -\frac{\Delta\vartheta_n}{\Delta t_n}\end{aligned} \tag{4.80}$$

and insert them into the time discrete weak form (4.71), where $\frac{\Delta\boldsymbol{\varphi}_n}{\Delta t_n} = \mathbf{v}_{n+1/2}$ and

$$\mathrm{sym}(\mathbf{F}^\top_{\varphi_{n+1/2}}\Delta\mathbf{F}_{\boldsymbol{\varphi}_n}) = \frac{1}{2}\Delta\mathbf{C}_{\boldsymbol{\varphi}_n} \tag{4.81}$$

yields

$$
\begin{aligned}
&\int_{\Omega_0} \rho_0 \frac{\Delta \mathbf{v}_n}{\Delta t_n} \mathbf{v}_{n+1/2} + \operatorname{sym}(\mathbf{F}_{\varphi_{n+1/2}}^{\top} \frac{\Delta \mathbf{F}_{\boldsymbol{\varphi}_n}}{\Delta t_n}) : \mathbf{S}_{1/2} - \frac{\Delta \boldsymbol{\varphi}_n}{\Delta t_n} \cdot \bar{\mathbf{b}} \, \mathrm{d}V \\
&\quad - \int_{\partial_\sigma \Omega_0} \frac{\Delta \boldsymbol{\varphi}_n}{\Delta t_n} \cdot \bar{\mathbf{t}}_{n+1/2} \, \mathrm{d}A = 0 \\
&\int_{\Omega_0} u_{\vartheta_{n+1}} \frac{\Delta \vartheta_n}{\Delta t_n} + \frac{u_{\vartheta_{n+1}}}{\eta_{\vartheta_{n+1}}} \eta_J J^{-1}_{\varphi_{n+1/2}} \mathbf{G}_{\varphi_{n+1/2}} : \operatorname{sym}(\mathbf{F}_{\varphi_{n+1/2}} \nabla \mathbf{v}_{n+1/2}) - \nabla\big(\frac{u_{\vartheta_{n+1}}}{u_{\vartheta_{n+1}}}\big) \cdot \mathbf{Q}_{1/2} \, \mathrm{d}V \\
&\quad + \int_{\partial\Omega_0} u_{\vartheta_{n+1}} \bar{q}_{n+1/2} \, \mathrm{d}A = 0 \\
&\int_{\Omega_0} \frac{\mathbf{u}_{\mathrm{C}_{n+1}}}{\Delta t_n} : \big[\Delta \mathbf{C}_n - \Delta \mathbf{C}_{\boldsymbol{\varphi}_n}\big] \, \mathrm{d}V = 0 \\
&\int_{\Omega_0} \frac{\mathbf{u}_{\mathrm{G}_{n+1}}}{\Delta t_n} : \big[\Delta \mathbf{G}_n - \mathbf{C}_{\boldsymbol{\varphi}_{n+1/2}} \barwedge \Delta \mathbf{C}_{\boldsymbol{\varphi}_n}\big] \, \mathrm{d}V = 0 \\
&\int_{\Omega_0} \frac{u_{J_{n+1}}}{\Delta t_n} \big[\Delta J_n - \frac{1}{2} J^{-1}_{\boldsymbol{\varphi}_{n+1/2}} \mathbf{G}_{\boldsymbol{\varphi}_{n+1/2}} : \Delta \mathbf{C}_{\boldsymbol{\varphi}_n}\big] \, \mathrm{d}V = 0 \\
&\int_{\Omega_0} -\frac{\Delta \mathbf{C}_n}{\Delta t_n} : \big[\mathbf{u}_{\mathrm{C}_{n+1}} - \mathrm{D}_{\mathrm{C}} u\big] \, \mathrm{d}V = 0 \\
&\int_{\Omega_0} -\frac{\Delta \mathbf{G}_n}{\Delta t_n} : \big[\mathbf{u}_{\mathrm{G}_{n+1}} - \mathrm{D}_{\mathrm{G}} u\big] \, \mathrm{d}V = 0 \\
&\int_{\Omega_0} -\frac{\Delta J_n}{\Delta t_n} \big[u_{J_{n+1}} - \mathrm{D}_J u\big] \, \mathrm{d}V = 0 \\
&\int_{\Omega_0} -\frac{\Delta \vartheta_n}{\Delta t_n} (u_{\vartheta_{n+1}} - \mathrm{D}_\vartheta u) \, \mathrm{d}V = 0.
\end{aligned}
\tag{4.82}
$$

By observing that

$$
\begin{aligned}
\operatorname{sym}(\mathbf{F}_{\varphi_{n+1/2}}^{\top} \frac{\Delta \mathbf{F}_{\boldsymbol{\varphi}_n}}{\Delta t_n}) : \mathbf{S}_{1/2} = \frac{1}{\Delta t_n} \big(&\Delta \mathbf{C}_{\boldsymbol{\varphi}_n} : \mathbf{u}_{\mathrm{C}_{n+1}} + \Delta \mathbf{C}_{\boldsymbol{\varphi}_n} : \mathbf{u}_{\mathrm{C}_{n+1}} \barwedge \mathbf{C}_{\boldsymbol{\varphi}_{n+1/2}} \\
&+ \frac{1}{2} \Delta \mathbf{C}_{\boldsymbol{\varphi}_n} : J^{-1}_{\boldsymbol{\varphi}_{n+1/2}} \mathbf{G}_{\boldsymbol{\varphi}_{n+1/2}} u_{J_{n+1}} - \frac{1}{2} \Delta \mathbf{C}_{\boldsymbol{\varphi}_n} : \Theta_{n+1} J^{-1}_{\boldsymbol{\varphi}_{n+1/2}} \mathbf{G}_{\boldsymbol{\varphi}_{n+1/2}} \mathrm{D}_J \eta \big),
\end{aligned}
\tag{4.83}
$$

we can add equations $(4.82)_1$ to $(4.82)_9$ and obtain

$$
\begin{aligned}
&\int_{\Omega_0} \rho_0 \frac{\Delta \mathbf{v}_n}{\Delta t_n} \mathbf{v}_{n+1/2} \, \mathrm{d}V - \int_{\Omega_0} \frac{\Delta \boldsymbol{\varphi}_n}{\Delta t_n} \cdot \bar{\mathbf{b}} \, \mathrm{d}V \\
&\quad + \int_{\Omega_0} \frac{\Delta \mathbf{C}_n}{\Delta t_n} : \mathrm{D}_{\mathrm{C}} u + \frac{\Delta \mathbf{G}_n}{\Delta t_n} : \mathrm{D}_{\mathrm{G}} u + \frac{\Delta J_n}{\Delta t_n} \mathrm{D}_J u + \mathrm{D}_\vartheta u \frac{\Delta \vartheta_n}{\Delta t_n} \, \mathrm{d}V = 0.
\end{aligned}
\tag{4.84}
$$

Hence, the total energy is conserved for thermally and mechanically closed systems, i.e., in the absence of external power input and Neumann boundary terms.

4.5.2. Time-discrete entropy production

According to the second law of thermodynamics, the total entropy must be non-decreasing, i.e.

$$
\Delta \mathcal{S}_n = \int_{\Omega_0} \Delta \eta_n \, \mathrm{d}V \geq 0 \tag{4.85}
$$

for all time steps Δt_n. Analogously to the proof of energy conservation, we choose the admissible test function

$$w_\vartheta = \eta_{\vartheta_{n+1}} \tag{4.86}$$

and insert it into equation $(4.71)_3$ to obtain

$$\begin{aligned}\int_{\Omega_0} \eta_{\vartheta_{n+1}} \frac{\vartheta_{n+1} - \vartheta_n}{\Delta t_n} + \frac{\eta_{\vartheta_{n+1}}}{\eta_{\vartheta_{n+1}}} \frac{1}{2\Delta t_n} \eta_{J_{n+1}} J^{-1}_{\varphi_{n+1/2}} \mathbf{G}_{\varphi_{n+1/2}} : \Delta \mathbf{C}_{\boldsymbol{\varphi}_n} \\ - \nabla\big(\frac{\eta_{\vartheta_{n+1}}}{u_{\vartheta_{n+1}}}\big) \cdot \mathbf{Q}_{1/2} \,\mathrm{d}V + \int_{\partial\Omega_0} \eta_{\vartheta_{n+1}} \bar{q}_{n+1/2} \,\mathrm{d}A = 0.\end{aligned} \tag{4.87}$$

From equations $(4.71)_9$, $(4.71)_{11}$ and $(4.71)_{12}$ we obtain $\eta_{\vartheta_{n+1}} = \mathrm{D}_\vartheta \eta$, $\eta_{J_{n+1}} = \mathrm{D}_J \eta$ and

$$\Delta J_n = \frac{1}{2} J^{-1}_{\boldsymbol{\varphi}_{n+1/2}} \mathbf{G}_{\boldsymbol{\varphi}_{n+1/2}} : \Delta \mathbf{C}_{\boldsymbol{\varphi}_n}, \tag{4.88}$$

yielding

$$\begin{aligned}\int_{\Omega_0} \Delta\eta \,\mathrm{d}V &= \int_{\Omega_0} \mathrm{D}_\vartheta \eta \Delta\vartheta_n + \mathrm{D}_J \eta \Delta J_n \,\mathrm{d}V + \int_{\partial\Omega_0} \mathrm{D}_\vartheta \eta \bar{q}_{n+1/2} \,\mathrm{d}A \\ &= \Delta t_n \int_{\Omega_0} \nabla\big(\frac{1}{\Theta_{n+1}}\big) \Theta^2_{n+1} k J^{-1}_{\boldsymbol{\varphi}_{n+1/2}} \mathbf{G}_{\boldsymbol{\varphi}_{n+1/2}} \nabla\big(\frac{1}{\Theta_{n+1}}\big) \,\mathrm{d}V \geq 0.\end{aligned} \tag{4.89}$$

Since the conductivity coefficient k is non-negative and $\mathbf{G}_{\boldsymbol{\varphi}_{n+1/2}}$ is positive definite, the time-discrete entropy production is indeed non-negative provided that the Neumann boundary contributions vanish.

Hence, the proposed discretization preserves the fundamental thermodynamic structure of the continuous GENERIC formulation at the time-discrete level.

4.6. Discretization in space

In this section, a spatial discretization of the weak formulation (4.68) is introduced. To this end, suitable finite element approximations for the trial and test functions are employed, resulting in a space-discrete counterpart of the weak formulation. Moreover, the proposed discretization is shown to preserve the thermodynamic structure of the continuous system.

4.6.1. Finite element approximation

In the framework of a Bubnov-Galerkin formulation, we employ a standard isoparametric finite element discretization.

The discrete approximation of the deformation mapping is introduced as

$$\boldsymbol{\varphi}^{\mathrm{h}} = \sum_{K=1}^{n_{\mathrm{node}}} N^K_\varphi \hat{\boldsymbol{\varphi}}^K = \mathbf{N}_\varphi \hat{\boldsymbol{\varphi}}, \tag{4.90}$$

with

$$\begin{aligned}\hat{\boldsymbol{\varphi}} &= \begin{bmatrix} \hat{\varphi}^1_x & \hat{\varphi}^1_y & \hat{\varphi}^1_z & \cdots & \hat{\varphi}^{n_{\mathrm{node}}}_x & \hat{\varphi}^{n_{\mathrm{node}}}_y & \hat{\varphi}^{n_{\mathrm{node}}}_z \end{bmatrix}^\top \in \mathbb{R}^{3n_{\mathrm{node}}}, \\ \mathbf{N}_\varphi &= \begin{bmatrix} N^1_\varphi \mathbf{I} & \cdots & N^{n_{\mathrm{node}}}_\varphi \mathbf{I} \end{bmatrix} \in \mathbb{R}^{3\times 3n_{\mathrm{node}}},\end{aligned} \tag{4.91}$$

where N^K_φ denotes the Lagrangian shape function corresponding to node K, and n_{node} represents the total number of nodes of the selected finite element. The collection of all nodal deformation values is

represented by the global vector $\hat{\boldsymbol{\varphi}}$, whereas the interpolation functions are assembled in the matrix $\mathbf{N}_\varphi$. Standard finite element assembly procedures yield a globally continuous approximation of the deformation field.

Using the same interpolation functions, the corresponding test functions as well as the discrete velocity field are expressed as

$$\begin{aligned} \mathbf{w}_\varphi^{\mathrm{h}} &= \sum_{K=1}^{n_{\mathrm{node}}} N_\varphi^K \hat{\mathbf{w}}_\varphi^K = \mathbf{N}_\varphi \hat{\mathbf{w}}_\varphi, \\ \mathbf{v}^{\mathrm{h}} &= \sum_{K=1}^{n_{\mathrm{node}}} N_\varphi^K \hat{\mathbf{v}}^K = \mathbf{N}_\varphi \hat{\mathbf{v}}. \end{aligned} \tag{4.92}$$

The approximated temperature field ϑ^{h} is given by

$$\vartheta^{\mathrm{h}} = \sum_{L=1}^{m_{\mathrm{node}}} N_\vartheta^L \hat{\vartheta}^L = \mathbf{N}_\vartheta \hat{\boldsymbol{\vartheta}}, \tag{4.93}$$

where

$$\begin{aligned} \hat{\boldsymbol{\vartheta}} &= \begin{bmatrix} \hat{\vartheta}^1 & \cdots & \hat{\vartheta}^{m_{\mathrm{node}}} \end{bmatrix}^\top \in \mathbb{R}^{m_{\mathrm{node}}}, \\ \mathbf{N}_\vartheta &= \begin{bmatrix} N_\vartheta^1 & \cdots & N_\vartheta^{m_{\mathrm{node}}} \end{bmatrix} \in \mathbb{R}^{m_{\mathrm{node}}}. \end{aligned} \tag{4.94}$$

In the above, m_{node} represents the total number of nodes of the selected finite element for the temperature field. Analogously, the approximation of the mixed fields $\{u_\vartheta, \eta_\vartheta\}$ as well as the corresponding test functions $\{w_\vartheta, w_{u_\vartheta}, w_{\eta_\vartheta}\}$ is given by

$$w_\vartheta^{\mathrm{h}} = \mathbf{N}_\vartheta \hat{\mathbf{w}}_\vartheta, \quad u_\vartheta^{\mathrm{h}} = \mathbf{N}_\vartheta \hat{\mathbf{u}}_\vartheta, \quad \eta_\vartheta^{\mathrm{h}} = \mathbf{N}_\vartheta \hat{\boldsymbol{\eta}}_\vartheta, \quad w_{u_\vartheta}^{\mathrm{h}} = \mathbf{N}_\vartheta \hat{\mathbf{w}}_{u_\vartheta}, \quad w_{\eta_\vartheta}^{\mathrm{h}} = \mathbf{N}_\vartheta \hat{\mathbf{w}}_{\eta_\vartheta}. \tag{4.95}$$

Note that the mixed quantities associated with the temperature derivatives, namely u_ϑ and η_ϑ, are approximated in the same finite element space as the temperature field itself. This choice is essential for preserving the thermodynamic structure of the semi-discrete system, in particular the discrete consistency of energy conservation and entropy production.

For tensor-valued mixed fields, a Voigt-type representation is adopted in order to facilitate the numerical implementation. A distinction is made between stress-like and strain-like second-order tensors. For a symmetric stress-like tensor $\mathbf{A} = \mathbf{A}^\top$ and a symmetric strain-like tensor $\mathbf{B} = \mathbf{B}^\top$, the corresponding Voigt mappings are defined as

$$\begin{aligned} \{\mathbf{A}\}_{\mathrm{V}} &= \begin{bmatrix} A_{11} & A_{22} & A_{33} & A_{12} & A_{23} & A_{13} \end{bmatrix}^\top, \\ \{\mathbf{B}\}_{\mathrm{V}} &= \begin{bmatrix} B_{11} & B_{22} & B_{33} & 2B_{12} & 2B_{23} & 2B_{13} \end{bmatrix}^\top. \end{aligned} \tag{4.96}$$

This distinction ensures that the Euclidean inner product of the Voigt vectors corresponds to the tensor contraction of the associated second-order tensors. Based on this notation, the finite element approximation of the kinematic mixed fields is introduced. These fields are treated in a discontinuous manner, as no inter-element continuity is required. In particular, the right Cauchy–Green deformation tensor $\mathbf{C}$ is approximated by

$$\begin{aligned} \mathbf{C}^{\mathrm{h}} &= \sum_{P=1}^{p_{\mathrm{node}}} N_C^P \hat{\mathbf{C}}^P, \\ \{\mathbf{C}^{\mathrm{h}}\}_{\mathrm{V}} &= \mathbf{N}_C \{\hat{\mathbf{C}}\}_{\mathrm{V}}, \end{aligned} \tag{4.97}$$

where

$$\begin{aligned}\left\{\hat{\mathbf{C}}\right\}_{\mathrm{V}} &= \begin{bmatrix}\left\{\hat{\mathbf{C}}^1\right\}_{\mathrm{V}}^{\top} & \cdots & \left\{\hat{\mathbf{C}}^{p_{\mathrm{node}}}\right\}_{\mathrm{V}}^{\top}\end{bmatrix}^{\top} \in \mathbb{R}^{6p_{\mathrm{node}}},\\ \mathbf{N}_C &= \begin{bmatrix}N_C^1\mathbf{I}_6 & \cdots & N_C^{p_{\mathrm{node}}}\mathbf{I}_6\end{bmatrix} \in \mathbb{R}^{6\times 6p_{\mathrm{node}}}.\end{aligned} \tag{4.98}$$

Here, p_{node} element-wise shape functions N_C^P are employed. Furthermore, $\mathbf{I}_6$ denotes the identity tensor in $\mathbb{R}^{6\times 6}$. Although $\mathbf{C}^{\mathrm{h}}$ is defined on a single element e, the element index is omitted for notational brevity.

In complete analogy, the remaining matrix-valued internal variables and their corresponding test functions are approximated via the same Voigt-based interpolation,

$$\begin{aligned}\left\{\mathbf{G}^{\mathrm{h}}\right\}_{\mathrm{V}} &= \mathbf{N}_C\left\{\hat{\mathbf{G}}\right\}_{\mathrm{V}}, & \left\{\mathbf{w}_{\mathbf{C}}^{\mathrm{h}}\right\}_{\mathrm{V}} &= \mathbf{N}_C\left\{\hat{\mathbf{w}}_{\mathbf{C}}\right\}_{\mathrm{V}},\\ & & \left\{\mathbf{w}_{\mathbf{G}}^{\mathrm{h}}\right\}_{\mathrm{V}} &= \mathbf{N}_C\left\{\hat{\mathbf{w}}_{\mathbf{G}}\right\}_{\mathrm{V}},\\ \left\{\mathbf{u}_{\mathbf{C}}^{\mathrm{h}}\right\}_{\mathrm{V}} &= \mathbf{N}_C\left\{\hat{\mathbf{u}}_{\mathbf{C}}\right\}_{\mathrm{V}}, & \left\{\mathbf{w}_{\boldsymbol{u}_{\mathbf{C}}}^{\mathrm{h}}\right\}_{\mathrm{V}} &= \mathbf{N}_C\left\{\hat{\mathbf{w}}_{\boldsymbol{u}_{\mathbf{C}}}\right\}_{\mathrm{V}},\\ \left\{\mathbf{u}_{\mathbf{G}}^{\mathrm{h}}\right\}_{\mathrm{V}} &= \mathbf{N}_C\left\{\hat{\mathbf{u}}_{\mathbf{G}}\right\}_{\mathrm{V}}, & \left\{\mathbf{w}_{\boldsymbol{u}_{\mathbf{G}}}^{\mathrm{h}}\right\}_{\mathrm{V}} &= \mathbf{N}_C\left\{\hat{\mathbf{w}}_{\boldsymbol{u}_{\mathbf{G}}}\right\}_{\mathrm{V}}.\end{aligned} \tag{4.99}$$

For the sake of simplicity, the same shape functions, i.e. $\mathbf{N}_C$, are employed for both $\mathbf{C}$- and $\mathbf{G}$-based variables. Finally, the remaining scalar valued mixed fields $\{J, u_J, \eta_J\}$ together with their corresponding test functions $\{w_J, w_{u_J}, w_{\eta_J}\}$ are interpolated using standard scalar shape functions N_J^L, without the need for a Voigt representation. This yields

$$J^{\mathrm{h}} = \sum_{Q=1}^{q_{\mathrm{node}}} N_J^Q \hat{J}^Q = \mathbf{N}_J\hat{\mathbf{J}}, \tag{4.100}$$

with

$$\begin{aligned}\hat{\mathbf{J}} &= \begin{bmatrix}\hat{J}^1 & \cdots & \hat{J}^{q_{\mathrm{node}}}\end{bmatrix}^{\top} \in \mathbb{R}^{q_{\mathrm{node}}},\\ \mathbf{N}_J &= \begin{bmatrix}N_J^1 & \cdots & N_J^{q_{\mathrm{node}}}\end{bmatrix} \in \mathbb{R}^{q_{\mathrm{node}}},\end{aligned} \tag{4.101}$$

where q_{node} element-wise shape functions N_J^Q are employed. Accordingly, the scalar mixed fields and associated test functions are represented as

$$w_J^{\mathrm{h}} = \mathbf{N}_J\hat{\mathbf{w}}_J, \quad u_J^{\mathrm{h}} = \mathbf{N}_J\hat{\mathbf{u}}_J, \quad w_{u_J}^{\mathrm{h}} = \mathbf{N}_J\hat{\mathbf{w}}_{u_J}, \quad \eta_J^{\mathrm{h}} = \mathbf{N}_J\hat{\boldsymbol{\eta}}_J, \quad w_{\eta_J}^{\mathrm{h}} = \mathbf{N}_J\hat{\mathbf{w}}_{\eta_J}. \tag{4.102}$$

In order to obtain discrete counterparts of the thermodynamic driving forces, we first recall the global energy and entropy functionals

$$\begin{aligned}\mathcal{U} &= \int_{\Omega_0} u(\mathbf{C}, \mathbf{G}, J, \vartheta)\,\mathrm{d}V,\\ \mathcal{S} &= \int_{\Omega_0} \eta(J, \vartheta)\,\mathrm{d}V.\end{aligned} \tag{4.103}$$

Based on the finite element approximations introduced above, their spatially discrete versions are defined by direct substitution of the discrete fields,

$$\begin{aligned}\mathcal{U}^{\mathrm{h}} &:= \int_{\Omega_0} u^{\mathrm{h}}\,\mathrm{d}V = \int_{\Omega_0} u(\mathbf{C}^{\mathrm{h}}, \mathbf{G}^{\mathrm{h}}, J^{\mathrm{h}}, \vartheta^{\mathrm{h}})\,\mathrm{d}V\\ &= \int_{\Omega_0} u(N_C^P\hat{\mathbf{C}}^P, N_C^P\hat{\mathbf{G}}^P, N_J^Q\hat{J}^Q, N_\vartheta^L\hat{\vartheta}^L)\,\mathrm{d}V = \mathcal{U}(\left\{\hat{\mathbf{C}}\right\}_{\mathrm{V}}, \left\{\hat{\mathbf{G}}\right\}_{\mathrm{V}}, \hat{\mathbf{J}}, \hat{\boldsymbol{\vartheta}}),\\ \mathcal{S}^{\mathrm{h}} &:= \int_{\Omega_0} \eta^{\mathrm{h}}\,\mathrm{d}V = \int_{\Omega_0} \eta(J^{\mathrm{h}}, \vartheta^{\mathrm{h}})\,\mathrm{d}V = \int_{\Omega_0} \eta(N_J^Q\hat{J}^Q, N_\vartheta^L\hat{\vartheta}^L)\,\mathrm{d}V = \mathcal{S}(\hat{\mathbf{J}}, \hat{\boldsymbol{\vartheta}}).\end{aligned} \tag{4.104}$$

With a slight abuse of notation, we retain the calligraphic symbols $\mathcal{U}$ and $\mathcal{S}$ for the finite-dimensional counterparts of the corresponding continuous functionals.

To obtain the discrete thermodynamic driving forces, the derivatives of the discrete functionals with respect to the nodal degrees of freedom are evaluated. For the internal energy functional this yields

$$\begin{aligned}
\partial_{\hat{\mathbf{C}}}\mathcal{U} &:= \int_{\Omega_0} \mathbf{N}_C^\top \left\{\partial_{\mathbf{C}} u^\mathrm{h}\right\}_\mathrm{V} \mathrm{d}V, \\
\partial_{\hat{\mathbf{G}}}\mathcal{U} &:= \int_{\Omega_0} \mathbf{N}_C^\top \left\{\partial_{\mathbf{G}} u^\mathrm{h}\right\}_\mathrm{V} \mathrm{d}V, \\
\partial_{\hat{\mathbf{j}}}\mathcal{U} &:= \int_{\Omega_0} \mathbf{N}_J^\top \partial_J u^\mathrm{h} \,\mathrm{d}V, \\
\partial_{\hat{\boldsymbol{\vartheta}}}\mathcal{U} &:= \int_{\Omega_0} \mathbf{N}_\vartheta^\top \partial_\vartheta u^\mathrm{h} \,\mathrm{d}V,
\end{aligned} \tag{4.105}$$

and analogously for the entropy,

$$\begin{aligned}
\partial_{\hat{\mathbf{j}}}\mathcal{S} &:= \int_{\Omega_0} \mathbf{N}_J^\top \partial_J \eta^\mathrm{h} \,\mathrm{d}V, \\
\partial_{\hat{\boldsymbol{\vartheta}}}\mathcal{S} &:= \int_{\Omega_0} \mathbf{N}_\vartheta^\top \partial_\vartheta \eta^\mathrm{h} \,\mathrm{d}V,
\end{aligned} \tag{4.106}$$

where $\partial_{(\hat{\bullet})}\mathcal{U}$ and $\partial_{(\hat{\bullet})}\mathcal{S}$ denote the gradients of the discrete functionals with respect to the nodal degrees of freedom, i.e. the vectors representing $\partial\mathcal{U}/\partial\{(\hat{\bullet})\}$ and $\partial\mathcal{S}/\partial\{(\hat{\bullet})\}$.

Applying the chain rule to the discrete functionals yields

$$\begin{aligned}
\frac{\mathrm{d}}{\mathrm{d}t}\mathcal{U}^\mathrm{h} &= \int_{\Omega_0} \partial_{\mathbf{C}} u^\mathrm{h} : \frac{\mathrm{d}}{\mathrm{d}t}\left(N_C^P \hat{\mathbf{C}}^P\right) + \partial_{\mathbf{G}} u^\mathrm{h} : \frac{\mathrm{d}}{\mathrm{d}t}\left(N_C^P \hat{\mathbf{G}}^P\right) \\
&\qquad + \partial_J u^\mathrm{h} \frac{\mathrm{d}}{\mathrm{d}t}\left(N_J^Q \hat{J}^Q\right) + \partial_\vartheta u^\mathrm{h} \frac{\mathrm{d}}{\mathrm{d}t}\left(N_\vartheta^L \hat{\vartheta}^L\right) \,\mathrm{d}V \\
&= \left\{\dot{\hat{\mathbf{C}}}\right\}_\mathrm{V}^\top \partial_{\hat{\mathbf{C}}}\mathcal{U} + \left\{\dot{\hat{\mathbf{G}}}\right\}_\mathrm{V}^\top \partial_{\hat{\mathbf{G}}}\mathcal{U} + \dot{\hat{\mathbf{j}}}^\top \partial_{\hat{\mathbf{j}}}\mathcal{U} + \dot{\hat{\boldsymbol{\vartheta}}}^\top \partial_{\hat{\boldsymbol{\vartheta}}}\mathcal{U}, \\
\frac{\mathrm{d}}{\mathrm{d}t}\mathcal{S}^\mathrm{h} &= \int_{\Omega_0} \partial_J \eta^\mathrm{h} \frac{\mathrm{d}}{\mathrm{d}t}\left(N_J^Q \hat{J}^Q\right) + \partial_\vartheta \eta^\mathrm{h} \frac{\mathrm{d}}{\mathrm{d}t}\left(N_\vartheta^L \hat{\vartheta}^L\right) \,\mathrm{d}V = \dot{\hat{\mathbf{j}}}^\top \partial_{\hat{\mathbf{j}}}\mathcal{S} + \dot{\hat{\boldsymbol{\vartheta}}}^\top \partial_{\hat{\boldsymbol{\vartheta}}}\mathcal{S}.
\end{aligned} \tag{4.107}$$

Now, the space-discrete counterpart of the weak form (4.68) leads to

$$
\begin{aligned}
&\int_{\Omega_0} \mathbf{w}_{\mathbf{p}}^{\mathrm{h}}(\dot{\boldsymbol{\varphi}}^{\mathrm{h}} - \mathbf{v}^{\mathrm{h}})\,\mathrm{d}V = 0\\
&\int_{\Omega_0} \mathbf{w}_{\boldsymbol{\varphi}}^{\mathrm{h}}\rho_0\dot{\mathbf{v}}^{\mathrm{h}} + \operatorname{sym}(\mathbf{F}_{\varphi^{\mathrm{h}}}^{\top}\nabla\mathbf{w}_{\boldsymbol{\varphi}}^{\mathrm{h}}) : \mathbf{S}^{\mathrm{h}} - \mathbf{w}_{\boldsymbol{\varphi}}^{\mathrm{h}}\cdot\bar{\mathbf{b}}\,\mathrm{d}V - \int_{\partial_\sigma\Omega_0}\mathbf{w}_{\boldsymbol{\varphi}}^{\mathrm{h}}\cdot\bar{\mathbf{t}}\,\mathrm{d}A = 0\\
&\int_{\Omega_0} w_{\vartheta}^{\mathrm{h}}\dot{\vartheta}^{\mathrm{h}} + \frac{w_{\vartheta}^{\mathrm{h}}}{\eta_{\vartheta}^{\mathrm{h}}}\eta_J^{\mathrm{h}}J_{\varphi^{\mathrm{h}}}^{-1}\mathbf{G}_{\varphi^{\mathrm{h}}} : \operatorname{sym}(\mathbf{F}_{\varphi^{\mathrm{h}}}^{\top}\nabla\mathbf{v}^{\mathrm{h}}) - \nabla\Big(\frac{w_{\vartheta}^{\mathrm{h}}}{u_{\vartheta}^{\mathrm{h}}}\Big)\cdot\mathbf{Q}^{\mathrm{h}}\,\mathrm{d}V - \int_{\partial_\sigma\Omega_0} w_{\vartheta}^{\mathrm{h}}\bar{q}\,\mathrm{d}A = 0\\
&\int_{\Omega_0} \mathbf{w}_{\mathrm{C}}^{\mathrm{h}} : \big[\dot{\mathbf{C}}^{\mathrm{h}} - 2\,\operatorname{sym}(\mathbf{F}_{\varphi^{\mathrm{h}}}^{\top}\nabla\mathbf{v}^{\mathrm{h}})\big]\,\mathrm{d}V = 0\\
&\int_{\Omega_0} \mathbf{w}_{\mathrm{G}}^{\mathrm{h}} : \big[\dot{\mathbf{G}}^{\mathrm{h}} - 2\mathbf{C}_{\varphi^{\mathrm{h}}} \barwedge \operatorname{sym}(\mathbf{F}_{\varphi^{\mathrm{h}}}^{\top}\nabla\mathbf{v}^{\mathrm{h}})\big]\,\mathrm{d}V = 0\\
&\int_{\Omega_0} w_J^{\mathrm{h}}\big[\dot{J}^{\mathrm{h}} - J_{\varphi^{\mathrm{h}}}^{-1}\mathbf{G}_{\varphi^{\mathrm{h}}} : \operatorname{sym}(\mathbf{F}_{\varphi^{\mathrm{h}}}^{\top}\nabla\mathbf{v}^{\mathrm{h}})\big]\,\mathrm{d}V = 0\\
&\int_{\Omega_0} \mathbf{w}_{\boldsymbol{u}_{\mathrm{C}}}^{\mathrm{h}} : \big[\mathbf{u}_{\mathrm{C}}^{\mathrm{h}} - \partial_{\mathrm{C}}u^{\mathrm{h}}\big]\,\mathrm{d}V = 0\\
&\int_{\Omega_0} \mathbf{w}_{\boldsymbol{u}_{\mathrm{G}}}^{\mathrm{h}} : \big[\mathbf{u}_{\mathrm{G}}^{\mathrm{h}} - \partial_{\mathrm{G}}u^{\mathrm{h}}\big]\,\mathrm{d}V = 0\\
&\int_{\Omega_0} w_{u_J}^{\mathrm{h}}\big[u_J^{\mathrm{h}} - \partial_J u^{\mathrm{h}}\big]\,\mathrm{d}V = 0\\
&\int_{\Omega_0} w_{u_\vartheta}^{\mathrm{h}}(u_{\vartheta}^{\mathrm{h}} - \partial_\vartheta u^{\mathrm{h}})\,\mathrm{d}V = 0\\
&\int_{\Omega_0} w_{\eta_J}^{\mathrm{h}}(\eta_J^{\mathrm{h}} - \partial_J\eta^{\mathrm{h}})\,\mathrm{d}V = 0\\
&\int_{\Omega_0} w_{\eta_\vartheta}^{\mathrm{h}}(\eta_{\vartheta}^{\mathrm{h}} - \partial_\vartheta\eta^{\mathrm{h}})\,\mathrm{d}V = 0,
\end{aligned}
\tag{4.108}
$$

where the space-discrete counterparts of the second Piola Kirchhoff stress tensor and the heat flux vector are given as

$$
\mathbf{S}^{\mathrm{h}} = 2\mathbf{u}_{\mathrm{C}}^{\mathrm{h}} + 2\mathbf{u}_{\mathrm{G}}^{\mathrm{h}} \barwedge \mathbf{C}_{\varphi^{\mathrm{h}}} + J_{\varphi^{\mathrm{h}}}^{-1}\mathbf{G}_{\varphi^{\mathrm{h}}}u_J^{\mathrm{h}} - \Theta^{\mathrm{h}}J_{\varphi^{\mathrm{h}}}^{-1}\mathbf{G}_{\varphi^{\mathrm{h}}}\eta_J^{\mathrm{h}}, \tag{4.109}
$$

and

$$
\mathbf{Q}^{\mathrm{h}} = (\Theta^{\mathrm{h}})^2 k J_{\varphi^{\mathrm{h}}}^{-1}\mathbf{G}_{\varphi^{\mathrm{h}}}\nabla\Big(\frac{1}{\Theta^{\mathrm{h}}}\Big), \tag{4.110}
$$

with

$$
\Theta^{\mathrm{h}} = \frac{u_{\vartheta}^{\mathrm{h}}}{\eta_{\vartheta}^{\mathrm{h}}}. \tag{4.111}
$$

Substituting the finite element approximations into (4.108) and performing a standard Galerkin projection yields the following semi discrete system of coupled algebraic equations

$$
\begin{aligned}
\dot{\hat{\boldsymbol{\varphi}}} - \hat{\mathbf{v}} &= \mathbf{0} \\
\hat{\mathbf{w}}_{\varphi}^{\top}\left[\mathbf{M}_{\varphi}^{\rho}\dot{\hat{\mathbf{v}}} + \boldsymbol{\Phi}\left\{\hat{\mathbf{u}}_{\mathrm{C}}\right\}_{\mathrm{V}} + \boldsymbol{\Psi}\left\{\hat{\mathbf{u}}_{\mathrm{G}}\right\}_{\mathrm{V}} + \Xi_{J}\hat{\mathbf{u}}_{J} - \Xi_{\vartheta}\hat{\mathbf{u}}_{\vartheta} - \mathbf{b} - \mathbf{t}\right] &= 0 \\
\hat{\mathbf{w}}_{\vartheta}^{\top}\left[\mathbf{M}_{\vartheta}\dot{\hat{\boldsymbol{\vartheta}}} + \Xi_{\vartheta}^{\top}\hat{\mathbf{v}} - \mathbf{y}_{Q} - \mathbf{q}\right] &= 0 \\
\left\{\hat{\mathbf{w}}_{\mathrm{C}}\right\}_{\mathrm{V}}^{\top}\left[\mathbf{M}_{\mathrm{C}}\left\{\dot{\hat{\mathbf{C}}}\right\}_{\mathrm{V}} - \boldsymbol{\Phi}^{\top}\hat{\mathbf{v}}\right] &= 0 \\
\left\{\hat{\mathbf{w}}_{\mathrm{G}}\right\}_{\mathrm{V}}^{\top}\left[\mathbf{M}_{\mathrm{C}}\left\{\dot{\hat{\mathbf{G}}}\right\}_{\mathrm{V}} - \boldsymbol{\Psi}^{\top}\hat{\mathbf{v}}\right] &= 0 \\
\hat{\mathbf{w}}_{J}^{\top}\left[\mathbf{M}_{J}\dot{\hat{\mathbf{J}}} - \Xi_{J}^{\top}\hat{\mathbf{v}}\right] &= 0 \\
\left\{\hat{\mathbf{w}}_{\boldsymbol{u}_{\mathrm{C}}}\right\}_{\mathrm{V}}^{\top}\left[\mathbf{M}_{\mathrm{C}}\left\{\hat{\mathbf{u}}_{\mathrm{C}}\right\}_{\mathrm{V}} - \partial_{\hat{\mathrm{C}}}\mathcal{U}\right] &= 0 \\
\left\{\hat{\mathbf{w}}_{\boldsymbol{u}_{\mathrm{G}}}\right\}_{\mathrm{V}}^{\top}\left[\mathbf{M}_{\mathrm{C}}\left\{\hat{\mathbf{u}}_{\mathrm{G}}\right\}_{\mathrm{V}} - \partial_{\hat{\mathrm{G}}}\mathcal{U}\right] &= 0 \\
\hat{\mathbf{w}}_{u_{J}}^{\top}\left[\mathbf{M}_{J}\hat{\mathbf{u}}_{J} - \partial_{\hat{\mathrm{J}}}\mathcal{U}\right] &= 0 \\
\hat{\mathbf{w}}_{u_{\vartheta}}^{\top}\left[\mathbf{M}_{\vartheta}\hat{\mathbf{u}}_{\vartheta} - \partial_{\hat{\boldsymbol{\vartheta}}}\mathcal{U}\right] &= 0 \\
\hat{\mathbf{w}}_{\eta_{J}}^{\top}\left[\mathbf{M}_{J}\hat{\boldsymbol{\eta}}_{J} - \partial_{\hat{\mathrm{J}}}\mathcal{S}\right] &= 0 \\
\hat{\mathbf{w}}_{\eta_{\vartheta}}^{\top}\left[\mathbf{M}_{\vartheta}\hat{\boldsymbol{\eta}}_{\vartheta} - \partial_{\hat{\boldsymbol{\vartheta}}}\mathcal{S}\right] &= 0
\end{aligned}
\tag{4.112}
$$

by defining the integrals

$$
\begin{aligned}
\mathbf{M}_{\varphi}^{\rho} &= \int_{\Omega_0} \rho_0 \mathbf{N}_{\varphi}^{\top}\mathbf{N}_{\varphi}\,\mathrm{d}V \\
\mathbf{M}_{\vartheta} &= \int_{\Omega_0} \mathbf{N}_{\vartheta}^{\top}\mathbf{N}_{\vartheta}\,\mathrm{d}V \\
\mathbf{M}_{\mathrm{C}} &= \int_{\Omega_0} \mathbf{N}_{C}^{\top}\mathbf{N}_{C}\,\mathrm{d}V \\
\mathbf{M}_{J} &= \int_{\Omega_0} \mathbf{N}_{J}^{\top}\mathbf{N}_{J}\,\mathrm{d}V \\
\boldsymbol{\Phi} &= \int_{\Omega_0} 2\mathbb{B}_{\hat{\boldsymbol{\varphi}}}^{\top}\mathbf{N}_{C}\,\mathrm{d}V \\
\boldsymbol{\Psi} &= \int_{\Omega_0} 2\mathbb{B}_{\hat{\boldsymbol{\varphi}}}^{\top}\mathcal{D}(\mathbf{C}_{\boldsymbol{\varphi}^{\mathrm{h}}})\mathbf{N}_{C}\,\mathrm{d}V \\
\Xi_{J} &= \int_{\Omega_0} \mathbb{B}_{\hat{\boldsymbol{\varphi}}}^{\top} J_{\varphi^{\mathrm{h}}}^{-1}\left\{\mathbf{G}_{\varphi^{\mathrm{h}}}\right\}_{\mathrm{V}}\mathbf{N}_{J}\,\mathrm{d}V \\
\Xi_{\vartheta} &= \int_{\Omega_0} \mathbb{B}_{\hat{\boldsymbol{\varphi}}}^{\top}\frac{1}{\eta_{\vartheta}^{\mathrm{h}}}\eta_{J}^{\mathrm{h}} J_{\varphi^{\mathrm{h}}}^{-1}\left\{\mathbf{G}_{\varphi^{\mathrm{h}}}\right\}_{\mathrm{V}}\mathbf{N}_{\vartheta}\,\mathrm{d}V \\
\mathbf{y}_{Q} &= \int_{\Omega_0} \left(\frac{u_{\vartheta}^{\mathrm{h}}\nabla(\mathbf{N}_{\vartheta}) - \mathbf{N}_{\vartheta}\nabla(u_{\vartheta}^{\mathrm{h}})}{(u_{\vartheta}^{\mathrm{h}})^{2}}\right)^{\top}\mathbf{Q}^{\mathrm{h}}\,\mathrm{d}V \\
\mathbf{b} &= \int_{\Omega_0} \mathbf{N}_{\varphi}^{\top}\bar{\mathbf{b}}\,\mathrm{d}V \\
\mathbf{t} &= \int_{\partial\Omega_0} \mathbf{N}_{\varphi}^{\top}\bar{\mathbf{t}}\,\mathrm{d}A \\
\mathbf{q} &= \int_{\partial\Omega_0} \mathbf{N}_{\vartheta}^{\top}\bar{q}\,\mathrm{d}A.
\end{aligned}
\tag{4.113}
$$

Within the assembled finite element formulation, the discrete strain-displacement relation is conveniently expressed in matrix form. To this end, we introduce the standard nodal kinematic operator via

$$\operatorname{sym}(\mathbf{F}_{\boldsymbol{\varphi}^{\mathrm{h}}}^{\top}\nabla \mathbf{w}_{\varphi}^{\mathrm{h}}) : \mathbf{A} = \left\{\mathbf{A}\right\}_{\mathrm{V}}^{\top} \mathbb{B}_{\hat{\boldsymbol{\varphi}}} \hat{\mathbf{w}}_{\varphi}. \tag{4.114}$$

Here, the matrix $\mathbb{B}_{\hat{\boldsymbol{\varphi}}} \in \mathbb{R}^{6\times 3n_{\mathrm{node}}}$ collects the spatial derivatives of the shape functions in Voigt representation and acts as the discrete counterpart of the symmetric gradient operator in the finite element setting.

The Voigt representation of tensor cross products combined with a double contraction can be expressed compactly by introducing the structural matrix $\mathcal{D}(\square) \in \mathbb{R}^{6\times 6}$, defined such that

$$(\mathbf{A} \overset{\times}{\otimes} \mathbf{B}) : \mathbf{C} = \left\{\mathbf{A}\right\}_{\mathrm{V}}^{\top} \mathcal{D}(\mathbf{C}) \left\{\mathbf{B}\right\}_{\mathrm{V}}, \tag{4.115}$$

where $\mathbf{A}$ denotes a symmetric strain-type tensor and $\mathbf{B}$ a symmetric stress-type tensor. For completeness, the explicit forms of the nodal operator matrix $\mathbb{B}_{\hat{\boldsymbol{\varphi}}}$ and the structural matrix $\mathcal{D}(\square)$ are collected in Appendices 4.9.1 and 4.9.2, respectively.

4.6.2. GENERIC-consistent semi-discrete formulation

We show that the above spatial discretization yields a GENERIC-consistent semi-discrete formulation in the sense that the space-discrete evolution equations can be written in GENERIC form for finite-dimensional systems. Unlike the continuous formulation, the finite element discretization naturally introduces mass matrices associated with the underlying approximation spaces. Therefore, it is convenient to formulate the semi-discrete GENERIC system in descriptor form.

Accordingly, we consider

$$\mathbf{E}\dot{\hat{\mathbf{x}}} = \mathbf{L}\mathbf{z}_{\mathcal{E}} + \mathbf{K}\mathbf{z}_{\mathcal{S}}, \tag{4.116}$$

where

$$\begin{aligned} \mathbf{E}^{\top}\mathbf{z}_{\mathcal{E}} &= \nabla \mathcal{E}(\hat{\mathbf{x}}), \\ \mathbf{E}^{\top}\mathbf{z}_{\mathcal{S}} &= \nabla \mathcal{S}(\hat{\mathbf{x}}). \end{aligned} \tag{4.117}$$

The vectors $\mathbf{z}_{\mathcal{E}}$ and $\mathbf{z}_{\mathcal{S}}$ play the role of discrete thermodynamic driving forces associated with the total energy and entropy functions, respectively. The matrices $\mathbf{L}$ and $\mathbf{K}$ represent the discrete counterparts of the GENERIC operators $\mathcal{L}$ and $\mathcal{K}$, governing the reversible and irreversible contributions to the semi-discrete dynamics. This descriptor representation naturally arises from the finite element discretization and the associated mass matrices. A similar formulation for the isothermal case has previously been employed in the context of structure-preserving discretizations of port-Hamiltonian systems in [A2]. The system is supplemented by the discrete non-interaction conditions

$$\begin{aligned} \mathbf{L}\mathbf{z}_{\mathcal{S}} &= \mathbf{0}, \\ \mathbf{K}\mathbf{z}_{\mathcal{E}} &= \mathbf{0}. \end{aligned} \tag{4.118}$$

The state vector $\hat{\mathbf{x}}$ collects the nodal values of its continuous counterpart X and is given by

$$\hat{\mathbf{x}} = \begin{bmatrix} \hat{\boldsymbol{\varphi}}^{\top} & \hat{\mathbf{v}}^{\top} & \left\{\hat{\mathbf{C}}\right\}_{\mathrm{V}}^{\top} & \left\{\hat{\mathbf{G}}\right\}_{\mathrm{V}}^{\top} & \hat{\mathbf{J}}^{\top} & \hat{\boldsymbol{\vartheta}}^{\top} \end{bmatrix}^{\top}. \tag{4.119}$$

The descriptor matrix $\mathbf{E}$ is defined as

$$\mathbf{E} = \operatorname{diag}\begin{bmatrix} \mathbf{I} & \mathbf{M}_{\varphi}^{\rho} & \mathbf{M}_{\mathrm{C}} & \mathbf{M}_{\mathrm{C}} & \mathbf{M}_{J} & \mathbf{M}_{\vartheta} \end{bmatrix}. \tag{4.120}$$

In the present setting, $\mathbf{E} = \mathbf{E}^\top$.

With regard to $(4.117)_1$, the discrete energy driving force is obtained as

$$\mathbf{z}_{\mathcal{E}} = \begin{bmatrix} -\mathbf{b}^\top & \hat{\mathbf{v}}^\top & \{\hat{\mathbf{u}}_{\mathrm{C}}\}_{\mathrm{V}}^\top & \{\hat{\mathbf{u}}_{\mathrm{G}}\}_{\mathrm{V}}^\top & \hat{\mathbf{u}}_J^\top & \hat{\mathbf{u}}_\vartheta^\top \end{bmatrix}^\top. \tag{4.121}$$

The discrete total energy follows from the total energy by inserting the space-discrete approximations introduced above. Thus,

$$\mathcal{E}(\hat{\mathbf{x}}) := \mathcal{E}^{\mathrm{h}} = \mathcal{T}^{\mathrm{h}} + \mathcal{U}^{\mathrm{h}} + \mathcal{V}^{\mathrm{h}}, \tag{4.122}$$

where the discrete internal energy $\mathcal{U}^{\mathrm{h}}$ has been introduced in (4.104). The discrete kinetic energy and the discrete external potential are given by

$$\mathcal{T}^{\mathrm{h}} = \int_{\Omega_0} \frac{1}{2}\rho_0 \mathbf{v}^{\mathrm{h}} \cdot \mathbf{v}^{\mathrm{h}} \,\mathrm{d}V = \frac{1}{2}\hat{\mathbf{v}}^\top \mathbf{M}_\varphi^\rho \hat{\mathbf{v}} \tag{4.123}$$

and

$$\mathcal{V}^{\mathrm{h}} = -\int_{\Omega_0} \bar{\mathbf{b}} \cdot \boldsymbol{\varphi}^{\mathrm{h}} \,\mathrm{d}V = -\hat{\boldsymbol{\varphi}}^\top \mathbf{b}. \tag{4.124}$$

Consequently, the gradient of the discrete total energy can be written as

$$\nabla\mathcal{E}(\hat{\mathbf{x}}) = \begin{bmatrix} \partial_{\hat{\boldsymbol{\varphi}}}\mathcal{V}^\top & \partial_{\hat{\mathbf{v}}}\mathcal{T}^\top & \partial_{\hat{\mathbf{C}}}\mathcal{U}^\top & \partial_{\hat{\mathbf{G}}}\mathcal{U}^\top & \partial_{\hat{\mathbf{J}}}\mathcal{U}^\top & \partial_{\hat{\boldsymbol{\vartheta}}}\mathcal{U}^\top \end{bmatrix}^\top. \tag{4.125}$$

The last four equations in $(4.117)_1$ follow directly from $(4.112)_7$–$(4.112)_{10}$, whereas the first two relations follow from the discrete external potential (4.124) and the discrete kinetic energy (4.123).

Similarly, $(4.117)_2$ gives rise to

$$\mathbf{z}_{\mathcal{S}} = \begin{bmatrix} \mathbf{0}^\top & \mathbf{0}^\top & \mathbf{0}^\top & \mathbf{0}^\top & \hat{\boldsymbol{\eta}}_J^\top & \hat{\boldsymbol{\eta}}_\vartheta^\top \end{bmatrix}^\top, \tag{4.126}$$

with

$$\nabla\mathcal{S}(\hat{\mathbf{x}}) = \begin{bmatrix} \partial_{\hat{\boldsymbol{\varphi}}}\mathcal{S}^\top & \partial_{\hat{\mathbf{v}}}\mathcal{S}^\top & \partial_{\hat{\mathbf{C}}}\mathcal{S}^\top & \partial_{\hat{\mathbf{G}}}\mathcal{S}^\top & \partial_{\hat{\mathbf{J}}}\mathcal{S}^\top & \partial_{\hat{\boldsymbol{\vartheta}}}\mathcal{S}^\top \end{bmatrix}^\top, \tag{4.127}$$

where the discrete counterpart of the system's total entropy is defined in $(4.104)_2$. The last two equations in $(4.117)_2$ follow directly from the last two equations in (4.112).

The Poisson matrix can be inferred from $(4.112)_1$–$(4.112)_6$ and is given by

$$\mathbf{L} = \begin{bmatrix} \mathbf{0} & \mathbf{I} & \mathbf{0} & \mathbf{0} & \mathbf{0} & \mathbf{0} \\ -\mathbf{I} & \mathbf{0} & -\boldsymbol{\Phi} & -\boldsymbol{\Psi} & -\Xi_J & \Xi_\vartheta \\ \mathbf{0} & \boldsymbol{\Phi}^\top & \mathbf{0} & \mathbf{0} & \mathbf{0} & \mathbf{0} \\ \mathbf{0} & \boldsymbol{\Psi}^\top & \mathbf{0} & \mathbf{0} & \mathbf{0} & \mathbf{0} \\ \mathbf{0} & \Xi_J^\top & \mathbf{0} & \mathbf{0} & \mathbf{0} & \mathbf{0} \\ \mathbf{0} & -\Xi_\vartheta^\top & \mathbf{0} & \mathbf{0} & \mathbf{0} & \mathbf{0} \end{bmatrix}. \tag{4.128}$$

By construction, $\mathbf{L}$ is skew-symmetric, i.e., $\mathbf{L} = -\mathbf{L}^\top$. Furthermore, the first discrete non-interaction condition $(4.118)_1$ is satisfied. Indeed, evaluation of $\mathbf{L}\mathbf{z}_{\mathcal{S}}$ shows that all rows vanish identically except for the second one, yielding

$$-\Xi_J \hat{\boldsymbol{\eta}}_J + \Xi_\vartheta \hat{\boldsymbol{\eta}}_\vartheta = \mathbf{0}. \tag{4.129}$$

This identity follows directly from the definitions of Ξ_J and Ξ_ϑ given in (4.113).

Furthermore, the friction matrix can be inferred from the heat-conduction contribution in $(4.112)_3$. The only non-zero block of $\mathbf{K}$ is the temperature-temperature block $\mathbf{K}_{\hat{\vartheta}\hat{\vartheta}}$, whose entries are

$$K_{\vartheta_A\vartheta_B} = \int_{\Omega_0} \mathbf{k}_A \cdot (\Theta^{\mathrm{h}})^2 k J_{\varphi^{\mathrm{h}}}^{-1} \mathbf{G}_{\varphi^{\mathrm{h}}} \mathbf{k}_B \,\mathrm{d}V \tag{4.130}$$

with

$$\mathbf{k}_A = \frac{1}{u_\vartheta^{\mathrm{h}}} \nabla N_\vartheta^A - \frac{N_\vartheta^A}{(u_\vartheta^{\mathrm{h}})^2} \nabla u_\vartheta^{\mathrm{h}}. \tag{4.131}$$

All remaining blocks of $\mathbf{K}$ vanish. For the positive semi-definiteness of $\mathbf{K}$, let $\mathbf{y}$ be an arbitrary vector. Then, the quadratic form associated with $\mathbf{K}$ reads

$$\mathbf{y}^\top \mathbf{K} \mathbf{y} = \sum_{A,B} y_A K_{\vartheta_A\vartheta_B} y_B = \int_{\Omega_0} \Big(\sum_A y_A \mathbf{k}_A \Big) \cdot (\Theta^{\mathrm{h}})^2 k J_{\varphi^{\mathrm{h}}}^{-1} \mathbf{G}_{\varphi^{\mathrm{h}}} \Big(\sum_B y_B \mathbf{k}_B \Big) \,\mathrm{d}V \geq 0. \tag{4.132}$$

Consequently, under the assumptions $k \geq 0$, $J_{\varphi^{\mathrm{h}}} > 0$ and $\mathbf{G}_{\varphi^{\mathrm{h}}} \succ 0$, the matrix $\mathbf{K}$ is indeed positive semi-definite.

Moreover, the discrete non-interaction condition $\mathbf{K}\mathbf{z}_{\mathcal{E}} = \mathbf{0}$ follows from

$$\sum_A \hat{u}_{\vartheta,A} \mathbf{k}_A = \frac{1}{u_\vartheta^{\mathrm{h}}} \nabla u_\vartheta^{\mathrm{h}} - \frac{u_\vartheta^{\mathrm{h}}}{(u_\vartheta^{\mathrm{h}})^2} \nabla u_\vartheta^{\mathrm{h}} = \mathbf{0}. \tag{4.133}$$

The GENERIC structure of the semi-discrete system thus immediately implies consistency with the first and second laws of thermodynamics. Indeed, using (4.116) and (4.117), the time derivative of the discrete total energy is given by

$$\dot{\mathcal{E}}(\hat{\mathbf{x}}) = \nabla \mathcal{E}(\hat{\mathbf{x}})^\top \dot{\hat{\mathbf{x}}} = \mathbf{z}_{\mathcal{E}}^\top \mathbf{E} \dot{\hat{\mathbf{x}}} = \mathbf{z}_{\mathcal{E}}^\top \mathbf{L} \mathbf{z}_{\mathcal{E}} + \mathbf{z}_{\mathcal{E}}^\top \mathbf{K} \mathbf{z}_{\mathcal{S}}. \tag{4.134}$$

The first term on the right-hand side of (4.134) vanishes due to the skew-symmetry of $\mathbf{L}$, whereas the second term vanishes by the discrete non-interaction condition $(4.118)_1$. Consequently,

$$\dot{\mathcal{E}}(\hat{\mathbf{x}}) = 0. \tag{4.135}$$

Similarly, the time derivative of the discrete total entropy is obtained as

$$\dot{\mathcal{S}}(\hat{\mathbf{x}}) = \nabla \mathcal{S}(\hat{\mathbf{x}})^\top \dot{\hat{\mathbf{x}}} = \mathbf{z}_{\mathcal{S}}^\top \mathbf{E} \dot{\hat{\mathbf{x}}} = \mathbf{z}_{\mathcal{S}}^\top \mathbf{L} \mathbf{z}_{\mathcal{E}} + \mathbf{z}_{\mathcal{S}}^\top \mathbf{K} \mathbf{z}_{\mathcal{S}}. \tag{4.136}$$

The first term on the right-hand side of (4.136) vanishes due to the discrete non-interaction condition $(4.118)_2$, while the second term is non-negative due to the positive semi-definiteness of $\mathbf{K}$. Hence,

$$\dot{\mathcal{S}}(\hat{\mathbf{x}}) = \mathbf{z}_{\mathcal{S}}^\top \mathbf{K} \mathbf{z}_{\mathcal{S}} \geq 0. \tag{4.137}$$

Thus, the semi-discrete formulation inherits the GENERIC structure and is consistent with the first and second laws of thermodynamics.

4.6.3. Verification of the discrete energy balance

Although energy conservation follows directly from the GENERIC structure, the following derivation verifies this property directly from the semi-discrete weak form and reveals the exact cancellation of the internal coupling terms.

Using the discrete energy functional introduced in (4.122), we investigate the evolution of $\mathcal{E}^{\mathrm{h}}$ through a specific admissible choice of discrete test functions

$$\begin{aligned} \hat{\mathbf{w}}_{\varphi} &= \dot{\hat{\boldsymbol{\varphi}}}, & \hat{\mathbf{w}}_{\vartheta} &= \hat{\mathbf{u}}_{\vartheta}, & \hat{\mathbf{w}}_{u_\vartheta} &= -\dot{\hat{\boldsymbol{\vartheta}}}, \\ \{\hat{\mathbf{w}}_{\boldsymbol{u}_{\mathrm{C}}}\}_{\mathrm{V}} &= -\{\dot{\hat{\mathbf{C}}}\}_{\mathrm{V}}, & \{\hat{\mathbf{w}}_{\boldsymbol{u}_{\mathrm{G}}}\}_{\mathrm{V}} &= -\{\dot{\hat{\mathbf{G}}}\}_{\mathrm{V}}, & \hat{\mathbf{w}}_{u_J} &= -\dot{\hat{\mathbf{J}}}, \\ \{\hat{\mathbf{w}}_{\mathrm{C}}\}_{\mathrm{V}} &= \{\hat{\mathbf{u}}_{\mathrm{C}}\}_{\mathrm{V}}, & \{\hat{\mathbf{w}}_{\mathrm{G}}\}_{\mathrm{V}} &= \{\hat{\mathbf{u}}_{\mathrm{G}}\}_{\mathrm{V}}, & \hat{\mathbf{w}}_{J} &= \hat{\mathbf{u}}_{J}. \end{aligned} \tag{4.138}$$

Inserting these relations into the spatially discrete weak formulation (4.112) and combining equations $(4.112)_2$–$(4.112)_{10}$, together with the identity $\hat{\mathbf{v}} = \dot{\hat{\boldsymbol{\varphi}}}$, yields a balance relation in which all internal coupling terms are retained explicitly:

$$\begin{aligned} &\hat{\mathbf{v}}^{\top}\mathbf{M}_{\varphi}^{\rho}\dot{\hat{\mathbf{v}}} + \dot{\hat{\boldsymbol{\varphi}}}^{\top}\boldsymbol{\Phi}(\hat{\boldsymbol{\varphi}})\{\hat{\mathbf{u}}_{\mathrm{C}}\}_{\mathrm{V}} + \dot{\hat{\boldsymbol{\varphi}}}^{\top}\boldsymbol{\Psi}(\hat{\boldsymbol{\varphi}})\{\hat{\mathbf{u}}_{\mathrm{G}}\}_{\mathrm{V}} + \dot{\hat{\boldsymbol{\varphi}}}^{\top}\Xi_J\hat{\mathbf{u}}_J - \dot{\hat{\boldsymbol{\varphi}}}^{\top}\Xi_\vartheta\hat{\mathbf{u}}_\vartheta - \dot{\hat{\boldsymbol{\varphi}}}^{\top}\mathbf{b} - \dot{\hat{\boldsymbol{\varphi}}}^{\top}\mathbf{t} \\ &\quad + \hat{\mathbf{u}}_\vartheta^{\top}\mathbf{M}_\vartheta\dot{\hat{\boldsymbol{\vartheta}}} + \hat{\mathbf{u}}_\vartheta^{\top}\Xi_\vartheta^{\top}\dot{\hat{\boldsymbol{\varphi}}} - \hat{\mathbf{u}}_\vartheta^{\top}\mathbf{y}_Q - \hat{\mathbf{u}}_\vartheta^{\top}\mathbf{q} \\ &\quad + \{\hat{\mathbf{u}}_{\mathrm{C}}\}_{\mathrm{V}}^{\top}\mathbf{M}_{\mathrm{C}}\{\dot{\hat{\mathbf{C}}}\}_{\mathrm{V}} - \{\hat{\mathbf{u}}_{\mathrm{C}}\}_{\mathrm{V}}^{\top}\boldsymbol{\Phi}^{\top}(\hat{\boldsymbol{\varphi}})\dot{\hat{\boldsymbol{\varphi}}} + \{\hat{\mathbf{u}}_{\mathrm{G}}\}_{\mathrm{V}}^{\top}\mathbf{M}_{\mathrm{C}}\{\dot{\hat{\mathbf{G}}}\}_{\mathrm{V}} - \{\hat{\mathbf{u}}_{\mathrm{G}}\}_{\mathrm{V}}^{\top}\boldsymbol{\Psi}^{\top}(\hat{\boldsymbol{\varphi}})\dot{\hat{\boldsymbol{\varphi}}} \\ &\quad - \{\dot{\hat{\mathbf{C}}}\}_{\mathrm{V}}^{\top}\mathbf{M}_{\mathrm{C}}\{\hat{\mathbf{u}}_{\mathrm{C}}\}_{\mathrm{V}} + \{\dot{\hat{\mathbf{C}}}\}_{\mathrm{V}}^{\top}\partial_{\hat{\mathrm{C}}}\mathcal{U} - \{\dot{\hat{\mathbf{G}}}\}_{\mathrm{V}}^{\top}\mathbf{M}_{\mathrm{C}}\{\hat{\mathbf{u}}_{\mathrm{G}}\}_{\mathrm{V}} + \{\dot{\hat{\mathbf{G}}}\}_{\mathrm{V}}^{\top}\partial_{\hat{\mathrm{G}}}\mathcal{U} \\ &\quad - \dot{\hat{\mathbf{J}}}^{\top}\mathbf{M}_J\hat{\mathbf{u}}_J + \dot{\hat{\mathbf{J}}}^{\top}\partial_{\hat{\mathbf{J}}}\mathcal{U} + \hat{\mathbf{u}}_J^{\top}\mathbf{M}_J\dot{\hat{\mathbf{J}}} - \hat{\mathbf{u}}_J^{\top}\Xi_J^{\top}\dot{\hat{\boldsymbol{\varphi}}} \\ &\quad - \dot{\hat{\boldsymbol{\vartheta}}}^{\top}\mathbf{M}_\vartheta\hat{\mathbf{u}}_\vartheta + \dot{\hat{\boldsymbol{\vartheta}}}^{\top}\partial_{\hat{\boldsymbol{\vartheta}}}\mathcal{U} = 0. \end{aligned} \tag{4.139}$$

The term involving $\mathbf{y}_Q$ does not contribute to the energy balance: Inserting $u_\vartheta^{\mathrm{h}} = \mathbf{N}_\vartheta\hat{\mathbf{u}}_\vartheta$ shows that the integrand cancels pointwise, implying

$$\hat{\mathbf{u}}_\vartheta^{\top}\mathbf{y}_Q = 0. \tag{4.140}$$

After elimination of this term, the remaining expression can be reorganized into

$$\hat{\mathbf{v}}^{\top}\mathbf{M}_{\varphi}^{\rho}\dot{\hat{\mathbf{v}}} - \dot{\hat{\boldsymbol{\varphi}}}^{\top}\mathbf{b} - \dot{\hat{\boldsymbol{\varphi}}}^{\top}\mathbf{t} - \hat{\mathbf{u}}_\vartheta^{\top}\mathbf{q} + \{\dot{\hat{\mathbf{C}}}\}_{\mathrm{V}}^{\top}\partial_{\hat{\mathrm{C}}}\mathcal{U} + \{\dot{\hat{\mathbf{G}}}\}_{\mathrm{V}}^{\top}\partial_{\hat{\mathrm{G}}}\mathcal{U} + \dot{\hat{\mathbf{J}}}^{\top}\partial_{\hat{\mathbf{J}}}\mathcal{U} + \dot{\hat{\boldsymbol{\vartheta}}}^{\top}\partial_{\hat{\boldsymbol{\vartheta}}}\mathcal{U} = 0. \tag{4.141}$$

Using the definitions of the discrete kinetic, internal, and external energies introduced above, the previous relation can be written as

$$\frac{\mathrm{d}}{\mathrm{d}t}\left(\mathcal{T}^{\mathrm{h}} + \mathcal{U}^{\mathrm{h}} + \mathcal{V}^{\mathrm{h}}\right) = \dot{\hat{\boldsymbol{\varphi}}}^{\top}\mathbf{t} + \hat{\mathbf{u}}_\vartheta^{\top}\mathbf{q}. \tag{4.142}$$

Hence, for vanishing Neumann-type boundary contributions, we again end at (4.135).

4.6.4. Verification of discrete entropy production

Likewise, non-negative entropy production can be verified directly from the semi-discrete weak form (4.112). We choose admissible discrete test functions

$$\hat{\mathbf{w}}_\vartheta = \hat{\boldsymbol{\eta}}_\vartheta,\ \hat{\mathbf{w}}_J = \hat{\boldsymbol{\eta}}_J,\ \hat{\mathbf{w}}_{\eta_J} = -\dot{\hat{\mathbf{J}}},\ \hat{\mathbf{w}}_{\eta_\vartheta} = -\dot{\hat{\boldsymbol{\vartheta}}}. \tag{4.143}$$

Summing equations $(4.112)_3$, $(4.112)_6$, $(4.112)_{11}$ and $(4.112)_{12}$ and inserting the above test functions yields

$$\begin{aligned}\hat{\boldsymbol{\eta}}_\vartheta^\top \mathbf{M}_\vartheta \dot{\hat{\boldsymbol{\vartheta}}} + \hat{\boldsymbol{\eta}}_\vartheta^\top \Xi_\vartheta^\top \hat{\mathbf{v}} - \hat{\boldsymbol{\eta}}_\vartheta^\top \mathbf{y}_Q - \hat{\boldsymbol{\eta}}_\vartheta^\top \mathbf{q} + \hat{\boldsymbol{\eta}}_J^\top \mathbf{M}_J \dot{\hat{\mathbf{J}}} - \hat{\boldsymbol{\eta}}_J^\top \Xi_J^\top \hat{\mathbf{v}} \\ - \dot{\hat{\mathbf{J}}}^\top \mathbf{M}_J \hat{\boldsymbol{\eta}}_J + \dot{\hat{\mathbf{J}}}^\top \partial_{\hat{\mathbf{J}}} \mathcal{S} - \dot{\hat{\boldsymbol{\vartheta}}}^\top \mathbf{M}_\vartheta \hat{\boldsymbol{\eta}}_\vartheta + \dot{\hat{\boldsymbol{\vartheta}}}^\top \partial_{\hat{\boldsymbol{\vartheta}}} \mathcal{S} = 0.\end{aligned} \tag{4.144}$$

A closer inspection shows that the coupling terms involving $\hat{\mathbf{v}}$ cancel exactly due to the structure of the finite element approximations, which implies

$$\begin{aligned}\hat{\boldsymbol{\eta}}_\vartheta^\top \Xi_\vartheta^\top \hat{\mathbf{v}} &= \int_{\Omega_0} \hat{\boldsymbol{\eta}}_\vartheta^\top \mathbf{N}_\vartheta^\top \frac{1}{\eta_\vartheta^{\mathrm{h}}} \eta_J^{\mathrm{h}} J_{\varphi^{\mathrm{h}}}^{-1} \left\{\mathbf{G}_{\varphi^{\mathrm{h}}}\right\}_{\mathrm{V}}^\top \mathbb{B}_{\hat{\boldsymbol{\varphi}}} \dot{\hat{\boldsymbol{\varphi}}} \, \mathrm{d}V \\ &= \int_{\Omega_0} \hat{\boldsymbol{\eta}}_J^\top \mathbf{N}_J^\top J_{\varphi^{\mathrm{h}}}^{-1} \left\{\mathbf{G}_{\varphi^{\mathrm{h}}}\right\}_{\mathrm{V}}^\top \mathbb{B}_{\hat{\boldsymbol{\varphi}}} \dot{\hat{\boldsymbol{\varphi}}} \, \mathrm{d}V = \hat{\boldsymbol{\eta}}_J^\top \Xi_J^\top \hat{\mathbf{v}}.\end{aligned} \tag{4.145}$$

Consequently, the entropy balance simplifies to

$$\dot{\hat{\boldsymbol{\vartheta}}}^\top \partial_{\hat{\boldsymbol{\vartheta}}} \mathcal{S} + \dot{\hat{\mathbf{J}}}^\top \partial_{\hat{\mathbf{J}}} \mathcal{S} - \hat{\boldsymbol{\eta}}_\vartheta^\top \mathbf{q} = \int_{\Omega_0} \nabla\Big(\frac{\eta_\vartheta^{\mathrm{h}}}{u_\vartheta^{\mathrm{h}}}\Big)^\top (\Theta^{\mathrm{h}})^2 k J_{\varphi^{\mathrm{h}}}^{-1} \mathbf{G}_{\varphi^{\mathrm{h}}} \nabla\Big(\frac{\eta_\vartheta^{\mathrm{h}}}{u_\vartheta^{\mathrm{h}}}\Big) \, \mathrm{d}V \geq 0. \tag{4.146}$$

Under the assumptions $k \geq 0$, $J_{\varphi^{\mathrm{h}}} > 0$, and $\mathbf{G}_{\varphi^{\mathrm{h}}} \succ 0$, the right-hand side is non-negative. Hence,

$$\dot{\mathcal{S}} = \dot{\hat{\boldsymbol{\vartheta}}}^\top \partial_{\hat{\boldsymbol{\vartheta}}} \mathcal{S} + \dot{\hat{\mathbf{J}}}^\top \partial_{\hat{\mathbf{J}}} \mathcal{S} - \hat{\boldsymbol{\eta}}_\vartheta^\top \mathbf{q} \geq 0, \tag{4.147}$$

which verifies non-negative entropy production at the semi-discrete level.

4.7. Numerical examples

The numerical examples presented in this section are intended to illustrate the performance and thermodynamic consistency of the proposed mixed GENERIC discretization framework. In particular, the numerical investigations focus on the preservation of the total energy for closed systems and the non-negative production of entropy in the presence of heat conduction.

4.7.1. Material models and discretization

In the first part of this Section, the general conditions of the simulations are introduced, including the employed constitutive models and the underlying spatial and temporal discretization.

4.7.1.1. Mooney–Rivlin-type material model

For the numerical investigations, a thermoelastic Mooney–Rivlin-type material model is employed. The chosen constitutive setting combines a polyconvex representation of the mechanical response with a simple thermo-mechanical coupling law and is particularly well suited for the present mixed formulation, since all kinematic quantities $\mathbf{C}$, $\mathbf{G}$, and J enter explicitly into the free energy function.

The Helmholtz free energy density is assumed in the additive form

$$\psi(\mathbf{C}, \mathbf{G}, J, \vartheta) = \psi_0(\vartheta) + \psi_1(\mathbf{C}, \mathbf{G}, J) - (\vartheta - \vartheta_0)\psi_2(J), \tag{4.148}$$

where ψ_0 denotes the purely thermal contribution, ψ_1 the purely mechanical contribution, and the last term represents a thermo-mechanical coupling contribution.

The purely thermal part is chosen as

$$\psi_0(\vartheta) = \kappa\big(\vartheta - \vartheta_0 - \vartheta \ln \frac{\vartheta}{\vartheta_0}\big), \tag{4.149}$$

where κ is a heat capacity parameter and ϑ_0 denotes the reference temperature. This contribution yields the classical logarithmic temperature dependence frequently employed in finite thermoelasticity and guarantees thermodynamic consistency of the thermal response.

The mechanical contribution is additively decomposed into an isochoric-type and a volumetric contribution according to

$$\psi_1(\mathbf{C}, \mathbf{G}, J) = \psi_{1\mathrm{a}}(\mathbf{C}, \mathbf{G}) + \psi_{1\mathrm{b}}(J), \tag{4.150}$$

with

$$\psi_{1\mathrm{a}}(\mathbf{C}, \mathbf{G}) = a(\operatorname{tr}\mathbf{C} - 3) + b(\operatorname{tr}\mathbf{G} - 3), \tag{4.151}$$

and

$$\psi_{1\mathrm{b}}(J) = \frac{c_1}{2}(J-1)^2 - d_1 \ln J, \tag{4.152}$$

where a, b, c_1, and d_1 are material parameters. Furthermore,

$$d_1 = 2(a + 2b), \tag{4.153}$$

guarantees a stress-free reference configuration.

The thermo-mechanical coupling is introduced exclusively through the volumetric response by means of

$$\psi_2(J) = 3\beta\big(c_2(J-1) - \frac{d_2}{J}\big), \tag{4.154}$$

where β denotes the coefficient of thermal expansion and c_2 and d_2 are additional material parameters.

To investigate the influence of the volumetric stiffness, two different parameter sets are considered throughout the numerical examples. The first parameter set corresponds to a compressible material ($\nu \approx 0.42$) and is summarized in Table 4.1. The second parameter set is obtained by increasing the bulk stiffness such that a Poisson ratio of $\nu = 0.499$ is obtained while keeping the shear modulus unchanged. The resulting quasi-incompressible parameter set is given in Table 4.2.

The second parameter set represents a nearly incompressible material and is therefore particularly suitable for assessing the performance of the proposed mixed formulation in the quasi-incompressible regime.

Since both parameter sets differ only in the numerical values of the material parameters, the constitutive expressions for the entropy, the internal energy, and their discrete derivatives remain unchanged.

The entropy associated with the Mooney–Rivlin-type material model follows from the thermodynamic relation

$$\eta = -\partial_\vartheta \psi = -\psi_0'(\vartheta) + \psi_2(J) = \kappa \ln \frac{\vartheta}{\vartheta_0} + \psi_2(J). \tag{4.155}$$

Using the Legendre transformation, the corresponding internal energy is obtained as

$$\begin{aligned} u &= \psi + \vartheta\eta \\ &= \psi_0(\vartheta) - \vartheta\psi_0'(\vartheta) + \psi_1(\mathbf{C}, \mathbf{G}, J) + \vartheta_0\psi_2(J) \\ &= \kappa(\vartheta - \vartheta_0) + \psi_1(\mathbf{C}, \mathbf{G}, J) + \vartheta_0\psi_2(J). \end{aligned} \tag{4.156}$$

Table 4.1.: Material parameters of the compressible Mooney–Rivlin-type material model.

Parameter	Value	Unit	Description
λ	5209	Pa	first Lamé constant
μ	997.5	Pa	shear modulus
a	249.375	Pa	material parameter
b	249.375	Pa	material parameter
c_1	4211.5	Pa	volumetric parameter
d_1	$2(a+2b) = 1496.25$	Pa	material parameter
ρ_0	10	$\mathrm{kg\,m^{-3}}$	mass density
c_2	5209	Pa	thermo-mech. coupl. parameter
d_2	665	Pa	thermo-mech. coupl. parameter
β	2.233×10^{-4}	$\mathrm{K^{-1}}$	coefficient of thermal expansion
κ	100	$\mathrm{J\,m^{-3}\,K^{-1}}$	heat capacity
ϑ_0	293.15	K	reference temperature
k	10	$\mathrm{W\,m^{-1}\,K^{-1}}$	thermal conductivity

Table 4.2.: Material parameters of the quasi-incompressible Mooney–Rivlin-type material model ($\nu = 0.499$).

Parameter	Value	Unit	Description
λ	4.977525×10^5	Pa	first Lamé constant
μ	997.5	Pa	shear modulus
a	249.375	Pa	material parameter
b	249.375	Pa	material parameter
c_1	4.96755×10^5	Pa	volumetric parameter
d_1	$2(a+2b) = 1496.25$	Pa	material parameter
ρ_0	10	$\mathrm{kg\,m^{-3}}$	mass density
c_2	4.977525×10^5	Pa	thermo-mech. coupl. parameter
d_2	665	Pa	thermo-mech. coupl. parameter
β	2.233×10^{-4}	$\mathrm{K^{-1}}$	coefficient of thermal expansion
κ	100	$\mathrm{J\,m^{-3}\,K^{-1}}$	heat capacity
ϑ_0	293.15	K	reference temperature
k	10	$\mathrm{W\,m^{-1}\,K^{-1}}$	thermal conductivity

The discrete derivatives of the Helmholtz free energy, the entropy, and the internal energy required in the formulation can now be evaluated explicitly. For the Mooney–Rivlin-type material model, we obtain

$$\begin{aligned}
\mathrm{D}_{\mathbf{C}} u &= a\mathbf{I} \\
\mathrm{D}_{\mathbf{G}} u &= b\mathbf{I} \\
\mathrm{D}_J u &= \frac{\psi_{1\mathrm{b}}(J_{n+1}) - \psi_{1\mathrm{b}}(J_n) - \vartheta_0\big(\psi_2(J_{n+1}) - \psi_2(J_n)\big)}{\Delta J} \\
\mathrm{D}_\vartheta u &= \frac{\psi_0(\vartheta_{n+1}) - \psi_0(\vartheta_n) - \vartheta_{n+1}\psi_0'(\vartheta_{n+1}) + \vartheta_n\psi_0'(\vartheta_n)}{\Delta\vartheta} = \kappa \\
\mathrm{D}_J \eta &= \frac{\psi_2(J_{n+1}) - \psi_2(J_n)}{\Delta J} \\
\mathrm{D}_\vartheta \eta &= \frac{-\psi_0'(\vartheta_{n+1}) + \psi_0'(\vartheta_n)}{\Delta\vartheta} = \kappa\frac{\ln(\vartheta_{n+1}) - \ln(\vartheta_n)}{\Delta\vartheta}.
\end{aligned} \tag{4.157}$$

Note that the discrete derivatives with respect to the scalar quantities J and ϑ reduce to the classical Greenspan formula [33]. The discrete derivatives with respect to $\mathbf{C}$ and $\mathbf{G}$ coincide with the midpoint

evaluation of their partial derivative counterparts due to the linearity of the Mooney-Rivlin-type material model with respect to these variables.

4.7.1.2. Spatial discretization and time integration

This subsection summarizes the spatial and temporal discretization schemes employed in the subsequent numerical examples.

For all formulations, the primary field variables $\boldsymbol{\varphi}$, $\mathbf{v}$, and ϑ are approximated by continuous Lagrange finite elements. The kinematic mixed quantities $\mathbf{C}$, $\mathbf{G}$, and J, together with the associated thermodynamic driving forces $\mathbf{u}_{\mathrm{C}}$, $\mathbf{u}_{\mathrm{G}}$, u_J, and η_J, are approximated by discontinuous finite element spaces. Depending on the considered formulation, the mixed quantities associated with the derivatives of the internal energy and entropy with respect to the temperature, namely u_ϑ and η_ϑ, are either approximated continuously or discontinuously.

To distinguish the different spatial discretizations, the notation

$$Q_\alpha Q_{\beta \mathrm{d}/\gamma \mathrm{c}} \tag{4.158}$$

is employed. Here, Q_α denotes the interpolation order of the primary field variables, while the first index in the second part specifies the interpolation order of the discontinuous mixed quantities associated with $\mathbf{C}$, $\mathbf{G}$, J, $\mathbf{u}_{\mathrm{C}}$, $\mathbf{u}_{\mathrm{G}}$, u_J, and η_J. The second index specifies the interpolation order of the mixed quantities u_ϑ and η_ϑ. The superscripts d and c indicate discontinuous and continuous interpolations, respectively.

For example, the notation $Q_1Q_{0d/1c}$ refers to continuous tri-linear Q_1 approximations of the primary fields, discontinuous constant Q_0 approximations of the kinematic mixed quantities and their associated thermodynamic driving forces, and continuous tri-linear Q_1 approximations of u_ϑ and η_ϑ.

For all formulations based on Q_0 and Q_1 interpolations, standard Lagrange finite elements are employed. The formulation denoted by $Q_2Q_{1d/2c}$ constitutes the only exception. In this case, the continuous quadratic approximations of the primary variables as well as of u_ϑ and η_ϑ are realized by quadratic Serendipity finite elements, while the remaining mixed quantities are still approximated by discontinuous linear Lagrange elements.

We have introduced these different formulations in order to compare their performance. It is important to emphasize that, in particular, discontinuous mixed variables can fundamentally reduce the size of the system of equations to be solved by employing static condensation (cf. [A2]).

For the temporal discretization, both the classical midpoint rule (MP) and the structure-preserving discrete derivative formulation introduced in Section 4.5 are considered. The latter is denoted by EME due to its preservation properties regarding the total energy, the angular momentum, and the entropy.

The nonlinear systems arising in each time step are solved using Newton's method. For simulations based on the midpoint rule, convergence is assessed solely by the Euclidean norm of the global residual vector,

$$|\mathbf{R}| \leq \epsilon_{\mathrm{R}}. \tag{4.159}$$

For the EME scheme, a combined residual- and energy-based stopping criterion is employed. In addition to the residual norm, a discrete energy balance defect is monitored according to

$$\mathcal{E}_{\mathrm{def}} = \left| \Delta \mathcal{T}^{\mathrm{h}} + \Delta \mathcal{U}^{\mathrm{h}} - \Delta \mathcal{W}^{\mathrm{h}}_{\mathrm{ext}} \right| < \epsilon_{\mathrm{E}}. \tag{4.160}$$

The Newton iteration is considered converged if both

$$\mathcal{E}_{\text{def}} < \epsilon_{\text{E}} \qquad \text{and} \qquad |\mathbf{R}| < \epsilon_{\text{R}} \tag{4.161}$$

are satisfied.

For all simulations, the tolerances

$$\epsilon_{\text{R}} = 10^{-6}, \qquad \epsilon_{\text{E}} = 10^{-10} \tag{4.162}$$

are employed.

The different formulations considered in the numerical examples are summarized in Table 4.3.

Table 4.3.: Overview of the discretization schemes employed in the numerical examples.

Method	Spatial discr.	Time integr.	Material model
$Q_1Q_{0\text{d}/1\text{d}}$-MP	$Q_1Q_{0d/1d}$	MP	compr. MR
$Q_1Q_{0\text{d}/1\text{c}}$-MP	$Q_1Q_{0d/1c}$	MP	compr. MR
$Q_1Q_{0\text{d}/1\text{d}}$-EME	$Q_1Q_{0d/1d}$	EME	compr. MR
$Q_1Q_{0\text{d}/1\text{c}}$-EME	$Q_1Q_{0d/1c}$	EME	compr. MR
$Q_2Q_{1\text{d}/2\text{c}}$-EME	$Q_2Q_{1d/2c}$	EME	compr. MR
$Q_1Q_{0\text{d}/1\text{c}}$-EME-incompr	$Q_1Q_{0d/1c}$	EME	quasi-incompr. MR
$Q_1Q_{0\text{d}/1\text{d}}$-EME-incompr	$Q_1Q_{0d/1d}$	EME	quasi-incompr. MR

4.7.2. Flying L-shape benchmark

The proposed formulation is assessed by means of a thermo-mechanical extension of the well-established flying L-shape benchmark originally introduced in the context of nonlinear elastodynamics. Owing to the combination of large rigid-body rotations, significant elastic deformations, and non-uniform temperature fields, this example provides a demanding test case for the proposed mixed GENERIC formulation. In particular, it allows for a simultaneous assessment of the mechanical response, the thermal equilibration process, and the preservation of the thermodynamic structure at the discrete level.

4.7.2.1. Problem setup

We consider the initial boundary value problem of an L-shaped body, following the work of [A2, 78].

The geometry and initial setting with boundary conditions are shown in Figure 4.3. In particular, the applied external mechanical tractions are

$$\bar{\mathbf{t}}_1(t) = -\bar{\mathbf{t}}_2(t) = f(t) \begin{bmatrix} 8 \\ 16 \\ 24 \end{bmatrix} \frac{\text{N}}{\text{m}^2}, \quad f(t) = \begin{cases} t & \text{for } t \leq 2.5\text{s} \\ 5 - t & \text{for } 2.5\text{s} < t \leq 5\text{s} \\ 0 & \text{for } t > 5\text{s} \end{cases}. \tag{4.163}$$

At the initial time t_0, the temperature field of the L-shaped body is prescribed uniformly as the reference temperature ϑ_0, except for the two colored boundary surfaces indicated in Fig. 4.3. On these surfaces, the temperature is initialized as

$$\vartheta_1 = \vartheta_0 + 30\,K. \tag{4.164}$$

The L-shaped domain is discretized with 117 finite elements, and the simulation time is set to $T = 200$ s with a total of 800 timesteps. This yields a timestep size of $\Delta t_n = 0.25$ s.

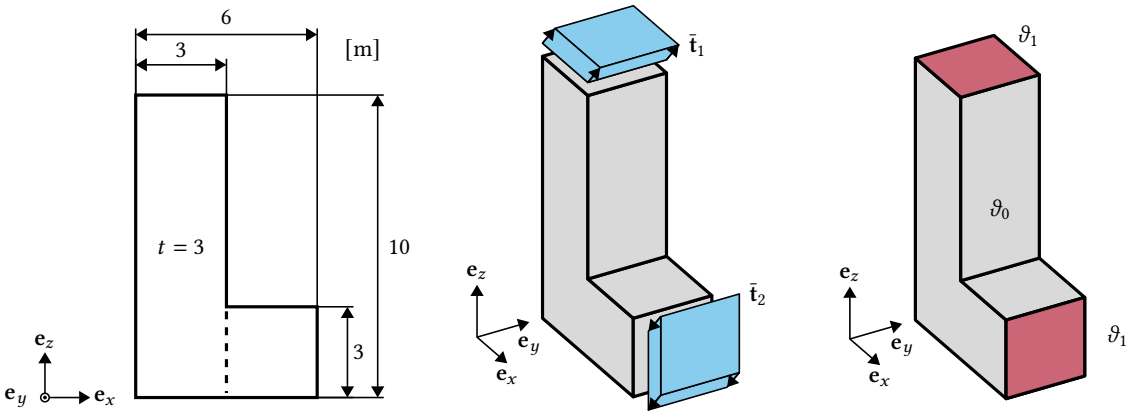


Figure 4.3.: Flying L-Shape: 2D projection of the geometry (left), 3D illustration of mechanical Neumann boundary conditions (center), and 3D illustration of thermal initial conditions (right).

4.7.2.2. Results

Figure 4.4 depicts selected snapshots of the deformation together with the corresponding von Mises stress distribution. The benchmark exhibits pronounced rigid-body rotations and large deformations throughout the simulation while maintaining a smooth stress evolution.

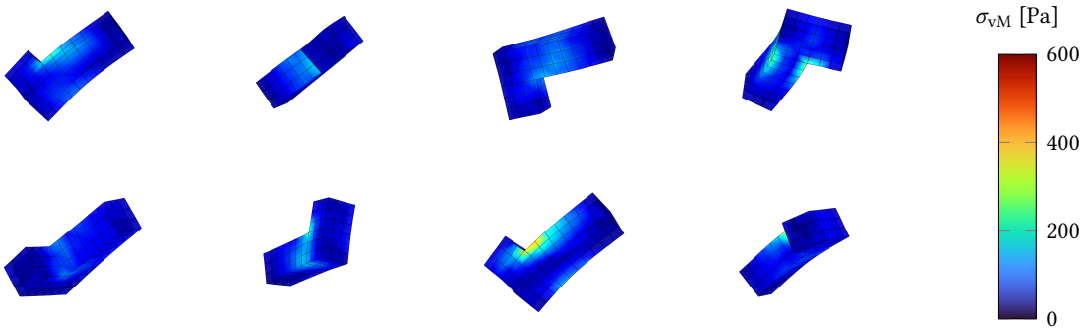


Figure 4.4.: Flying L-Shape: snapshots with von Mises stress distribution σ_{vM} [Pa] of the $Q_1Q_{0\mathrm{d}/1\mathrm{c}}$-EME formulation at times $t \in \{20.0, 40.0, 60.0, 80.0, 100.0, 120.0, 140.0, 160.0\}$s.

Figure 4.5 shows the corresponding temperature distribution for the same simulation. It can be observed that the initially imposed temperature gradients gradually diminish due to heat conduction, resulting in an increasingly homogeneous temperature field. Consequently, the system evolves towards a state of thermodynamic equilibrium.

All snapshots shown in Figs. 4.4 and 4.5 are obtained using the $Q_1Q_{0\mathrm{d}/1\mathrm{c}}$-EME formulation.

The energies obtained with the integrators under investigation are shown in Figure 4.6.

The energies obtained with the integrators under investigation are shown in Figure 4.6. In the left panel, two distinct energy levels can be identified. The uppermost curve corresponds to the $Q_2Q_{1\mathrm{d}/2\mathrm{c}}$-EME formulation. The remaining Q_1Q_0 formulations exhibit significantly lower energy levels, with only minor differences between the compressible and quasi-incompressible variants.

For the EME formulations, the total energy varies during the loading phase and remains constant up to the prescribed energy tolerance of 10^{-10} once the external tractions have vanished. This behavior

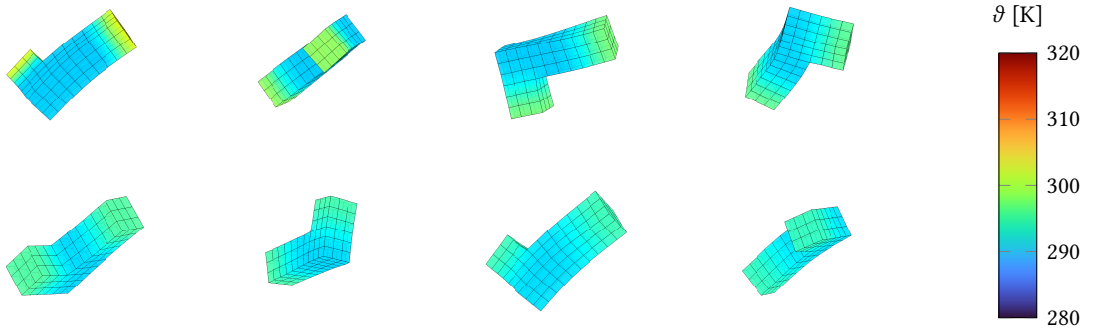


Figure 4.5.: Flying L-Shape: snapshots of the temperature field ϑ [K] obtained with the $Q_1Q_{0d/1c}$-EME formulation at times $t \in \{20.0, 40.0, 60.0, 80.0, 100.0, 120.0, 140.0, 160.0\}$s.

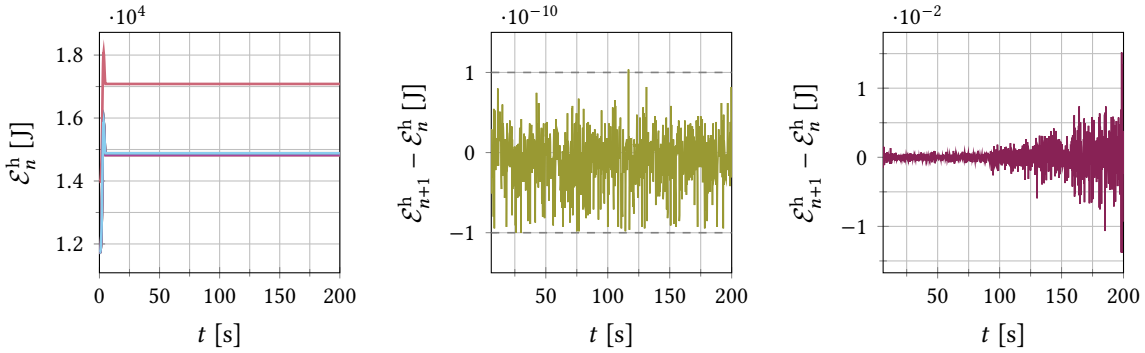


Figure 4.6.: Flying L-Shape: total energy $\mathcal{E}_n^h$ for $Q_1Q_{0d/1d}$-EME —, $Q_1Q_{0d/1c}$-EME —, $Q_2Q_{1d/2c}$-EME —, $Q_1Q_{0d/1c}$-EME-incompr —, $Q_1Q_{0d/1d}$-EME-incompr —, $Q_1Q_{0d/1d}$-MP —, and $Q_1Q_{0d/1c}$-MP — formulation (left); energy difference $\mathcal{E}_{n+1}^h - \mathcal{E}_n^h$ for $Q_1Q_{0d/1d}$-EME — formulation (middle); and energy difference $\mathcal{E}_{n+1}^h - \mathcal{E}_n^h$ for $Q_1Q_{0d/1d}$-MP — formulation (right).

is consistent with the theoretical properties established in Section 4.5. In contrast, the observed bounded energy oscillations of the $Q_1Q_{0d/1d}$-MP and $Q_1Q_{0d/1c}$-MP formulation are consistent with the well-known long-term behavior of symplectic midpoint-type schemes.

The total angular momentum is preserved up to numerical accuracy by all investigated formulations. Exemplarily, the three total angular momenta as well as the norm of the difference of the total angular momenta obtained with the $Q_1Q_{0d/1d}$-EME formulation is shown in Figure 4.7.

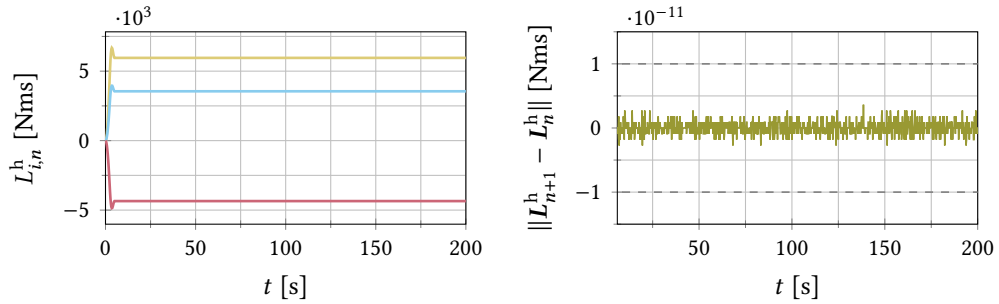


Figure 4.7.: Flying L-Shape: angular momentum components $L_{i,n}^h$, $i \in \{1$ —, 2 —, 3 —$\}$, obtained with $Q_1Q_{0d/1d}$-EME (left); and norm of the time difference of the total angular momentum $\|\boldsymbol{L}_{n+1}^h - \boldsymbol{L}_n^h\|$ — (right).

Figure 4.8 illustrates the evolution of the total entropy and the corresponding entropy increments for the considered discretizations. In the left panel, three distinct groups of curves can be identified. The

uppermost curve corresponds to the $Q_2Q_{1d/2c}$-EME formulation, exhibiting a rapid initial increase in entropy followed by a gradual approach towards a nearly constant value. The intermediate group represents the compressible formulations $Q_1Q_{0d/1d}$-EME, $Q_1Q_{0d/1c}$-EME, $Q_1Q_{0d/1d}$-MP and $Q_1Q_{0d/1c}$-MP. Although their initial entropy levels are lower than those of the $Q_2Q_{1d/2c}$-EME formulation, they exhibit a similar temporal evolution. In contrast, the lowermost group corresponds to the quasi-incompressible formulations $Q_1Q_{0d/1c}$-EME-incompr and $Q_1Q_{0d/1d}$-EME-incompr, which show an approximately linear increase in entropy over the considered simulation time.

The middle panel depicts the entropy increments $\mathcal{S}^{\mathrm{h}}_{n+1} - \mathcal{S}^{\mathrm{h}}_{n}$ of the EME formulations on a logarithmic scale. While the compressible formulations exhibit a similar decay in their entropy increments, the quasi-incompressible formulations show a distinctly different behavior, with the increments remaining at approximately 10^{-3} J/K over an extended period. The right panel presents the corresponding entropy increments for the two midpoint formulations, which exhibit nearly identical behavior and gradually decrease throughout the simulation. Furthermore, no significant differences are observed between discontinuous and continuous shape functions for the mixed quantities u_ϑ and η_ϑ. Therefore, all mixed quantities may be discretized using discontinuous shape functions, enabling static condensation and thereby significantly reducing the computational cost.

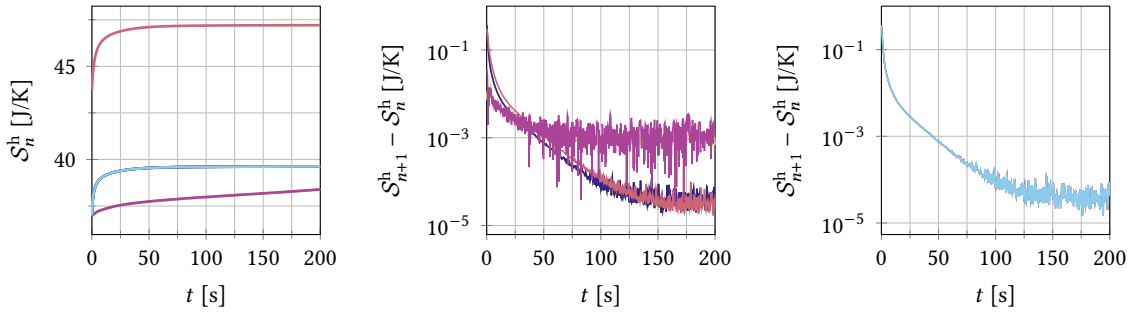


Figure 4.8.: Flying L-Shape: total entropy $\mathcal{S}^{\mathrm{h}}_n$ for $Q_1Q_{0d/1d}$-EME ——, $Q_1Q_{0d/1c}$-EME ——, $Q_2Q_{1d/2c}$-EME ——, $Q_1Q_{0d/1c}$-EME-incompr ——, $Q_1Q_{0d/1d}$-EME-incompr ——, $Q_1Q_{0d/1d}$-MP ——, and $Q_1Q_{0d/1c}$-MP —— formulation (left); entropy difference $\mathcal{S}^{\mathrm{h}}_{n+1} - \mathcal{S}^{\mathrm{h}}_n$ for $Q_1Q_{0d/1d}$-EME ——, $Q_1Q_{0d/1c}$-EME ——, $Q_2Q_{1d/2c}$-EME ——, $Q_1Q_{0d/1c}$-EME-incompr ——, and $Q_1Q_{0d/1d}$-EME-incompr —— formulation (middle); and entropy difference $\mathcal{S}^{\mathrm{h}}_{n+1} - \mathcal{S}^{\mathrm{h}}_n$ for $Q_1Q_{0d/1d}$-MP —— and $Q_1Q_{0d/1c}$-MP —— formulation (right).

For all EME formulations, the entropy increases monotonically throughout the simulation, in agreement with the theoretical results established in Section 4.6 and 4.5. The entropy difference plot confirms that the discrete entropy production remains non-negative throughout the simulation.

For the MP based discretizations, a monotonic entropy increase is likewise observed for the present benchmark. However, in contrast to the EME formulations, this behavior is not enforced by the underlying discretization and should therefore be regarded as an empirical observation rather than a theoretically guaranteed property.

The numerical results confirm the theoretical properties derived for the EME formulations. In particular, the total energy is preserved up to the prescribed energy tolerance and the entropy production remains non-negative throughout the simulation. Furthermore, the benchmark demonstrates that both considered MP based discretizations exhibit the expected long-term behavior with bounded energy oscillations and preservation of angular momentum.

4.8. Conclusion

We have proposed a mixed GENERIC formulation of finite-strain thermoelasticity together with a structure-preserving discretization in space and time. The proposed framework combines the thermodynamic structure provided by GENERIC with a mixed Hu–Washizu-type formulation based on polyconvex energy functions. In this way, reversible and irreversible processes are treated within a unified variational setting while maintaining consistency with the first and second laws of thermodynamics.

Starting from a special form of GENERIC presented in [56], a mixed thermo-mechanical formulation has been derived in terms of the kinematic quantities $\mathbf{C}$, $\mathbf{G}$, and J, together with their associated thermodynamic driving forces. The resulting framework is formulated for a general thermodynamic variable τ and therefore inherits the flexibility of the underlying special GENERIC structure. For the subsequent discretization and numerical investigations, the choice $\tau = \vartheta$ is adopted, leading to a reduced system of equations due to the vanishing entropy derivatives with respect to $\mathbf{C}$ and $\mathbf{G}$, while preserving the thermodynamic structure of the formulation.

We have shown that the proposed temporal discretization based on discrete derivatives in the sense of [32] yields a thermodynamically consistent extension of midpoint-type schemes. In particular, the resulting time-discrete formulation preserves the total energy of closed systems while guaranteeing non-negative entropy production. Furthermore, the spatial discretization of the mixed weak form leads to a semi-discrete GENERIC system satisfying discrete symmetry and non-interaction properties.

A particular feature of the present approach is that the kinematic constraints originating from the Hu–Washizu functional are enforced on the rate level. This feature is closely related to the port-Hamiltonian formulation recently proposed in [A2]. Consequently, the proposed framework is not restricted to the specific mixed finite element formulation considered in the present work. Instead, it provides a general structure-preserving setting that can accommodate a broader class of mixed finite element formulations.

The numerical investigations demonstrate the robustness of the proposed framework and confirm the theoretical findings. In particular, the structure-preserving discretization accurately reproduces the expected thermodynamic behavior, including energy conservation and non-negative entropy production.

Future research may address the extension of the present framework to inelastic constitutive models, additional multiphysics couplings, and alternative mixed finite element formulations. Another interesting topic for future work concerns the investigation of alternative thermodynamic variables within the present framework, such as the internal energy or the entropy, whose influence on the resulting discretization and numerical performance remains to be investigated.

4.9. Appendix

4.9.1. Nodal operator matrix

The matrix $\mathbb{B}_{\dot{\boldsymbol{\varphi}}}$ provides the finite-dimensional representation of the operator

$$\operatorname{sym}(\mathbf{F}^{\top}_{\boldsymbol{\varphi}^{\mathrm{h}}} \nabla \mathbf{w}^{\mathrm{h}}_{\varphi}), \tag{4.165}$$

appearing in the weak formulation. It is introduced through the relation

$$\operatorname{sym}(\mathbf{F}_{\boldsymbol{\varphi}^{\mathrm{h}}}^{\top}\nabla\mathbf{w}_{\varphi}^{\mathrm{h}}) : \mathbf{A} = \left\{\mathbf{A}\right\}_{\mathrm{V}}^{\top}\mathbb{B}_{\hat{\boldsymbol{\varphi}}}\hat{\mathbf{w}}_{\varphi}, \tag{4.166}$$

for an arbitrary symmetric second-order tensor $\mathbf{A}$.

Using the finite element interpolation of the virtual displacement field together with the identity

$$\operatorname{sym}(\mathbf{F}_{\boldsymbol{\varphi}^{\mathrm{h}}}^{\top}\nabla\mathbf{w}_{\varphi}^{\mathrm{h}}) : \mathbf{A} = \mathbf{A} : \left(\mathbf{F}_{\boldsymbol{\varphi}^{\mathrm{h}}}^{\top}\nabla\mathbf{w}_{\varphi}^{\mathrm{h}}\right) = \sum_{K=1}^{n_{\mathrm{node}}} \nabla N_{\varphi}^{K} \cdot \left(\mathbf{A}^{\top}\mathbf{F}_{\boldsymbol{\varphi}^{\mathrm{h}}}^{\top}\hat{\mathbf{w}}_{\varphi}^{K}\right), \tag{4.167}$$

one obtains

$$\mathbb{B}_{\hat{\boldsymbol{\varphi}}} = \left[\mathbb{B}_{\hat{\boldsymbol{\varphi}}}^{1} \quad \cdots \quad \mathbb{B}_{\hat{\boldsymbol{\varphi}}}^{n_{\mathrm{node}}}\right]. \tag{4.168}$$

Since

$$\mathbf{F}_{\boldsymbol{\varphi}^{\mathrm{h}}} = \sum_{K=1}^{n_{\mathrm{node}}} \hat{\boldsymbol{\varphi}}^{K} \otimes \nabla N_{\varphi}^{K}, \tag{4.169}$$

the matrices $\mathbb{B}_{\hat{\boldsymbol{\varphi}}}^{K}$ depend linearly on the nodal position vectors. Their explicit form reads

$$\mathbb{B}_{\hat{\boldsymbol{\varphi}}}^{K} = \begin{bmatrix} F_{11}N_{,x}^{K} & F_{21}N_{,x}^{K} & F_{31}N_{,x}^{K} \\ F_{12}N_{,y}^{K} & F_{22}N_{,y}^{K} & F_{32}N_{,y}^{K} \\ F_{13}N_{,z}^{K} & F_{23}N_{,z}^{K} & F_{33}N_{,z}^{K} \\ F_{11}N_{,y}^{K} + F_{12}N_{,x}^{K} & F_{21}N_{,y}^{K} + F_{22}N_{,x}^{K} & F_{31}N_{,y}^{K} + F_{32}N_{,x}^{K} \\ F_{12}N_{,z}^{K} + F_{13}N_{,y}^{K} & F_{22}N_{,z}^{K} + F_{23}N_{,y}^{K} & F_{32}N_{,z}^{K} + F_{33}N_{,y}^{K} \\ F_{11}N_{,z}^{K} + F_{13}N_{,x}^{K} & F_{21}N_{,z}^{K} + F_{23}N_{,x}^{K} & F_{31}N_{,z}^{K} + F_{33}N_{,x}^{K} \end{bmatrix}. \tag{4.170}$$

4.9.2. Matrix related to the tensor cross product

For the finite element implementation it is convenient to introduce a matrix representation of the tensor cross product. To this end, the matrix $\mathcal{D}(\mathbf{Q})$ is defined through

$$(\mathbf{O} \overset{\times}{\times} \mathbf{P}) : \mathbf{Q} = \left\{\mathbf{O}\right\}_{\mathrm{V}}^{\top}\mathcal{D}(\mathbf{Q})\left\{\mathbf{P}\right\}_{\mathrm{V}}, \tag{4.171}$$

where $\mathbf{O}$ denotes a symmetric strain-type tensor and $\mathbf{P}$ a symmetric stress-type tensor.

Starting from the definition of the tensor cross product and employing the Voigt representations introduced in (4.96), one obtains

$$\mathcal{D}(\mathbf{Q}) = \begin{bmatrix} 0 & Q_{33} & Q_{22} & 0 & -2Q_{23} & 0 \\ Q_{33} & 0 & Q_{11} & 0 & 0 & -2Q_{13} \\ Q_{22} & Q_{11} & 0 & -2Q_{12} & 0 & 0 \\ 0 & 0 & -Q_{12} & -Q_{33} & Q_{13} & Q_{23} \\ -Q_{23} & 0 & 0 & Q_{13} & -Q_{11} & Q_{12} \\ 0 & -Q_{13} & 0 & Q_{23} & Q_{12} & -Q_{22} \end{bmatrix}. \tag{4.172}$$

The matrix $\mathcal{D}(\mathbf{Q})$ is generally non-symmetric. This property originates from the different Voigt conventions adopted for strain-type and stress-type tensors, which differ by factors of two in the off-diagonal components.

5. Conclusion

5.1. Summary

This thesis has investigated mixed formulations for nonlinear continuum mechanics and their integration into structure-preserving modeling and discretization frameworks. The central objective was to study how additional independent fields, as they arise in mixed Hu–Washizu-type formulations inspired by polyconvexity, can be incorporated consistently into formulations that preserve fundamental mechanical and thermodynamic structures.

The first step was concerned with coupled nonlinear electro-thermo-elastodynamics. Starting from an existing polyconvexity-inspired mixed formulation for nonlinear elastodynamics, the framework was augmented by additional field equations associated with thermodynamics and electrostatics. It shows how mixed mechanical formulations can be extended by additional potential or non-potential fields and their corresponding balance or constraint equations, while retaining the structural advantages of the underlying mixed formulation. In particular, the resulting coupled system was discretized in time by means of discrete derivatives, leading to an energy–momentum consistent scheme for the nonlinear multiphysics problem.

The second step addressed the integration of mixed formulations into the port-Hamiltonian framework. For this purpose, the mixed kinematic compatibility relations were reformulated at rate level and incorporated into an energy-based state description. This made it possible to interpret the additional mixed fields not merely as auxiliary finite element quantities, but as part of a structured port-Hamiltonian formulation. The resulting weak form and finite element discretization preserve the characteristic power-based structure of the port-Hamiltonian setting and provide a basis for energy–momentum consistent time integration schemes.

The third step transferred the same guiding principle to the GENERIC framework for nonlinear thermoelasticity. A mixed GENERIC formulation was developed in which reversible mechanical dynamics and irreversible heat conduction are represented within a thermodynamically consistent operator structure. The additional mixed kinematic fields were incorporated in such a way that the GENERIC degeneracy conditions are preserved. Moreover, compatible temporal and spatial discretizations were constructed that preserve the total energy and angular momentum of closed systems while ensuring consistent entropy production.

The results show that mixed formulations can be combined with structure-preserving principles in a consistent and flexible way. In the numerical examples considered in this thesis, the resulting schemes also exhibit stable and robust behavior. The specific polyconvexity-inspired Hu–Washizu-type setting used throughout this thesis serves as a representative and particularly suitable framework for demonstrating this idea. At the same time, the developed concepts point beyond this specific choice and provide a methodological basis for the broader integration of mixed finite element formulations into structure-preserving computational mechanics.

5.2. Outlook

The developments presented in this thesis open several directions for future research. A first natural extension concerns more general classes of material behavior. Since the GENERIC formulation developed in this work is restricted to nonlinear thermoelasticity with heat conduction, future work could extend the mixed GENERIC framework to inelastic, dissipative, or microstructure-informed solid models. Existing GENERIC-based developments for inelastic solid mechanics, thermodynamically consistent damage modeling, and heterogeneous solids provide useful starting points for such extensions [39, 41, 59, 73]. Such developments would require the consistent incorporation of the additional variables and dissipative mechanisms associated with the respective material model while preserving the GENERIC degeneracy conditions and the corresponding energy and entropy balances.

The choice of constitutive models also offers room for further investigation. In the examples considered in this thesis, the numerical behavior depends strongly on the structure of the stored energy function and on the way in which the energy is expressed in terms of the mixed variables. It would therefore be valuable to identify material models for which the mixed formulation yields clear advantages over purely displacement-based formulations or standard midpoint-type time discretizations. In particular, strongly nonlinear polyconvexity-inspired or genuinely polyconvex models may provide useful test cases for assessing the benefits of structure-preserving time integration schemes based on discrete derivatives. Promising candidates in this direction are provided by near-incompressible generalized-polynomial and Arruda–Boyce-type strain-energy functions studied from the viewpoint of polyconvexity, as well as by more recent polyconvex hyperelastic models for rubberlike materials [36, 81].

Another direction concerns more general coupled multiphysics problems. The first contribution of this thesis considered electro-thermo-elastodynamics within a mixed variational framework, whereas the GENERIC contribution focused on thermoelasticity with heat conduction. Combining these viewpoints suggests the development of mixed GENERIC formulations for broader classes of coupled multiphysics systems. Existing GENERIC-based developments for dissipative electromagnetism, reactive fluid flows, reaction–diffusion systems, and non-Fourier heat conduction provide useful starting points for such extensions [37, 42, 82, 90]. Building on these developments, mixed GENERIC formulations could provide a thermodynamically consistent framework for multiphysics problems involving large deformations, field interactions, chemical or thermal transport processes, and the corresponding irreversible mechanisms.

Beyond the specific Hu–Washizu-type formulations considered in this thesis, future work may assess the practical implications of applying the proposed structure-preserving methodology to other mixed finite element technologies. Examples include pressure-based elements of the Simo–Taylor–Pister type, enhanced assumed strain formulations, related combinations of pressure and enhanced strain fields, and Hellinger–Reissner-type assumed-stress approaches [2, B2, 67, 76, 77, 79]. Since the generality of the approach is tied to the consistent treatment of additional fields and their constraint or compatibility relations, such studies could clarify how different choices of mixed variables affect approximation quality, robustness, implementation effort, and the preservation of the relevant energy, power, or entropy structures.

Finally, the connection between structure-preserving methods and data-driven modeling provides a promising long-term perspective. GENERIC-informed neural-network approaches have already shown how energy conservation, entropy production, and the associated degeneracy conditions can be incorporated into data-driven models of thermodynamic systems [87, 91]. In computational mechanics, related developments in physics-augmented neural networks demonstrate how constitutive requirements such as objectivity, material symmetry, polyconvexity, and thermodynamic consistency can be enforced

by construction, and how such models can be combined with mixed finite element formulations and energy–momentum consistent time integration [27, 49]. Combining these developments with mixed finite element formulations, port-Hamiltonian systems, or GENERIC may lead to new methods for learning constitutive behavior or reduced-order dynamics while preserving energy, power, and entropy structures by construction.

Overall, the thesis provides a foundation for the systematic development of mixed structure-preserving formulations in nonlinear continuum mechanics. The extension to more general dissipative materials, coupled multiphysics systems, broader classes of mixed finite element formulations, efficient computational implementations, and data-driven structure-preserving models remains a rich field for future research.

Declaration of authorship

The initials Moritz Hille (MH), Peter Betsch (PB), Marlon Franke (MF) and Felix Zähringer (FZ) are used below to mark the contributions of the respective author to the publications.



Available online at www.sciencedirect.com

ScienceDirect

IFAC PapersOnline CONFERENCE PAPER ARCHIVE

IFAC PapersOnLine 58-6 (2024) 113–118

Structure-Preserving Discretization of a Polyconvexity-Inspired Formulation for Coupled Nonlinear Electro-Thermo-Elastodynamics

Moritz Hille * Marlon Franke * Felix Zähringer * Peter Betsch *

* *Institute of Mechanics, Karlsruhe Institute of Technology (KIT), Germany (e-mail: Peter.Betsch@kit.edu).*

Abstract: A consistent, structure-preserving space-time discretization for coupled nonlinear electro-thermo-elastodynamical problems is presented. The underlying polyconvexity-inspired mixed framework is facilitated by the properties of the tensor cross product. The elastodynamic problem is then extended by the energy balance as well as Gauss's and Faraday's law to integrate the thermodynamic and electrostatic contribution, respectively. A suitable polyconvexity-inspired internal energy function is chosen to complete the nonlinear, fully coupled electro-thermo-elastodynamical formulation. Additionally, we present a structure-preserving, second-order accurate time integration scheme, utilizing discrete derivatives in the sense of Gonzalez (1996), ensuring a stable and robust simulation even for large time steps. Finally, we assess the numerical performance of our newly developed method through representative examples also showing the possibilities of the framework in the field of boundary control.

Copyright © 2024 The Authors. This is an open access article under the CC BY-NC-ND license (https://creativecommons.org/licenses/by-nc-nd/4.0/)

Keywords: Nonlinear electro-thermo-elastodynamics, Polyconvexity, Tensor cross product, Structure-preserving discretization

1. INTRODUCTION

Dielectric elastomers (DEs) are classified as smart materials within the group of electroactive polymers, showcasing great potential in the field of control owing to their electrically induced actuation properties. In their basic configuration, DEs comprise an elastomer layer sandwiched between two electrodes. The application of a voltage results in a Coulomb force, leading to a compression of the elastomer layer. DEs can undergo large deformations, with area expansions of up to 1600% (Keplinger et al. (2012)), albeit exhibiting sensitivity to temperature variations (see e.g. Mehnert et al. (2021)). Thus, this paper provides a fully coupled nonlinear thermo-electro-mechanical framework to simulate DEs.

For long-term time-dependent finite element simulations of DEs, employing a stable and robust spatial and temporal discretization is crucial. Energy-momentum (EM) time integration schemes offer superior stability and robustness compared to other classical time integration methods (Simo and Tarnow (1992)). This superiority arises from their inherent ability to preserve the conservation of the total energy, total linear momentum, and total angular momentum of the system.

Betsch et al. (2018) leveraged the tensor cross product, originally introduced by de Boer (1982) and reintroduced to the field of nonlinear continuum mechanics by Bonet et al. (2016). They subsequently adapted an EM scheme based on discrete gradients in the sense of Gonzalez (1996), to suit a mixed polyconvexity inspired elastodynamic framework. To achieve the desired multiphysics framework, we incorporate the mixed polyconvexity-inspired elastodynamics formulation by Betsch et al. (2018). This formulation is then extended by introducing additional fields from thermodynamics and electrostatics.

The paper is therefore organized as follows: In Section 2, fundamental concepts are presented, including the basics of the tensor cross products, a mixed Hu-Washizu-like variational potential for elastodynamics, balance equations derived from thermodynamics and electrostatics, and a suitable coupling energy density function. These elements collectively give rise to the mixed polyconvexity-inspired thermo-electro-mechanical framework. The temporal and spatial discretization is then discussed in Section 3. Using two examples, the structure-preserving properties of the formulation are investigated in Section 4, before brief conclusions are drawn in Section 5.

2. FRAMEWORK

In this section we give an overview of the balance equations of elastodynamics, thermodynamics and electrostatics along with a suitable material model yielding the fully coupled, mixed, polyconvexity-inspired framework we use.

2.1 Elastodynamics

We start with the elastodynamic part of the framework. The deformation gradient $\boldsymbol{F}$ defined as

$$\mathrm{d}\boldsymbol{x} = \boldsymbol{F}\cdot\mathrm{d}\boldsymbol{X} \tag{1}$$

2405-8963 Copyright © 2024 The Authors. This is an open access article under the CC BY-NC-ND license.
Peer review under responsibility of International Federation of Automatic Control.
10.1016/j.ifacol.2024.08.266

Citation:
Hille M, Franke M, Zähringer F, and Betsch P. "Structure-Preserving Discretization of a Polyconvexity-Inspired Formulation for Coupled Nonlinear Electro-Thermo-Elastodynamics". In: *IFAC-PapersOnLine*, 58(6): 113–118, 2024. DOI: 10.1016/j.ifacol.2024.08.266

Declaration:
Conceptualization, formal analysis, project administration, validation, writing – review & editing: MH, MF, PB • investigation, software: MH, MF, FZ • methodology: MH, MF, FZ, PB • funding acquisition, resources, supervision: MF, PB • visualization, writing – original draft: MH.



Computer Methods in Applied Mechanics and Engineering 458 (2026) 118790

Contents lists available at ScienceDirect

Comput. Methods Appl. Mech. Engrg.

journal homepage: www.elsevier.com/locate/cma

Port-Hamiltonian formulation and structure-preserving discretization of finite elasticity based on a mixed Hu-Washizu-type formulation

Moritz Hille, Peter Betsch, Marlon Franke

Institute of Mechanics, Karlsruhe Institute of Technology (KIT), Germany

ARTICLE INFO

Keywords:
Nonlinear elastodynamics
Livens principle
Hu-Washizu principle
Port-Hamiltonian formulation
Mixed finite elements
Energy-momentum methods

ABSTRACT

We propose a port-Hamiltonian formulation and structure-preserving discretization of finite elasticity. The energy functional (or Hamiltonian) is based on a polyconvex representation of the stored energy and gives rise to three strain-type fields, which play the role of energy variables in the port-Hamiltonian formulation. We show that a Hu-Washizu-type extension of the variational principle of Livens can be used (i) to derive the continuous port-Hamiltonian formulation and (ii) to perform a structure-preserving spatial discretization. In particular, we show that the spatial finite element discretization of the underlying mixed formulation yields a discrete port-Hamiltonian system. Moreover, the temporal discretization of the underlying continuous formulation yields a new energy-momentum consistent framework, which accommodates alternative finite element formulations. The new framework, in particular, covers mixed finite elements that have been shown to be well suited for handling quasi-incompressible material behavior. Numerical examples are provided to evaluate the numerical performance and stability of the newly devised energy-momentum schemes.

1. Introduction

The port-Hamiltonian (pH) formulation of evolution equations related to multiphysics systems provides an appealing framework for modeling, simulation, and control [1,2]. The energy-based pH description takes into account dissipation and interaction with the environment by means of ports, and can thus be considered as an extension of classical Hamiltonian systems to open systems.

Finite-dimensional pH systems have been originally introduced in [3] and are based on a Dirac structure, which encodes system properties such as passivity and energy consistency into system equations. The extension of the pH modeling paradigm to infinite-dimensional systems is based on a Stokes-Dirac structure and can be traced back to [4]. Since then, distributed pH systems have been subject to extensive research in the areas of multiphysics system modeling, analysis and design of control techniques, and structure-preserving discretization methods, as categorized in the comprehensive literature review [5].

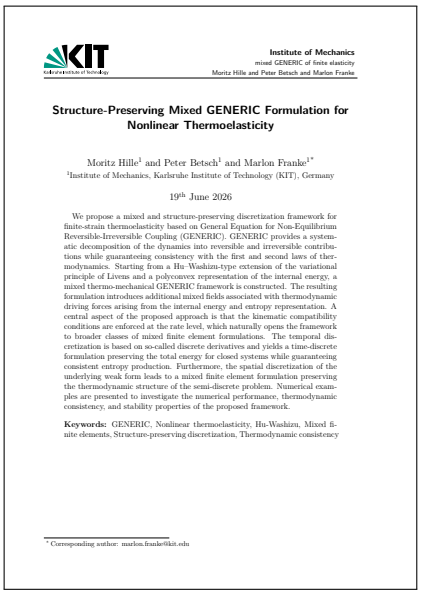
The design of structure-preserving discretization techniques is a natural objective in preserving the intrinsic structure and properties of pH systems, such as passivity and energy consistency. Galerkin-based numerical methods for the structure-preserving discretization of pH systems have become more popular only recently [6]. In particular, finite element methods have been applied to discretize pH formulations of viscoelastic strings [7], beams [8–11], plates [12], the wave equation [13], piezoelasticity [14], and

* Corresponding author.
E-mail address: peter.betsch@kit.edu (P. Betsch).

https://doi.org/10.1016/j.cma.2026.118790
Received 30 September 2025; Received in revised form 1 January 2026; Accepted 27 January 2026
Available online 29 April 2026
0045-7825/© 2026 The Authors. Published by Elsevier B.V. This is an open access article under the CC BY license (http://creativecommons.org/licenses/by/4.0/).

Citation:
Hille M, Betsch P, and Franke M. "Port-Hamiltonian Formulation and Structure-Preserving Discretization of Finite Elasticity Based on a Mixed Hu–Washizu-Type Formulation". In: *Computer Methods in Applied Mechanics and Engineering*, 458: 118790, 2026. DOI: 10.1016/j.cma.2026.118790

Declaration:
Conceptualization, formal analysis, methodology, project administration, validation, writing – original draft, writing – review & editing: MH, PB, MF • software, visualization: MH, MF • funding acquisition: PB, MF • resources, supervision: PB • data curation, investigation: MF.



Institute of Mechanics
mixed GENERIC of finite elasticity
Moritz Hille and Peter Betsch and Marlon Franke

Structure-Preserving Mixed GENERIC Formulation for Nonlinear Thermoelasticity

Moritz Hille[1] and Peter Betsch[1] and Marlon Franke[1*]
[1]Institute of Mechanics, Karlsruhe Institute of Technology (KIT), Germany

19th June 2026

We propose a mixed and structure-preserving discretization framework for finite-strain thermoelasticity based on General Equation for Non-Equilibrium Reversible-Irreversible Coupling (GENERIC). GENERIC provides a systematic decomposition of the dynamics into reversible and irreversible contributions while guaranteeing consistency with the first and second laws of thermodynamics. Starting from a Hu–Washizu-type extension of the variational principle of Livens and a polyconvex representation of the internal energy, a mixed thermo-mechanical GENERIC framework is constructed. The resulting formulation introduces additional mixed fields associated with thermodynamic driving forces arising from the internal energy and entropy representation. A central aspect of the proposed approach is that the kinematic compatibility conditions are enforced at the rate level, which naturally opens the framework to broader classes of mixed finite element formulations. The temporal discretization is based on so-called discrete derivatives and yields a time-discrete formulation preserving the total energy for closed systems while guaranteeing consistent entropy production. Furthermore, the spatial discretization of the underlying weak form leads to a mixed finite element formulation preserving the thermodynamic structure of the semi-discrete problem. Numerical examples are presented to investigate the numerical performance, thermodynamic consistency, and stability properties of the proposed framework.

Keywords: GENERIC, Nonlinear thermoelasticity, Hu-Washizu, Mixed finite elements, Structure-preserving discretization, Thermodynamic consistency

* Corresponding author: marlon.franke@kit.edu

Citation:
Hille M, Betsch P, and Franke M. *Structure-Preserving Mixed GENERIC Formulation for Nonlinear Thermoelasticity*. Manuscript submitted to Journal of Computational Physics. Preprint available at SSRN. 2026. DOI: 10.2139/ssrn.7029051

Declaration:
Conceptualization, formal analysis, methodology, project administration, validation, writing – original draft, writing – review & editing: MH, PB, MF • data curation, investigation, software, visualization: MH, MF • funding acquisition: PB, MF • resources, supervision: PB.

Declaration of AI-assisted tools: During the preparation of this work, the author used generative artificial intelligence (AI) tools exclusively for language editing and stylistic improvements. After using these tools, the author carefully reviewed and edited the content as necessary and takes full responsibility for the content of this publication.

Data availability: The article-based chapters of this thesis are accompanied by open-source implementations of the corresponding numerical methods. For Chapters 3 and 4, the availability of the code is specified in the respective article or submitted manuscript on which the chapters are based. The proceedings contribution underlying Chapter 2 does not contain a separate data availability statement; however, the numerical results reported there were generated with the same version of the institute research code whose open-source availability is documented in the extended journal contribution [B3].

Publications and talks

Peer-reviewed publications and submitted manuscripts included in this thesis

[A1] **Hille M**, Franke M, Zähringer F, and Betsch P. "Structure-Preserving Discretization of a Polyconvexity-Inspired Formulation for Coupled Nonlinear Electro-Thermo-Elastodynamics". In: *IFAC-PapersOnLine*, 58(6): 113–118, 2024. DOI: 10.1016/j.ifacol.2024.08.266.

[A2] **Hille M**, Betsch P, and Franke M. "Port-Hamiltonian Formulation and Structure-Preserving Discretization of Finite Elasticity Based on a Mixed Hu–Washizu-Type Formulation". In: *Computer Methods in Applied Mechanics and Engineering*, 458: 118790, 2026. DOI: 10.1016/j.cma.2026.118790.

[A3] **Hille M**, Betsch P, and Franke M. *Structure-Preserving Mixed GENERIC Formulation for Nonlinear Thermoelasticity*. Manuscript submitted to Journal of Computational Physics. Preprint available at SSRN. 2026. DOI: 10.2139/ssrn.7029051.

Further publications

[B1] Franke M, Ortigosa R, Gil A, and **Hille M**. "Energy-Momentum Scheme For Nonlinear Thermo-Electro-Elastodynamics". In: *14th World Congress on Computational Mechanics (WCCM) ECCOMAS Congress 2020*. 2020. DOI: 10.23967/wccm-eccomas.2020.134.

[B2] **Hille M**, Pfefferkorn R, and Betsch P. "Locking-Free Mixed Finite Element Methods and Their Spurious Hourglassing Patterns". In: *Current Trends and Open Problems in Computational Mechanics*. Ed. by Aldakheel F, Hudobivnik B, Soleimani M, Wessels H, Weißenfels C, and Marino M. Cham: Springer, 2022. DOI: 10.1007/978-3-030-87312-7_19.

[B3] Franke M, Zähringer F, **Hille M**, Ortigosa R, Betsch P, and Gil AJ. "A Novel Mixed and Energy–Momentum Consistent Framework for Coupled Nonlinear Thermo–Electro–Elastodynamics". In: *International Journal for Numerical Methods in Engineering*, 124: 2135–2170, 2023. DOI: 10.1002/nme.7209.

Conference contributions

[C1] **Hille M**, Pfefferkorn R, and Betsch P. *Spurious Hourglassing Patterns of Locking-Free Mixed Finite-Element Methods for Nearly Incompressible Large Deformation Solid Mechanics*. 92nd Annual Meeting of the International Association of Applied Mathematics and Mechanics. Aachen, Germany, Aug. 15–19, 2022.

[C2] **Hille M**, Franke M, Zähringer F, Ortigosa R, Betsch P, and Gil A. *A Polyconvexity-Inspired Mixed Formulation and Structure-Preserving Discretization for Coupled Nonlinear Electro-Thermo-Elastodynamics*. 10th International Conference of Computational Methods for Coupled Problems in Science and Engineering. Chania, Crete, Greece, June 5–7, 2023.

[C3] **Hille M**, Franke M, Zähringer F, and Betsch P. *Structure-Preserving Discretization of a Polyconvexity-Inspired Formulation for Nonlinear Electro-Thermo-Elastodynamics*. 8th IFAC Workshop on Lagrangian and Hamiltonian Methods for Nonlinear Control – LHMNC 2024. Besançon, France, June 10–12, 2024.

[C4] **Hille M**, Franke M, and Betsch P. *Space-Time Discretization of Nonlinear Coupled Thermo-Elastodynamical Problems in a Novel, Polyconvexity-Inspired, Mixed GENERIC Framework*. 95th Annual Meeting of the International Association of Applied Mathematics and Mechanics. Poznań, Poland, Apr. 7–11, 2025.

[C5] **Hille M**, Franke M, and Betsch P. *On Structure Preserving Properties of a Polyconvexity-Inspired, Mixed GENERIC Formalism to Simulate Nonlinear Coupled Thermo-Elastodynamical Problems*. 11th International Conference on Computational Methods for Coupled Problems in Science and Engineering. Accepted abstract; talk presented by Peter Betsch. Villasimius, Sardinia, Italy, 2025.

[C6] **Hille M**, Betsch P, and Franke M. *Structure Preserving Discretization of Polyconvexity-Inspired, Mixed Nonlinear Thermoelasticity Using Port-Hamiltonian and GENERIC Frameworks*. 17th World Congress on Computational Mechanics and 10th European Congress on Computational Methods in Applied Sciences and Engineering. Accepted abstract; talk to be presented by Marlon Franke. Munich, Germany, 2026.

List of figures

1.1. Conceptual structure of the thesis. . . . 2

2.1. Flying L-Shape: reference configuration. . . . 15
2.2. Flying L-Shape: total energy and angular momentum evolution. . . . 16
2.3. Flying L-Shape: total energy and angular momentum difference. . . . 16
2.4. Microfluid pump: initial configuration. . . . 17
2.5. Microfluid pump: top and side view. . . . 17
2.6. Microfluid pump: applied electric Dirichlet boundary conditions. . . . 17
2.7. Microfluid pump: total energy and energy difference. . . . 18
2.8. Microfluid pump: simulation snapshots. . . . 18

3.1. Configuration and kinematics of a deformable body. . . . 23
3.2. Flying L-Shape: Geometry and boundary conditions. . . . 48
3.3. Flying L-Shape: motion snapshots with von Mises stress distribution. . . . 49
3.4. Flying L-Shape: total energy and energy difference. . . . 49
3.5. Flying L-Shape: angular momentum components and difference. . . . 50
3.6. Flying L-Shape: convergence results. . . . 50
3.7. Bending and twisting beam: initial configuration. . . . 51
3.8. Bending beam: motion snapshots with von Mises stress distribution. . . . 51
3.9. Twisting beam: motion snapshots with von Mises stress distribution. . . . 52
3.10. Bending and twisting beam: total energy ($\nu = 0.495$). . . . 52
3.11. Bending and twisting beam: total energy ($\nu = 0.499$). . . . 53
3.12. Bending beam: quasi-incompressibility verification. . . . 53

4.1. Configuration and kinematics of a deformable body with mechanical boundaries. . . . 60
4.2. Configuration and kinematics of a deformable body with thermal boundaries. . . . 62
4.3. Flying L-Shape: Geometry, boundary and initial conditions. . . . 91
4.4. Flying L-Shape: motion snapshots with von Mises stress distribution. . . . 91
4.5. Flying L-Shape: motion snapshots with temperature distribution. . . . 92
4.6. Flying L-Shape: total energy and energy difference. . . . 92
4.7. Flying L-Shape: angular momentum components and total angular momentum difference. 92
4.8. Flying L-Shape: total entropy and entropy difference. . . . 93

List of tables

3.1. Considered discretizations and associated abbreviations. 46
3.2. Mooney Rivlin model parameters. 47
3.3. Modified Mooney–Rivlin model parameters with effective Poisson's ratio of $\nu = 0.495$. . . 47
3.4. Modified Mooney-Rivlin model parameters with effective Poisson's ratio of $\nu = 0.499$. . . 47

4.1. Material parameters of the compressible Mooney–Rivlin-type material model. 88
4.2. Material parameters of the quasi-incompressible Mooney–Rivlin-type material model ($\nu = 0.499$). 88
4.3. Overview of the discretization schemes employed in the numerical examples. 90

Bibliography

[1] Altmann R, Mehrmann V, and Unger B. "Port-Hamiltonian formulations of poroelastic network models". In: *Mathematical and Computer Modelling of Dynamical Systems*, 27(1): 429–452, 2021. DOI: 10.1080/13873954.2021.1975137 (see pp. 4, 22).

[2] Armero F. "On the locking and stability of finite elements in finite deformation plane strain problems". In: *Computers & Structures*, 75(3): 261–290, 2000. DOI: 10.1016/S0045-7949(99)00136-4 (see p. 98).

[3] Ball JM. "Convexity conditions and existence theorems in nonlinear elasticity". In: *Archive for Rational Mechanics and Analysis*, 63(4): 337–403, 1976. DOI: 10.1007/BF00279992 (see p. 2).

[4] Bell L and Struchtrup H. "13-moment-equations from nonequilibrium thermodynamics and kinetic theory: Comparison for non-linear one-dimensional flows". In: *Physics of Fluids*, 37(6): 067122, 2025. DOI: 10.1063/5.0270910 (see p. 4).

[5] Betsch P and Steinmann P. "Conservation properties of a time FE method. Part II: time-stepping schemes for nonlinear elastodynamics". In: *International Journal for Numerical Methods in Engineering*, 50: 1931–1955, 2001. DOI: 10.1002/nme.103 (see pp. 3, 22).

[6] Betsch P, ed. *Structure-preserving integrators in nonlinear structural dynamics and flexible multibody dynamics*. Vol. 565. CISM International Centre for Mechanical Sciences Courses and Lectures. Springer-Verlag, 2016. DOI: 10.1007/978-3-319-31879-0 (see p. 3).

[7] Betsch P, Janz A, and Hesch C. "A mixed variational framework for the design of energy-momentum schemes inspired by the structure of polyconvex stored energy functions". In: *Computer Methods in Applied Mechanics and Engineering*, 335: 660–696, 2018. DOI: 10.1016/j.cma.2018.01.013 (see pp. 2, 10, 11, 18, 22, 46, 48, 53, 58).

[8] Betsch P and Schiebl M. "Energy-momentum-entropy consistent numerical methods for large-strain thermoelasticity relying on the GENERIC formalism". In: *International Journal for Numerical Methods in Engineering*, 119(12): 1216–1244, 2019. DOI: 10.1002/nme.6089 (see pp. 4, 58).

[9] Betsch P and Schiebl M. "GENERIC-based formulation and discretization of initial boundary value problems for finite strain thermoelasticity". In: *Computational Mechanics*, 65(2): 503–531, 2020. DOI: 10.1007/s00466-019-01781-5 (see pp. 4, 58).

[10] Boer R de. *Vektor- und Tensorrechnung für Ingenieure*. Springer-Verlag Berlin Heidelberg, 1982 (see pp. 10, 24, 61).

[11] Boffi D, Brezzi F, and Fortin M. *Mixed finite element methods and applications*. Vol. 44. Springer Series in Computational Mathematics. Berlin, Heidelberg: Springer, 2013. DOI: 10.1007/978-3-642-36519-5 (see p. 1).

[12] Bonet J, Gil A, Lee C, Aguirre M, and Ortigosa R. "A first order hyperbolic framework for large strain computational solid dynamics. Part I: total Lagrangian isothermal elasticity". In: *Computer Methods in Applied Mechanics and Engineering*, 283: 689–732, 2015. DOI: 10.1016/j.cma.2014.09.024 (see p. 53).

[13] Bonet J, Gil AJ, and Ortigosa R. "A computational framework for polyconvex large strain elasticity". In: *Computer Methods in Applied Mechanics and Engineering*, 283: 1061–1094, 2015. DOI: 10.1016/j.cma.2014.10.002 (see p. 2).

[14] Bonet J, Gil AJ, and Ortigosa R. "On a tensor cross product based formulation of large strain solid mechanics". In: *International Journal of Solids and Structures*, 84: 49–63, 2016. DOI: 10.1016/j.ijsolstr.2015.12.030 (see pp. 2, 10, 24, 61).

[15] Brezzi F and Fortin M. *Mixed and hybrid finite element methods*. Vol. 15. Springer Series in Computational Mathematics. New York: Springer, 1991. DOI: 10.1007/978-1-4612-3172-1 (see p. 1).

[16] Brugnoli A, Alazard D, Pommier-Budinger V, and Matignon D. "A port-Hamiltonian formulation of linear thermoelasticity and its mixed finite element discretization". In: *Journal of Thermal Stresses*, 44(6): 643–661, 2021. DOI: 10.1080/01495739.2021.1917322 (see pp. 4, 22).

[17] Brugnoli A, Alazard D, Pommier-Budinger V, and Matignon D. "Structure-preserving discretization of port-Hamiltonian plate models". In: *IFAC-PapersOnLine*, 54(39): 359–364, 2021. DOI: 10.1016/j.ifacol.2021.06.094 (see pp. 4, 22).

[18] Brugnoli A, Rashad R, Califano F, Stramigioli S, and Matignon D. "Mixed finite elements for port-Hamiltonian models of von Kármán beams". In: *IFAC-PapersOnLine*, 54(19): 186–191, 2021. DOI: 10.1016/j.ifacol.2021.11.076 (see pp. 4, 22).

[19] Brugnoli A, Matignon D, and Morlier J. "A linearly-implicit energy–momentum preserving scheme for geometrically nonlinear mechanics based on non-canonical Hamiltonian formulations". In: *Nonlinear Dynamics*, 2025. DOI: 10.1007/s11071-025-11601-6 (see pp. 22, 31, 50).

[20] Cardoso-Ribeiro FL, Matignon D, and Lefèvre L. "A structure-preserving partitioned finite element method for the 2D wave equation". In: *IFAC-PapersOnLine*, 51(3): 119–124, 2018. DOI: 10.1016/J.IFACOL.2018.06.033 (see p. 22).

[21] Cardoso-Ribeiro FL, Matignon D, and Pommier-Budinger V. "Piezoelectric beam with distributed control ports: a power-preserving discretization using weak formulations". In: *IFAC-PapersOnLine*, 49(8): 290–297, 2016. DOI: 10.1016/j.ifacol.2016.07.456 (see p. 22).

[22] Ciarlet PG. *Mathematical Elasticity, Volume I: Three-Dimensional Elasticity*. Vol. 20. Studies in Mathematics and Its Applications. Amsterdam: North-Holland, 1988 (see pp. 2, 60).

[23] Duindam V, Macchelli A, Stramigioli S, and Bruyninckx H, eds. *Modeling and control of complex physical systems. The port-Hamiltonian approach*. Berlin, Heidelberg: Springer-Verlag, 2009. DOI: 10.1007/978-3-642-03196-0 (see pp. 3, 21).

[24] Esen O, Grmela M, and Pavelka M. "On the role of geometry in statistical mechanics and thermodynamics. I. Geometric perspective". In: *Journal of Mathematical Physics*, 63(12): 122902, 2022. DOI: 10.1063/5.0099923 (see p. 4).

[25] Esen O, Grmela M, and Pavelka M. "On the role of geometry in statistical mechanics and thermodynamics. II. Thermodynamic perspective". In: *Journal of Mathematical Physics*, 63(12): 123305, 2022. DOI: 10.1063/5.0099930 (see p. 4).

[B3] Franke M, Zähringer F, Hille M, Ortigosa R, Betsch P, and Gil AJ. "A Novel Mixed and Energy–Momentum Consistent Framework for Coupled Nonlinear Thermo–Electro–Elastodynamics". In: *International Journal for Numerical Methods in Engineering*, 124: 2135–2170, 2023. DOI: 10.1002/nme.7209 (see pp. 5, 14, 16, 58, 102).

[26] Franke M, Janz A, Schiebl M, and Betsch P. "An energy-momentum consistent integration scheme using a polyconvexity-based framework for non-linear thermo-elastodynamics". In: *International Journal for Numerical Methods in Engineering*, 115(5): 549–577, 2018. DOI: 10.1002/nme.5816 (see pp. 48, 58).

[27] Franke M, Klein DK, Weeger O, and Betsch P. "Advanced discretization techniques for hyperelastic physics-augmented neural networks". In: *Computer Methods in Applied Mechanics and Engineering*, 416: 116333, 2023. DOI: 10.1016/j.cma.2023.116333 (see pp. 46, 47, 99).

[28] Ghandi K and Hagood NW. "Hybrid Finite Element Model for Phase Transitions in Nonlinear Electromechanically Coupled Material". In: *Smart Structures and Materials 1997: Mathematics and Control in Smart Structures*. Ed. by Varadan VV and Chandra J. Vol. 3039. International Society for Optics and Photonics. SPIE, 1997, pp. 97–112. DOI: 10.1117/12.276529 (see p. 12).

[29] Gil AJ, Lee CH, Bonet J, and Aguirre M. "A stabilised Petrov–Galerkin formulation for linear tetrahedral elements in compressible, nearly incompressible and truly incompressible fast dynamics". In: *Computer Methods in Applied Mechanics and Engineering*, 276: 659–690, 2014. DOI: 10.1016/j.cma.2014.04.006 (see p. 50).

[30] Gil AJ and Ortigosa R. "A new framework for large strain electromechanics based on convex multivariable strain energies: variational formulation and material characterisation". In: *Computer Methods in Applied Mechanics and Engineering*, 302: 293–328, 2016. DOI: 10.1016/j.cma.2015.11.036 (see pp. 2, 60).

[31] Gonzalez O. "Time integration and discrete Hamiltonian systems". In: *Journal of Nonlinear Science*, 6(5): 449–467, 1996. DOI: 10.1007/BF02440162 (see pp. 3, 9, 10, 14, 19, 33, 58, 74).

[32] Gonzalez O. "Exact energy and momentum conserving algorithms for general models in nonlinear elasticity". In: *Computer Methods in Applied Mechanics and Engineering*, 190: 1763–1783, 2000. DOI: 10.1016/S0045-7825(00)00189-4 (see pp. 3, 22, 45, 46, 58, 94).

[33] Greenspan D. "Conservative numerical methods for $\ddot{x} = f(x)$". In: *Journal of Computational Physics*, 56(1): 28–41, 1984. DOI: 10.1016/0021-9991(84)90081-0 (see pp. 34, 88).

[34] Grmela M and Öttinger HC. "Dynamics and thermodynamics of complex fluids. I. Development of a general formalism". In: *Physical Review E*, 56(6): 6620–6632, 1997. DOI: 10.1103/PhysRevE.56.6620 (see pp. 4, 58).

[35] Groß M, Betsch P, and Steinmann P. "Conservation properties of a time FE method. Part IV: higher order energy and momentum conserving schemes". In: *International Journal for Numerical Methods in Engineering*, 63: 1849–1897, 2005. DOI: 10.1002/nme.1339 (see pp. 3, 22).

[36] Hartmann S and Neff P. "Polyconvexity of generalized polynomial-type hyperelastic strain energy functions for near-incompressibility". In: *International Journal of Solids and Structures*, 40(11): 2767–2791, 2003. DOI: 10.1016/S0020-7683(03)00086-6 (see p. 98).

[B2] Hille M, Pfefferkorn R, and Betsch P. "Locking-Free Mixed Finite Element Methods and Their Spurious Hourglassing Patterns". In: *Current Trends and Open Problems in Computational Mechanics*. Ed. by Aldakheel F, Hudobivnik B, Soleimani M, Wessels H, Weißenfels C, and Marino M. Cham: Springer, 2022. DOI: 10.1007/978-3-030-87312-7_19 (see p. 98).

[A2] Hille M, Betsch P, and Franke M. "Port-Hamiltonian Formulation and Structure-Preserving Discretization of Finite Elasticity Based on a Mixed Hu–Washizu-Type Formulation". In: *Computer Methods in Applied Mechanics and Engineering*, 458: 118790, 2026. DOI: 10.1016/j.cma.2026.118790 (see pp. 5, 7, 21, 58, 82, 89, 90, 94, 101).

[A3] Hille M, Betsch P, and Franke M. *Structure-Preserving Mixed GENERIC Formulation for Nonlinear Thermoelasticity*. Manuscript submitted to Journal of Computational Physics. Preprint available at SSRN. 2026. DOI: 10.2139/ssrn.7029051 (see pp. 5, 7, 57, 102).

[A1] Hille M, Franke M, Zähringer F, and Betsch P. "Structure-Preserving Discretization of a Polyconvexity-Inspired Formulation for Coupled Nonlinear Electro-Thermo-Elastodynamics". In: *IFAC-PapersOnLine*, 58(6): 113–118, 2024. DOI: 10.1016/j.ifacol.2024.08.266 (see pp. 5, 7, 9, 101).

[37] Hoyuelos M. *GENERIC framework for reaction diffusion systems*. 2012. arXiv: 1210.0373 (see p. 98).

[38] Huang S, He Z, Dirr N, Zimmer J, and Reina C. "Statistical-Physics-Informed Neural Networks (Stat-PINNs): A machine learning strategy for coarse-graining dissipative dynamics". In: *Journal of the Mechanics and Physics of Solids*, 194: 105908, 2025. DOI: 10.1016/j.jmps.2024.105908 (see p. 4).

[39] Hütter M and Svendsen B. "On the Formulation of Continuum Thermodynamic Models for Solids as General Equations for Non-equilibrium Reversible-Irreversible Coupling". In: *Journal of Elasticity*, 104: 357–368, 2011. DOI: 10.1007/s10659-011-9327-4 (see p. 98).

[40] Hütter M and Svendsen B. "Thermodynamic model formulation for viscoplastic solids as general equations for non-equilibrium reversible–irreversible coupling". In: *Continuum Mechanics and Thermodynamics*, 24(2–4): 211–227, 2012. DOI: 10.1007/s00161-011-0232-7 (see pp. 4, 58).

[41] Hütter M and Svendsen B. "Formulation of strongly non-local, non-isothermal dynamics for heterogeneous solids based on the GENERIC with application to phase-field modeling". In: *Materials Theory*, 1: 2, 2017. DOI: 10.1186/s41313-017-0004-2 (see p. 98).

[42] Jelić A, Hütter M, and Öttinger HC. "Dissipative electromagnetism from a nonequilibrium thermodynamics perspective". In: *Physical Review E*, 74(4): 041126, 2006. DOI: 10.1103/PhysRevE.74.041126 (see p. 98).

[43] Keplinger C, Li T, Baumgartner R, Suo Z, and Bauer S. "Harnessing Snap-Through Instability in Soft Dielectrics to Achieve Giant Voltage-Triggered Deformation". In: *Soft Matter*, 8: 285–288, 2012. DOI: 10.1039/C1SM06736B (see p. 9).

[44] Kinon PL, Betsch P, and Eugster SR. "Energy-momentum-consistent simulation of planar geometrically exact beams in a port-Hamiltonian framework". In: *Multibody System Dynamics*, 2025. DOI: 10.1007/s11044-025-10087-9 (see pp. 4, 22, 53).

[45] Kinon PL, Betsch P, and Schneider S. "Structure-preserving integrators based on a new variational principle for constrained mechanical systems". In: *Nonlinear Dynamics*, 111: 14231–14261, 2023. DOI: 10.1007/s11071-023-08522-7 (see pp. 26, 63).

[46] Kinon PL, Thoma T, Betsch P, and Kotyczka P. "Generalized Maxwell viscoelasticity for geometrically exact strings: nonlinear port-Hamiltonian formulation and structure-preserving discretization". In: *IFAC-PapersOnLine*, 58(6): 101–106, 2024. DOI: 10.1016/j.ifacol.2024.08.264 (see pp. 4, 22).

[47] Kotyczka P, Maschke B, and Lefèvre L. "Weak form of Stokes–Dirac structures and geometric discretization of port-Hamiltonian systems". In: *Journal of Computational Physics*, 361: 442–476, 2018. DOI: 10.1016/j.jcp.2018.02.006 (see pp. 4, 22).

[48] Kraus A, Wriggers P, Viebahn N, and Schröder J. "Low-order locking-free mixed finite element formulation with approximation of the minors of the deformation gradient". In: *International Journal for Numerical Methods in Engineering*, 120(8): 1011–1026, 2019. DOI: 10.1002/nme.6168 (see pp. 2, 22, 30, 43, 44, 50, 53, 58).

[49] Linden L, Klein DK, Kalina KA, Brummund J, Weeger O, and Kästner M. "Neural networks meet hyperelasticity: A guide to enforcing physics". In: *Journal of the Mechanics and Physics of Solids*, 179: 105363, 2023. DOI: 10.1016/j.jmps.2023.105363 (see p. 99).

[50] Marsden JE and Hughes TJR. *Mathematical foundations of elasticity*. Dover Civil and Mechanical Engineering. Dover Publications, 1994 (see p. 2).

[51] Maschke B and van der Schaft A. "Port-controlled Hamiltonian systems: modelling origins and systemtheoretic properties". In: *IFAC Proceedings Volumes*, 25(13): 359–365, 1992. DOI: 10.1016/S1474-6670(17)52308-3 (see pp. 3, 21).

[52] Mehnert M, Hossain M, and Steinmann P. "A complete thermo–electro–viscoelastic characterization of dielectric elastomers, Part I: Experimental investigations". In: *Journal of the Mechanics and Physics of Solids*, 157: 104603, 2021. DOI: 10.1016/j.jmps.2021.104603 (see p. 9).

[53] Mehnert M, Pelteret JP, and Steinmann P. "Numerical Modelling of Nonlinear Thermo-Electro-Elasticity". In: *Mathematics and Mechanics of Solids*, 22(11): 2196–2213, 2017. DOI: 10.1177/1081286517729867 (see p. 16).

[54] Mehrmann V and Morandin R. "Structure-preserving discretization for port-Hamiltonian descriptor systems". In: *Proceedings of the 58th IEEE Conference on Decision and Control*. Nice, France, 2019, pp. 6863–6868. DOI: 10.1109/CDC40024.2019.9030180 (see pp. 4, 27, 39).

[55] Mehrmann V and Unger B. "Control of port-Hamiltonian differential-algebraic systems and applications". In: *Acta Numerica*, 32: 395–515, 2023. DOI: 10.1017/S0962492922000083 (see pp. 27, 39).

[56] Mielke A. "Formulation of thermoelastic dissipative material behavior using GENERIC". In: *Continuum Mechanics and Thermodynamics*, 23: 233–256, 2011. DOI: 10.1007/s00161-010-0179-0 (see pp. 4, 58, 64, 69, 94).

[57] Mielke A. "An Eulerian formulation for dissipative materials using Lie derivatives and GENERIC". In: *Advances in continuum physics: In Memoriam Wolfgang Dreyer*. Ed. by Fuhrmann J, Hömberg D, Müller WH, and Weiss W. Cham: Springer Nature Switzerland, 2025, pp. 13–38. DOI: 10.1007/978-3-031-93918-1_2 (see pp. 4, 58).

[58] Mielke A, Peletier MA, and Zimmer J. "Deriving a GENERIC system from a Hamiltonian system". In: *Archive for Rational Mechanics and Analysis*, 249(5): 62, 2025. DOI: 10.1007/s00205-025-02119-7 (see p. 4).

[59] Mielke A and Roubíček T. "A general thermodynamical model for finitely-strained continuum with inelasticity and diffusion, its GENERIC derivation in Eulerian formulation, and some application". In: *Zeitschrift für angewandte Mathematik und Physik*, 76: 11, 2025. DOI: 10.1007/s00033-024-02391-9 (see pp. 4, 58, 98).

[60] Ortigosa R and Gil AJ. "A new framework for large strain electromechanics based on convex multi-variable strain energies: conservation laws, hyperbolicity and extension to electro-magneto-mechanics". In: *Computer Methods in Applied Mechanics and Engineering*, 309: 202–242, 2016. DOI: 10.1016/j.cma.2016.05.019 (see p. 2).

[61] Ortigosa R and Gil AJ. "A new framework for large strain electromechanics based on convex multi-variable strain energies: finite element discretisation and computational implementation". In: *Computer Methods in Applied Mechanics and Engineering*, 302: 329–360, 2016. DOI: 10.1016/j.cma.2015.12.007 (see p. 2).

[62] Öttinger HC. *Beyond equilibrium thermodynamics*. John Wiley & Sons, 2005 (see pp. 4, 19, 58, 59).

[63] Öttinger HC and Grmela M. "Dynamics and thermodynamics of complex fluids. II. Illustrations of a general formalism". In: *Physical Review E*, 56(6): 6633–6655, 1997. DOI: 10.1103/PhysRevE.56.6633 (see p. 4).

[64] Öttinger HC, Struchtrup H, and Torrilhon M. "Formulation of moment equations for rarefied gases within two frameworks of non-equilibrium thermodynamics: RET and GENERIC". In: *Philosophical Transactions of the Royal Society A: Mathematical, Physical and Engineering Sciences*, 378(2170): 20190174, 2020. DOI: 10.1098/rsta.2019.0174 (see p. 4).

[65] Park JSR, Hashim AH, Cheung SW, Choi Y, and Shin Y. *WGFINNs: Weak formulation-based GENERIC formalism informed neural networks*. 2026. arXiv: 2604.02601 [cs.LG] (see p. 4).

[66] Pavelka M, Klika V, and Grmela M. *Multiscale Thermo-Dynamics, Introduction to GENERIC*. Berlin, Boston: De Gruyter, 2018 (see pp. 4, 58, 59).

[67] Pian THH and Sumihara K. "Rational approach for assumed stress finite elements". In: *International Journal for Numerical Methods in Engineering*, 20(9): 1685–1695, 1984. DOI: 10.1002/nme.1620200911 (see p. 98).

[68] Ponce C, Ramirez H, Gorrec YL, and Wu Y. "Constrained port-Hamiltonian modeling and structure-preserving discretization of the Rayleigh beam". In: *IFAC-PapersOnLine*, 59(8): 108–113, 2025. DOI: 10.1016/j.ifacol.2025.08.075 (see pp. 4, 22).

[69] Ponce C, Wu Y, Le Gorrec Y, and Ramirez H. "A port-Hamiltonian framework for the modeling and FEM discretization of hyperelastic systems". In: *Applied Mathematical Modelling*, 150: 116403, 2025. DOI: 10.1016/j.apm.2025.116403 (see pp. 4, 22, 31).

[70] Rashad R, Califano F, van der Schaft A, and Stramigioli S. "Twenty years of distributed port-Hamiltonian systems: a literature review". In: *IMA Journal of Mathematical Control and Information*, 37(1): 1400–1422, 2020. DOI: 10.1093/imamci/dnaa018 (see pp. 3, 22).

[71] Romero I. "An analysis of the stress formula for energy-momentum methods in nonlinear elastodynamics". In: *Computational Mechanics*, 50(5): 603–610, 2012. DOI: 10.1007/s00466-012-0693-y (see pp. 22, 45).

[72] Romero I. "Thermodynamically consistent time-stepping algorithms for non-linear thermomechanical systems". In: *International Journal for Numerical Methods in Engineering*, 79(6): 706–732, 2009. DOI: 10.1002/nme.2588 (see pp. 4, 58).

[73] Schiebl M and Betsch P. "Structure-preserving space-time discretization of large-strain thermoviscoelasticity in the framework of GENERIC". In: *International Journal for Numerical Methods in Engineering*, 122(14): 3448–3488, 2021. DOI: 10.1002/nme.6670 (see pp. 4, 19, 98).

[74] Schröder J, Wriggers P, and Balzani D. "A new mixed finite element based on different approximations of the minors of deformation tensors". In: *Computer Methods in Applied Mechanics and Engineering*, 200(49–52): 3583–3600, 2011. DOI: 10.1016/j.cma.2011.08.009 (see pp. 2, 22, 30, 43, 44, 46, 47, 50, 53, 58).

[75] Scovazzi G, Carnes B, Zeng X, and Rossi S. "A simple, stable, and accurate linear tetrahedral finite element for transient, nearly, and fully incompressible solid dynamics: a dynamic variational multiscale approach". In: *International Journal for Numerical Methods in Engineering*, 106(10): 799–839, 2016. DOI: 10.1002/nme.5138 (see pp. 50, 53).

[76] Simo JC and Armero F. "Geometrically non-linear enhanced strain mixed methods and the method of incompatible modes". In: *International Journal for Numerical Methods in Engineering*, 33(7): 1413–1449, 1992. DOI: 10.1002/nme.1620330705 (see p. 98).

[77] Simo JC and Rifai MS. "A class of mixed assumed strain methods and the method of incompatible modes". In: *International Journal for Numerical Methods in Engineering*, 29(8): 1595–1638, 1990. DOI: 10.1002/nme.1620290802 (see pp. 1, 98).

[78] Simo JC and Tarnow N. "The discrete energy-momentum method. conserving algorithms for nonlinear elastodynamics". In: *Zeitschrift für angewandte Mathematik und Physik ZAMP*, 43: 757–792, 1992. DOI: 10.1007/BF00913408 (see pp. 3, 9, 22, 32, 48, 90).

[79] Simo JC, Taylor RL, and Pister KS. "Variational and projection methods for the volume constraint in finite deformation elasto-plasticity". In: *Computer Methods in Applied Mechanics and Engineering*, 51(1–3): 177–208, 1985. DOI: 10.1016/0045-7825(85)90033-7 (see pp. 1, 98).

[80] Struchtrup H and Öttinger HC. "Thermodynamically admissible 13-moment equations". In: *Physics of Fluids*, 34(1): 017105, 2022. DOI: 10.1063/5.0078780 (see p. 4).

[81] Suchocki C and Jemioło S. "Polyconvex hyperelastic modeling of rubberlike materials". In: *Journal of the Brazilian Society of Mechanical Sciences and Engineering*, 43(7): 352, 2021. DOI: 10.1007/s40430-021-03062-w (see p. 98).

[82] Szücs M, Pavelka M, Kovács R, Fülöp T, Ván P, and Grmela M. "A case study of non-Fourier heat conduction using internal variables and GENERIC". In: *Journal of Non-Equilibrium Thermodynamics*, 47(1): 31–60, 2022. DOI: 10.1515/jnet-2021-0022 (see p. 98).

[83] Thoma T, Kotyczka P, and Egger H. "On the velocity-stress formulation for geometrically nonlinear elastodynamics and its structure-preserving discretization". In: *Mathematical and Computer Modelling of Dynamical Systems*, 30(1): 701–720, 2024. DOI: 10.1080/13873954.2024.2397486 (see pp. 22, 31).

[84] Tierz A, Alfaro I, González D, Chinesta F, and Cueto E. "Graph neural networks informed locally by thermodynamics". In: *Engineering Applications of Artificial Intelligence*, 144: 110108, 2025. DOI: 10.1016/j.engappai.2025.110108 (see p. 4).

[85] van der Schaft A and Jeltsema D. "Port-Hamiltonian systems theory: an introductory overview". In: *Foundations and Trends in Systems and Control*, 1(2–3): 173–378, 2014. DOI: 10.1561/2600000002 (see pp. 3, 21).

[86] van der Schaft A and Maschke B. "Hamiltonian formulation of distributed-parameter systems with boundary energy flow". In: *Journal of Geometry and Physics*, 42(1–2): 166–194, 2002. DOI: 10.1016/S0393-0440(01)00083-3 (see pp. 3, 21).

[87] Votruba V, He Z, Qiu W, Reina C, and Pavelka M. *Nonlinear GENERIC Informed Neural Networks (N-GINNs): learning GENERIC dynamics with non-quadratic dissipation potentials*. 2026. arXiv: 2605.09058 [math.NA] (see pp. 4, 98).

[88] Washizu K. *Variational methods in elasticity and plasticity*. 2nd. Pergamon Press, 1975 (see pp. 1, 26).

[89] Wriggers P. *Nonlinear finite element methods*. Berlin; Heidelberg: Springer, 2008. DOI: 10.1007/978-3-540-71001-1 (see pp. 1, 3, 35).

[90] Zafferi A, Peschka D, and Thomas M. "GENERIC framework for reactive fluid flows". In: *Zeitschrift für Angewandte Mathematik und Mechanik*, 103(7): e202100254, 2023. DOI: 10.1002/zamm.202100254 (see pp. 4, 98).

[91] Zhang Z, Shin Y, and Karniadakis GE. "GFINNs: GENERIC formalism informed neural networks for deterministic and stochastic dynamical systems". In: *Philosophical Transactions of the Royal Society A: Mathematical, Physical and Engineering Sciences*, 380(2229): 20210207, 2022. DOI: 10.1098/rsta.2021.0207 (see pp. 4, 98).

[92] Zienkiewicz OC, Taylor RL, and Zhu JZ. *The Finite Element Method: Its Basis and Fundamentals*. 7th ed. Oxford: Butterworth-Heinemann, 2013 (see p. 3).